Experimental Investigation on the Effects of Power Actuated Fasteners on Open Web Steel Joists

by

Zachary Dean Kates, B.S.C.E.

Thesis

Presented to the Faculty of the Graduate School of

The University of Texas at Austin

in Partial Fulfillment

of the Requirements

for the Degree of

Master of Science in Engineering

The University of Texas at Austin

August 1998

Experimental Investigation on the Effects of Power Actuated Fasteners on Open Web Steel Joists

Approved by
Supervising Committee:

Michael D. Engelhardt

Sharon L. Wood

Dedication

This thesis is dedicated to my grandfather, Zach Nicolopulos, a man who always had words of encouragement and praise for all of my endeavors and accomplishments, a man who had a friendly handshake and smile for everyone.

Acknowledgements

I would like to gratefully acknowledge funding for this study provided by the Hilti Corporation. In particular, I would like to thank Tommy Wilson and Hermann Beck for their assistance throughout the course of this study.

I would like to thank my supervisor, Dr. Michael D. Engelhardt, for all his guidance and support. He was instrumental in moving the project over many of the obstacles encountered along the way. I would also like to thank my second reader, Dr. Sharon L. Wood, for her time and advice on this thesis. In addition, I would like to thank the FSEL Staff for putting up with my somewhat large demands. In particular, I would like to thank Mike Bell who stuck by his word even when the babysitter didn't show.

I would like to send out a special thank you to my parents and family, who quietly but steadfastly provided me with nothing but love, support, and encouragement.

An extra special thanks goes out to my fiancee, Debra Ann. The motivation of our new life together pushed me through right to the end.

Date Submitted: August 1998

Abstract

Experimental Investigation on the Effects of Power Actuated Fasteners on Open Web Steel Joists

Zachary Dean Kates, M.S.E.

The University of Texas at Austin, 1998

Supervisor: Michael D. Engelhardt

A series of 10 full scale tests were conducted on roof subassemblages consisting of open web steel joists and roof deck. In these specimens the roof deck was fastened to the joists by using either 5/8 inch diameter puddle welds or by using power actuated fasteners (PAFs). PAFs are small high strength nails pneumatically or power driven through the roof deck into the joist top chord angles. In these tests, the joists and roof deck were loaded to failure under downward acting vertical loads. The purpose of the tests was to determine if the presence of the PAFs produced any detrimental effects on the gravity load capacity of a joist roof system. The test results showed essentially identical performance for specimens using puddle welds as for specimens using PAFs. The tests demonstrated that the use of PAFs had no detrimental effects on the joists.

Table of Contents

List of Tables

List of Figures

Chapter 1:

Introduction

1.1 BACKGROUND

Many steel buildings currently being constructed utilize a roof system which incorporates metal roof decking. The roof decking is often supported on open-web steel joists. The connection between the roof decking and the top chord of the joists is typically made with puddle welds or self-tapping screws. An alternative to the use of welds or screws are power actuated fasteners (PAFs).

A power actuated fastener is a mechanical fastener that provides a means for connecting steel elements. Figure 1.1 shows a PAF installed in the top chord of a roof joist. The fastener consists of a small high-strength nail that is driven into the base material using an explosive charge (powder actuated) or using compressed air (pneumatically driven). Figure 1.2 shows PAF installation using a pneumatic tool. Several potential advantages of power actuated fasteners over puddle welds for metal roof deck attachment have been noted, including a greater speed of installation and more consistent quality (Glaser 1994).

Dimensions, material properties, and structural performance characteristics of PAFs are not standardized among manufacturers as is the case, for example, with high strength bolts. Rather, each manufacturer produces their own proprietary line of fasteners and installation tools. Load capacity values and other design related information for particular fasteners can be found in

manufacturers' literature and in reports published by the ICBO Evaluation Service and other code approval bodies. Safety related issues, particularly with respect to powder actuated systems, are covered by several standards and regulations (PATMI 1991; American 1995; Occupational 1981). Test methods are covered by ASTM Standard E 1190 (American 1987).

The use of PAFs for fastening roof deck has long been common practice in Europe, where puddle welding is virtually unknown. A recent survey (Glaser 1994) indicated that within the United States, acceptance of PAFs has been rather slow, and the use of puddle welds still predominates for fastening roof deck. This survey further indicated that structural engineers have been hesitant to specify PAFs because of an overall lack of familiarity and information on these fasteners. In the case of roof joists, concerns have been raised that the PAFs may damage the very thin top chord angles frequently found in steel roof joists and thereby impair the load capacity of the joists.

1.2 INVESTIGATION OBJECTIVES

The remainder of this report describes a large scale testing program intended to address the concerns noted above. In particular, the objective of this investigation was to determine if the use of power actuated fasteners produced any detrimental effects on the vertical load capacity of open web steel joists. This was accomplished by comparing the vertical load capacity of roof subassemblages constructed with puddle welds with the load capacity of roof subassemblages constructed with power actuated fasteners.

An additional objective of this investigation was to further study the effects of power actuated fasteners on the behavior of double angle steel chord members subjected to tensile stress. The investigation focused on the strength and ductility of the members, considering factors such as loss of area and the introduction of stress concentrations. This was accomplished by comparing the elongation and load capacity of double angle chord members without PAFs, with PAFs, and with drilled holes.

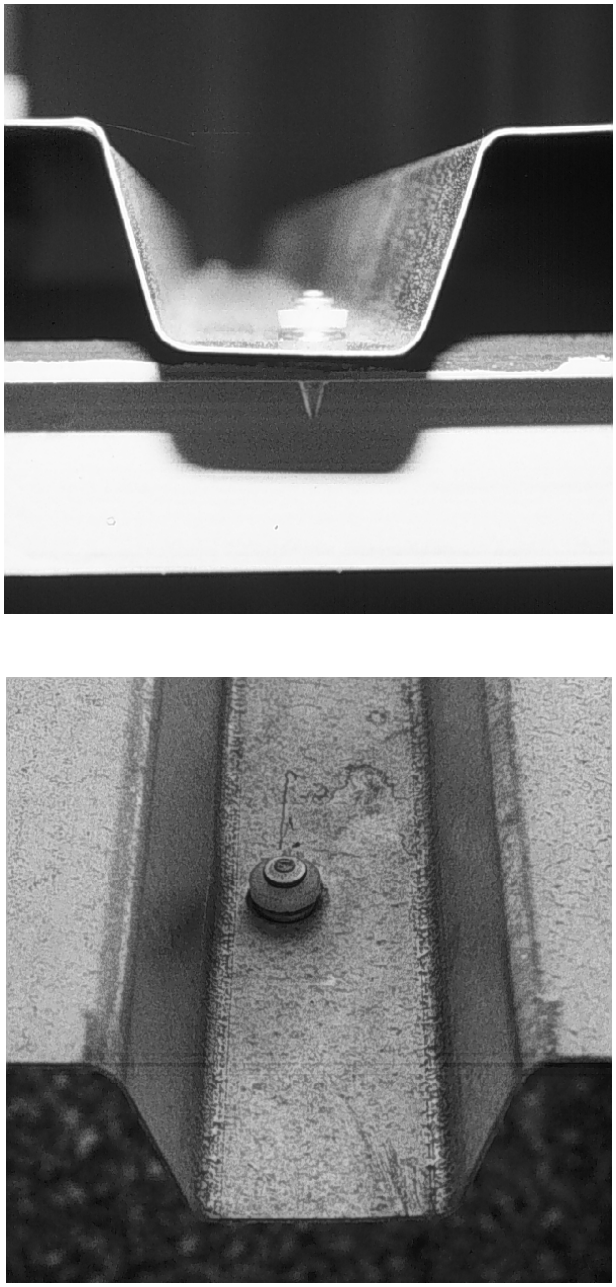

Figure 1.1 PAF Installed in the Top Chord of a Joist

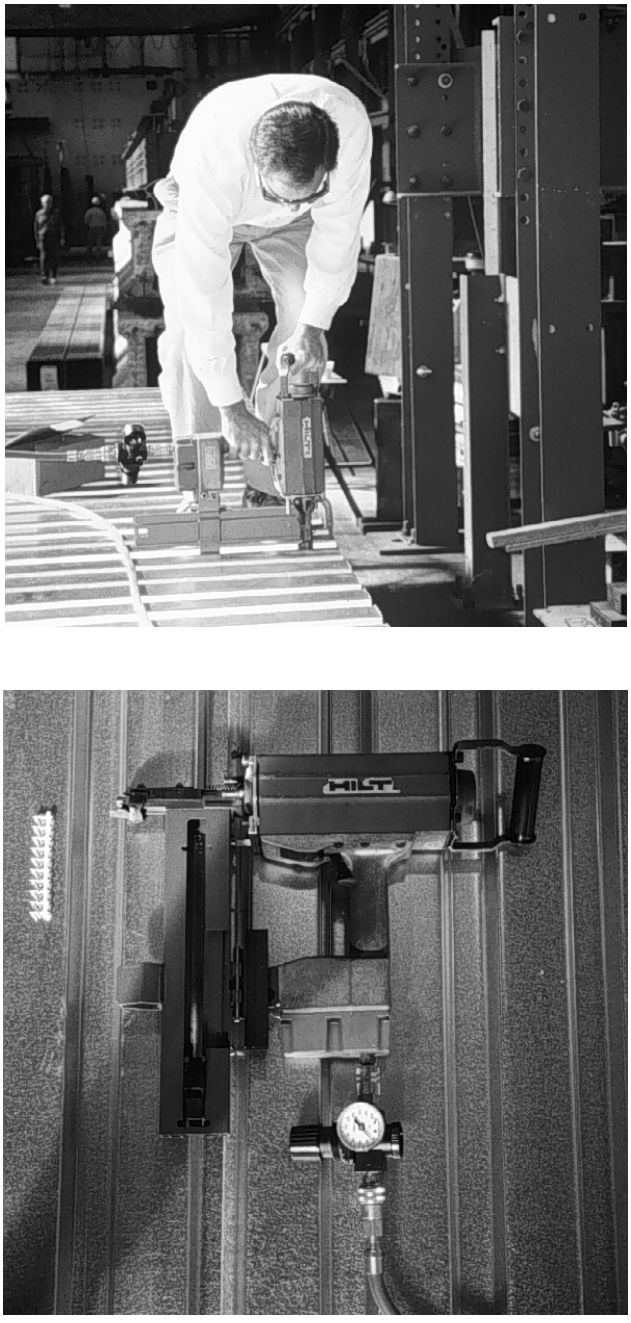

Figure 1.2 Installation Using a Pneumatically Driven Tool

Chapter 2:

Testing of Roof Subassemblages

2.1 GENERAL

Ten full scale tests on roof subassemblages were completed during this testing program. Each specimen consisted of two simply-supported joists approximately 26 feet in length, spaced 4 feet apart, and covered by metal roof decking. The specimens were loaded to failure under downward-acting vertical loads. The three main variables considered within each test were deck fastener type, joist size, and fastener pattern.

2.2 DESCRIPTION OF TEST SPECIMENS

2.2.1 Description of Joists

The nominal dimensions and configurations for the joists used in the testing program are shown in Figure 2.1. Two types of joists, designated as the 16K2 joist and the 26K5 joist, were used in the investigation. A complete listing of both the nominal and measured member sizes for each joist is given in Appendix A and is to be used with Figure 2.1.

The 16K2 joist represented a relatively light joist. The maximum allowable load capacity for this joist, according to the manufacturer's literature, was 216 lbs./ft. The top and bottom chord members consisted of double angles (top chord: 2L-1.5"x1.5"x0.113"; bottom chord: 2L-1.25"x1.25"x0.109"). The

diagonals consisted of round bars which varied between 0.5” and 19/32” in diameter. The depth of the 16K2 joist was 16 inches.

The 26K5 joist represented a heavier joist. The maximum allowable load capacity for this joist, according to the manufacturer’s literature, was 542 lbs./ft. The top and bottom chord consisted of double angles (top chord: 2L-1.75”x1.75”x0.155”; bottom chord: 2L-1.5”x1.5”x0.123”). The diagonals consisted of a variety of single angle and round members. The depth of the 26K5 joist was 26 inches.

Steps were taken within the testing program to minimize the effects of material variation on the performance of the specimens. For a particular joist designation, the different types of members making up each joist (the top chord, the bottom chord, and diagonals) were produced from the same heat of steel. For example, all of the bottom chord angles of the 26K5 joists were produced from the same heat of steel, etc.

2.2.2 Description of Roof Subassemblages

The specimens developed for this testing program consisted of a roof subassemblage intended to simulate a portion of a typical metal roof system. Figures 2.2 and 2.3 show the configuration for the test specimens. Each specimen consisted of two parallel joists with metal roof decking spanning between the joists. The joists were simply-supported at both ends and were spaced at 4 feet on center. The metal roof decking was attached to the top chord of each joist using

either puddle welds or power actuated fasteners. Horizontal bridging was also provided for each specimen, according to the manufacturer's recommendations.

The roof deck used in this test program was designated as a Type 1.5B galvanized roof deck with a 22 gage (0.0295 inches) thickness. The depth of the deck was 1.5 inches, with ribs spaced at 6 inches. The length of the deck was 56 inches, allowing the deck to span the 4 feet between joists and still provide for a 4 inch overhang at each joist. The deck was supplied in 36 inch wide panels. Eight deck panels were used for each specimen. Sidelap connections between deck panels were made using #10 self-drilling and self-tapping screws. Four screws were used for each sidelap.

The horizontal bridging used in the testing program consisted of two horizontal single angles (L-1"x1"x7/64"), one attached to the top chord of both joists and the other attached to the bottom chord of both joists. Each end of the bridging angle was attached to the chord member using one fillet weld on each angle of the chord member, as shown in Figure 2.3. Three sets of horizontal bridging were provided for the specimens using 16K2 joists. The first set was placed 6" from midspan. The other two sets were placed at a distance of 6'-6" from midspan. Two sets of horizontal bridging were provided for the specimens using 26K5 joists. Each set of bridging was placed at a distance of 8'-8" from each end of the specimen. The bridging locations for each of the specimens are shown in Figure 2.2. The bridging worked in conjunction with the external lateral bracing system (described later) to restrain the joists against lateral movement. The location of the horizontal bridging members, the size of the bridging

members, and the bridging member connection details followed specifications of the Steel Joist Institute (Steel 1994).

2.3 EXPERIMENTAL SETUP

2.3.1 Overall Setup

An overall view of the experimental setup is shown in Figures 2.4 and 2.5. The experimental setup consisted of four W12x65 columns that were bolted to the laboratory floor. Each joist end was supported on a roller, which in turn rested on a stiffened seat that was bolted to the columns. Two parallel W12x72 beams spanned between the column members. These beams provided a reaction for the hydraulic loading rams and supported the upper end of the lateral bracing system (described later). Two single angles were bolted to the laboratory floor under each reaction beam to serve as the support for the lower end of the lateral bracing system. Photographs of the overall test setup are shown in Figure 2.6.

2.3.2 Joist End Supports

Figure 2.7 shows the configuration for the joist end supports. A roller support was provided at each of the joist ends. The upper portion of the support consisted of the roller assembly. The roller assembly provided a vertical reaction but offered minimal horizontal or rotational restraint, in keeping with the simply-supported design assumption. The lower portion of the support consisted of a load cell (described later).

In order to protect against the possibility of a local failure occurring at the reaction points of each joist, a thin plate of steel (PL 3”x4”x3/16”) was tack welded over the reaction area at each joist end. The plate was provided to distribute the concentrated reaction from the roller assembly.

2.3.3 Joist Loading System

The joist loading system consisted of a series of hydraulic rams secured to the W12x72 reaction beams using brackets, as shown in Figure 2.8. The rams were centered over each of the upper chord panel points and over the longitudinal centerline of each joist. The 16K2 specimens required 12 hydraulic rams for each joist. The 26K5 specimens required 11 hydraulic rams for each joist. The points of load application for each of the specimens are shown in Figures 2.2 and 2.3. The arrangement of hydraulic rams was intended to approximate a uniformly distributed load on each joist.

The loading system was developed to apply nominally identical downward forces at each of the load points. The rams were connected to a common hydraulic line. This configuration caused the same oil pressure to be applied to each ram. Therefore, the force of each ram, which is a function of the oil pressure, was nominally equal and independent of the ram extension. The system was powered by a pneumatically-driven hydraulic pump. In addition, a series of needle valves was provided to facilitate the loading of one joist independently of the other, if necessary.

2.3.4 Joist Lateral Support System

An external lateral bracing system was provided to restrain lateral movement of the specimens during the loading process. Figure 2.9 shows the configuration for the bracing system.

Lateral braces were provided at the same locations as the horizontal bridging, in order to provide complete lateral bracing of the top and bottom chords at the bridging locations. As shown in Figure 2.9, out-of-plane movement of the chords was restricted by vertical steel plates at the brace locations. A small portion of the metal deck was cut away at each brace location to permit the vertical plate to be placed immediately adjacent to the chord members. A very small gap was left between the vertical steel bracing plate and the joist chord members to minimize friction.

Figure 2.4 shows the locations for the bracing frames for each of the specimen types. The test specimens using 16K2 joists required 3 bracing frames. The test specimens using 26K5 joists required 2 bracing frames.

2.4 INSTRUMENTATION

2.4.1 Data Collection

The data collected for each of the full-scale tests included information on the load applied to the specimen, the displacement of the specimen, and strain levels within selected members. The electronic data sets were recorded using a Hewlett Packard computerized data acquisition system. The data were taken at selected intervals throughout the test.

2.4.2 Load

A load cell was located underneath the roller bearing assembly at each of the joist ends, as shown in Figure 2.7. The load cells were used to measure the vertical reactions at each of the joist ends caused by the loading of the test specimen. The total load applied to a particular joist was found by summing the load cell readings for each of the joist ends.

2.4.3 Displacement

Vertical displacements were measured at the midspan and the quarter points for each joist. The measurement locations are shown in Figure 2.10. The displacements were measured using electronic string potentiometers. Each potentiometer was anchored to the laboratory floor using a steel weight. The potentiometer string was attached to the bottom chord of the joist using a line extension fabricated from 50 pound test line and metal swivels.

Each string potentiometer had a maximum travel length of 5 inches. Many of the potentiometers had to be reset during testing because the maximum travel length was exceeded.

2.4.4 Strain Gages

Selected members of the joists were instrumented with electrical resistance strain gages to monitor strain levels during the test. For each joist, the

first compression diagonal at each end as well as the top and bottom chord members near midspan were provided with strain gages. Figure 2.10 shows the gage locations for both the 16K2 and 26K5 joists. Figure 2.11 shows the gage layout for round and angle members.

Each test specimen using 16K2 joists was instrumented with 56 strain gages, 28 gages on each joist. A group of 4 strain gages was provided on each of the round compression diagonals. A group of 10 strain gages was provided on each of the top and bottom chords. Each test specimen using 26K5 joists was instrumented with 60 strain gages, 30 gages on each joist. A group of 5 strain gages was provided on each compression diagonal. A group of 10 strain gages was provided on each of the top and bottom chords.

All gages were oriented parallel to the longitudinal axis of the member. The layout of the gages was chosen to facilitate the computation of the average axial strain in the member from the individual strain gage readings (described in Chapter 3).

2.5 TEST METHODOLOGY

2.5.1 Variables Considered

The three variables investigated during this testing program consisted of fastener type, joist size, and fastener pattern. The most important variable was the fastener type used in connecting the roof deck to the joists. The two types of fasteners considered within this testing program consisted of a power actuated fastener and a 5/8” puddle weld. The fastener type used for each specimen is

listed in Table 2.1. All fasteners were located on the outer angle of the upper chord members.

The power actuated fastener used in this testing program is produced by the Hilti Corporation and designated as the "X-EDNK22THQ12M." The fastener is shown in Figure 2.12. The fastener has an overall length of 0.96" and a maximum shaft width of 0.146 inches. The fastener consists of a slightly tapered knurled shaft, a flat washer, and a conical washer. The knurled shaft increases the grip of the fastener. Upon impact with the base material, the flat washer is pushed against the conical washer. The conical washer compresses and acts like a spring to keep the deck in contact with the base material. The flat washer acts not only to increase the bearing area of the fastener but also to align the fastener within the installation tool. According to the manufacturer, this fastener is specifically intended for use in the fastening of metal deck to steel joists, with joist angle thickness in the range of about 1/8 inch to 3/8 inch. The minimum thickness encountered on the top chord of the test joists was just under 1/8 inch. The deck fasteners were installed using a pnuematically driven tool. In order to simulate the flexibility of a typical roof system, the joists were supported only at their ends during installation.

The puddle welds used in this testing program had a nominal diameter of 5/8 inch. The welds were made using the shielded metal arc welding process (stick welding) using an E7010-A1 3/32 inch diameter rod. No weld washers were used. An elongated weld measuring 3/8 inch in width and 1-1/4 inches in

length was used for the locations where the puddle weld was located within a deck overlap.

The effect of joist size was also considered. Two different types of joists, designated as the 16K2 joist and the 26K5 joist, were used in the investigation. Table 2.1 describes the joist size used for each specimen.

The final variable that was considered involved the connection pattern used to secure the roof decking to the joists. The two fastener patterns considered were designated as the 36/7 pattern and the 36/3 pattern. For specimens with a 36/7 pattern, a fastener was provided in each deck rib, resulting in 7 fasteners for every 36 inches of deck panel. For specimens with the 36/3 pattern, a fastener was provided in every third deck rib, resulting in 3 fasteners for every 36 inches of deck panel. These patterns were chosen to represent upper and lower bounds on the number of fasteners used in typical design practice. Table 2.1 describes the fastener pattern used for each specimen.

For specimens with power actuated deck fasteners, several PAFs were also installed in the bottom chord angles of the joists. These fasteners were installed to investigate the influence of PAFs on the tensile capacity of thin chord members. The fastener used for this application is designated as the "DAK-16-P8-T" and was installed using a powder actuated installation tool. This fastener, also manufactured by Hilti, has a maximum shank diameter of 0.146 inch. The maximum shaft diameter of these fasteners is nominally equal to the shaft diameter of the deck fasteners. Two fasteners were installed in the central bottom chord for each joist. One fastener was driven into the horizontal leg of each angle

forming the bottom chord. A more comprehensive investigation on the effects of PAFs on the capacity of double angle chord members subjected to tensile stress can be found in Chapter 4.

The two tests designated as 16K2-ND and 26K5-ND were included for comparison purposes. These specimens were provided with no decking or deck fasteners but were provided with the same horizontal bridging and lateral bracing as all other specimens.

2.5.2 Testing Procedure

Each roof subassemblage was subjected to a slowly applied downward vertical load. The load increments used during each test were determined by the test administrator. Larger load increments were taken during the elastic portion of response. Smaller load increments were taken as the response neared first yield. The test data were recorded following each load increment.

The specimens were loaded until failure of the joists occurred. Typically, one joist failed at a slightly smaller load than the other. For these cases, once failure of one joist occurred, the loading of that joist was terminated. This was accomplished by preventing additional hydraulic flow to the rams over the failed joist. Loading was then continued on the other joist until failure occurred.

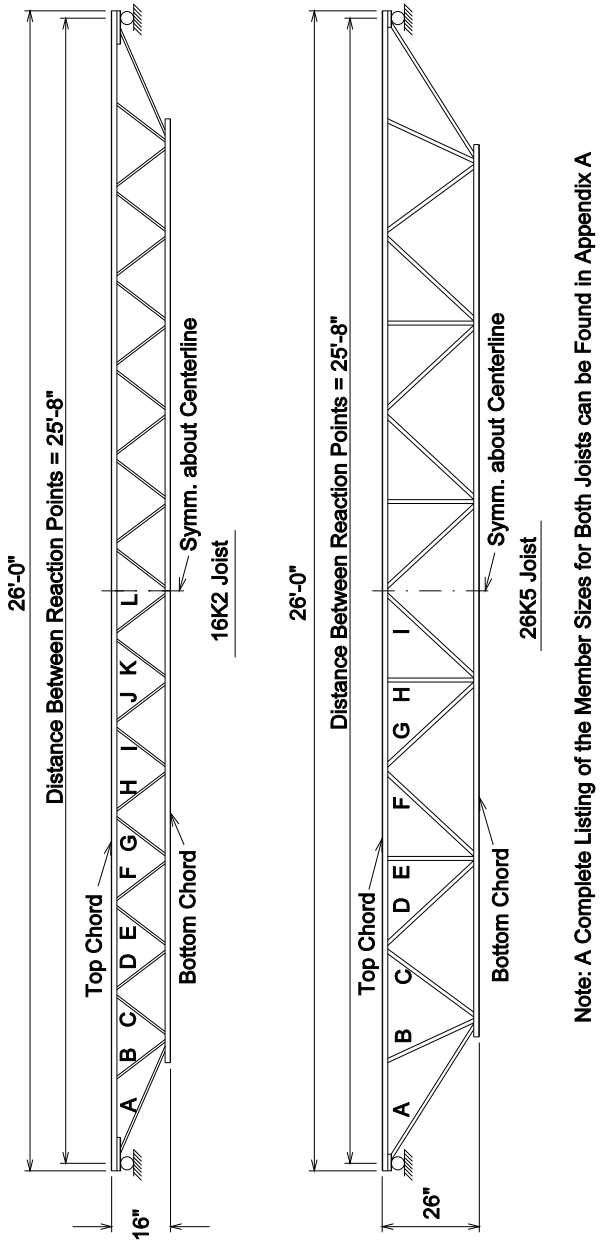

Figure 2.1 Configuration of Joists Used in the Testing Program

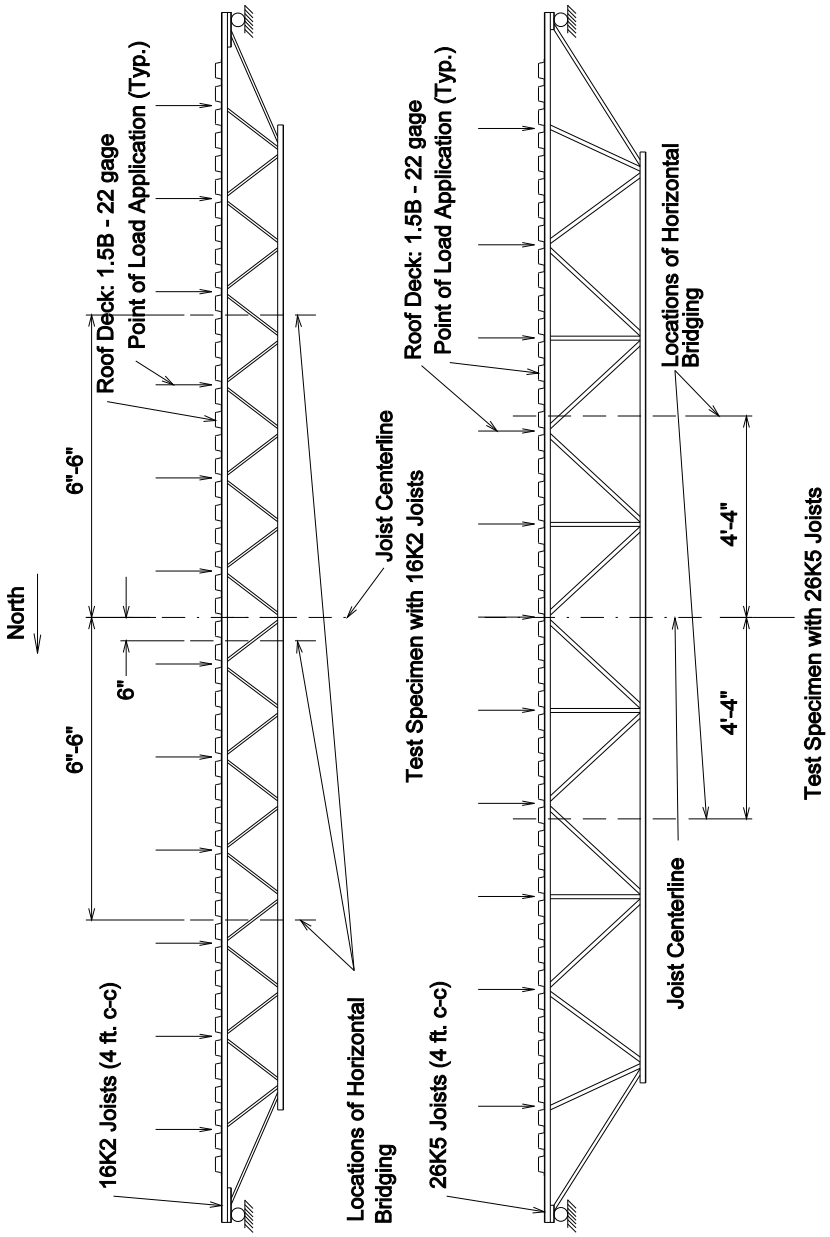

Figure 2.2 Configuration of Test Specimens

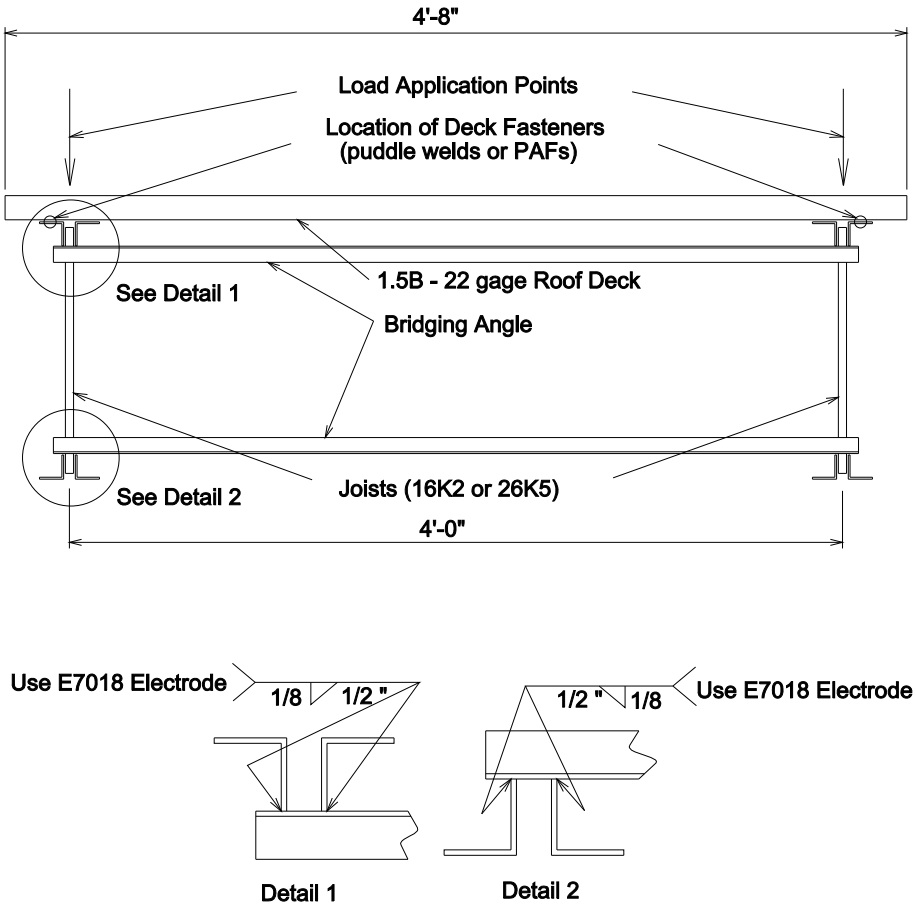

Figure 2.3 Cross Section of Test Specimen

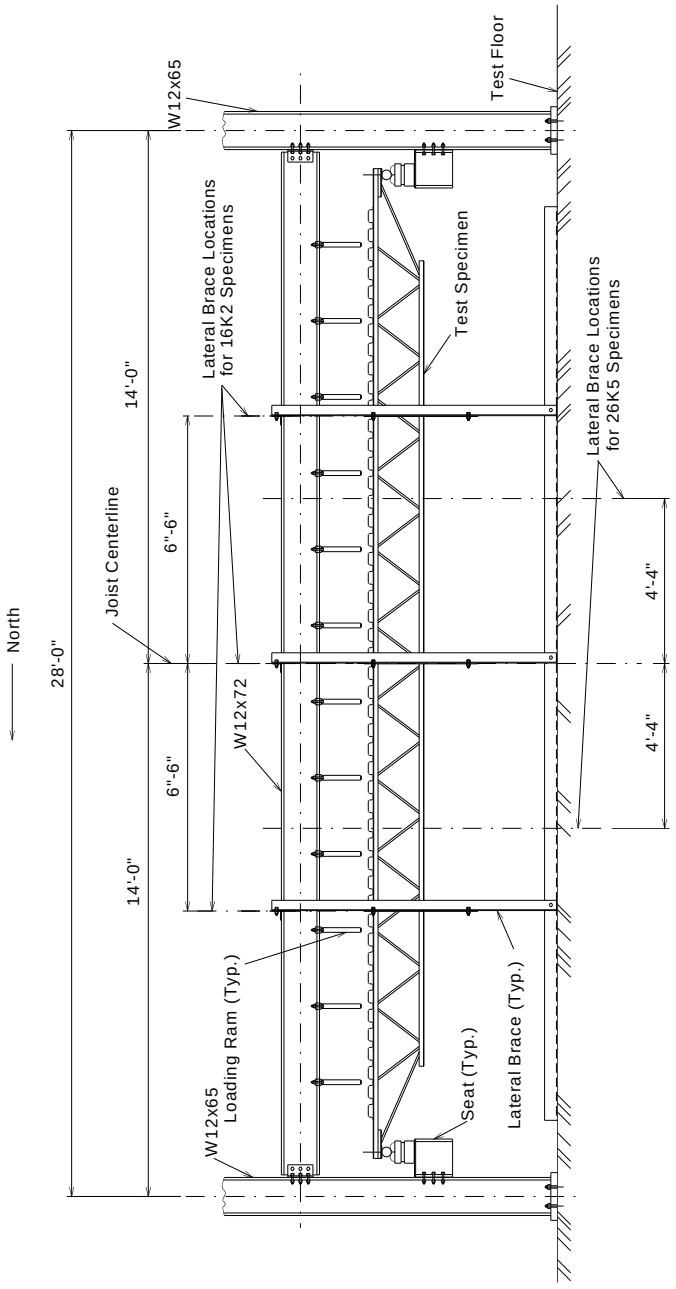

Figure 2.4 Overall View of Experimental Setup

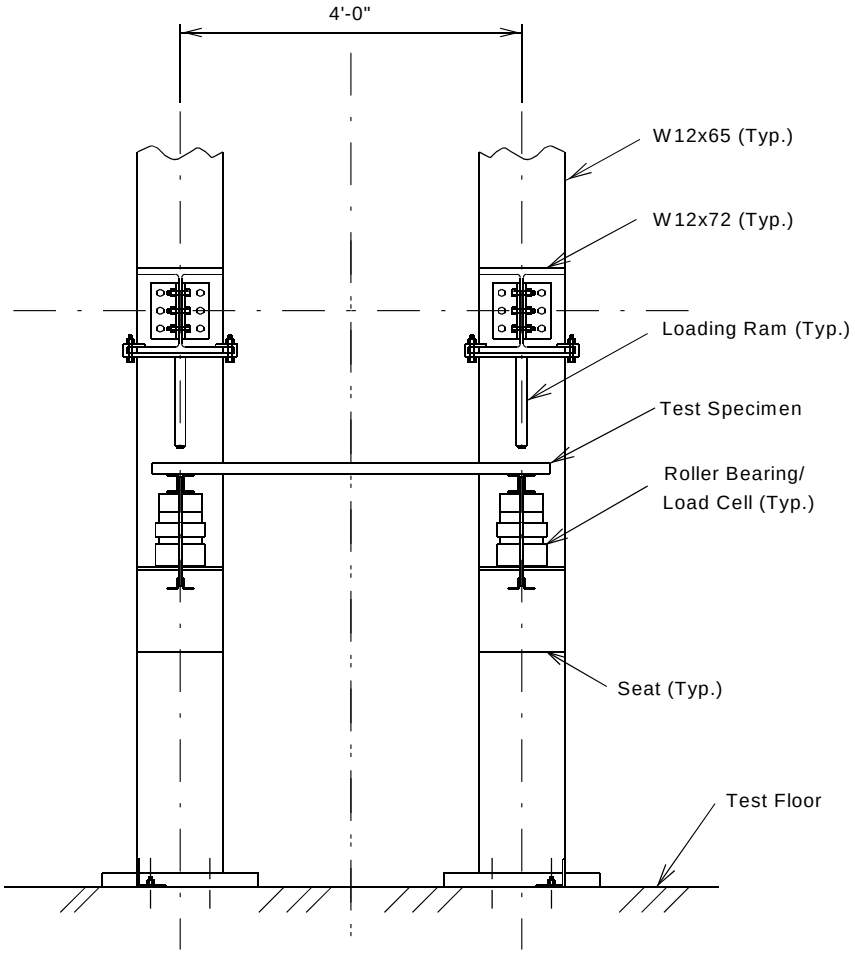

Figure 2.5 Cross Section of Experimental Setup

Figure 2.6 Photographs of Experimental Setup

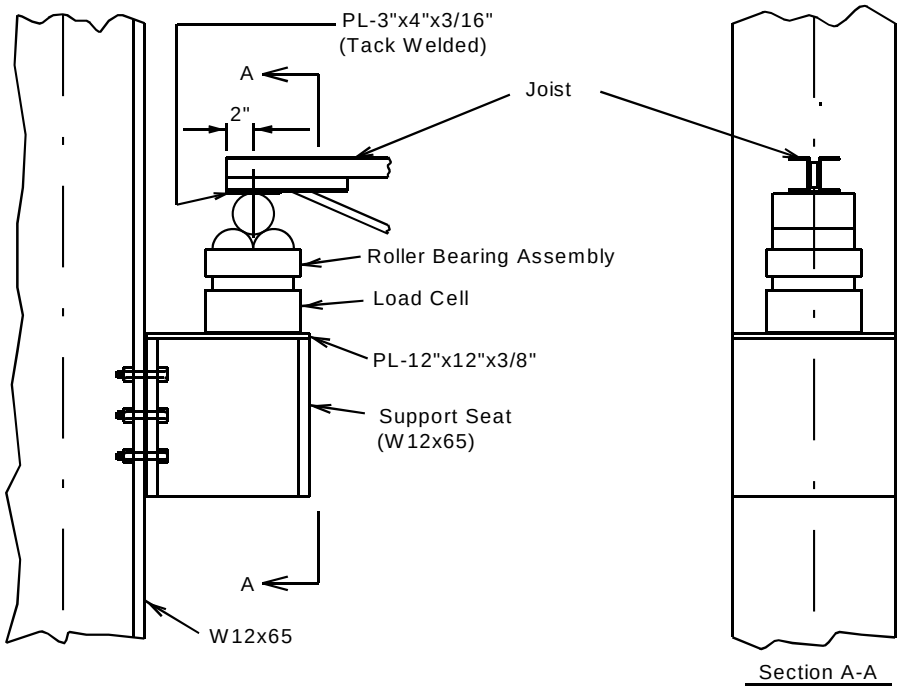

Figure 2.7 Joist End Support Details

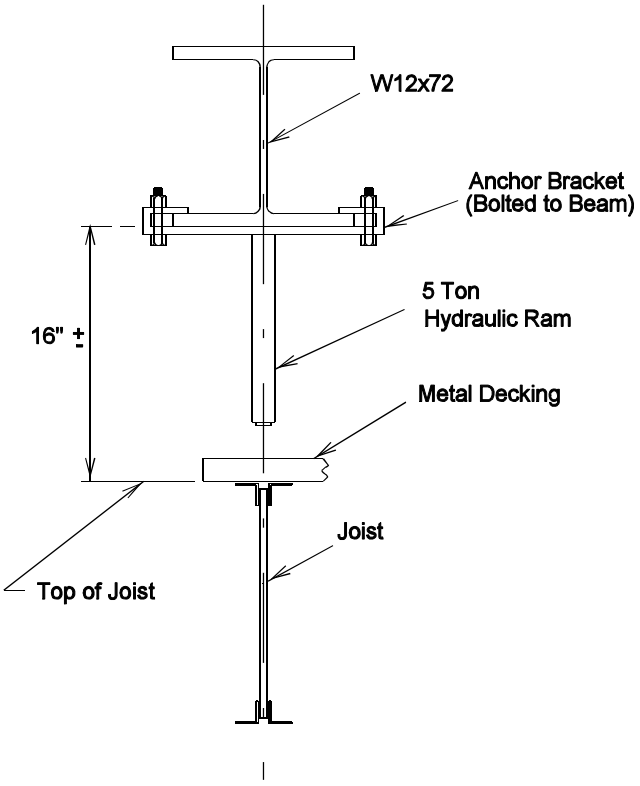

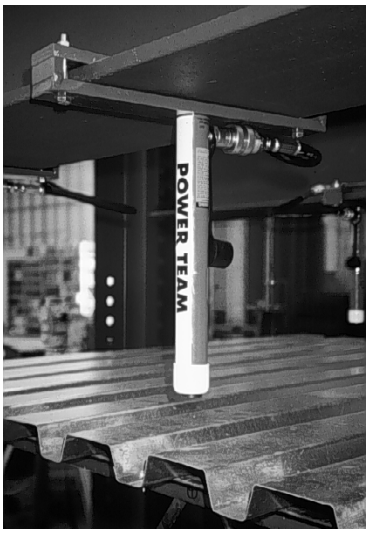

Figure 2.8 Hydraulic Ram Configuration

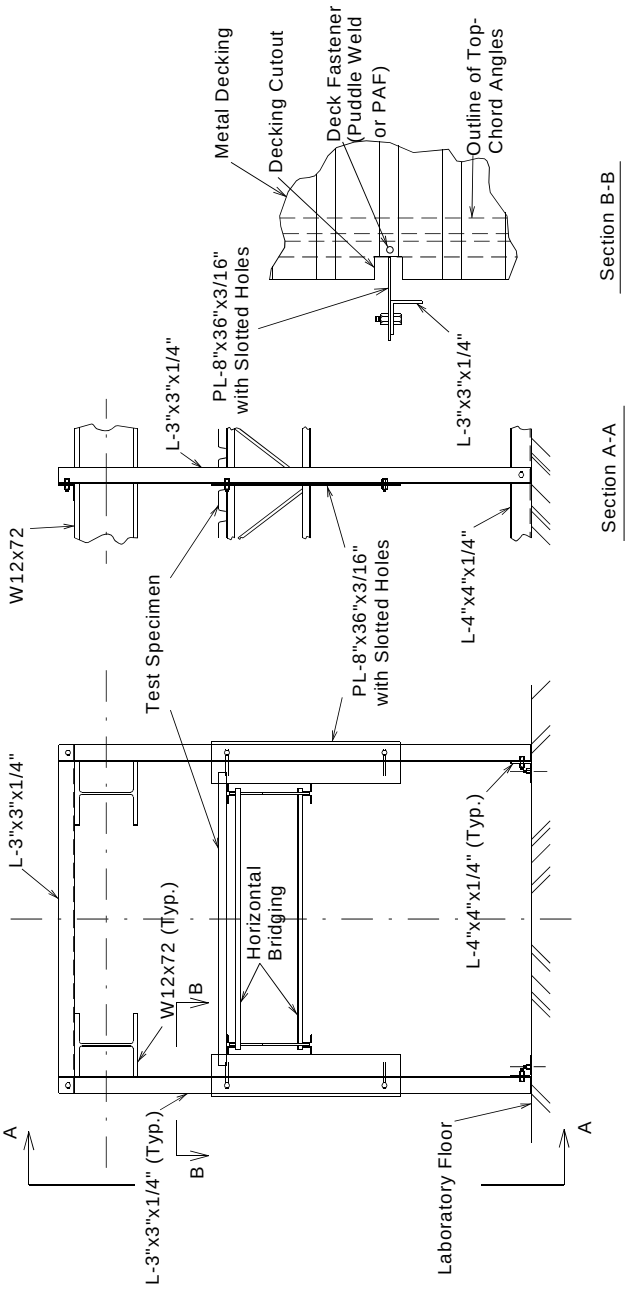

Figure 2.9 Configuration for Lateral Bracing System

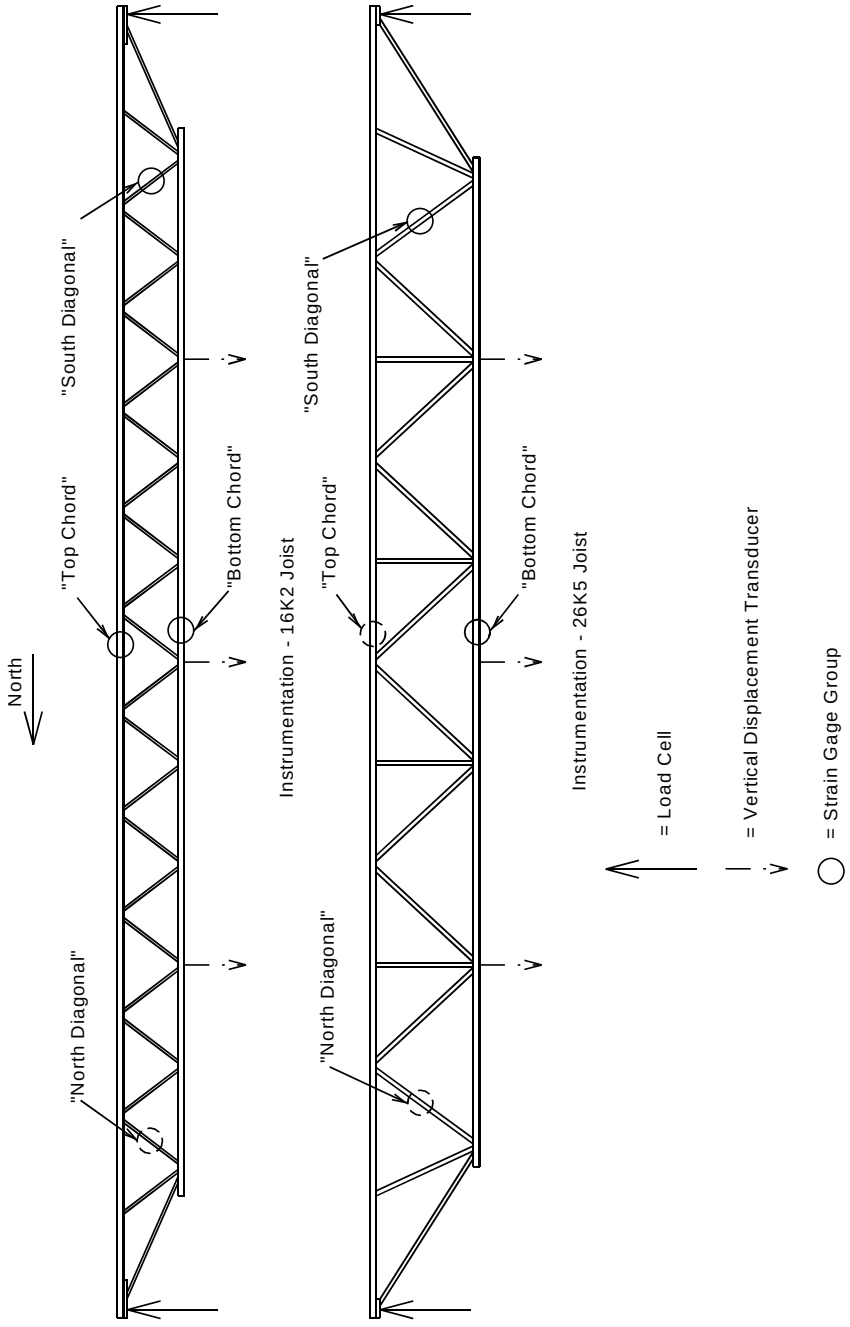

Figure 2.10 Instrumentation Locations

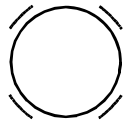

Strain Gage Layout on
Round Diagonal Members

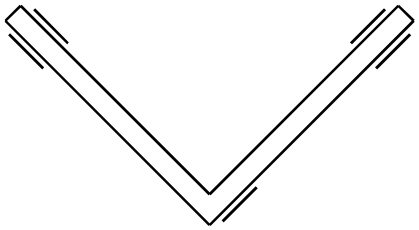

Strain Gage Layout on
Single Angle Diagonal Members

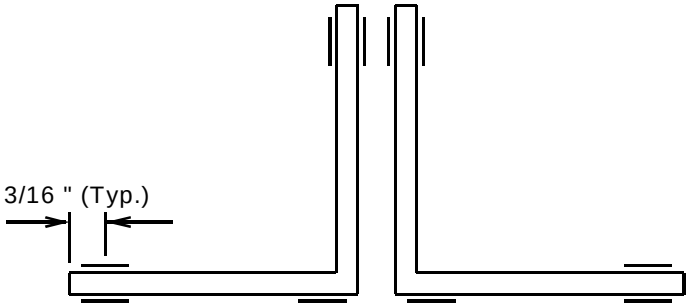

Strain Gage Layout on
Double Angle Chord Members

Figure 2.11 Gage Layout for Round and Angle Members

Fastener Designation: X-EDNK22THQ12M

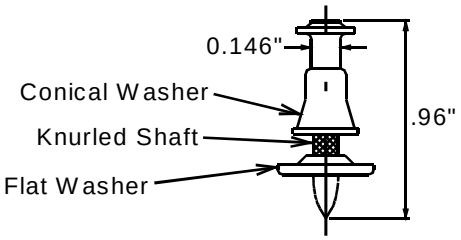

Figure 2.12 Fastener Used in Test Specimens

Table 2.1 Description of Test Specimens

Specimen Designation	Joist Type	Deck Fastener Type	Deck Fastener Pattern
16K2-PW-1	16K2	puddle welds	36/7
16K2-PW-2	16K2	puddle welds	36/3
16K2-DX-1	16K2	PAFs	36/7
16K2-DX-2	16K2	PAFs	36/3
16K2-ND	16K2	no deck	no deck
26K5-PW-1	26K5	puddle welds	36/7
26K5-PW-2	26K5	puddle welds	36/3
26K5-DX-1	26K5	PAFs	36/7
26K5-DX-2	26K5	PAFs	36/3
26K5-ND	26K5	no deck	no deck

Chapter 3:

Results for Tests on Roof Subassemblages

3.1 GENERAL

A series of 10 full scale tests was completed on specimens consisting of roof subassemblages. Each specimen was subjected to a slowly applied uniform load, approximated by a series of hydraulic rams. The load was applied until failure of the joists occurred, as discussed in Chapter 2. The total load and vertical displacements were recorded for each joist during the tests. In addition, strain readings were collected for selected members.

The remainder of this chapter describes the behavior of the joists during each test. This includes a discussion of the failure modes for each of the joists, a discussion of the joist behavior, and a discussion of the individual response for each of the instrumented members.

3.2 JOIST BEHAVIOR AND MODES OF FAILURE

3.2.1 General

The load capacity and failure mode for each of the joists is listed in Table 3.1. In addition, the load versus displacement plots for each joist are provided in Appendix B. The individual responses for the members instrumented with strain gages are provided in Appendix C.

3.2.2 Behavior of Specimens with 16K2 Joists

3.2.2.1 Specimen 16K2-PW-1

Yielding of the central bottom chord for both the east and west joists was the first event noticed during the initial loading of the specimen. After continued loading, it was noticed that the travel of the midspan linear potentiometers was exhausted. To recover the midspan displacement readings, the specimen was unloaded, and the midspan potentiometers were reset. During reloading, the central top chord of the east joist buckled in the plane of the joist, as shown in Figure 3.1. The east joist sustained a maximum load of 9.99 kips.

After the buckling of the east joist, loading was continued only on the west joist. Additional load on the west joist caused slight local buckling of the east, horizontal leg of the central top chord of the west joist, as shown in Figure 3.2. The west joist suistained a maximum load of 10.11 kips. After this event, the specimen was unloaded, and the test was terminated.

3.2.2.2 Specimen 16K2-PW-2

Yielding of the central bottom chord for both the east and west joists was the first event noticed during the initial loading of the specimen. After significant yielding of the bottom chord occurred for both joists, the central top chord of the east joist buckled in the plane of the joist, as shown in Figure 3.3. The east joist sustained a maximum load of 9.97 kips.

After the buckling of the east joist occurred, loading was continued only on the west joist. During reloading, the central top chord of the west joist also

buckled in the plane of the joist, as shown in Figure 3.4. The west joist sustained a maximum load of 10.06 kips. After the buckling of the west joist occurred, the west joist was loaded until the stroke limit was reached on the west loading rams. This extreme loading was done to investigate the holding capacity of the puddle welds through large and excessive deformations. The specimen was then unloaded, and the test was terminated.

3.2.2.3 Specimen 16K2-DX-1

Before loading of the specimen began, it was noticed that the installation of the power actuated fasteners caused slight distortions of the top chord at several locations on both the east and west joists, as shown in Figure 3.5. This typically occurred at locations on the 16K2 joists where the fasteners were installed toward the outer edge of the top chord angle, a location where the stiffening effects of the vertical leg were minimal.

Yielding of the central bottom chord for both the east and west joists was the first event noticed during the initial loading of the specimen. After significant yielding of the bottom chord occurred for both joists, the central top chord of the east joist buckled in the plane of the joist, as shown in Figure 3.6. The east joist sustained a maximum load of 9.98 kips.

After the buckling of the east joist occurred, loading was continued only on the west joist. Shortly after the reloading of the west joist began, the central top chord of the west joist also buckled in the plane of the joist, as shown in Figure 3.7. The west joist sustained a maximum load of 10.04 kips. After the

buckling of the west joist occurred, the west joist was loaded until the stroke limit was reached on the west loading rams. This extreme loading was also done to determine the holding capacity of the PAF's through large and excessive deformations, as demonstrated in Figure 3.8. The specimen was then unloaded, and the test was terminated.

3.2.2.4 Specimen 16K2-DX-2

Before loading of the specimen began, it was noticed that the installation of the power actuated fasteners also caused slight distortions of the top chord at several locations on both joists for this specimen. Again, this typically occurred at locations on the 16K2 joists where the fasteners were installed toward the outer edge of the top chord angle, a location where the stiffening effects of the vertical leg were minimal.

Yielding of the central bottom chord for both the east and west joists was the first event noticed during the initial loading of the specimen. After significant yielding of the bottom chord occurred for both joists, the central top chord of both the west and east joists buckled simultaneously in the plane of the joists, as shown in Figures 3.9 and 3.10, respectively. The east joist and west joist sustained maximum loads of 10.08 kips and 9.74 kips, respectively. After the buckling of both joists occurred, the specimen was loaded for several more increments before the test was terminated.

3.2.2.5 Specimen 16K2-ND

The first event which took place during the initial loading of the specimen was the out-of-plane buckling of the top-chord of the west joist, as shown in Figure 3.11. The buckle was caused by inadequate lateral bracing of the top chord, aggravated by the non-existence of the metal deck. This event occurred without any yielding in the bottom chord of the west joist. The west joist sustained a maximum load of 9.65 kips.

After the buckling of the west joist, loading was continued only on the east joist. A small amount of yielding was observed in the bottom chord of the east joist. This was followed by an out-of-plane buckling of the top chord of the east joist, and shown in Figure 3.12. Again, this was due to inadequate lateral bracing on the top chord, aggravated by the non-existence of the metal deck. The east joist sustained a maximum load of 9.85 kips. The specimen was then unloaded, and the test was terminated.

3.2.3 Behavior of Specimens with 26K5 Joists

3.2.3.1 Specimen 26K5-PW-1

During the initial loading of the specimen, it was noticed that a small fracture was developing in the weld connecting one of the compression diagonals to the bottom chord of the east joist. The location of the affected diagonal on the east joist is shown in Figure 3.13. The propagation of the fracture seemed to be aggravated by the eccentricity caused by the offset in the line of action of the member force and the location of the weld. Upon further loading, the weld failed

and the compression diagonal buckled, as shown in Figure 3.14. The east joist sustained a maximum load of 22.45 kips.

After the buckle of the east compression diagonal, loading was continued only on the west joist. The loading of the west joist caused the central bottom chord to yield. The yielding of the bottom chord continued until the stroke limit was reached on the west loading rams, as shown in Figure 3.15. The west joist sustained a maximum load of 23.86 kips. The specimen was then unloaded, and the test was terminated.

In addition, it was noticed that localized shear yielding occurred at each end of the bottom chord for both joists, as shown in Figure 3.16. This yielding occurred because of an eccentricity caused by the offsets in the lines of action for the diagonal members and the bottom chord. This yielding may have caused a premature softening of the overall joist stiffness and may have led to increased deformation of the joist.

3.2.3.2 Specimen 26K5-PW-2

During the initial loading of the specimen, it was noticed that a small fracture was developing in the weld connecting one of the compression diagonals to the bottom chord of the west joist. The location of the affected diagonal on the west joist is shown in Figure 3.13. Upon further loading, the weld failed and the compression diagonal buckled, as shown in Figure 3.17. The west joist sustained a maximum load of 19.79 kips.

After the buckle of the west compression diagonal, loading was continued only on the east joist. The loading of the east joist caused the central bottom chord to yield. The yielding of the bottom chord continued until the stroke limit was reached on the east loading rams, as shown in Figure 3.18. The east joist sustained a maximum load of 22.98 kips. The specimen was then unloaded, and the test was terminated. Localized shear yielding was noticed at each end of the bottom chord for the joists of this specimen, as well.

3.2.3.3 Specimen 26K5-DX-1

During the initial loading of the specimen, it was noticed that a small fracture was developing in the weld connecting one of the compression diagonals to the bottom chord of the east joist. The location of the affected diagonal on the east joist is shown in Figure 3.13. Upon further loading, the weld failed and the compression diagonal buckled, as shown in Figure 3.19. The east joist sustained a maximum load of 21.59 kips.

After the buckle of the east compression diagonal, loading was continued only on the west joist. As the load was increased, the weld securing a tension diagonal to the bottom chord of the west joist failed, and the tension diagonal pulled away from the bottom chord, as shown in Figure 3.20. The location of the affected diagonal on the west joist is shown in Figure 3.13. The west joist sustained a maximum load of 21.66 kips. The specimen was then unloaded, and the test was terminated.

Localized shear yielding was noticed at each end of the bottom chord for the joists of this specimen, as well. It also should be mentioned that no top chord distortion caused by the installation of the PAF's was found for the specimens with 26K5 joists.

3.2.3.4 Specimen 26K5-DX-2

During the initial loading of the specimen, it was noticed that a small fracture was developing in the weld connecting one of the compression diagonals to the bottom chord of the west joist. The location of the affected diagonal on the west joist is shown in Figure 3.13. Upon further loading, the weld failed and the compression diagonal buckled, as shown in Figure 3.21. The west joist sustained a maximum load of 21.73 kips.

After the buckle of the west compression diagonal, loading was continued only on the east joist. As the load was increased, the weld securing a compression diagonal to the bottom chord of the east joist failed, and the compression diagonal buckled, as shown in Figure 3.22. The location of the affected diagonal on the east joist is shown in Figure 3.13. The east joist sustained a maximum load of 22.41 kips. The specimen was then unloaded, and the test was terminated.

Localized shear yielding was noticed at each end of the bottom chord for the joists of this specimen, as well. It also should be mentioned that no top chord distortion caused by the installation of the PAF's was found for this specimen.

3.2.3.5 Specimen 26K5-ND

During the initial loading of the specimen, it was noticed that a small fracture was developing on the weld connecting one of the compression diagonals to the bottom chord of the west joist. The location of the affected diagonal on the west joist is shown in Figure 3.13. Upon further loading, the weld failed and the compression diagonal buckled, as shown in Figure 3.23. The west joist sustained a maximum load of 20.00 kips.

After the buckle of the west compression diagonal, loading was continued only on the east joist. As the load was increased, the weld securing a compression diagonal to the bottom chord of the east joist failed, and the compression diagonal buckled, as shown in Figure 3.24. The location of the affected diagonal on the east joist is shown in Figure 3.13. The east joist sustained a maximum load of 21.82 kips. The specimen was then unloaded, and the test was terminated. Localized shear yielding was noticed at each end of the bottom chord for the joists of this specimen, as well.

3.3 DISCUSSION OF JOIST BEHAVIOR

3.3.1 Discussion of Specimens with 16K2 Joists

All of the specimens with 16K2 joists showed nearly the same maximum load capacity, regardless of deck fastener type or pattern. The maximum load capacity for each 16K2 joist is shown in Figure 3.25. The largest variation in the maximum load capacity between the ten 16K2 joists was less than 4 percent. The results are even more favorable for the specimens with similar deck fastener

patterns. In particular, the largest variation in maximum load capacity for the joists of both the 16K2-PW-1 and 16K2-DX-1 specimens was less than 2 percent. The largest variation in maximum load capacity for the joists of both the 16K2-PW-2 and 16K2-DX-2 specimens was less than 3 percent.

The failure modes for the 16K2 joists were very similar between the specimens (excluding the specimens with no deck), as stated in Table 3.1. In general, the central bottom chord was the first member to yield. This was typically followed by an in-plane buckling of the central top chord member which then resulted in unloading of the joist. The maximum load capacities for the 16K2 joists were typically attained during yielding of the bottom chord. Because the failure modes were similar, it follows that the maximum load capacities should also be similar.

The results for the 16K2 joists show that the use of PAFs has no detrimental impact on the maximum load capacity of the joists when compared with joists constructed with puddle welds. Figure 3.26 compares the load versus midspan displacment for the Specimen 16K2-PW-1 (puddle welds at the 36/7 pattern) and the Specimen 16K2-DX-1 (PAFs at the 36/7 pattern). Figure 3.27 compares the load versus midspan displacement for the Specimen 16K2-PW-2 (puddle welds at the 36/3 pattern) and the Specimen 16K2-DX-2 (PAFs at the 36/3 pattern). The similarity in maximum load between the joists as well as the similarity in load vs. displacement behavior are evident. Visually, the similarity in the failure modes between specimens constructed with puddle welds and specimens constructed with PAFs can be seen in Figure 3.28.

The top chord distortions observed in the Specimens 16K2-DX-1 and 16K2-DX-2 were found not to be detrimental to the maximum load capacity of the joists. Even though the distortions were located in an area of high compressive stress, the distortions did not lower the buckling capacity of the top chord members. The resistance to buckling may have been a result of the additional restraint from the deck or from the undistorted vertical legs of the top chord member.

The west joists of Specimens 16K2-PW-2 and 16K2-DX-1 were subjected to an extreme loading condition to determine the holding capacity of the puddle welds and PAFs through large and excessive deformations. It was observed that for both specimens, the deck remained fastened to the top chord despite the large deformations caused by the continued loading of the specimen in the buckled state. This behavior was observed for specimens with both puddle welds and PAFs.

Despite yield level stresses in the bottom chord of the 16K2 joists, the PAFs installed in the bottom chord produced no detrimental effects. It was observed that yielding of the bottom chord often began at the locations of the fasteners (because of the introduction of stress concentrations at these locations), but this was not the limit state which caused failure of the joist.

Specimen 16K2-ND failed by an out-of-plane buckling of the top chord as compared to the in-plane buckling of the top chord in specimens with metal roof decking. Thus, the in-plane stiffness and strength of the decking and fasteners

(both PAFs and puddle welds) was sufficient to stabilize the the top chord against any out-of-plane movement.

3.3.2 Discussion of Specimens with 26K5 Joists

The specimens constructed with 26K5 joists showed much greater variability in the maximum load capacity. Figure 3.29 shows the maximum load capacities for all of the 26K5 joists. The largest variation in the maximum load capacity was 12 percent for these specimens. This large variation in load capacity is thought to be related to the variability in the joists themselves and appears to be unrelated to the deck fastener type or deck fastener pattern. This is evident in the variety of failure modes observed for the 26K5 joists.

Three failure modes were observed for the 26K5 joists. The most common failure mode involved a weld failure on the lower portion of a compression diagonal, resulting in the subsequent buckling of that diagonal. The other modes of failure involved yielding of the central bottom chord or a weld failure on the lower portion of a tension diagonal, resulting in a pull-out of that tension diagonal. The failure modes involving the diagonal members were often brittle and occurred with little warning. Because of the large variation in failure modes and the brittle behavior of the failure modes, it follows that the maximum load capacities should contain larger variations.

The load versus midspan displacement behavior of Specimens 26K5-PW-1 and 26K5-DX-1 is shown in Figure 3.30. The load versus midspan displacement behavior of Specimens 26K5-PW-2 and 26K5-DX-2 is shown in

Figure 3.31. These plots show no correlation between the fastener type or pattern and the failure mode. The maximum load capacity is also independent of the deck fastener type or pattern. As indicated in Table 3.1, the average capacity of the joists with puddle welds was essentially identical to the average capacity of the joists with PAFs.

Despite yield level stresses in the bottom chord for a few of the 26K5 joists, the PAFs installed in the bottom chord produced no detrimental effects. It was observed that yielding of the bottom chord often began at the locations of the fasteners (because of the introduction of stress concentrations at these locations), but this was not the limit state which caused failure of the joist.

Specimen 26K5-ND failed by the buckling of a compression diagonal on both the east and west joists, in a manner similar to the specimens which possessed metal roof decking. Thus, the larger top chord members of the 26K5 joists were sufficiently strong to resist any out-of-plane lateral movement and did not rely on the deck and fasteners for lateral stability.

3.4 DISCUSSION OF STRAIN GAGE DATA

3.4.1 General

Selected members on each joist were instrumented with electrical resistance strain gages, as discussed in Chapter 2. The strain gage locations for each joist can be found in Figure 2.10. Figure 2.11 shows the typical gage layouts for round and angle members.

The strain gages were intended to provide an estimate of the axial force in the instrumented members throughout the test. In general, the joist members were subjected to both axial force and bending moments. As a result, the strain at any point on the member cross-section may have resulted from both axial strain and strain due to bending moments. Because the axial force is a function only of the axial strain, it was necessary to determine the strain at the centroid of each member. Computation of the strain at this location removed the influence of the bending moments on the member strain. The strain gages were positioned to facilitate the computation of the strain at this location.

Four strain gages were provided on the round diagonal members, as shown in Figure 2.11. Because of the symmetry of the circular cross-section, the neutral axis must pass through the centroid of the member. As a result, the axial strain was computed by taking the average of the four strain gage readings.

Ten strain gages were provided on the double angle chord members, as shown in Figure 2.11. Because the double angle chord members can bend both as a unit and individually, the location of the neutral axis is generally not known. In order to determine the strain at the centroid of the member, a technique was used which does not require knowledge of the neutral axis location. The method used to compute the axial strain in double angle chord members is explained in Figure 3.32. The method uses the assumption that plane sections remain plane to determine the strain at the centroid of each angle.

The axial strain values given within this report represent changes in strain with respect to the unloaded condition of the joists at the start of the test. They do

not include any residual strains which may have been present within the joist members because of the initial forming of the steel members or fabrication of the joists.

The axial stress for each of the instrumented members was calculated by multiplying the modulus of elasticity of steel (29,600 ksi) by the computed axial strain in the member. This relationship is valid as long as the material remains elastic in the location of the strain gages. In order to determine the applicability of the relationship, the computed axial strain for each member was compared with the elastic strain limit for that member type. The elastic strain limits were based on the material property tests discussed in Chapter 5 and were computed by dividing the static yield stress for each member type by the modulus of elasticity of steel. The linear relationship between stress and strain was used as long as the computed axial strain stayed at or below the elastic strain limit.

The axial force in each member was calculated by multiplying the computed axial stress by the nominal cross-sectional area of that member. As presented in Appendix A, the difference between the measured cross-sectional dimensions and the nominal cross-sectional dimensions is small. Therefore, the nominal cross-sectional dimensions were used in the axial force calculations.

3.4.2 Discussion of Results

The results of the axial strain and axial force calculations are presented in Appendix C. Plots of average axial strain versus total load on the joist and estimated axial force versus total load on the joist are provided for each of the

instrumented members. It should be re-emphasized that the data points within the axial force plots only represent elastic member behavior. The plots denoted as "Not Available" indicate that either one or more of the strain gages at a particular location failed during the test and that the necessary data could not be recovered.

In general, the behavior of the joist members, as indicated by the strain gage data, does agree with the overall behavior and failure modes of the specimens. As discussed earlier, many of the 16K2 joists failed by yielding of the bottom chord followed by the in-plane buckling of the top chord. The axial strain data for many of these joists indicated that the diagonal members remained completely elastic throughout the test, as expected. In addition, the data indicated that the central bottom chord yielded in a nearly elasto-plastic manner. More importantly, the strain data also displayed the buckling point of the central top chord.

Many of the 26K5 joists failed by the buckling of a compression diagonal. The strain data for many of these joists indicated that the diagonal members remained elastic throughout the test. The data also indicated that, in many cases, the top chord and bottom chord remained elastic, or nearly elastic, at the buckling point. For the joists in which the bottom chord was observed to yield, the strain data also indicates nearly elasto-plastic behavior from the bottom chord.

3.5 CONCLUSIONS

The results of the ten tests performed on roof subassemblages indicate that the use of PAFs to fasten metal roof deck to open web steel joists has no

detrimental effect on the vertical load capacity of the joists. The performance of the specimens with PAFs was essentially identical to the specimens with puddle welds, for both the 16K2 and the 26K5 joist series.

As noted in Chapter 1, concerns have been raised in the past that PAFs driven into very thin top chord joist members may adversely affect the joists. The top chord of a joist will normally be in compression, and the capacity of a top chord member will therefore be controlled by its buckling strength. The deck fasteners may influence the buckling strength in several ways. First, if installation of the fasteners produces significant permanent distortions of the top chord member, the buckling capacity of the member may be reduced due to initial crookedness effects. Further, if the fasteners do not have sufficient shear strength or stiffness, the deck may no longer serve as an effective lateral brace, and the out-of-plane buckling may potentially occur at a lower load. Despite the very thin top chord members in the test specimen, neither of these potentially detrimental effects were observed.

An additional potential concern involves the use of PAFs in thin chord members under tension. This can occur when PAFs are used in the bottom chord of a joist to hang ceilings, ductwork or other appurtenances from the joists. Tension can also occur in the top chord if the roof is subjected to net uplift forces. PAFs may potentially affect tension capacity due to loss of cross-sectional area or due to stress concentrations introduced by the fastener. In these tests, despite the very thin bottom chord members and despite the development of yield level

stresses in the bottom chords, the presence of PAF's had no detrimental effect on these members.

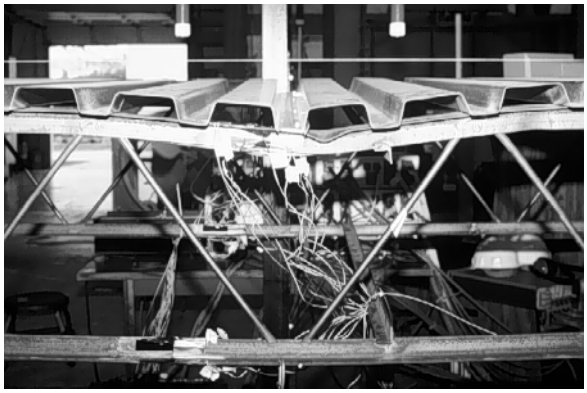

Figure 3.1 Failure Mode for 16K2-PW-1 East Joist

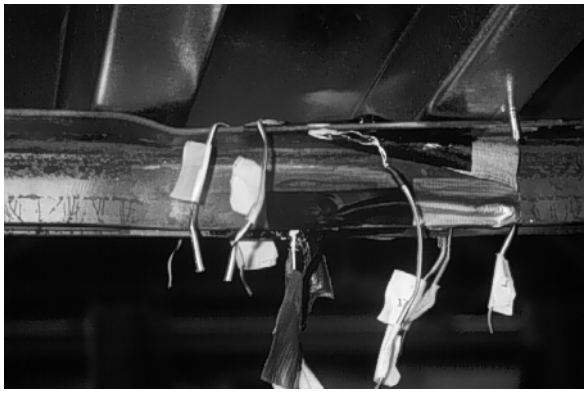

Figure 3.2 Failure Mode for 16K2-PW-1 West Joist

Figure 3.3 Failure Mode for 16K2-PW-2 East Joist

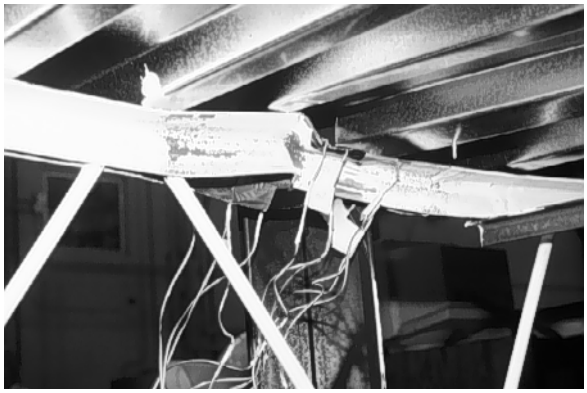

Figure 3.4 Failure Mode for 16K2-PW-2 West Joist

Figure 3.5 Distortions in Top Chord on Specimen 16K2-DX-1

Figure 3.6 Failure Mode for 16K2-DX-1 East Joist

Figure 3.7 Failure Mode for 16K2-DX-1 West Joist

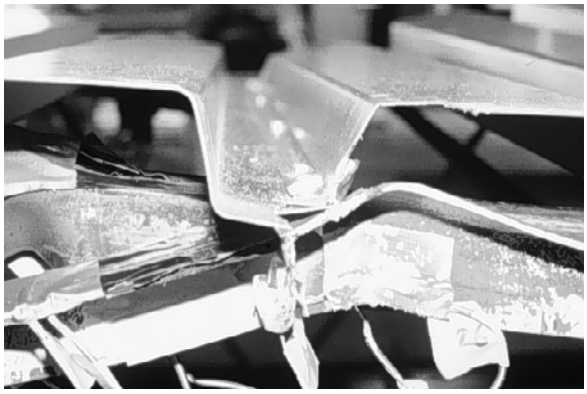

Figure 3.8 Holding Capacity of PAF through Large Deformations

Figure 3.9 Failure Mode for 16K2-DX-2 West Joist

Figure 3.10 Failure Mode for 16K2-DX-2 East Joist

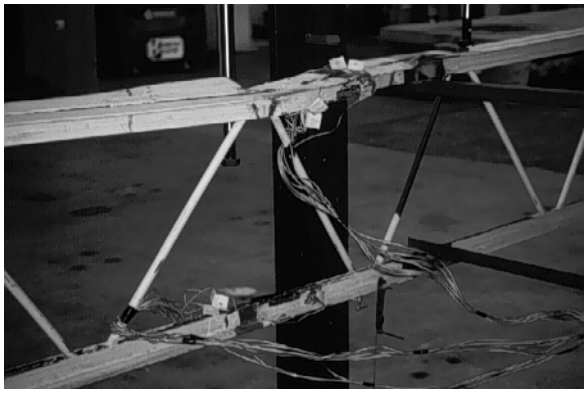

Figure 3.11 Failure Mode for 16K2-ND West Joist

Figure 3.12 Failure Mode for 16K2-ND East Joist

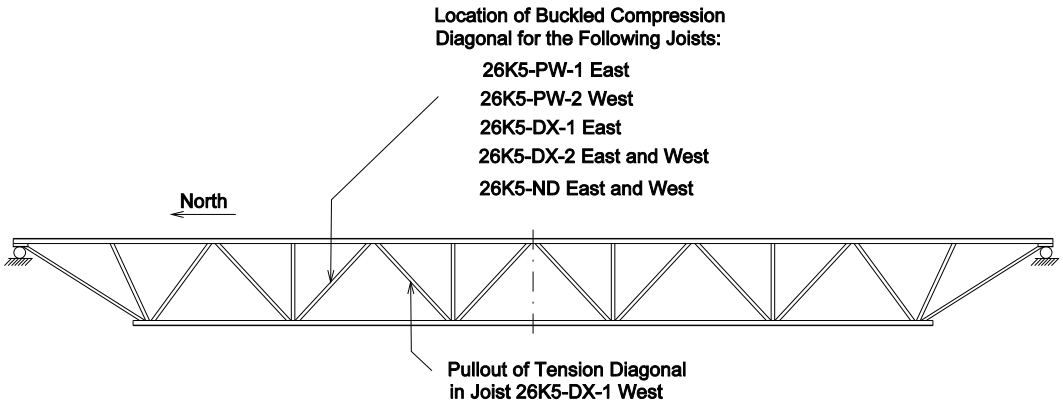

Figure 3.13 Locations for Failed Diagonal Members

Figure 3.14 Failure Mode for 26K5-PW-1 East Joist

Figure 3.15 Failure Mode for 26K5-PW-1 West Joist

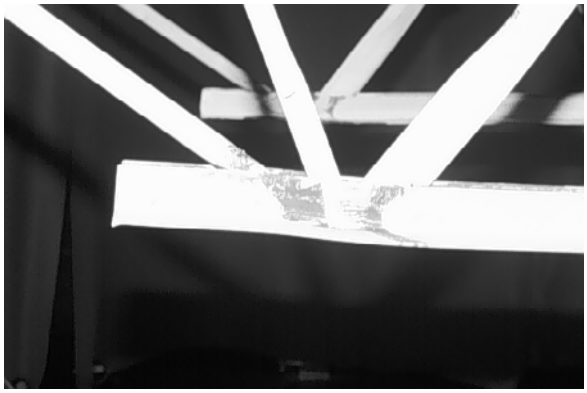

Figure 3.16 Localized Shear Yielding at Bottom Chord Ends

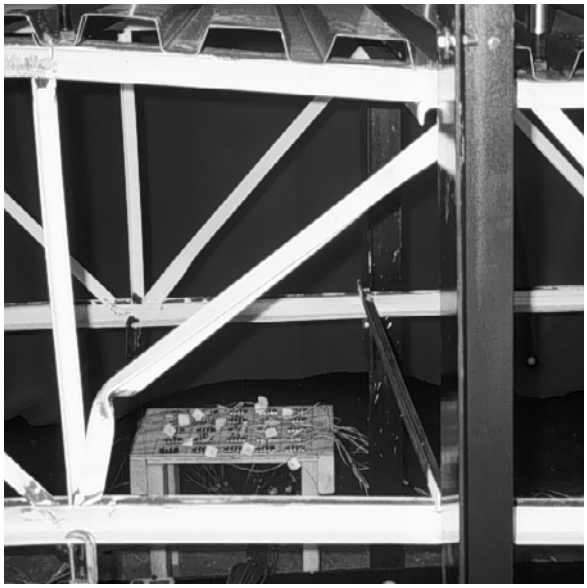

Figure 3.17 Failure Mode for 26K5-PW-2 West Joist

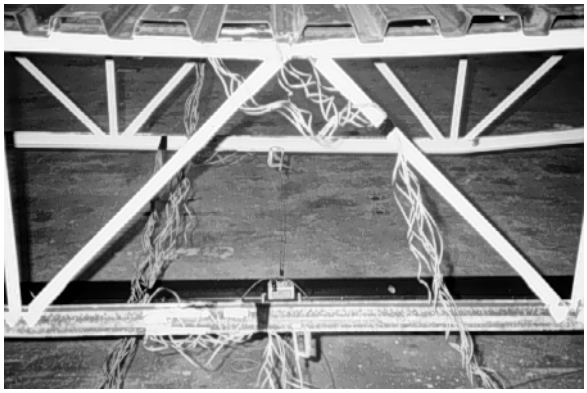

Figure 3.18 Failure Mode for 26K5-PW-2 East Joist

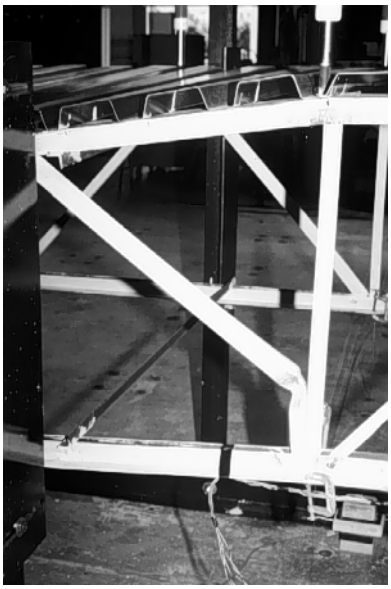

Figure 3.19 Failure Mode for 26K5-DX-1 East Joist

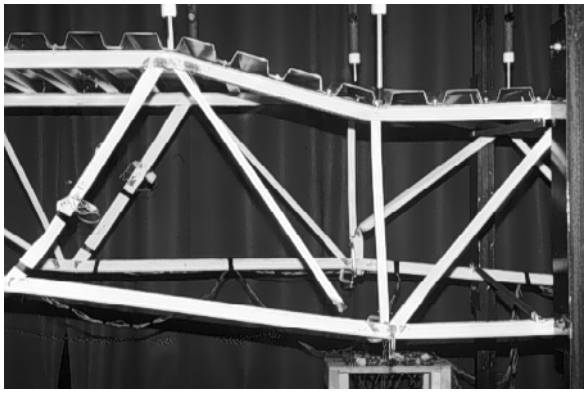

Figure 3.20 Failure Mode for 26K5-DX-1 West Joist

Figure 3.21 Failure Mode for 26K5-DX-2 West Joist

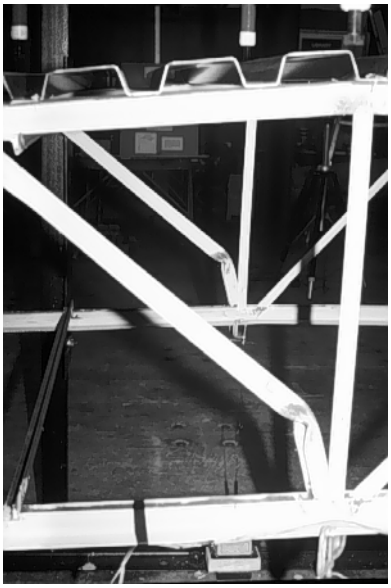

Figure 3.22 Failure Mode for 26K5-DX-2 East Joist

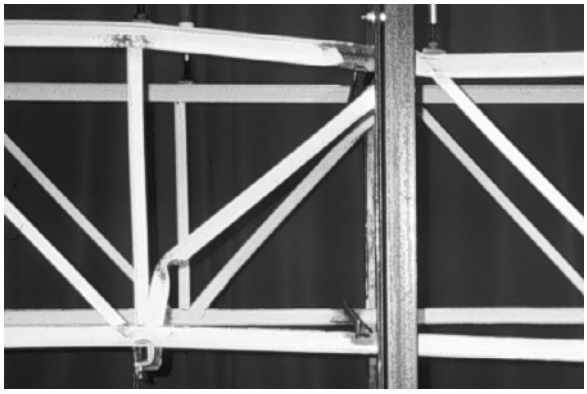

Figure 3.23 Failure Mode for 26K5-ND West Joist

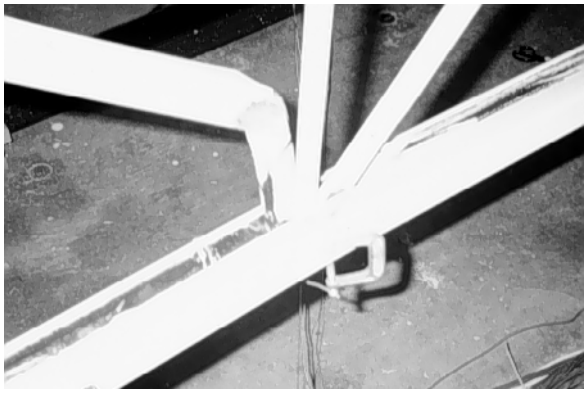

Figure 3.24 Failure Mode for 26K5-ND East Joist

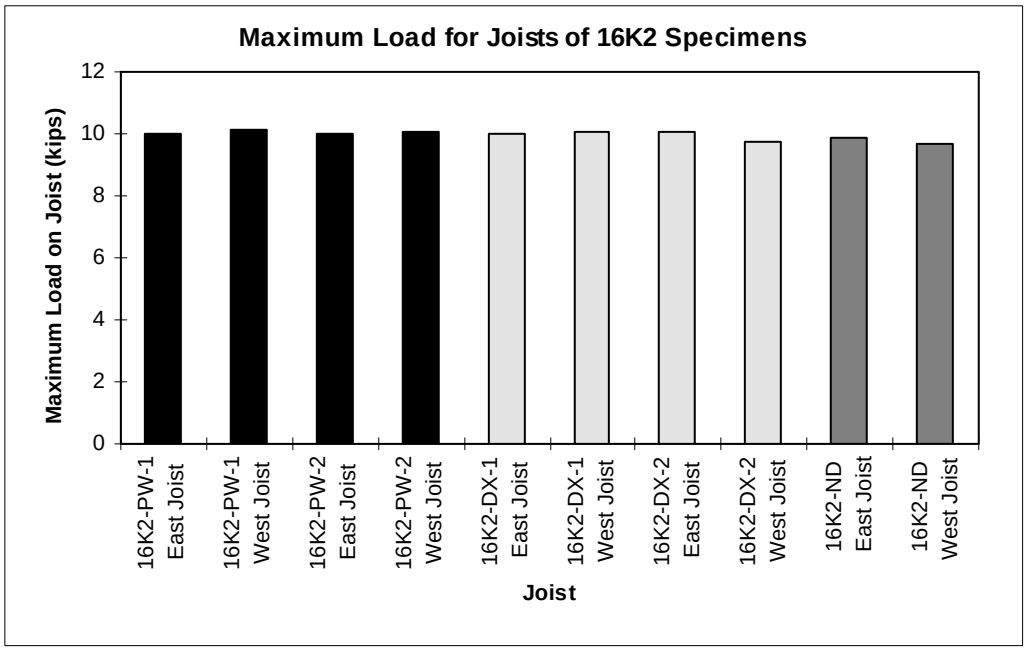

Figure 3.25 Maximum Load for Joists of 16K2 Specimens

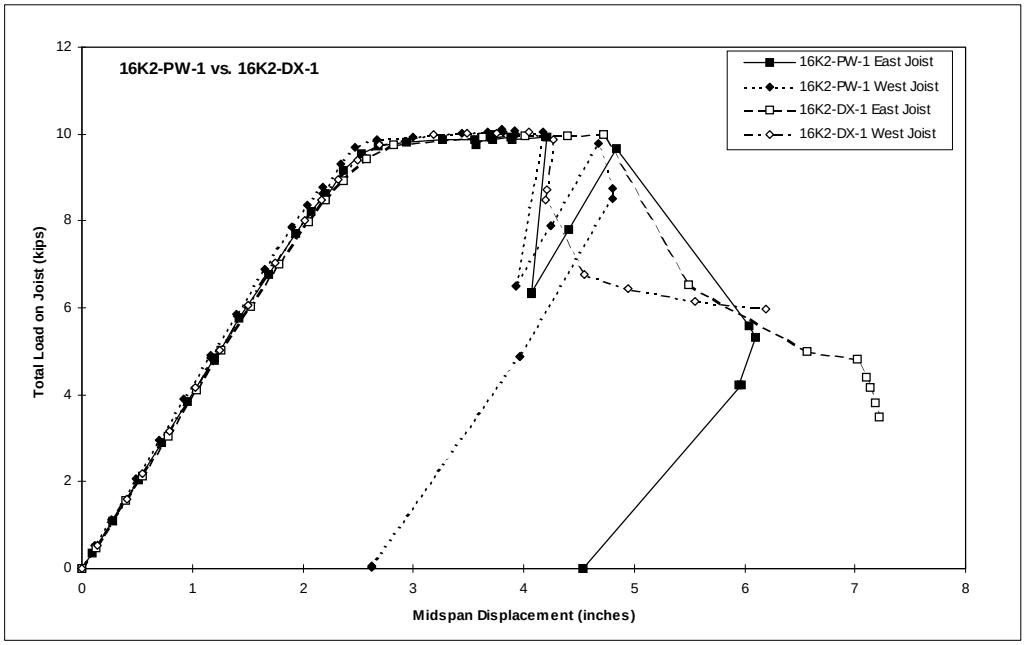

Figure 3.26 Load vs. Midspan Displacement for 16K2-PW-1 and 16K2-DX-1

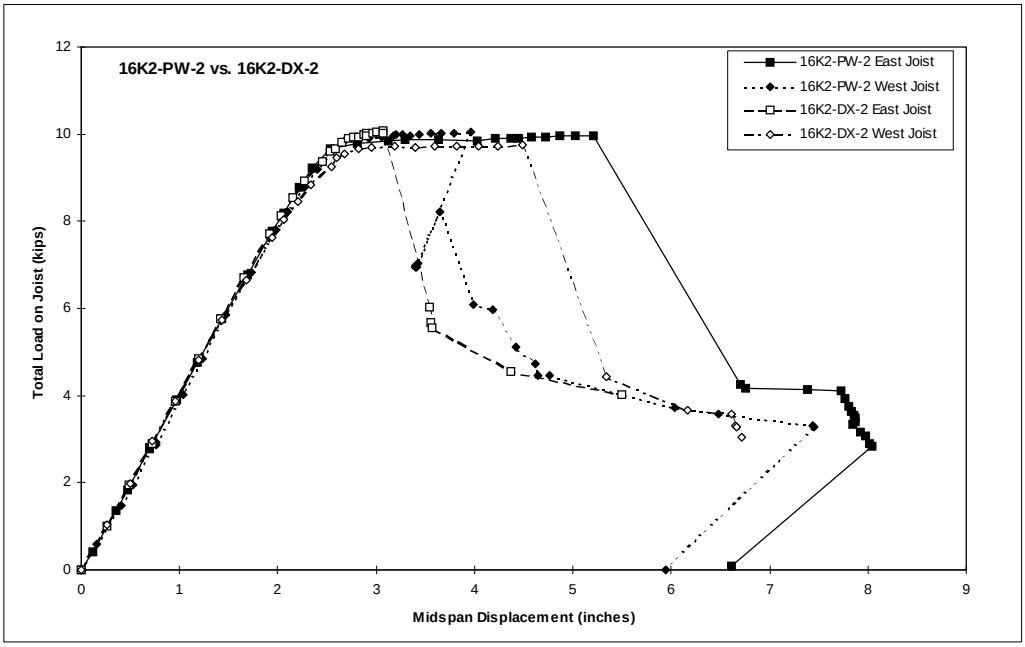

Figure 3.27 Load vs. Midspan Displacement for 16K2-PW-2 and 16K2-DX-2

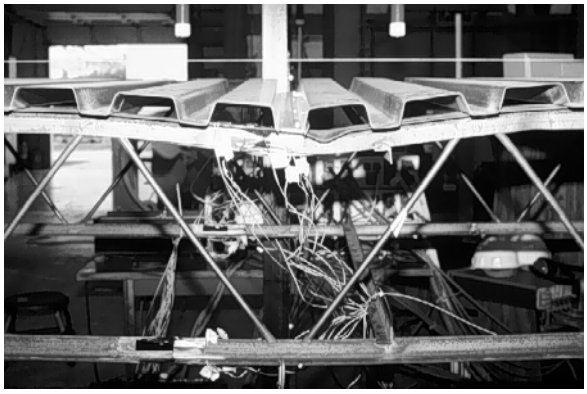

16K2-PW-1 East Joist

16K2-DX-1 East Joist

Figure 3.28 Similarity of Failure Modes

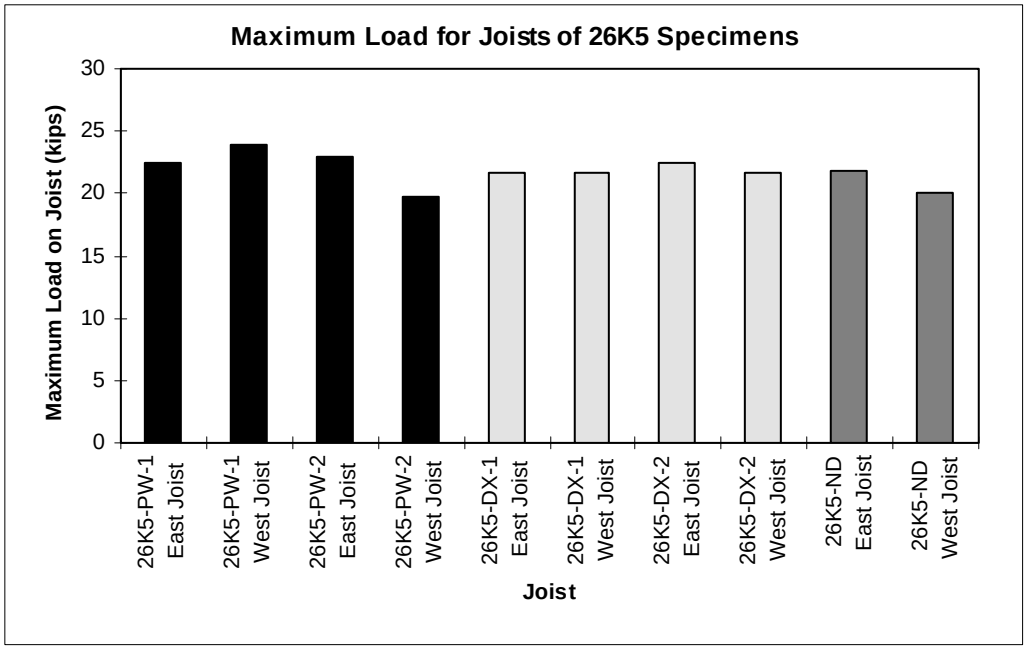

Figure 3.29 Maximum Load for Joist of 26K5 Specimens

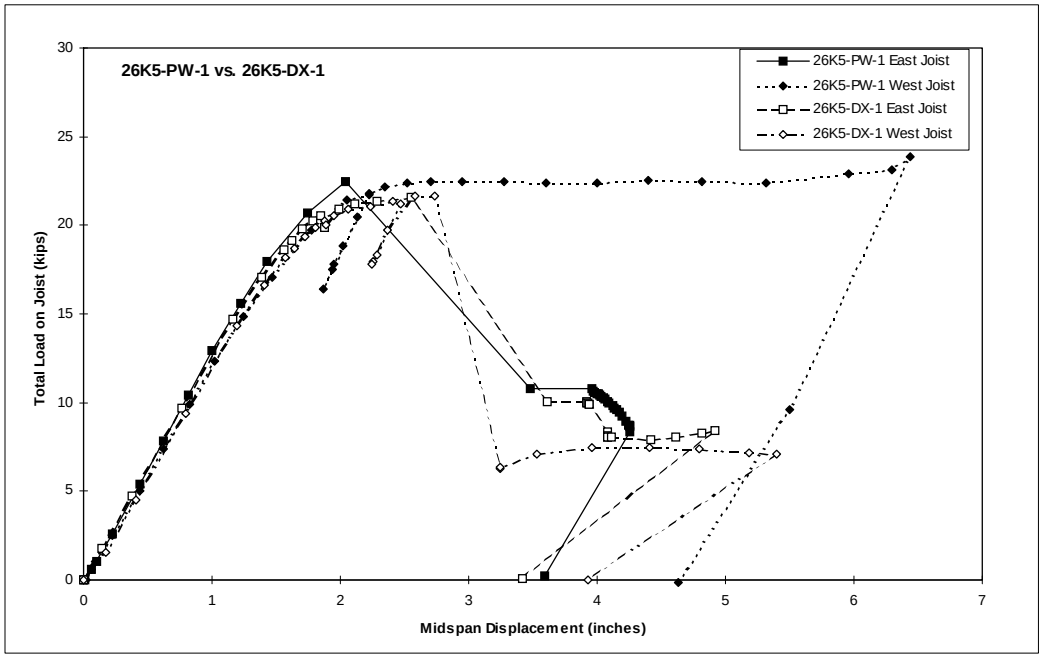

Figure 3.30 Load vs. Midspan Displacment for 26K5-PW-1 and 26K5-DX-1

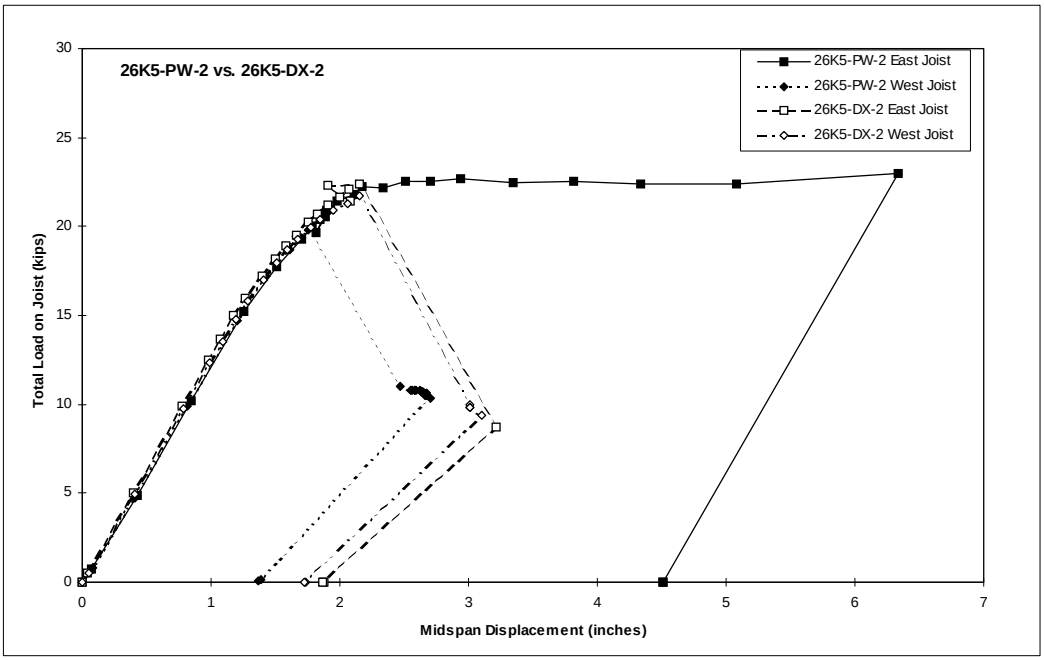

Figure 3.31 Load vs. Midspan Displacement for 26K5-PW-2 and 26K5-DX-2

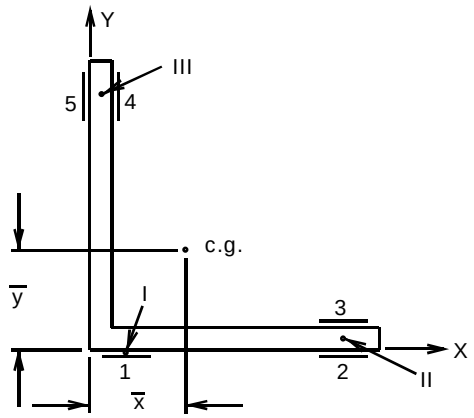

$\varepsilon_1, \varepsilon_2, \varepsilon_3, \varepsilon_4, \varepsilon_5 =$ measured strains at strain gage locations

Compute:

$$\varepsilon_I = \varepsilon_1$$

$$\varepsilon_{II} = \left(\varepsilon_2 + \varepsilon_3\right) / 2$$

$$\varepsilon_{III} = \left(\varepsilon_4 + \varepsilon_5\right) / 2$$

At any location $\left(x, y\right)$, compute strain from: $\varepsilon\left(x, y\right) = Ax + By + C$

where: $A, B, C =$ constants

Solve for A, B, C from $\varepsilon_I, \varepsilon_{II}, \varepsilon_{III}$, by solving this system of equations

$$\varepsilon_I = Ax_I + By_I + C$$

$$\varepsilon_{II} = Ax_{II} + By_{II} + C$$

$$\varepsilon_{III} = Ax_{III} + By_{III} + C$$

where: $\left(x_I, y_I\right)$ = coordinates of point I, etc.

Solve for $\bar{\varepsilon} =$ strain at centroid of angle: $\bar{\varepsilon} = A\bar{x} + B\bar{y} + C$

For elastic response: $\bar{\sigma} = E\bar{\varepsilon}$

where: $\bar{\sigma} =$ axial stress at centroid, E=29,600 ksi

Axial Force in angle = $\bar{\sigma}$ x cross-sectional area of angle

Total axial force in double angle member:

Repeat above calculations for other angle, and sum forces

Figure 3.32 Computation of Axial Strain and Force in Double Angle Members

Table 3.1 Summary of Test Results on Roof Subassemblages

Specimen	Joist	Maximum Load (kips)	Failure Mode
16K2-PW-1	West	10.11	yielding of bottom chord, followed by local buckling in one leg of top chord
	East	9.99	yielding of bottom chord, followed by in-plane buckling of top chord
16K2-PW-2	West	10.06	yielding of bottom chord, followed by in-plane buckling of top chord
	East	9.97	yielding of bottom chord, followed by in-plane buckling of top chord
16K2-DX-1	West	10.04	yielding of bottom chord, followed by in-plane buckling of top chord
	East	9.98	yielding of bottom chord, followed by in-plane buckling of top chord
16K2-DX-2	West	9.74	yielding of bottom chord, followed by in-plane buckling of top chord
	East	10.08	yielding of bottom chord, followed by in-plane buckling of top chord
16K2-ND	West	9.65	out-of-plane buckling of top chord
	East	9.85	out-of-plane buckling of top chord
26K5-PW-1	West	23.86	yielding of bottom chord
	East	22.45	buckling of diagonal member
26K5-PW-2	West	19.79	buckling of diagonal member
	East	22.98	yielding of bottom chord
26K5-DX-1	West	21.66	failure of weld on tension diagonal
	East	21.59	buckling of diagonal member
26K5-DX-2	West	21.73	buckling of diagonal member
	East	22.41	buckling of diagonal member
26K5-ND	West	20.00	buckling of diagonal member
	East	21.82	buckling of diagonal member

Chapter 4:

Angle Tests

4.1 INTRODUCTION

Power actuated fasteners have numerous applications beyond metal deck attachment. The majority of these uses involve the attachment of non-structural elements to steel members. These non-structural elements include pipe hangers, suspended ceilings, and HVAC ductwork. It is not uncommon to fasten these elements to the tension chord of roof or floor joists. Concerns have been raised over the installation of these fasteners into chord members which are subjected to tensile stress. These concerns involve factors such as loss of area and the introduction of stress concentrations.

A series of tests on double angle chord members was conducted to further study the effects of power actuated fasteners on members subjected to tensile stress. This was accomplished by comparing the elongation and load capacities of specimens with power actuated fasteners, without power actuated fasteners, and with drilled holes.

4.2 SPECIMEN DESCRIPTION

The overall specimen configuration can be seen in Figure 4.1. Each specimen consisted of two back-to-back angle members that were attached at each end to a gusset plate. The orientation of the angle members in the specimen was

intended to simulate the orientation of the members within the joists. The cross-sectional area of the angle members was reduced in the section between the gusset plates to force the yielding and failure of the specimen to occur within the reduced section.

In order to study the influence of angle size and leg thickness, two different chord members were considered within the investigation. The first series of test specimens was constructed with angle members from the bottom chord of the 16K2 joists. The bottom chord angles had a leg thickness of 0.109 inch. The second series of test specimens was constructed with angle members from the top chord of the 26K5 joists. The top chord angles had a leg thickness of 0.155 inch. The leg width for the reduced section of both specimens was 1.0 inch. These chord members were chosen because they represent the upper and lower limits on angle size and thickness considered within this investigation.

Power actuated fasteners were installed on eight of the double angle specimens. The fasteners used on these specimens were the same fasteners used in the full size joist tests. The location of the fasteners is shown in Figure 4.1. Each fastener was positioned along the centerline of the specimen and was centered within the reduced leg width. For the specimens incorporating only one fastener per angle, each fastener was located on the angle leg not attached to the gusset plate. For the specimens incorporating two fasteners per angle, one fastener was located on each leg of the angle member.

Four of the double angle specimens incorporated drilled holes as a means of reducing the cross-sectional area. A hole diameter of 0.144” was used. The

hole diameter nominally equaled the shaft diameter of the fasteners used on the test specimens. The hole locations are also shown in Figure 4.1.

The gusset plates (PL-2.5”x11.0”x0.75”) were attached to the chord angles using a series of fillet welds. The fillet welds were sized to equal the leg thickness of the angles and were located along the edges of each angle which extended over the gusset plate. The gusset plates extended 6 inches past each end of the double angles to provide adequate surface area for the grip mechanism of the testing machine.

4.3 TESTING

The double angle specimens were loaded using a Tinius Olsen testing machine, which is shown in Figure 4.2. The testing machine had a stationary upper cross-head and a movable lower cross-head. A screw apparatus provided the drive mechanism for the lower cross-head. The lower cross-head moved at a constant rate which was controlled by the operator. The specimen was held in the machine by a pair of vice grips which were connected to the upper and lower cross-heads. The orientation of a double angle specimen in the testing machine is shown in Figure 4.3.

Each angle was instrumented with an extensometer. The extensometer measured the elongation of the specimen over its 8 inch gage length. A computerized data acquisition system was used to record the data sets for each test. The data sets included information on the elongation of the specimen over the gage length and the load acting on the specimen. This information was then

used to determine the force-displacement response of the specimen. The plots of force versus displacement for each of the test specimens can be found in Appendix D. In addition, a series of values were manually recorded from the testing machine to supplement the computerized data.

Three sets of dynamic and static yield loads were recorded during each test. In addition, a series of static and dynamic loads were recorded in the range between initial strain hardening and fracture of the specimen. Each static load was reached following a 3 minute pause in loading of the specimen. This time period was adequate in allowing the full relaxation of the specimen to occur.

Two different cross-head rates were used during each test. A cross-head rate of 0.02 in./min. was used in the range up to initial strain-hardening of the material. A cross-head rate of 0.05 in./min. was used in the range from initial strain-hardening through fracture of the material. These cross-head rates were used consistently during each test in order to minimize any variation in the material properties caused by strain rate effects.

In order to determine the elongation of the specimen, a set of two gage marks, spaced at approximately 8 inches, was placed on each angle before loading. The initial distances between the gage marks and the final distances between the gage marks after fracture were recorded for each angle. The elongation of the each angle was calculated as the change in length of the angle divided by the initial distance between the gage marks. The elongation of the specimen was taken to be the average elongation between the two angles. In many cases, one angle fractured before the other, and the test was terminated

before fracture of the second angle occurred. For these instances, the elongation was also calculated as the average elongation between the two angles.

4.4 TESTING SCHEME

A total of 16 tests were completed on double angle specimens during this testing program. Table 4.1 gives a description for each of the test specimens.

4.5 RESULTS

The results from the double angle tests are summarized in Table 4.2 and Table 4.3. Table 4.2 reports the load values before any normalization was performed on the data. Table 4.3 reports load values that were normalized with respect to the theoretical gross area for each of the angle types. The following equation was used to normalize the load values:

$$\text{Normalized Value} = \text{Original Value}\left(\frac{Ag_{theoretical}}{Ag_{measured}}\right)$$

The normalization was done to remove any variation in the test data due to dimensional inconsistencies of the angle cross-sections. The elongation values reported in Table 4.3 are not normalized. Figures 4.4 through 4.11 show photographs of the failures for each of the test specimens.

4.6 DISCUSSION

In order to investigate the effects of power actuated fasteners on members subjected to tensile stress, the elongation and load capacities of the double angle specimens with PAFs, without PAFs, and with drilled holes were compared.

Insignificant variations in the dynamic and static yield loads were observed for the test specimens. In particular, the maximum variation in dynamic and static yield loads for the specimens of the 16K2 joist series was 4.0 and 0.7 percent, respectively. The maximum variation in the dynamic and static yield loads for the specimens of the 26K5 joist series was 3.3 and 3.6 percent, respectively. Because no trends were observed in the yield data, it was concluded that the introduction of power actuated fasteners or holes has a minimal impact on the yield loads of chord members subjected to tensile stress. This behavior is expected because the yield loads are a function of the gross area of the member. Therefore, any reasonable reduction in the cross-sectional area should not heavily impact the yield loads.

Larger differences were seen in the ultimate load capacities. In general, the largest ultimate load capacities were observed in the specimens with no fasteners. As fasteners were introduced into the specimens, the ultimate load capacities decreased. The specimens with 2 PAFs in each angle showed lower ultimate capacities than the specimens with 1 PAF in each angle. Finally, the specimens with 2 holes per angle showed the greatest decrease in the ultimate load capacities.

Table 4.4 shows the percent decrease in dynamic ultimate load, static ultimate load, and cross-sectional area for each specimen type. The reported values were normalized with respect to the specimens with no fasteners for each joist series.

The results show that similar reductions in the ultimate load capacities occurred between the specimens with 2 PAFs per angle and the specimens with 2 holes per angle. For the specimens from the 16K2 joist series, the decrease in the dynamic ultimate load in the specimens with 2 holes per angle was 10.8 percent. The decrease in the dynamic ultimate load for the specimens with 2 fasteners per angle was 9.2 percent. For the specimens from the 26K5 joist series, the decrease in the dynamic ultimate load for the specimens with 2 holes per angle was 12.8 percent. The decrease in the dynamic ultimate load for the specimens with 2 fasteners per angle was 11.6 percent. A similar trend was also observed for the decrease in static ultimate load for the two specimen types. The similar reductions in the ultimate load capacities show that the behavior of the specimens with 2 PAFs in each angle resemble the behavior of the specimens with 2 holes in each angle.

Table 4.4 also shows the percent decrease in cross-sectional area for each specimen type. For specimens with PAFs, the decrease in cross-sectional area from each fastener was assumed to equal the fastener diameter multiplied by the leg thickness. It should be noted that this approximation may not correspond with the actual decrease in cross-sectional area.

For the specimens from the 16K2 joist series, the percent decrease in the ultimate loads was consistently smaller than the percent decrease in cross-sectional area. Therefore, the capacities of these members would be underestimated if a net section approach is used in design. The majority of the specimens from the 26K5 joist series also yielded a percent decrease in the ultimate loads that was slightly smaller than the percent decrease in cross-sectional area. The specimens with 1 PAF per angle showed a percent decrease in the ultimate loads which was higher than the percent decrease in cross-sectional area. The results for the specimens with 1 PAF per angle do not follow the trend set forth by the other test specimens. Further testing should be completed before any conclusions are made.

The elongation capacity of the specimens was greatly reduced by the introduction of PAFs or drilled holes. In general, the specimens with no fasteners had the largest elongation capacity. An approximate reduction in elongation capacity of 70 percent was observed when PAFs or holes were introduced into the specimens, as shown in Table 4.5. Insignificant variations in the elongation capacity of the specimens with PAFs or holes were observed. Because no trends were observed in the specimens with PAFs or holes, further testing should be completed to determine the difference, if any, in the elongation capacity of these specimen types.

4.6 CONCLUSIONS

A series of 16 tests was completed on double angle chord members to further study the effects of PAFs on members subjected to tensile stress. The testing program showed that the presence of PAFs does not influence the yield loads of double angle chord members subjected to tensile stress. The tests also revealed that the presence of PAFs does reduce the elongation capacity and ultimate load capacities of the specimens. In addition, the decreases in the elongation capacity and the ultimate load capacities in the specimens with PAF's resemble the decreases in the elongation capacity and ultimate load capacities of the specimens with drilled holes.

Due to the limited size of the data set, it is recommended that additional testing be completed on similar types of specimens.

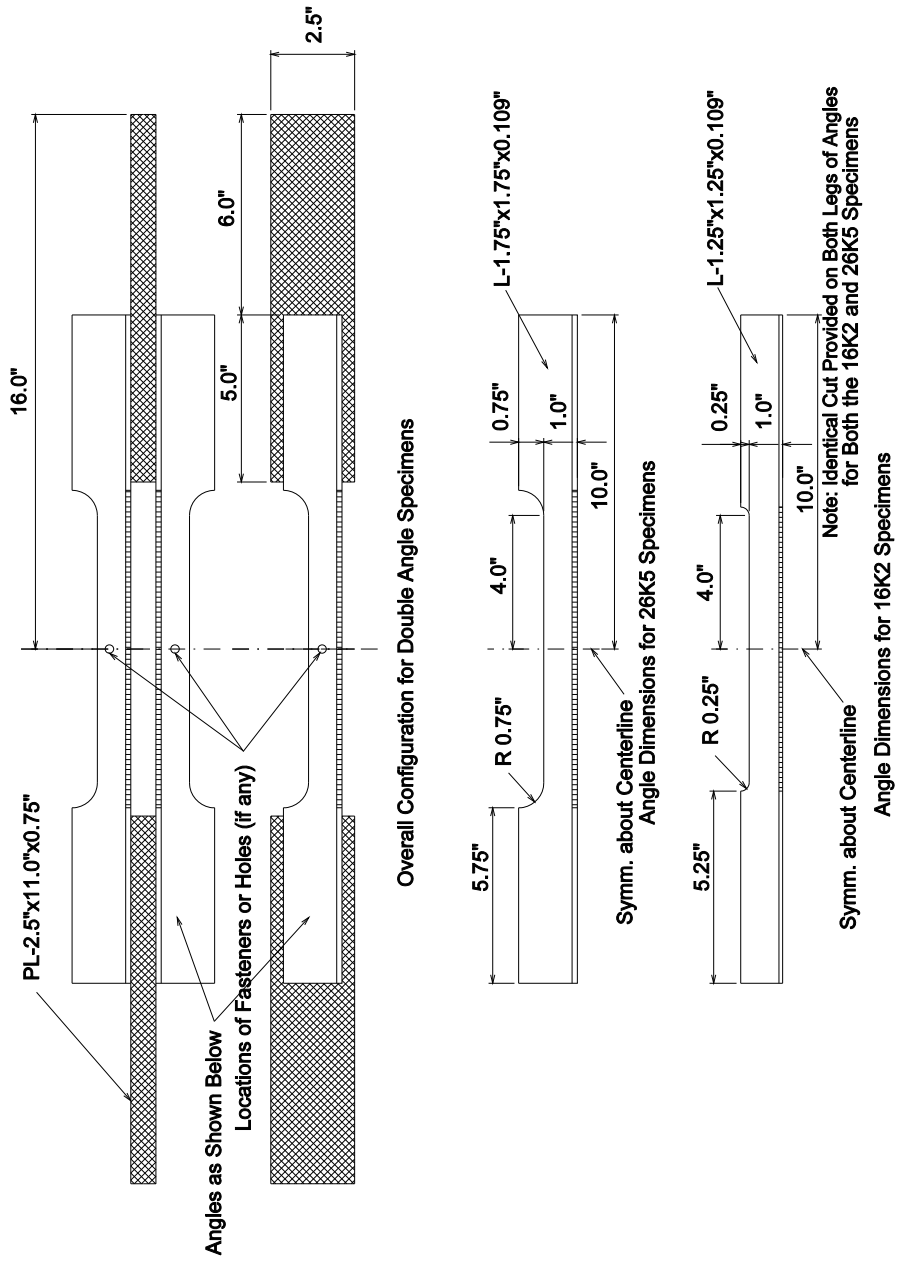

Figure 4.1 Configuration for Double Angle Specimens

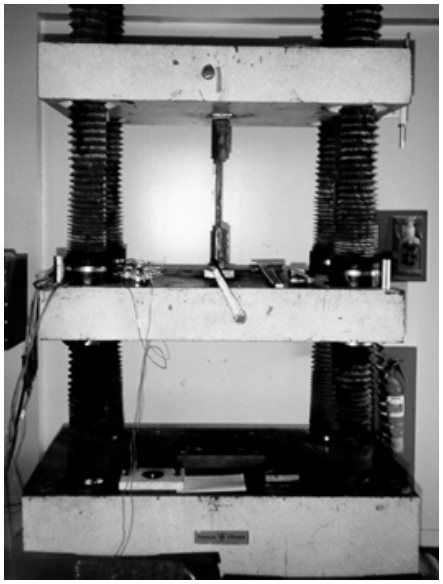

Figure 4.2 Testing Machine Used for Double Angle Specimens

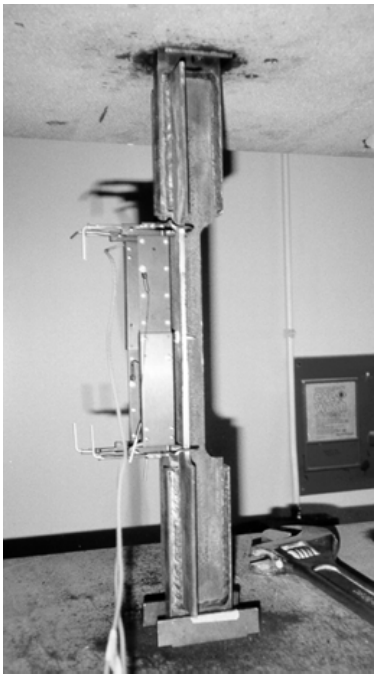

Figure 4.3 Orientation of Double Angle Specimens in the Testing Machine

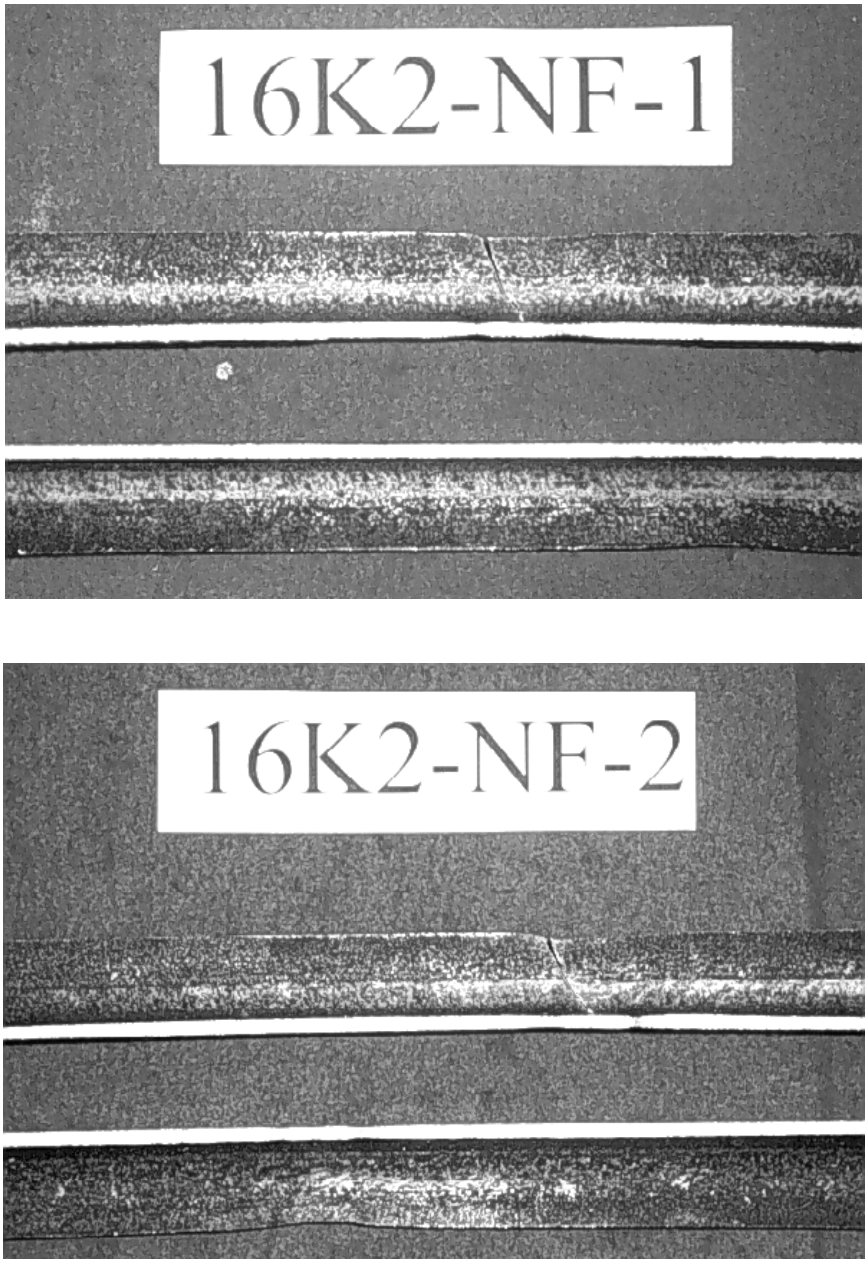

Figure 4.4 Failures in 16K2 Specimens with No Fasteners

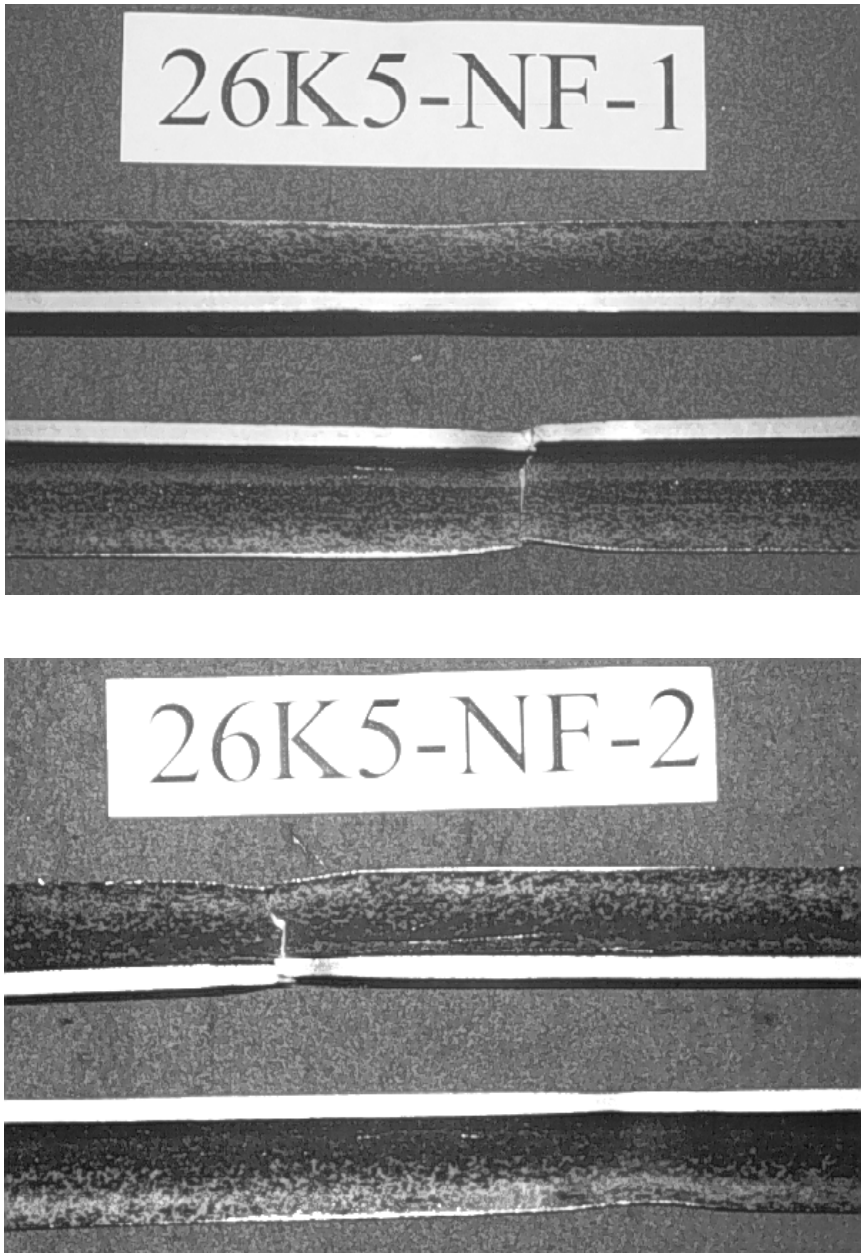

Figure 4.5 Failures in 26K5 Specimens with No Fasteners

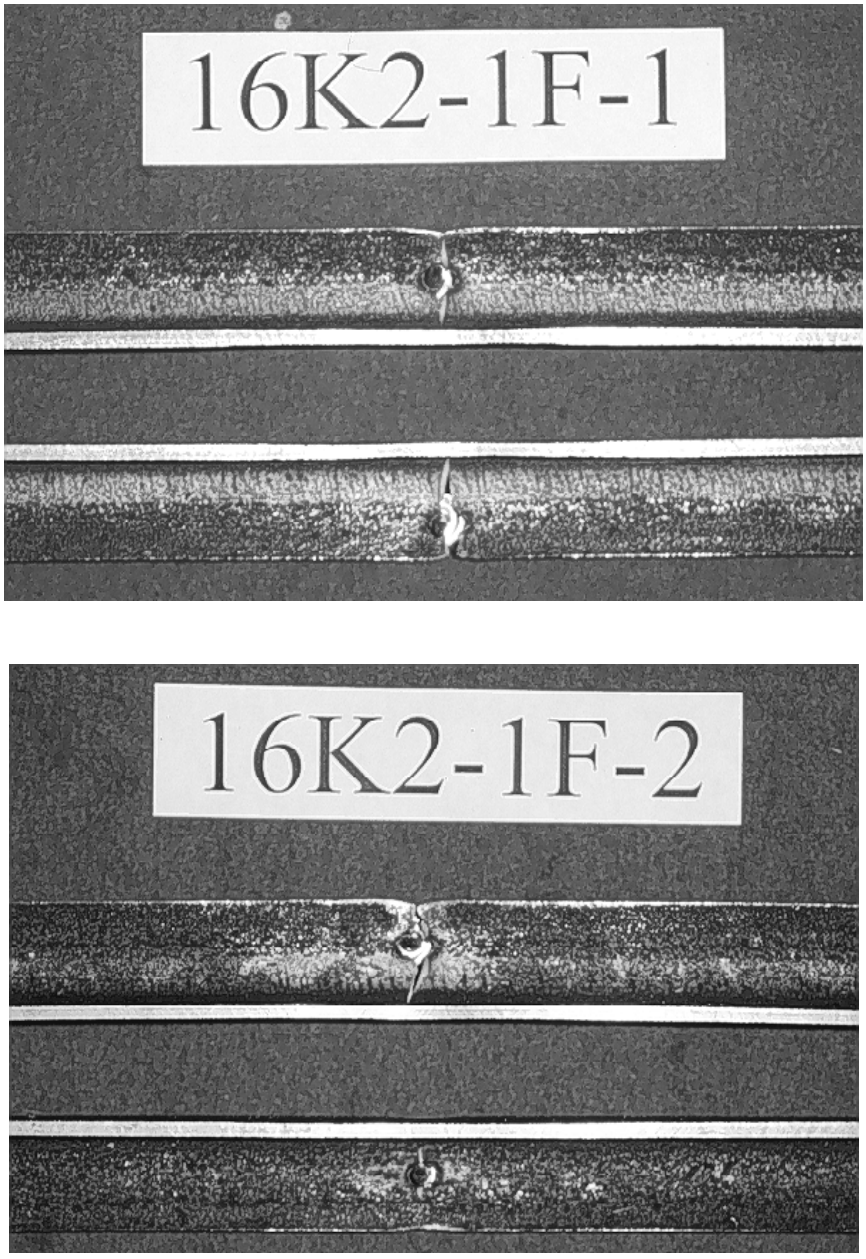

Figure 4.6 Failures in 16K2 Specimens with 1 PAF per Angle

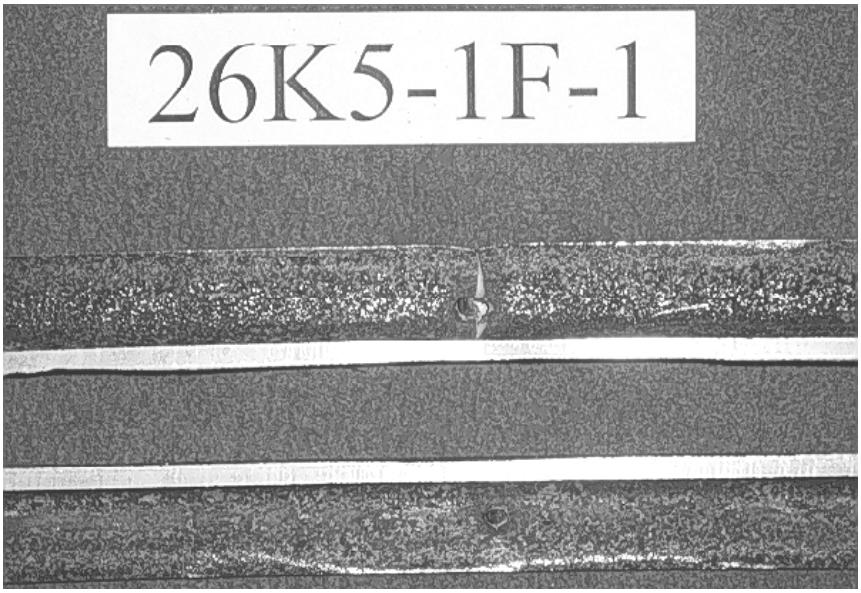

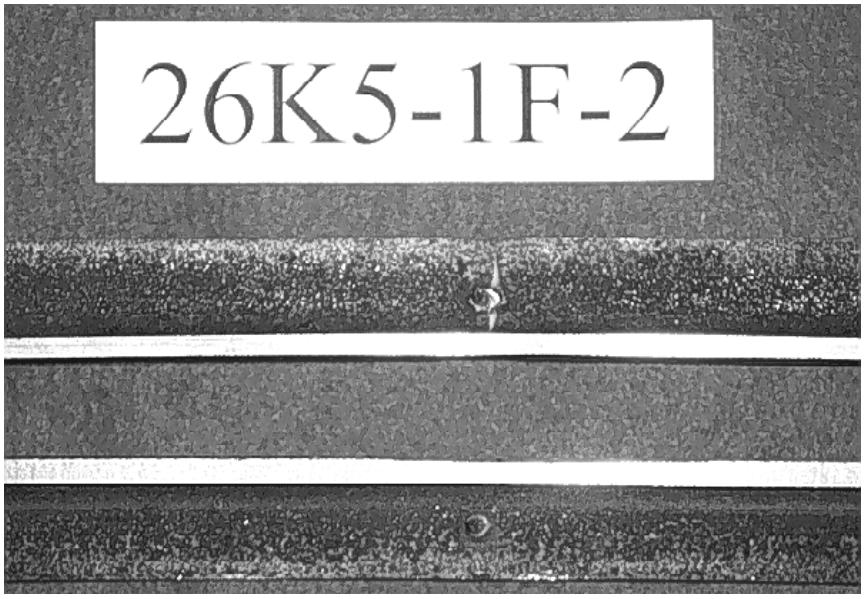

Figure 4.7 Failures in 26K5 Specimens with 1 PAF per Angle

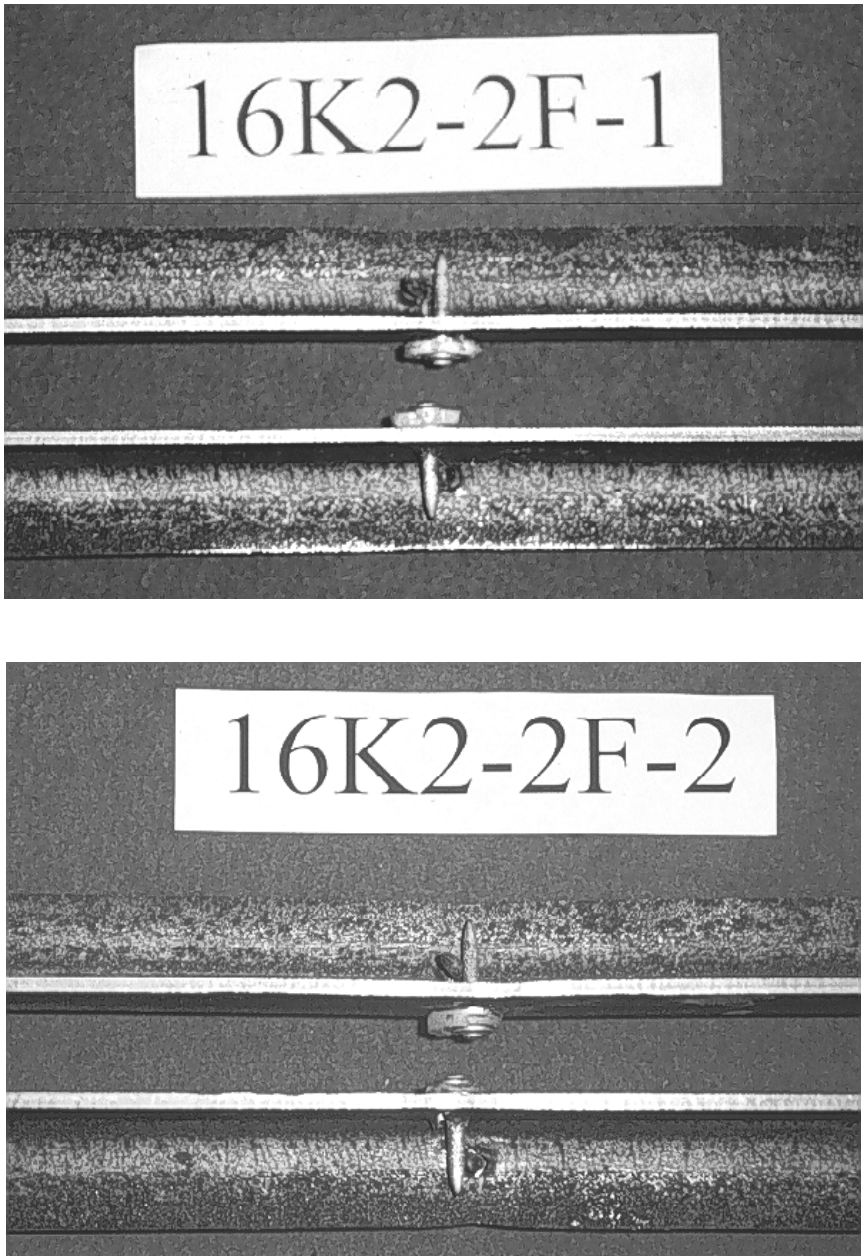

Figure 4.8 Failures in 16K2 Specimens with 2 PAFs per Angle

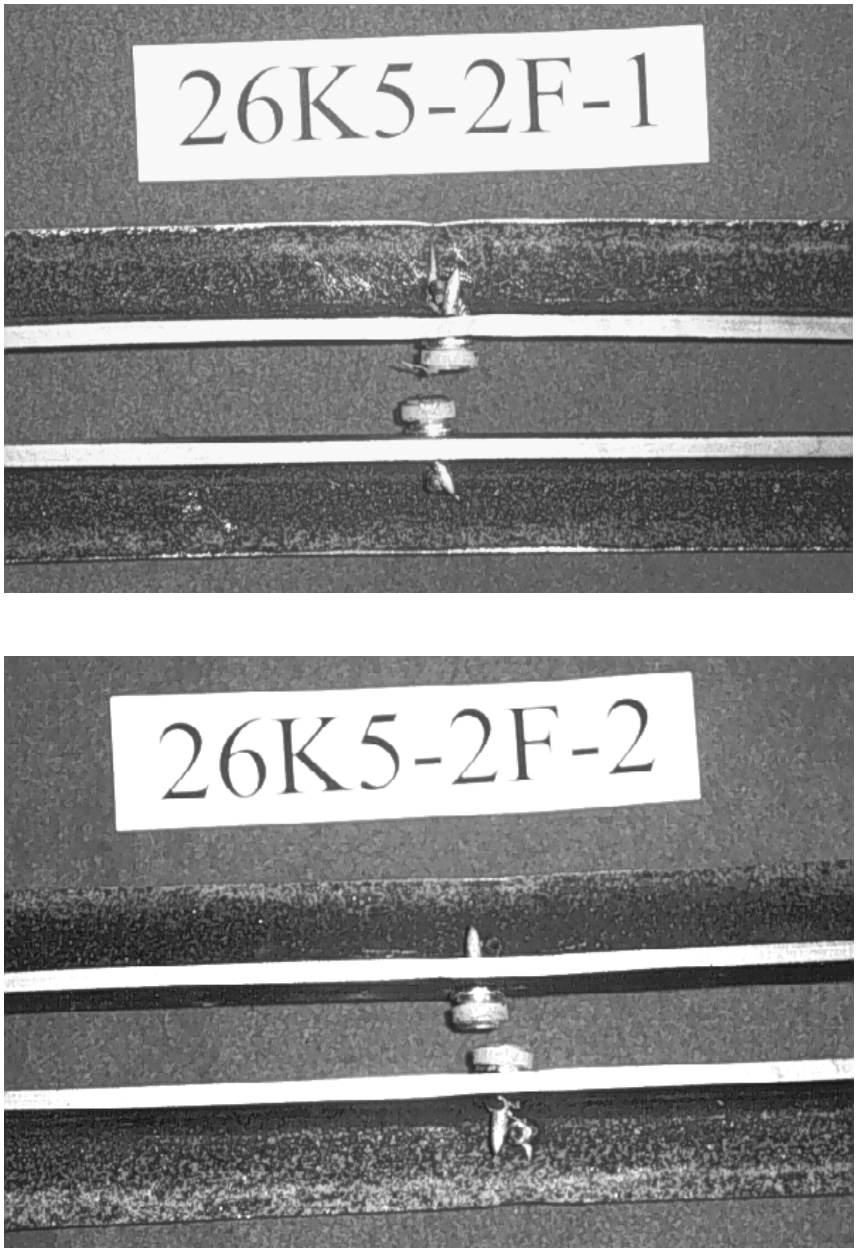

Figure 4.9 Failures in 26K5 Specimens with 2 PAFs per Angle

Figure 4.10 Failures in 16K2 Specimens with 2 Holes per Angle

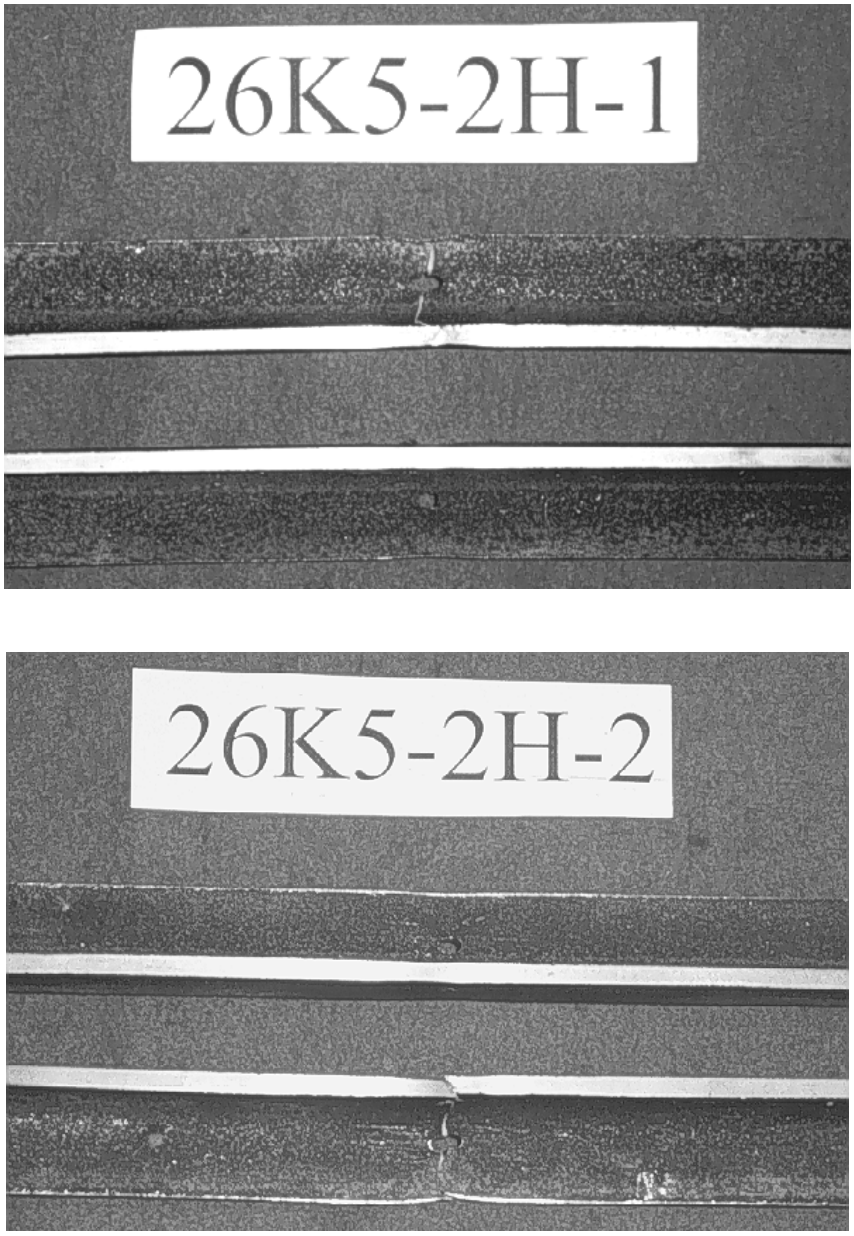

Figure 4.11 Failures in 26K5 Specimens with 2 Holes per Angle

Table 4.1 Description of Double Angle Specimens

Chord Location and Size	Specimen Designation	Descritpion	Number of Specimens	Ag-theoretical (in.^2)	An-theoretical (in.^2)
16K2 - Bottom Chord (2L-1.25"x1.25"x0.109")	16K2-NF	No Fasteners	2	0.4122	0.4122
	16K2-1F	1 PAF per Angle	2	0.4122	0.3804
	16K2-2F	2 PAFs per Angle	2	0.4122	0.3485
	16K2-2H	2 Holes per Angle	2	0.4122	0.3494
26K5 - Top Chord (2L-1.75"x1.75"x0.155")	26K5-NF	No Fasteners	2	0.5720	0.5720
	26K5-1F	1 PAF per Angle	2	0.5720	0.5267
	26K5-2F	2 PAFs per Angle	2	0.5720	0.4815
	26K5-2H	2 Holes per Angle	2	0.5720	0.4827

Notes: Each hole diameter corresponds to the maximum shaft diameter of the PAF.

The area loss for the specimens with the power actuated fasteners is calculated using an equivalent hole with a diameter equal to the maximum shaft diameter of the fastener

Table 4.2 Results of Double Angle Tests Before Normalization

Joist Series	Description	Coupon Designation	Dynamic Yield (kips)	Static Yield (kips)	Dynamic Ultimate (kips)	Static Ultimate (kips)	% Elongation
16K2	No Fasteners	16K2-NF-1	24.31	23.12	32.19	30.66	22.4%
		16K2-NF-2	24.40	23.25	32.25	30.76	22.7%
		Average	**24.36**	**23.19**	**32.22**	**30.71**	**22.6%**
	1 PAF per Angle	16K2-1F-1	24.18	22.92	30.01	28.61	7.3%
		16K2-1F-2	24.24	22.98	29.97	28.62	7.3%
		Average	**24.21**	**22.95**	**29.99**	**28.62**	**7.3%**
	2 PAFs per Angle	16K2-2F-1	23.85	22.66	28.69	27.34	5.5%
		16K2-2F-2	24.01	22.80	28.48	27.20	5.2%
		Average	**23.93**	**22.73**	**28.59**	**27.27**	**5.4%**
	2 Holes per Angle	16K2-2H-1	23.99	22.89	28.71	27.41	6.1%
		16K2-2H-2	23.97	22.86	28.68	27.40	7.1%
		Average	**23.98**	**22.88**	**28.70**	**27.41**	**6.6%**
26K5	No Fasteners	26K5-NF-1	40.26	38.38	57.39	54.83	22.1%
		26K5-NF-2	40.32	38.46	57.46	54.90	22.6%
		Average	**40.29**	**38.42**	**57.43**	**54.87**	**22.4%**
	1 PAF per Angle	26K5-1F-1	37.99	36.21	48.82	46.92	5.9%
		26K5-1F-2	37.57	35.71	49.16	47.01	6.1%
		Average	**37.78**	**35.96**	**48.99**	**46.97**	**6.0%**
	2 PAFs per Angle	26K5-2F-1	40.19	38.30	50.61	48.47	4.9%
		26K5-2F-2	40.57	38.63	51.83	49.70	5.3%
		Average	**40.38**	**38.47**	**51.22**	**49.09**	**5.1%**
	2 Holes per Angle	26K5-2H-1	37.41	35.58	48.04	46.14	5.7%
		26K5-2H-2	37.74	35.86	48.38	46.50	5.8%
		Average	**37.58**	**35.72**	**48.21**	**46.32**	**5.8%**

Notes:
Cross-head Rate 0.02 in./min. up to initial strain hardening
0.05 in./min. from initial strain hardening through fracture

Elongation: % elongation based on an 8 inch gage length

Normalization: None

Table 4.3 Results of Double Angle Tests After Normalization

Joist Series	Description	Coupon Designation	Dynamic Yield (kips)	Static Yield (kips)	Dynamic Ultimate (kips)	Static Ultimate (kips)	% Elongation	Ag-measured (in^2)	Ag-theoretical (in^2)
16K2	No Fasteners	16K2-NF-1	23.79	22.63	31.50	30.00	22.4%	0.4212	0.4122
		16K2-NF-2	24.08	22.95	31.83	30.36	22.7%	0.4176	0.4122
		Average	**23.94**	**22.79**	**31.67**	**30.18**	**22.6%**	-	-
	1 PAF per Angle	16K2-1F-1	23.87	22.62	29.62	28.24	7.3%	0.4176	0.4122
		16K2-1F-2	24.05	22.80	29.74	28.40	7.3%	0.4154	0.4122
		Average	**23.96**	**22.71**	**29.68**	**28.32**	**7.3%**	-	-
	2 PAFs per Angle	16K2-2F-1	24.04	22.84	28.92	27.56	5.5%	0.4089	0.4122
		16K2-2F-2	24.12	22.91	28.61	27.33	5.2%	0.4103	0.4122
		Average	**24.08**	**22.87**	**28.77**	**27.44**	**5.4%**	-	-
	2 Holes per Angle	16K2-2H-1	23.46	22.38	28.07	26.80	6.1%	0.4216	0.4122
		16K2-2H-2	23.76	22.66	28.42	27.16	7.1%	0.4159	0.4122
		Average	**23.61**	**22.52**	**28.25**	**26.98**	**6.6%**	-	-
26K5	No Fasteners	26K5-NF-1	36.52	34.81	52.05	49.73	22.1%	0.6306	0.5720
		26K5-NF-2	36.16	34.49	51.53	49.23	22.6%	0.6378	0.5720
		Average	**36.34**	**34.65**	**51.79**	**49.48**	**22.4%**	-	-
	1 PAF per Angle	26K5-1F-1	35.28	33.63	45.34	43.57	5.9%	0.6159	0.5720
		26K5-1F-2	36.21	34.42	47.38	45.31	6.1%	0.5934	0.5720
		Average	**35.75**	**34.02**	**46.36**	**44.44**	**6.0%**	-	-
	2 PAFs per Angle	26K5-2F-1	35.56	33.89	44.78	42.89	4.9%	0.6464	0.5720
		26K5-2F-2	36.62	34.87	46.78	44.86	5.3%	0.6337	0.5720
		Average	**36.09**	**34.38**	**45.78**	**43.87**	**5.1%**	-	-
	2 Holes per Angle	26K5-2H-1	34.92	33.21	44.84	43.07	5.7%	0.6127	0.5720
		26K5-2H-2	35.46	33.69	45.45	43.69	5.8%	0.6088	0.5720
		Average	**35.19**	**33.45**	**45.15**	**43.38**	**5.8%**	-	-

Notes: Cross-head Rat 0.02 in./min. up to initial strain hardening
0.05 in./min. from initial strain hardening through fracture

Elongation: % elongation based on an 8 inch gage length

Normalization: Data normalized w.r.t. the theoretical gross area

Table 4.4 Percent Decrease in Average Ultimate Loads and Cross Sectional Area

Percent Decrease in Avgerage Ultimate Loads and Cross-Sectional Area:				
Joist Series	Description	% Decrease in Avg. Dynamic Ultimate	% Decrease in Avg. Static Ultimate	% Decrease in Cross-Sectional Area
16K2	No Fasteners	0.0%	0.0%	0.0%
	1 PAF per Angle	-6.3%	-6.2%	-7.7%
	2 PAFs per Angle	-9.2%	-9.1%	-15.4%
	2 Holes per Angle	-10.8%	-10.6%	-15.2%
26K5	No Fasteners	0.0%	0.0%	0.0%
	1 PAF per Angle	-10.5%	-10.2%	-7.9%
	2 PAFs per Angle	-11.6%	-11.3%	-15.8%
	2 Holes per Angle	-12.8%	-12.3%	-15.6%

Notes: Decreases are reported with respect to the specimens with no fasteners

Theoretical decreases in cross-sectional area considered

Table 4.5 Percent Decrease in Elongation Capacity

Percent Reduction in Elongation Capacity:		
Joist Series	Description	% Decrease in Elongation Capacity
16K2	No Fasteners	0.0%
	1 PAF per Angle	-67.6%
	2 PAFs per Angle	-76.3%
	2 Holes per Angle	-70.7%
26K5	No Fasteners	0.0%
	1 PAF per Angle	-73.2%
	2 PAFs per Angle	-77.2%
	2 Holes per Angle	-74.3%

Notes: Decreases are reported with respect to the specimens with no fasteners

Chapter 5:

Joist Material Properties

5.1 GENERAL

In order to ascertain the material properties of the joists used in the testing program, a series of material tests was performed. The results from the material tests were used to assist in the analysis of the test data.

5.2 COUPON DESCRIPTION

Material samples were extracted from the upper chord, lower chord, and the first compression diagonal of both the 16K2 and 26K5 joists. These locations correspond to the chord members that were instrumented with strain gages during the testing program. The material samples were extracted from surplus joists that were not used in any previous tests. This was deemed appropriate because the chord members of the surplus joists were rolled from the same heats of steel as the chord members of the tested joists.

The material samples were machined into tension coupons according to current ASTM standards (American 1996). Coupon configurations with reduced overall dimensions were used due to the limitations on the length and width of the material samples. The different shapes of the material samples required that both rectangular and round specimens be used. The round specimens were used for the diagonals of the 16K2 joists. All other material samples consisted of angle

members which were made into rectangular coupons. A list of the tension coupons used for this testing program is shown in Table 5.1.

The configuration for the rectangular coupons is shown in Figure 5.1. The coupons had an overall width of 0.75" and an overall length which varied between 14 and 16 inches, depending on the rough length of the material sample. The reduced section for each of these samples measured 0.5" in width and 3" in length. This was used to support an extensometer with a 2 inch gage length. The thickness of the coupons corresponded to the original thickness of the sample. One rectangular coupon was machined from each leg of the angle member provided, as shown in Figure 5.1.

The configuration for the round coupons is shown in Figure 5.2. These coupons had an overall length of 10 inches and an overall width of 19/32 inch. They had a reduced section which measured 3 inches in length and 0.35" in diameter. A 2 inch gage length was also used for the round coupons. The overall diameter of the coupon corresponded to the original diameter of the compression diagonal sample.

5.3 TESTING

The tension coupons were tested in a Tinius Olsen testing machine, which is shown in Figure 5.3. The testing machine had a stationary upper cross-head and a movable lower cross-head. A screw apparatus provided the drive mechanism for the lower cross-head. The lower cross-head moved at a constant rate which was controlled by the operator. The specimen was held by a pair of

vice grips which were connected to the upper and lower cross-heads. The orientation of the tension coupon in the testing machine is shown in Figure 5.4.

Each coupon was instrumented with an extensometer. The extensometer measured the elongation of the coupon over its 2 inch gage length. A computerized data acquisition system was used to the record the data sets for each test. The data sets included information on the elongation of the coupon over the gage length and the load acting on the coupon. This information was then used to determine the stress-strain response of the material. In addition, a series of values were manually recorded from the testing machine to supplement the computerized data.

Three sets of dynamic and static yield loads were recorded during each test. Each static yield load was reached following a 3 minute pause in loading of the coupon. This time period was adequate in allowing the full relaxation of the coupon. Dynamic yield values were taken with the machine cross-head in motion along the yield plateau.

Two different cross-head rates were used during each test. A cross-head rate of 0.02 in./min. was used in the range up to the initial strain-hardening of the material. A cross-head rate of 0.05 in./min. was used in the range from initial strain-hardening through fracture of the material. These cross-head rates were used consistently during each test to minimize any variation in the material properties caused by strain rate effects.

In order to determine the elongation of the coupon, a set of two gage marks, spaced at approximately 2 inches, was placed on each coupon before

loading. The initial and final distance between the gage marks were used to determine the elongation.

5.4 RESULTS

The data set recorded for each test was used to determine both the dynamic and static yield stresses, the dynamic ultimate strength, and the percent elongation of the material. Table 5.2 shows the results from the material testing program. The average values from each of the coupon groups were used in the analysis of the joist data.

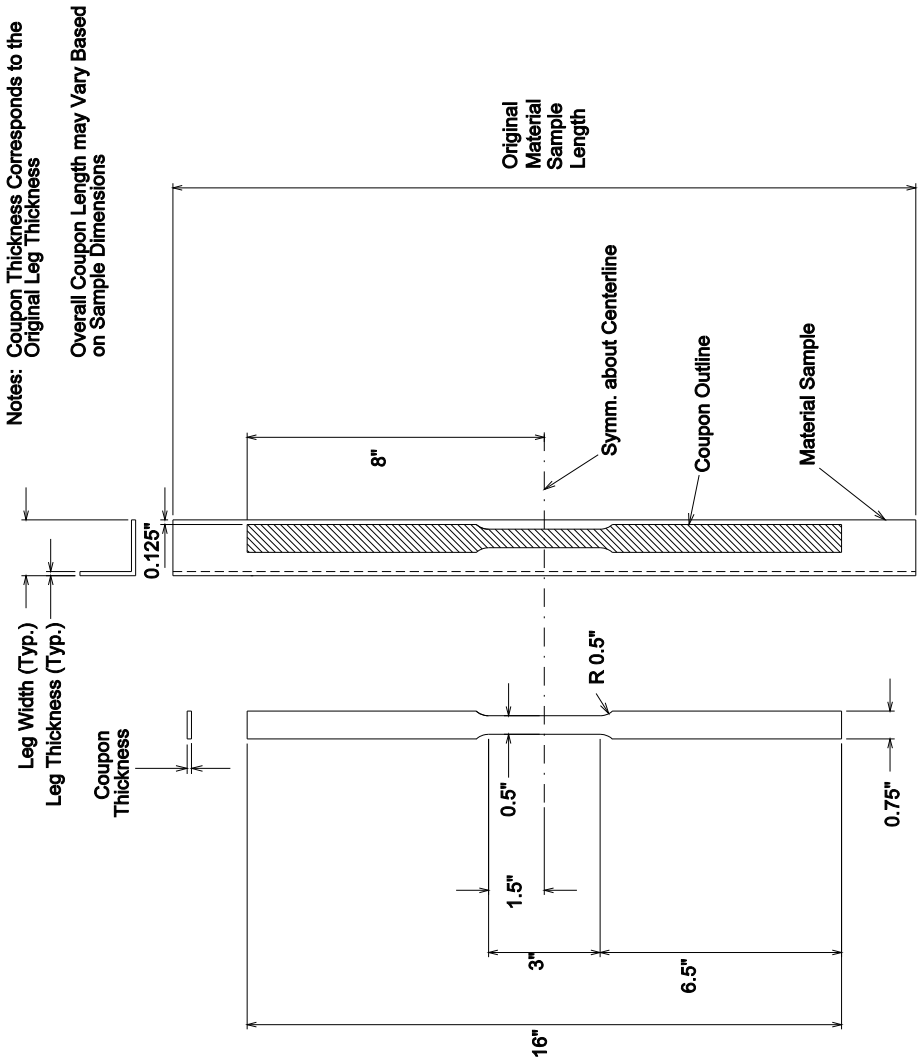

Figure 5.1 Rectangular Coupon Configuration

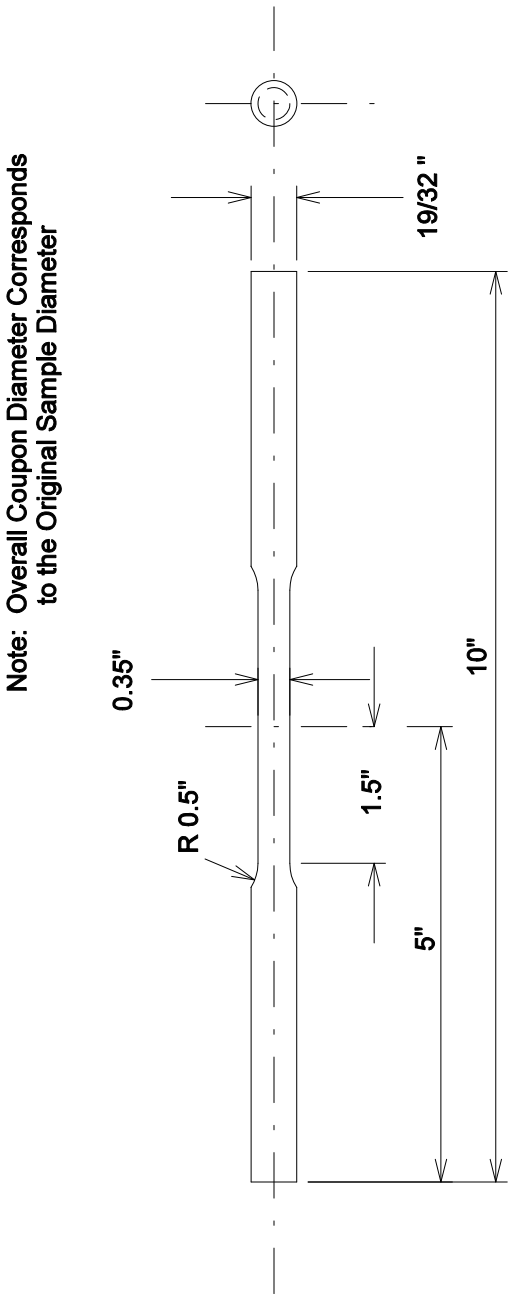

Figure 5.2 Round Coupon Configuration

Figure 5.3 Testing Machine Used for Tension Coupons

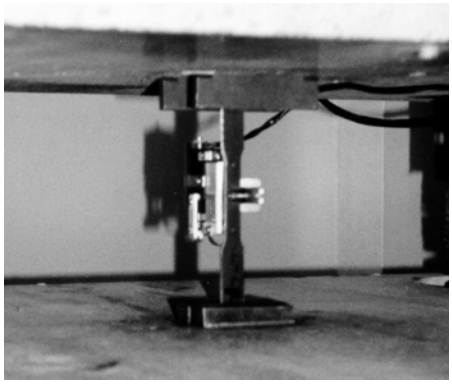

Figure 5.4 Orientation of Tension Coupon in Testing Machine

Table 5.1 Description of Tension Coupons

Coupon Designation	Coupon Type	Joist Type	Sample Location	Number of Coupons
16K2-TC	Rectangular	16K2	Top Chord	3
16K2-BC	Rectangular	16K2	Bottom Chord	3
16K2-CD	Round	16K2	Diagonal Member	3
26K5-TC	Rectangular	26K5	Top Chord	3
26K5-BC	Rectangular	26K5	Bottom Chord	3
26K5-CD	Rectangular	26K5	Diagonal Member	3

Table 5.2 Results of Material Testing Program

Joist Series	Location	Coupon Designation	Dynamic Yield (ksi)	Static Yield (ksi)	Dynamic Ultimate (ksi)	% Elongation
16K2	Top Chord	16K2-TC-1	58.1	54.7	77.9	31.2%
		16K2-TC-2	55.4	51.1	75.2	31.6%
		16K2-TC-3	55.8	51.7	75.6	31.3%
		Average	**56.4**	**52.5**	**76.2**	**31.4%**
	Bottom Chord	16K2-BC-1	56.7	53.5	75.9	31.4%
		16K2-BC-2	57.3	54.2	76.6	29.0%
		16K2-BC-3	55.9	51.8	74.2	30.6%
		Average	**56.6**	**53.2**	**75.6**	**30.3%**
	Diagonal	16K2-CD-1	56.0	52.0	80.6	30.6%
		16K2-CD-2	55.8	52.2	80.6	28.5%
		16K2-CD-3	56.3	51.8	80.1	28.0%
		Average	**56.0**	**52.0**	**80.4**	**29.0%**
26K5	Top Chord	26K5-TC-1	60.8	56.9	80.8	27.8%
		26K5-TC-2	60.0	56.0	84.7	30.0%
		26K5-TC-3	60.2	56.1	84.7	28.5%
		Average	**60.3**	**56.3**	**83.4**	**28.8%**
	Bottom Chord	26K5-BC-1	61.0	56.9	74.8	29.0%
		26K5-BC-2	58.8	55.4	73.7	31.3%
		26K5-BC-3	59.3	55.7	74.4	30.1%
		Average	**59.7**	**56.0**	**74.3**	**30.1%**
	Diagonal	26K5-CD-1	60.0	56.2	85.0	29.6%
		26K5-CD-2	59.6	56.1	84.5	29.8%
		26K5-CD-3	59.8	56.5	85.0	31.1%
		Average	**59.8**	**56.3**	**84.8**	**30.2%**

Notes: Cross-head Rate: 0.02 in./min. up to initial strain hardening
0.05 in./min. from initial strain hardening through fracture

Elongation: % elongation based on a 2 inch gage length

Chapter 6:

Conclusions

A power actuated fastener is a mechanical fastener that provides a means for connecting steel elements. PAFs are an alternative to puddle welds for fastening roof deck to steel joists. PAFs may offer several advantages over puddle welds, including greater speed of installation and more consistent quality.

The acceptance of power actuated fasteners has been slow within the United States. This is related to an overall lack of familiarity and information on these fasteners. In addition, concerns have been raised that PAFs may damage the very thin top chord angles of roof joists and thereby impair the load capacity of the joists. Concerns have also been raised that PAF's may decrease the tensile capacity of joist members subjected to tensile loadings.

A large scale testing program was performed to address the above concerns. A series of ten full-scale roof subassemblages consisting of open web steel joists and roof deck were subjected to a slowly applied downward load until failure of the joists occurred. The objective of this investigation was to determine if the use of PAFs produced any detrimental effects on the vertical load capacity of the open web steel joists. An additional objective of this investigation was to further study the effects of PAFs on the behavior of double angle steel chord members subjected to tensile stress. To accomplish this, a series of tension tests on double angle chord members was completed.

The results of the tests on the roof subassemblages indicated that the use of PAF's to fasten metal roof deck to open web steel joists had no detrimental effect on the vertical load capacity of the joists. The performance of the specimens with PAFs was essentially identical to the specimens with puddle welds.

It was also found that any permanent distortions placed in the thin top chord members by the PAFs had no detrimental effect on the buckling capacity of those members or on the overall load capacity of the joists. The fasteners were also found to provide enough shear strength so that the deck served as an effective lateral brace in preventing out-of-plane movements of the chord members.

The results of the tension tests on double angle specimens indicated that the addition of PAFs or holes into the cross-section reduced the ultimate load capacities and elongation capacities of the specimens. In particular, the ultimate load capacities and elongation capacities of double angle specimens with PAFs resembled those of double angle specimens with drilled holes. Due to the limited size of the data set, it was recommended that additional testing be completed on similar types of specimens.

Appendix A:

Nominal and Measured Member Sizes for 16K2 and 26K5 Joists

Table A.1 Nominal Member Sizes for 16K2 Joists

Nominal Member Sizes for 16K2 Joists:	
Member Location	Member Size
Top Chord	2L 1-1/2 x 1-1/2 x 0.113
Bottom Chord	2L 1-1/4 x 1-1/4 x 0.109
A	9/16 Round
B	19/32 Round
C	19/32 Round
D	19/32 Round
E	19/32 Round
F	19/32 Round
G	19/32 Round
H	1/2 Round
I	1/2 Round
J	1/2 Round
K	1/2 Round
L	1/2 Round

Notes: All dimensions are in inches,
List to be used with Figure 2.1

Table A.2 Nominal Member Sizes for 26K5 Joists

Nominal Member Sizes for 26K5 Joists:	
Member Location	Member Size
Top Chord	2L 1-3/4 x 1-3/4 x 0.155
Bottom Chord	2L 1-1/2 x 1-1/2 x 0.123
A	7/8 Round
B	L 1 x 1 x 0.109
C	L 1-3/4 x 1-3/4 x 0.155
D	L 1 x 1 x 0.109
E	L 1 x 1 x 0.109
F	L 1-1/2 x 1-1/2 x 0.113
G	L 1 x 1 x 0.109
H	L 1 x 1 x 0.109
I	L 1-1/4 x 1-1/4 x 0.109

Notes: All dimensions are in inches,
List to be used with Figure 2.1

Table A.3 Measured Member Sizes for 16K2 Joists

Measured Member Sizes for 16K2 Joists:	
Member Location	Member Size
Top Chord	2L 1.518 x 1.518 x 0.113
Bottom Chord	2L 1.249 x 1.249 x 0.110
A	.573 Round
B	.601 Round
C	.594 Round
D	.598 Round
E	.596 Round
F	.598 Round
G	.593 Round
H	.509 Round
I	.508 Round
J	.506 Round
K	.508 Round
L	.507 Round

Notes: All dimensions are in inches,
List to be used with Figure 2.1

Table A.4 Measured Member Sizes for 26K5 Joists

Measured Member Sizes for 26K5 Joists:	
Member Location	Member Size
Top Chord	2L 1.754 x 1.754 x 0.164
Bottom Chord	2L 1.507 x 1.507 x 0.122
A	.861 Round
B	L 1.007 x 1.007 x 0.114
C	L 1.75 x 1.75 x 0.162
D	L 1.007 x 1.007 x 0.114
E	L 1.007 x 1.007 x 0.114
F	L 1.532 x 1.532 x 0.113
G	L 1.007 x 1.007 x 0.114
H	L 1.007 x 1.007 x 0.114
I	L 1.282 x 1.282 x 0.112

Notes: All dimensions are in inches,
List to be used with Figure 2.1

Appendix B:

Load vs. Displacement Response for Roof Subassemblages

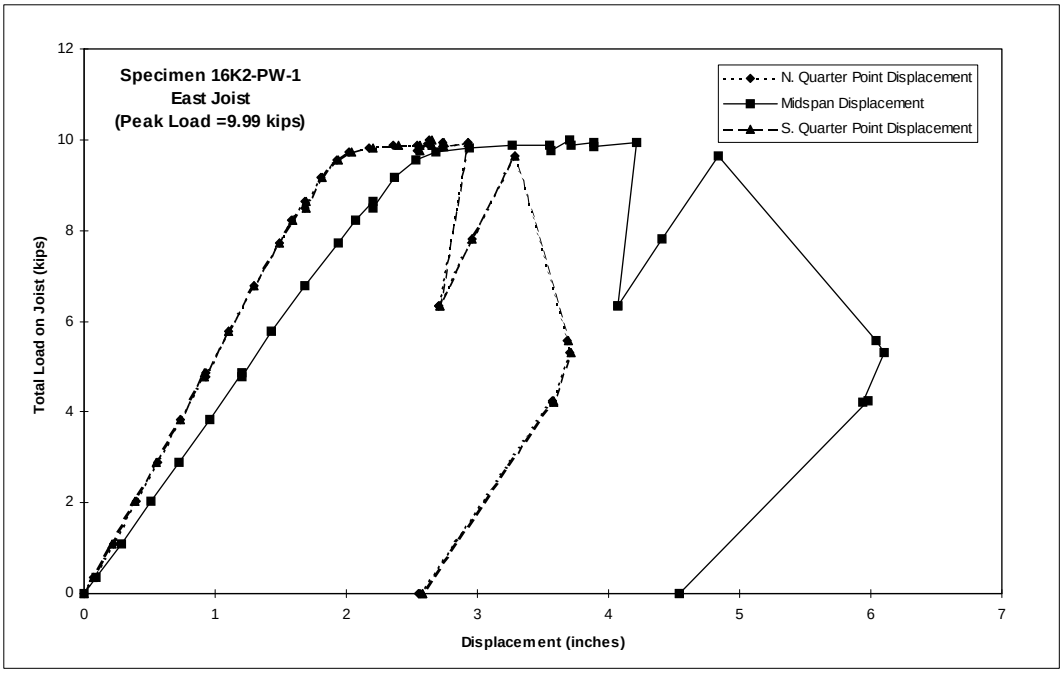

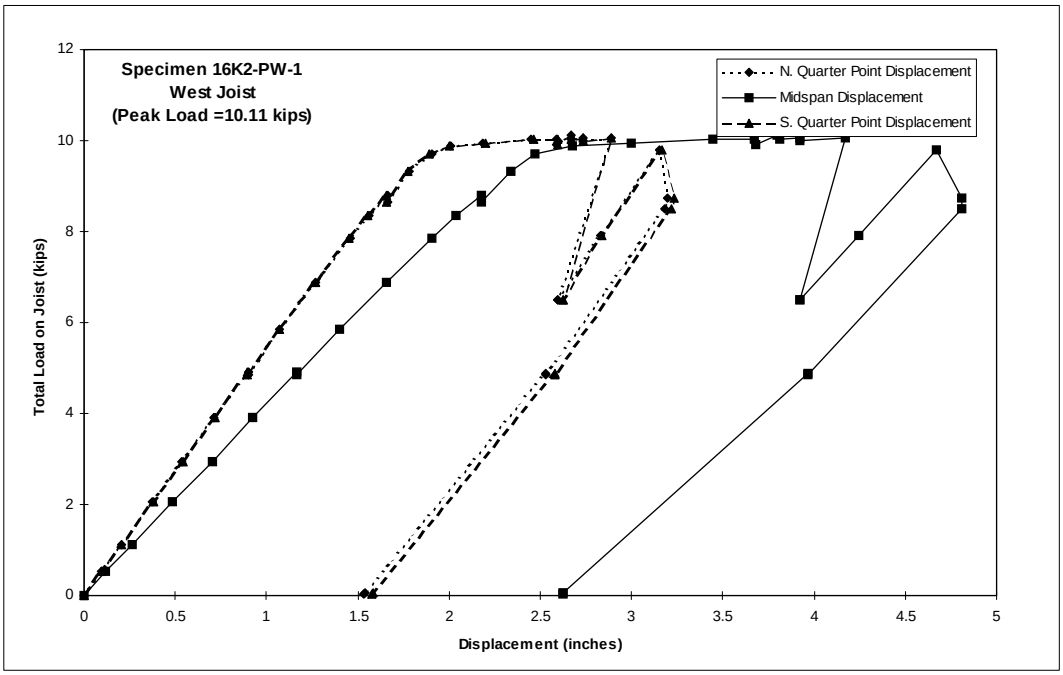

Figure B.1 Load vs. Displacement Response for Specimen 16K2-PW-1

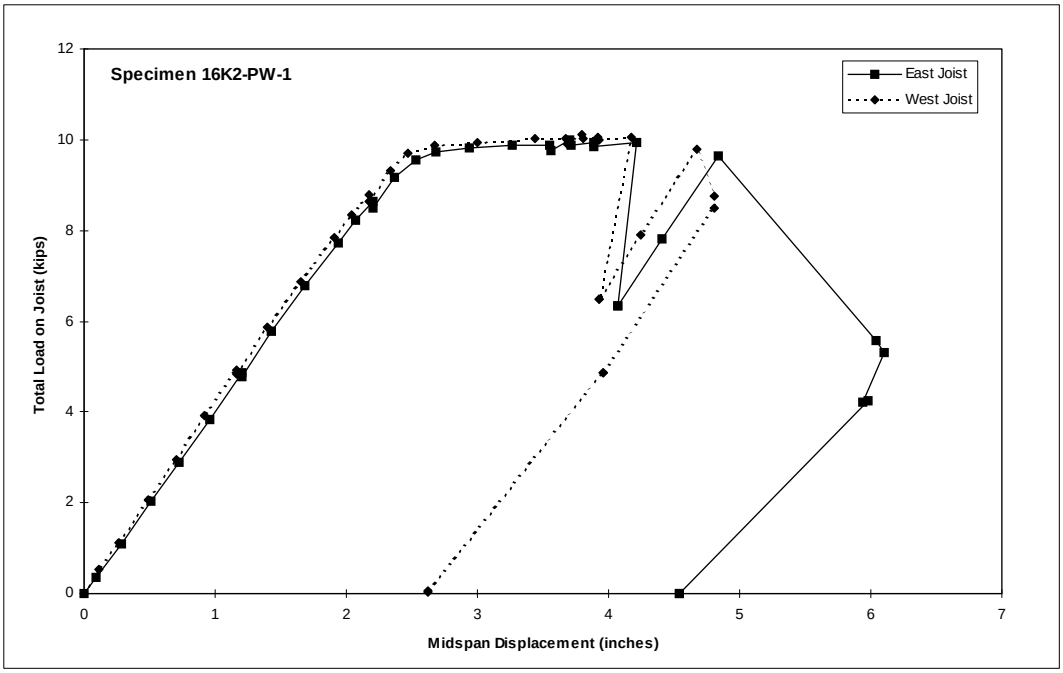

Figure B.2 Load vs. Midspan Displacement for 16K2-PW-1 East and West Joists

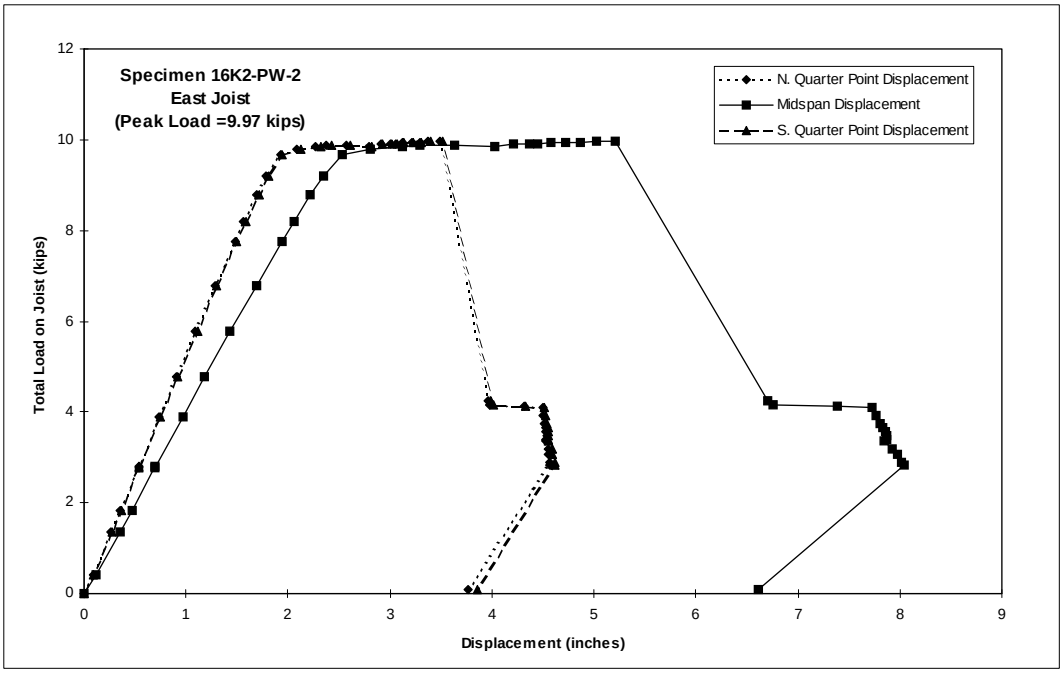

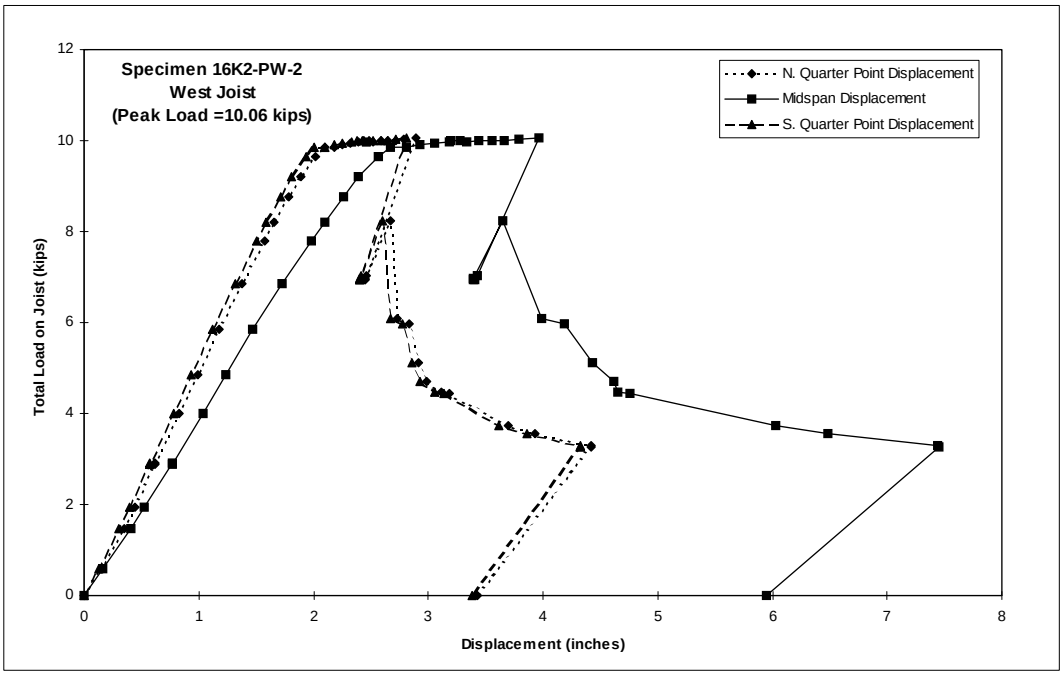

Figure B.3 Load vs. Displacement Response for Specimen 16K2-PW-2

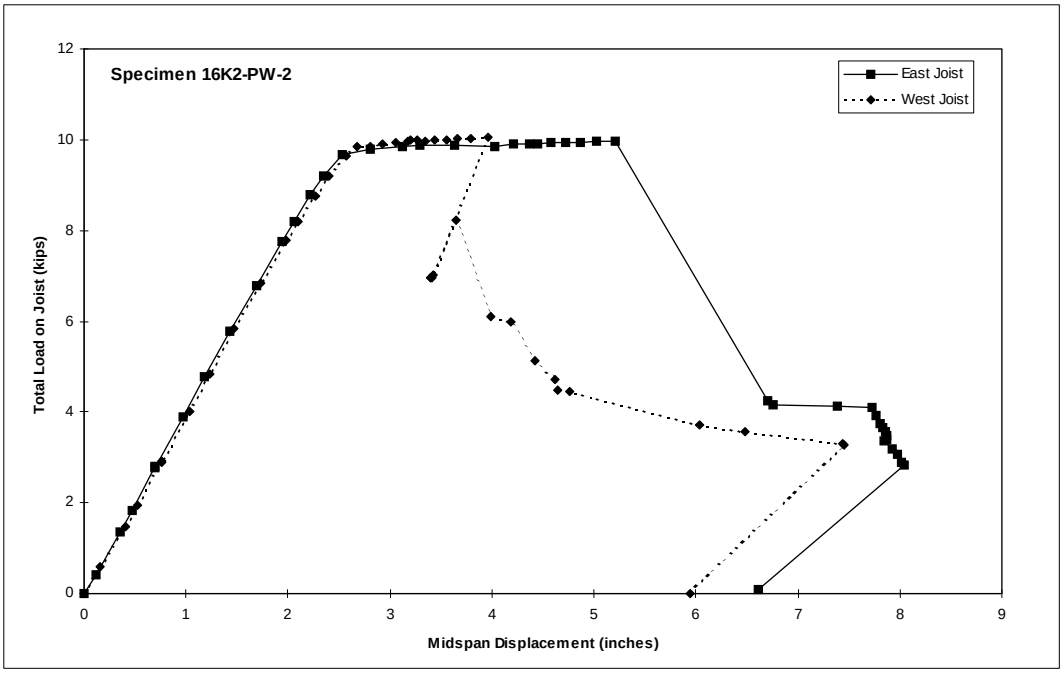

Figure B.4 Load vs. Midspan Displacement for 16K2-PW-2 East and West Joists

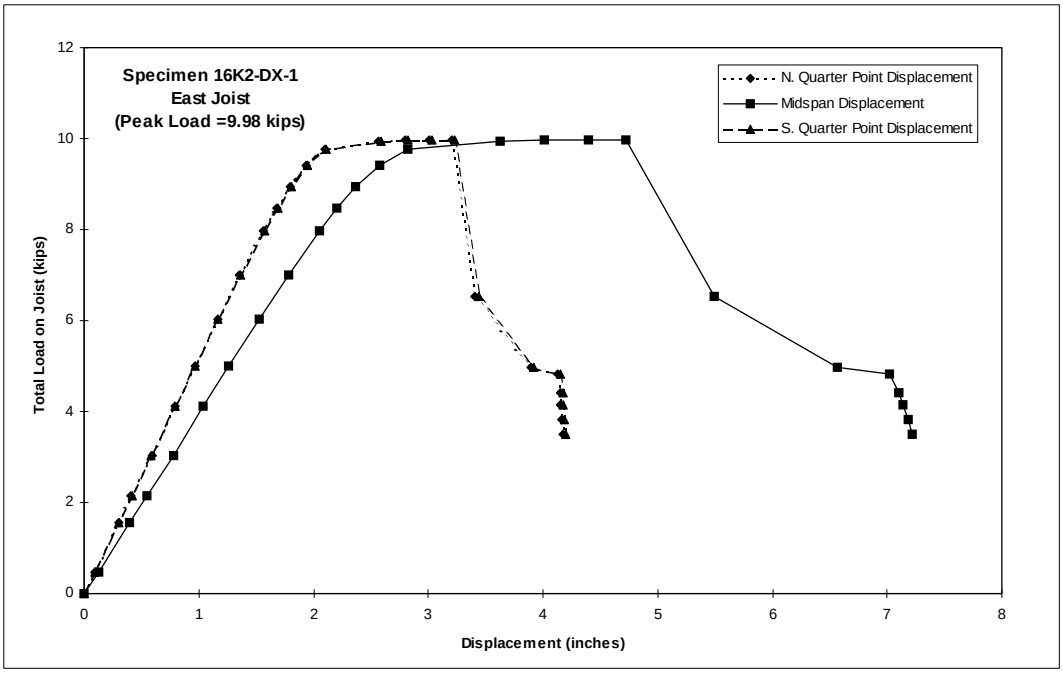

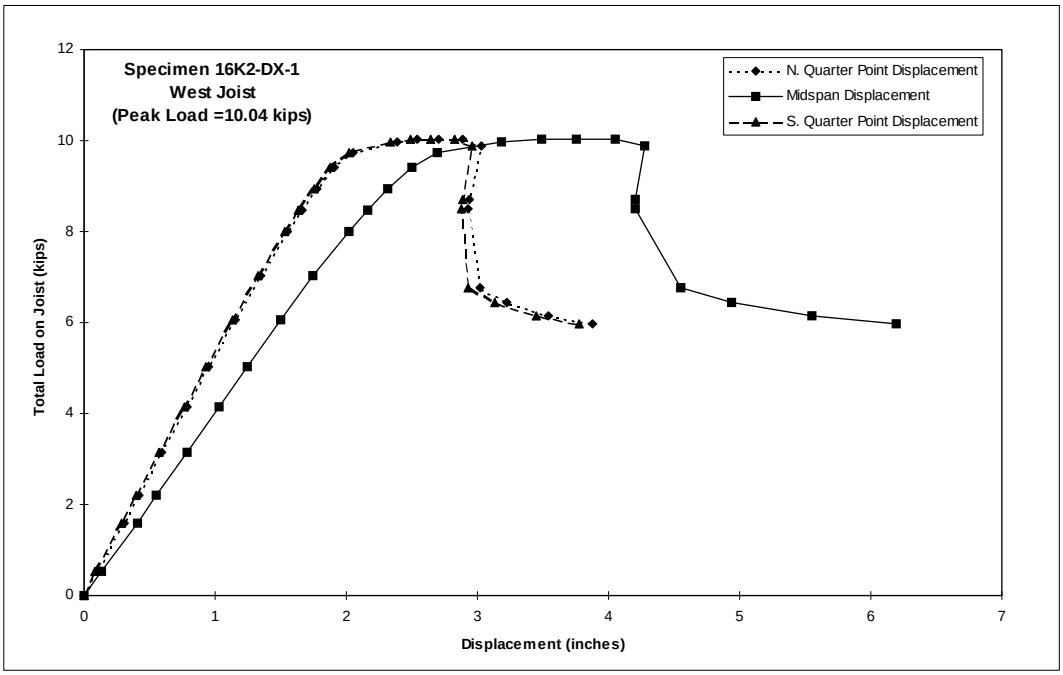

Figure B.5 Load vs. Displacement Response for Specimen 16K2-DX-1

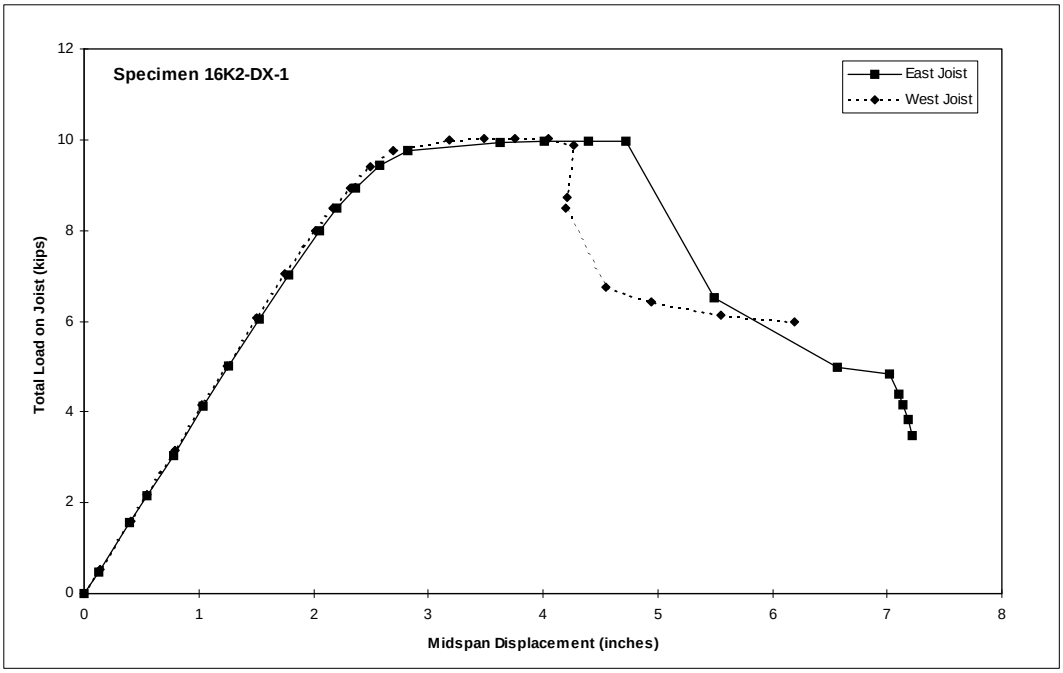

Figure B.6 Load vs. Midspan Displacement for 16K2-DX-1 East and West Joists

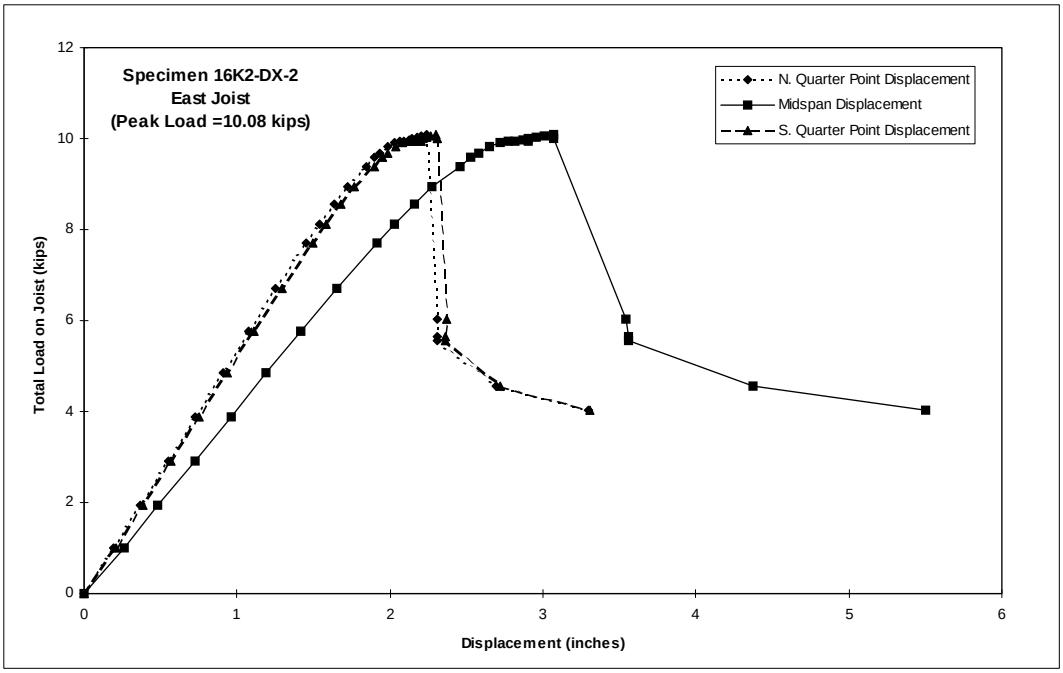

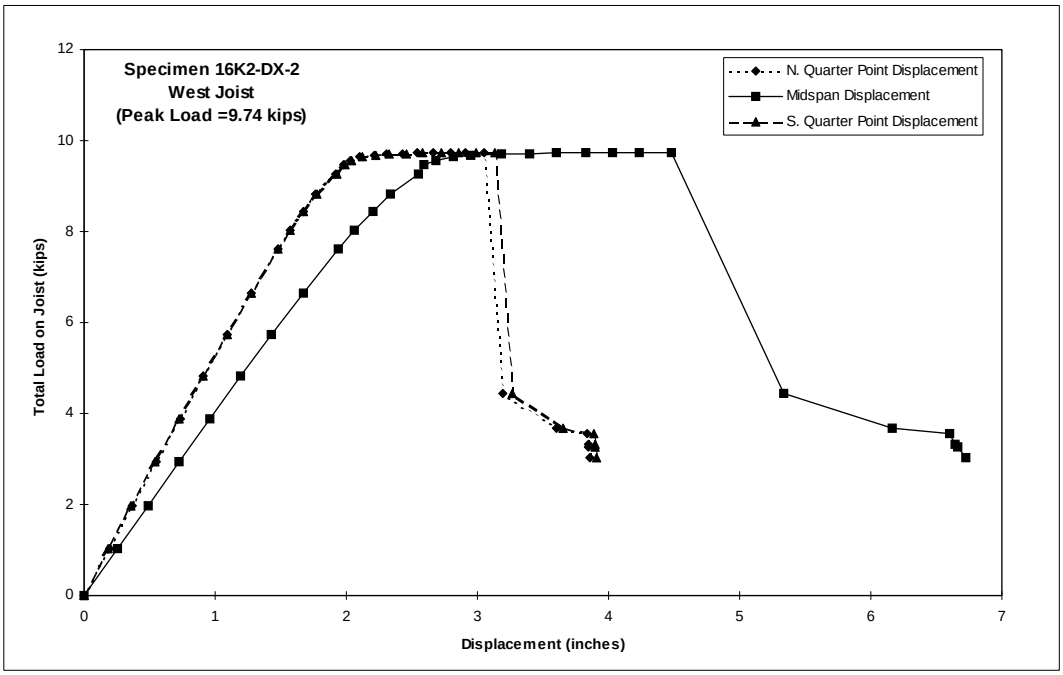

Figure B.7 Load vs. Displacement Response for Specimen 16K2-DX-2

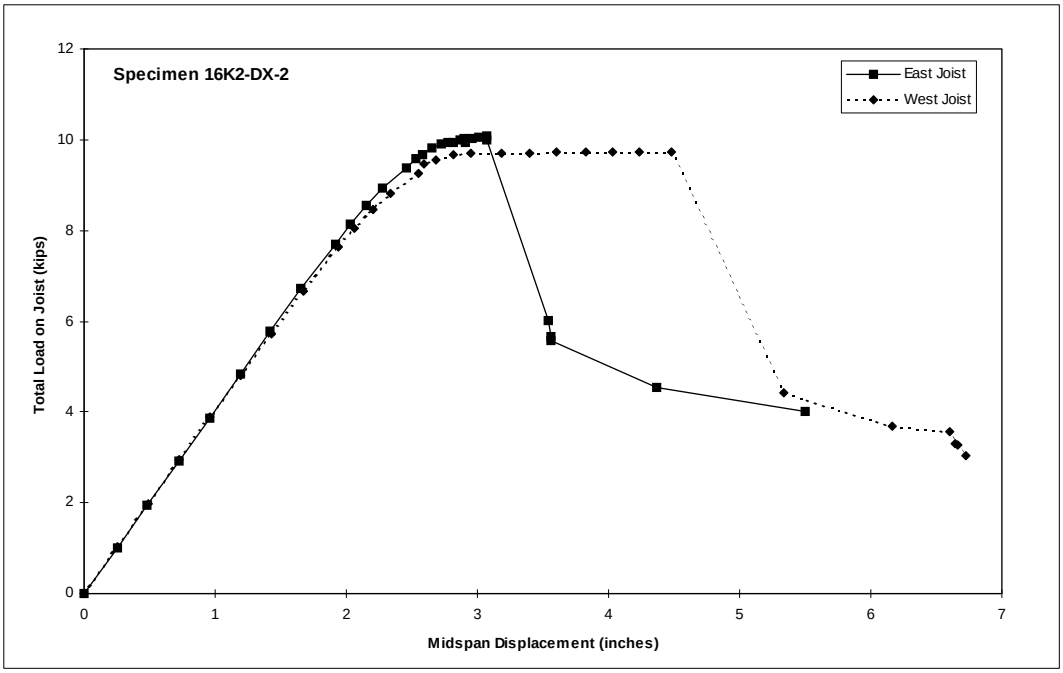

Figure B.8 Load vs. Midspan Displacement for 16K2-DX-2 East and West Joists

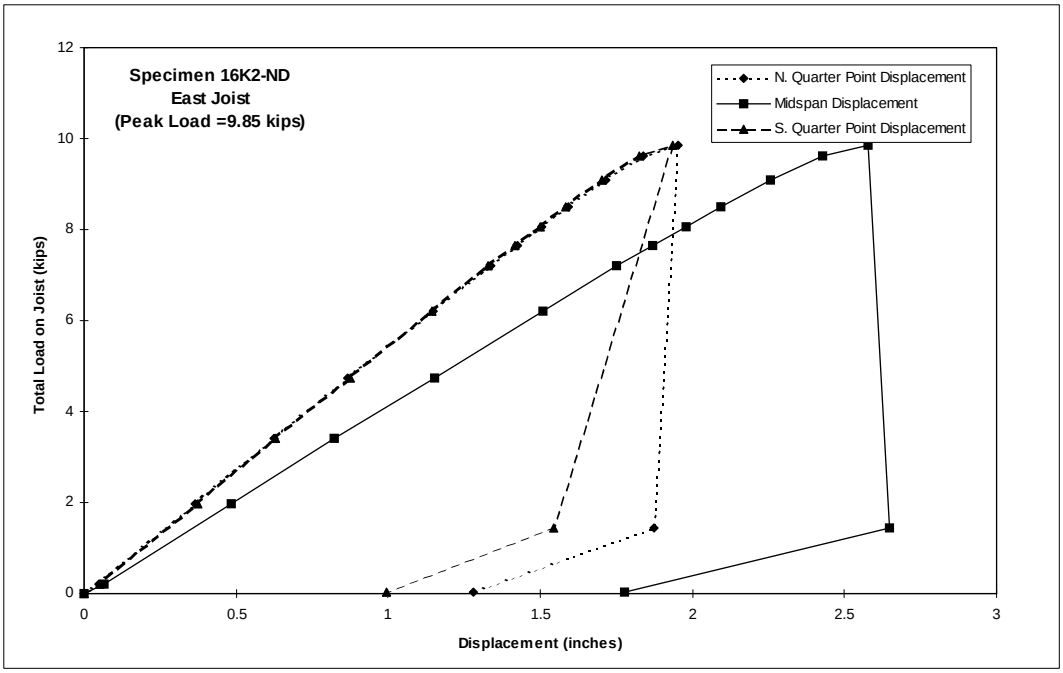

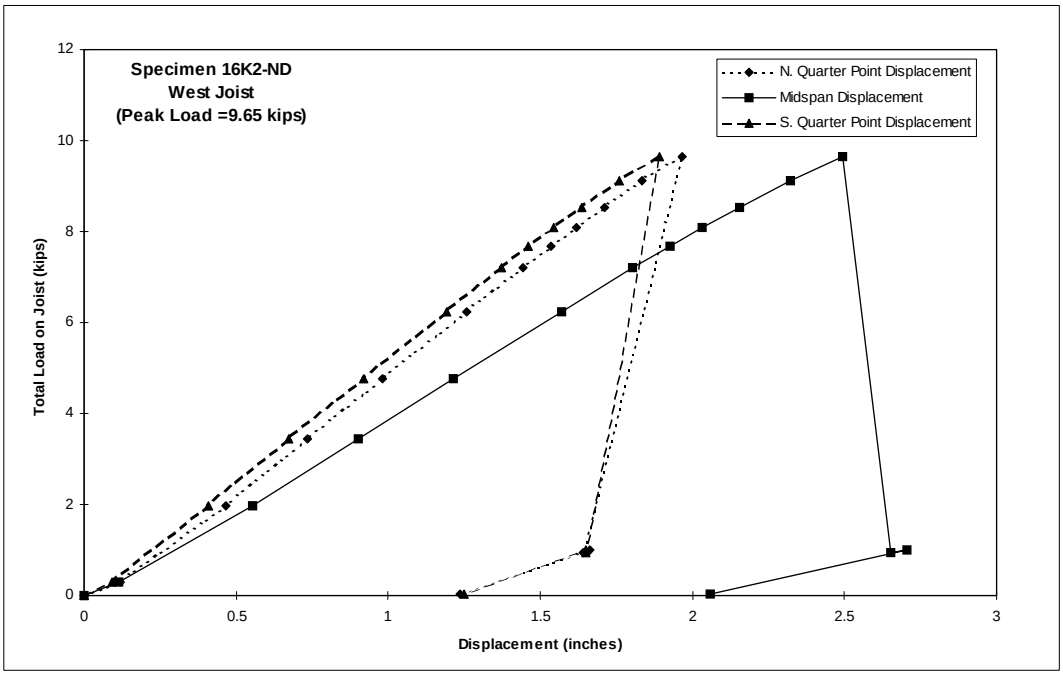

Figure B.9 Load vs. Displacement Response for Specimen 16K2-ND

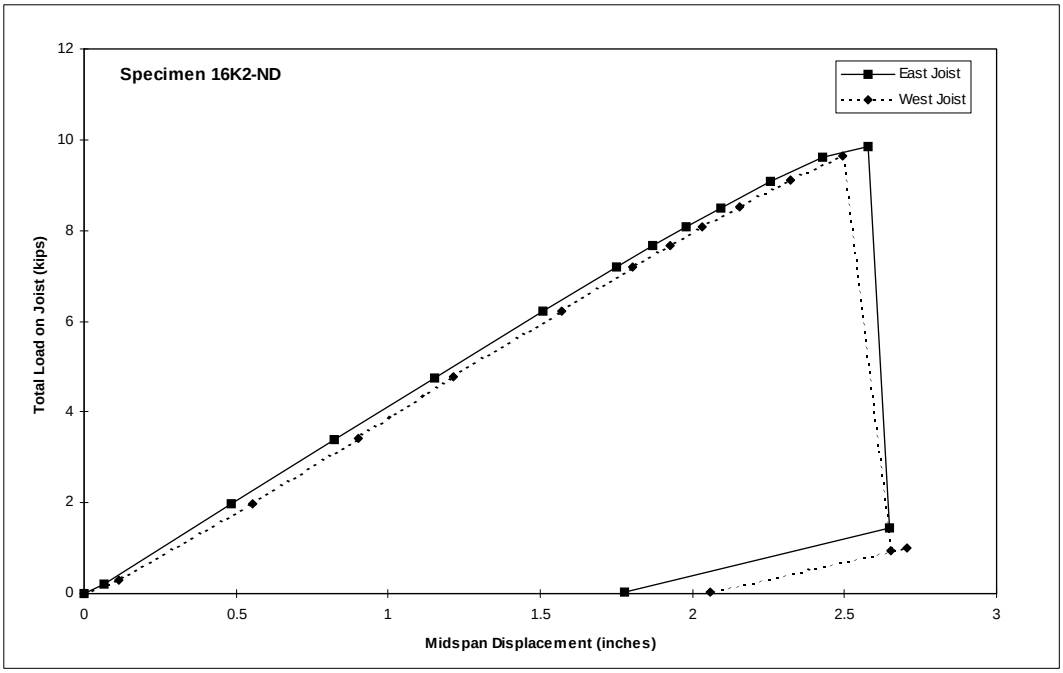

Figure B.10 Load vs. Midspan Displacement for 16K2-ND East and West Joists

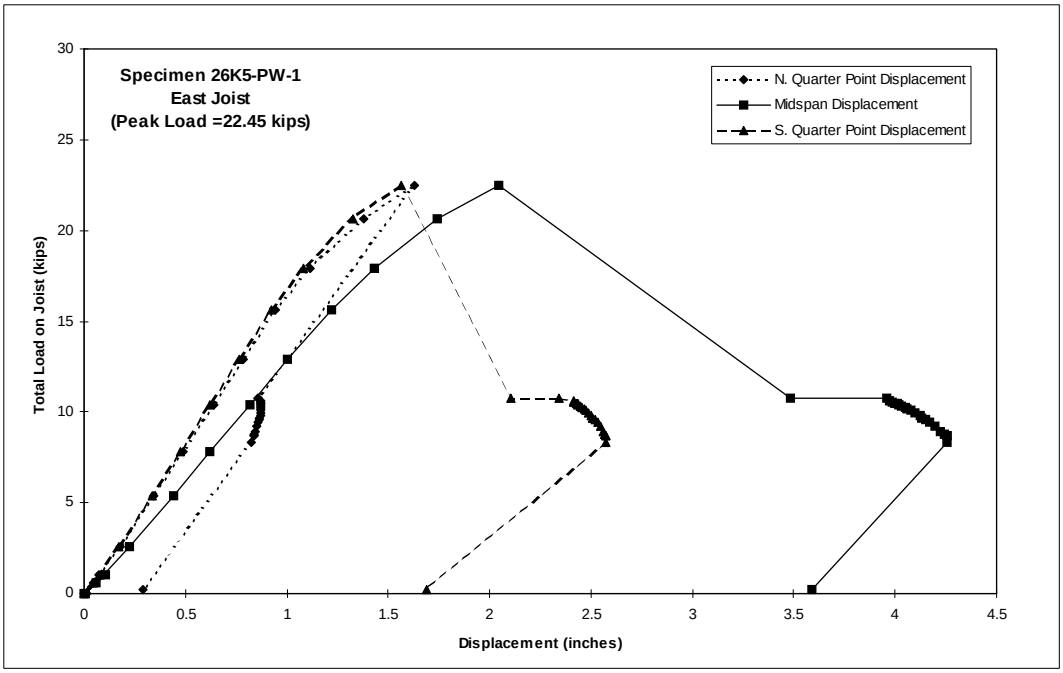

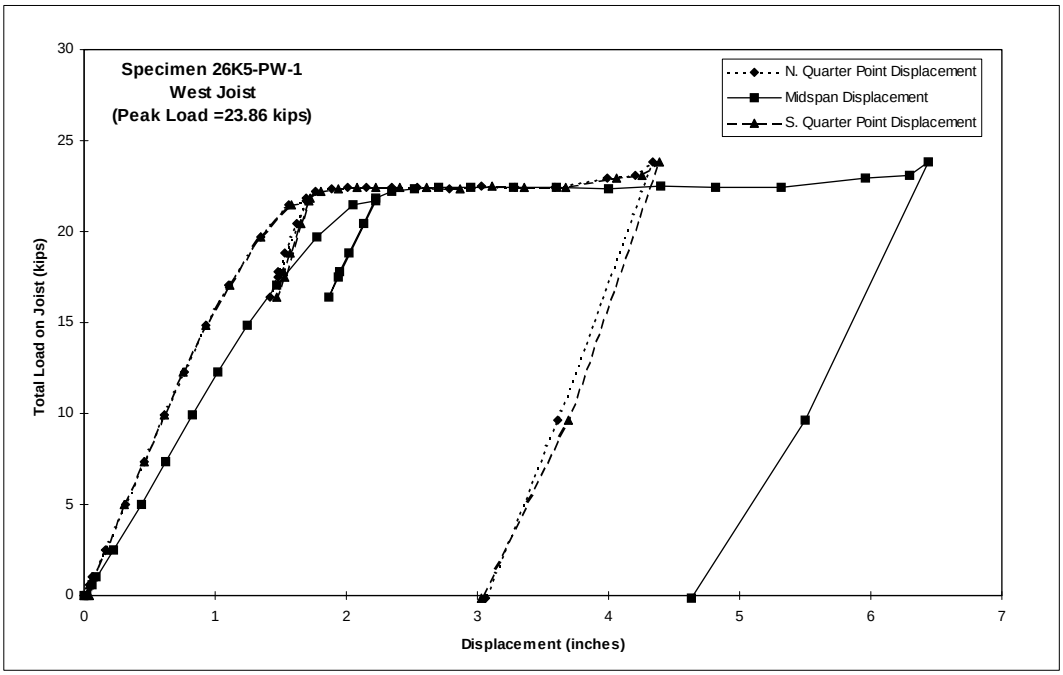

Figure B.11 Load vs. Displacement Response for Specimen 26K5-PW-1

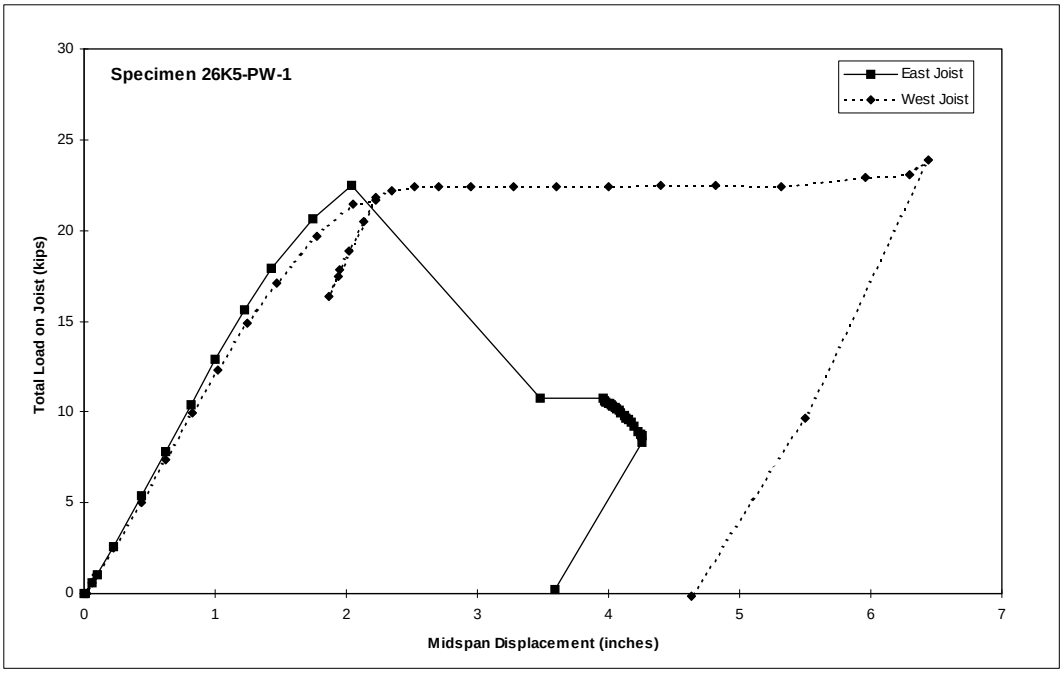

Figure B.12 Load vs. Midspan Displacement for 26K5-PW-1 East and West Joists

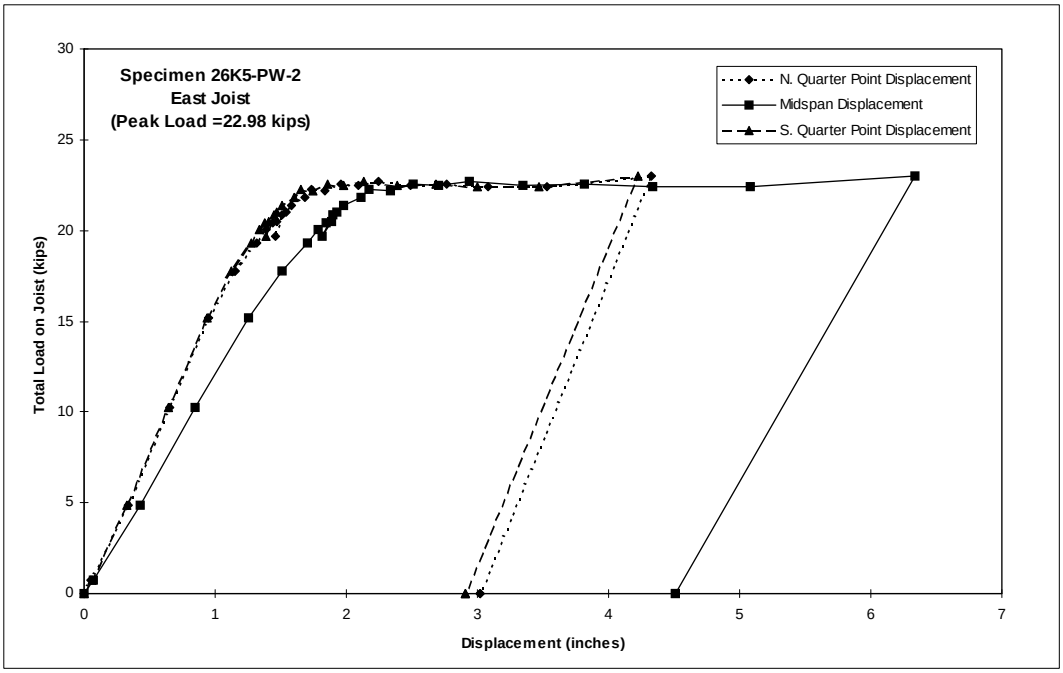

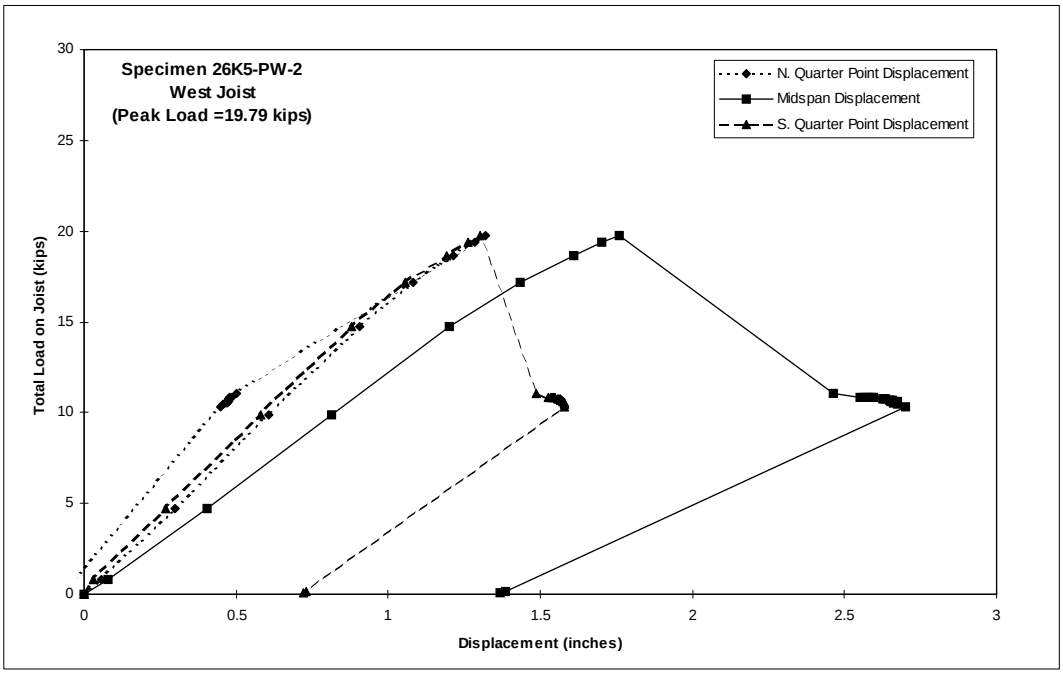

Figure B.13 Load vs. Displacement Response for Specimen 26K5-PW-2

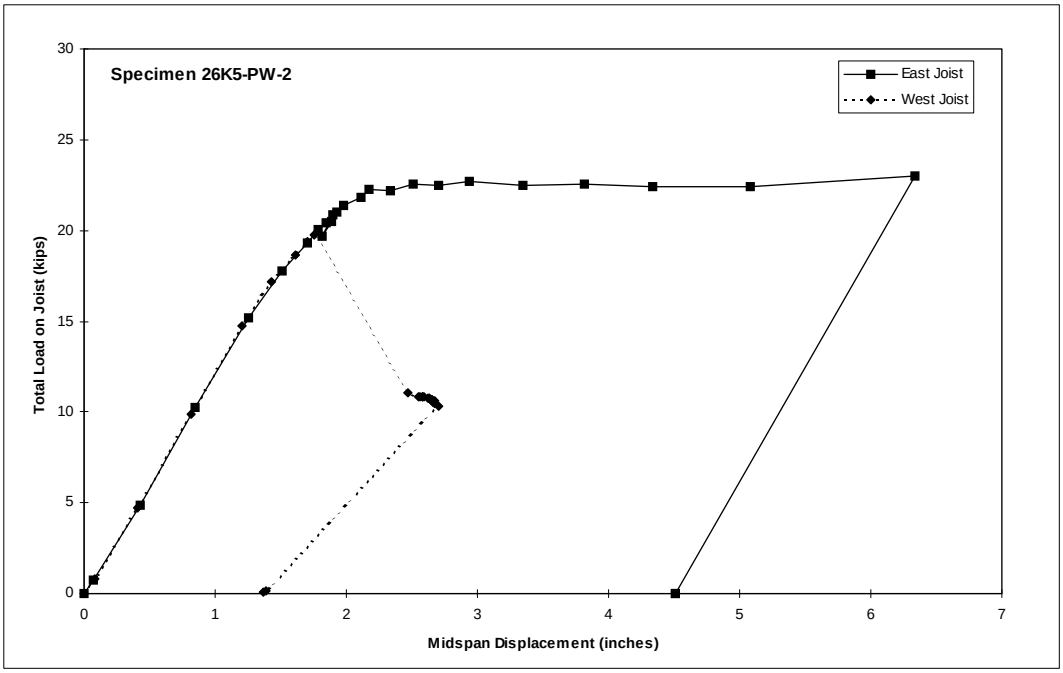

Figure B.14 Load vs. Midspan Displacement for 26K5-PW-2 East and West Joists

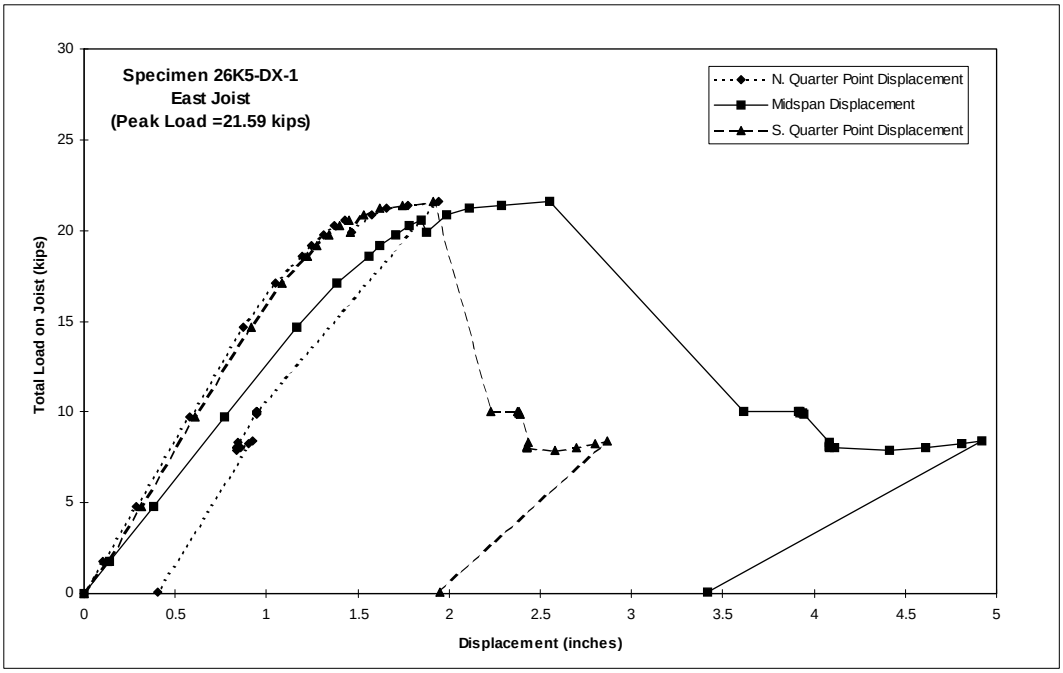

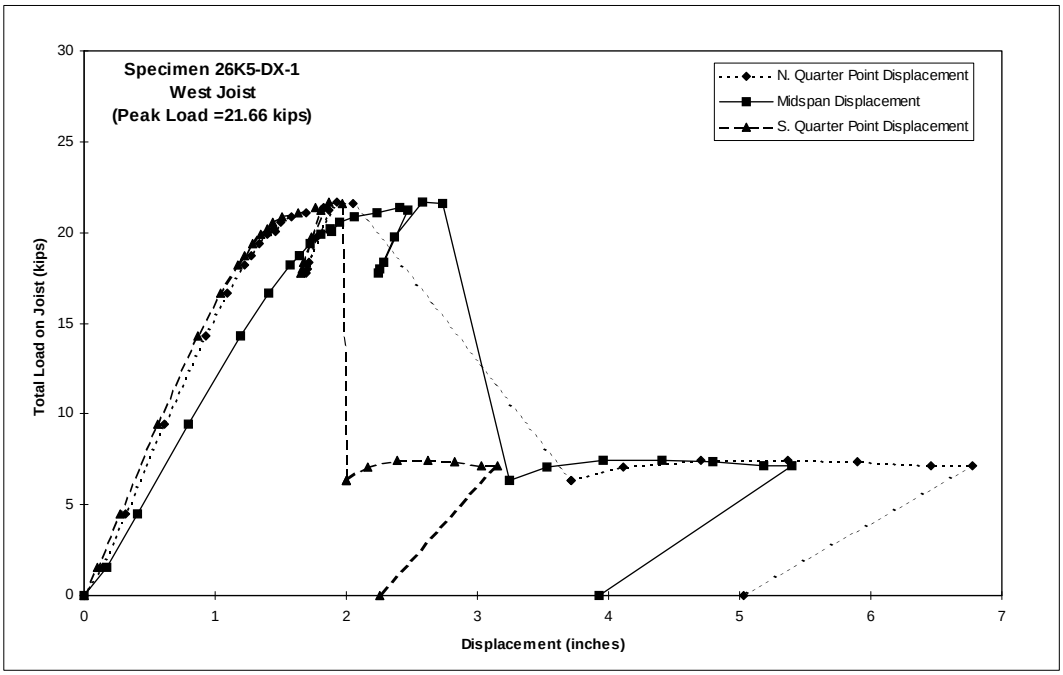

Figure B.15 Load vs. Displacement Response for Specimen 26K5-DX-1

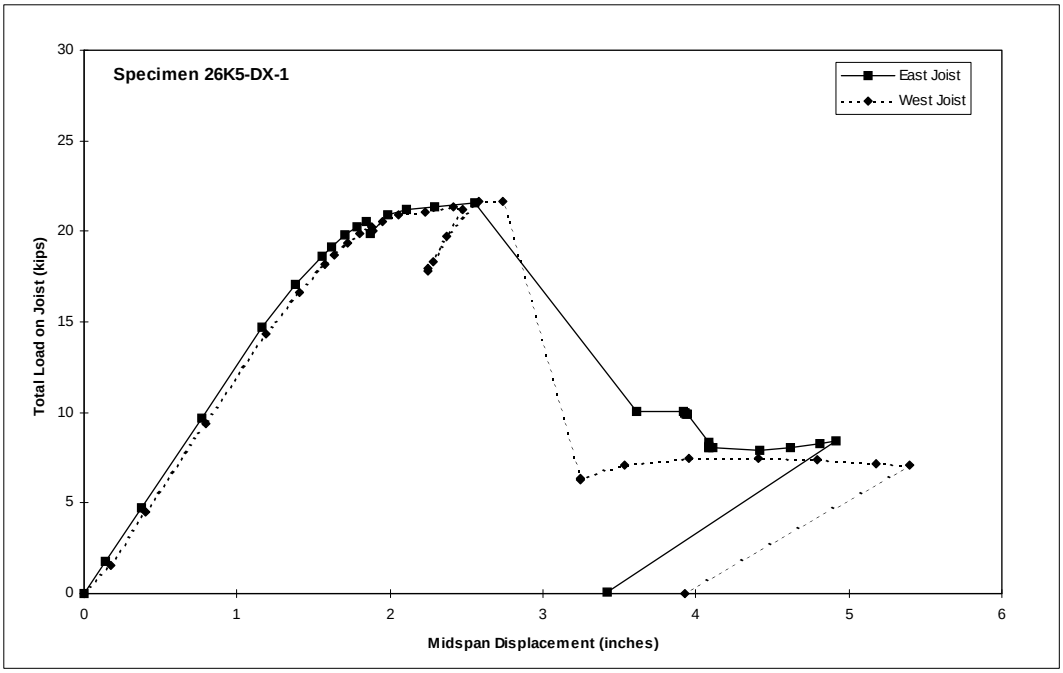

Figure B.16 Load vs. Midspan Displacement for 26K5-DX-1 East and West Joists

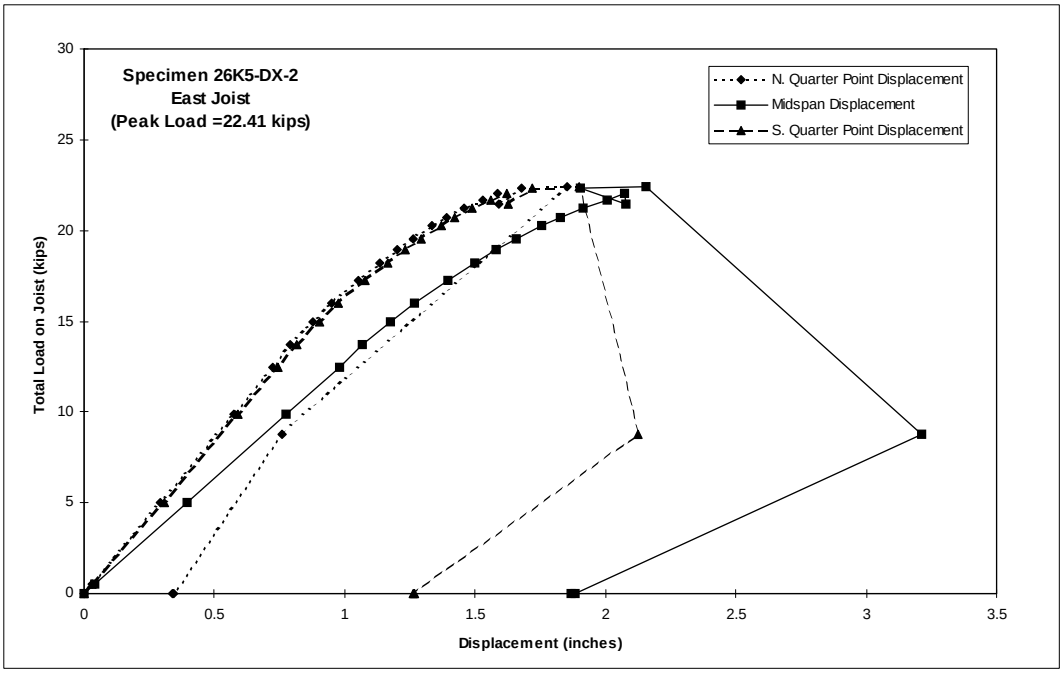

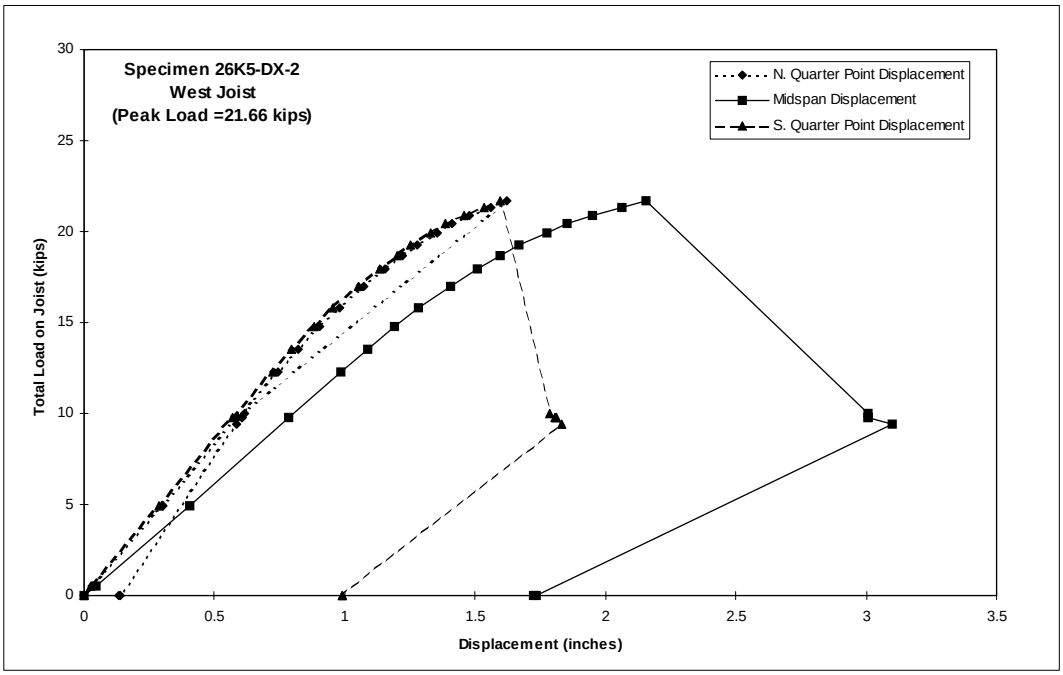

Figure B.17 Load vs. Displacement Response for Specimen 26K5-DX-2

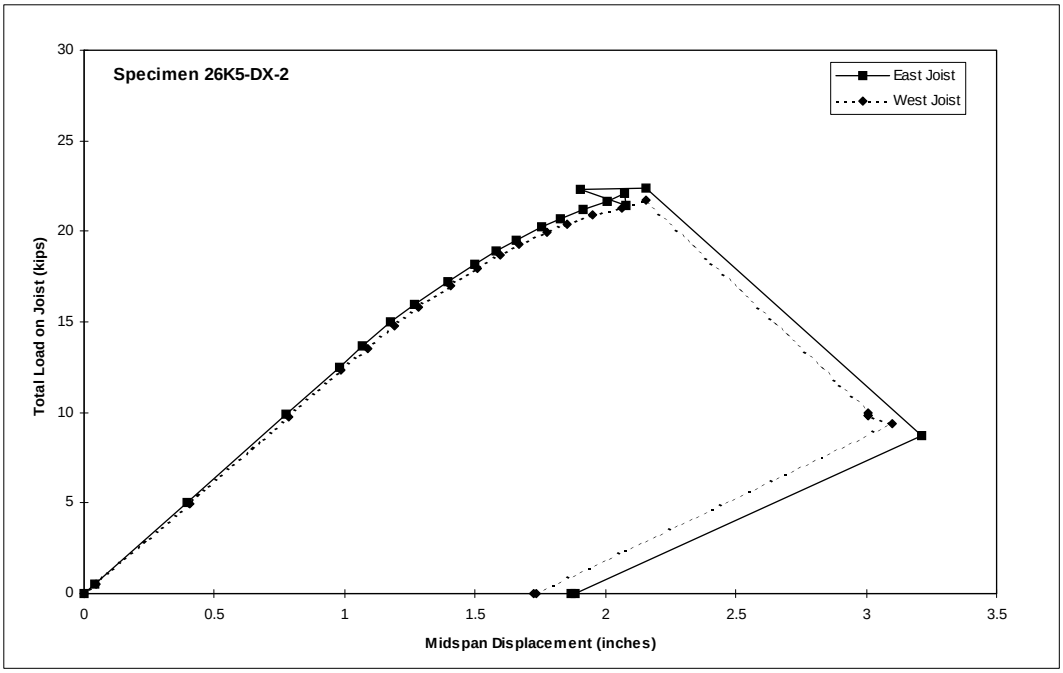

Figure B.18 Load vs. Midspan Displacement for 26K5-DX-2 East and West Joists

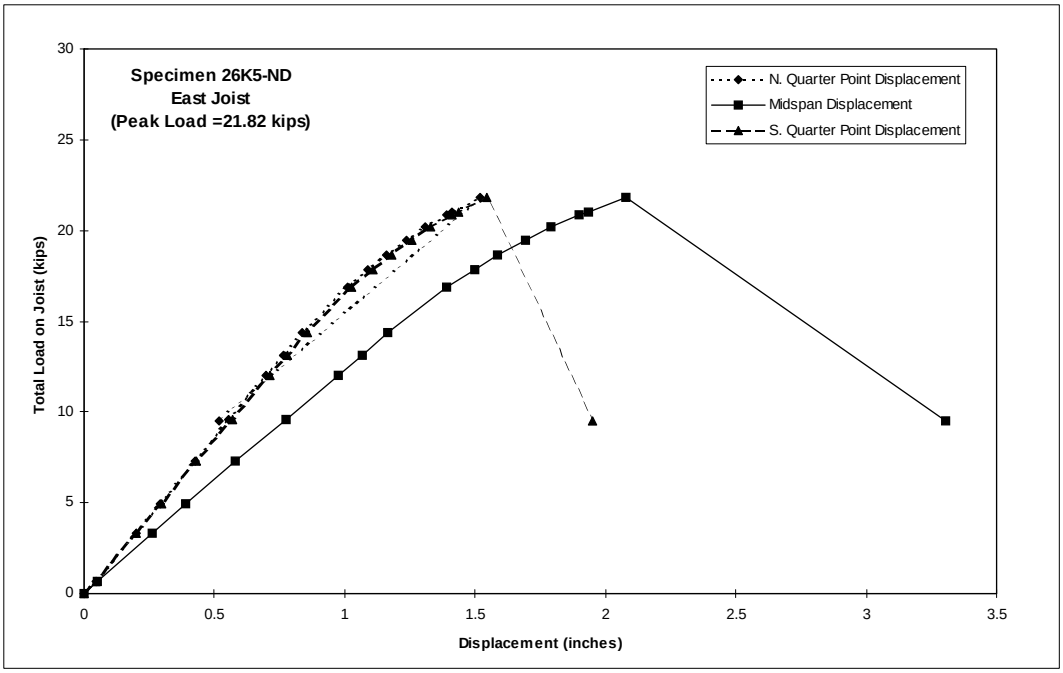

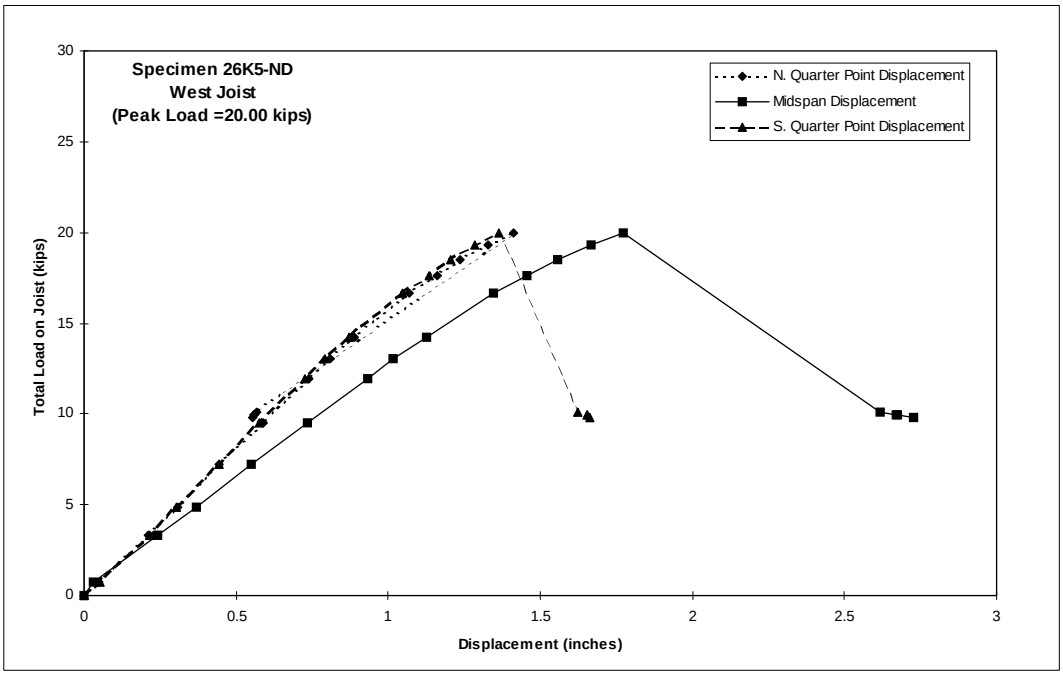

Figure B.19 Load vs. Displacement Response for Specimen 26K5-ND

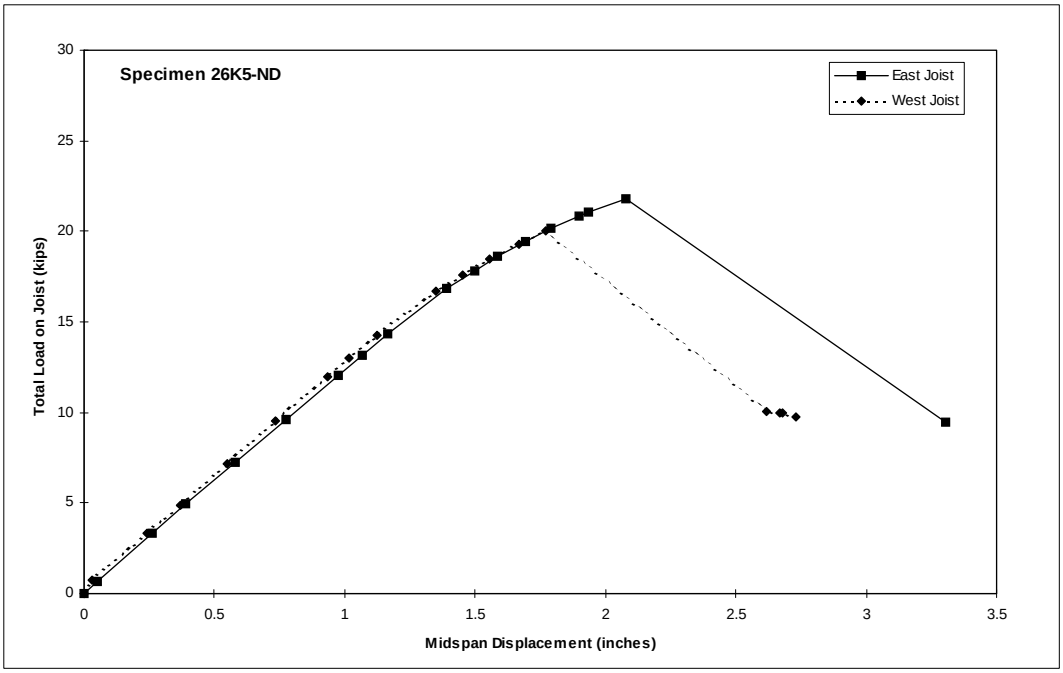

Figure B.20 Load vs. Midspan Displacement for 26K5-ND East and West Joists

Appendix C:

Results from Instrumented Members

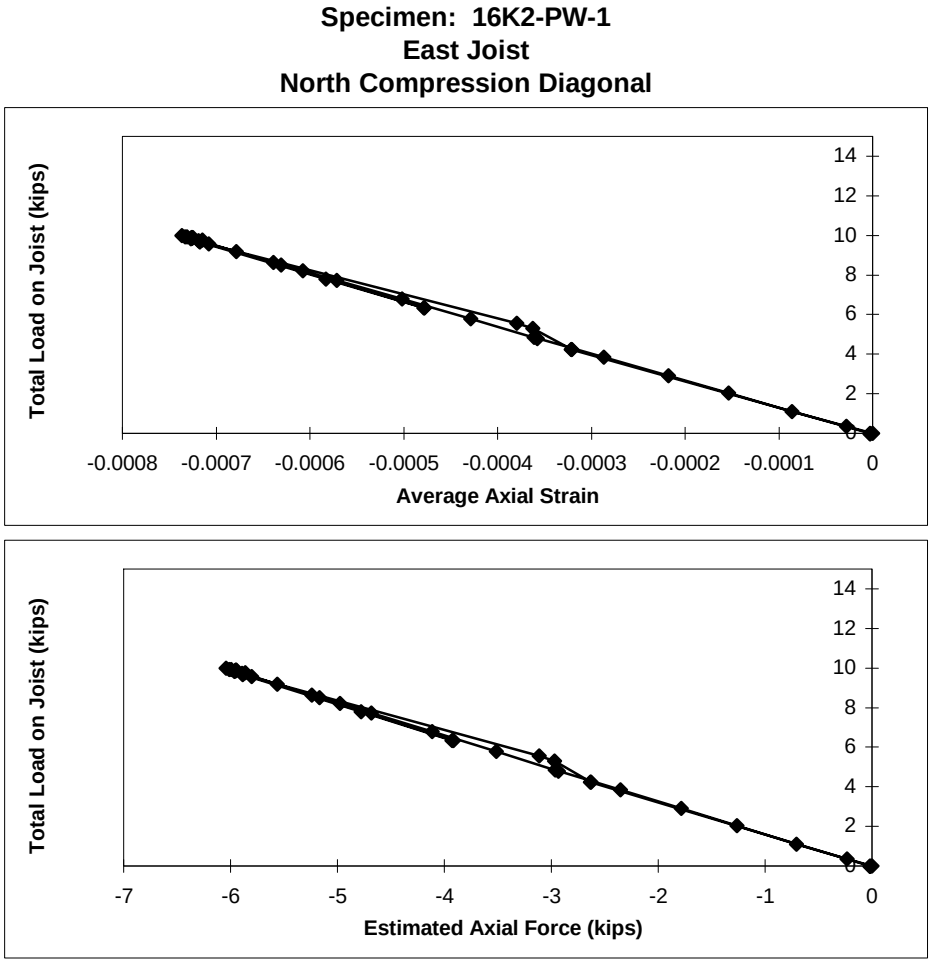

Figure C.1 16K2-PW-1 East Joist North Compression Diagonal

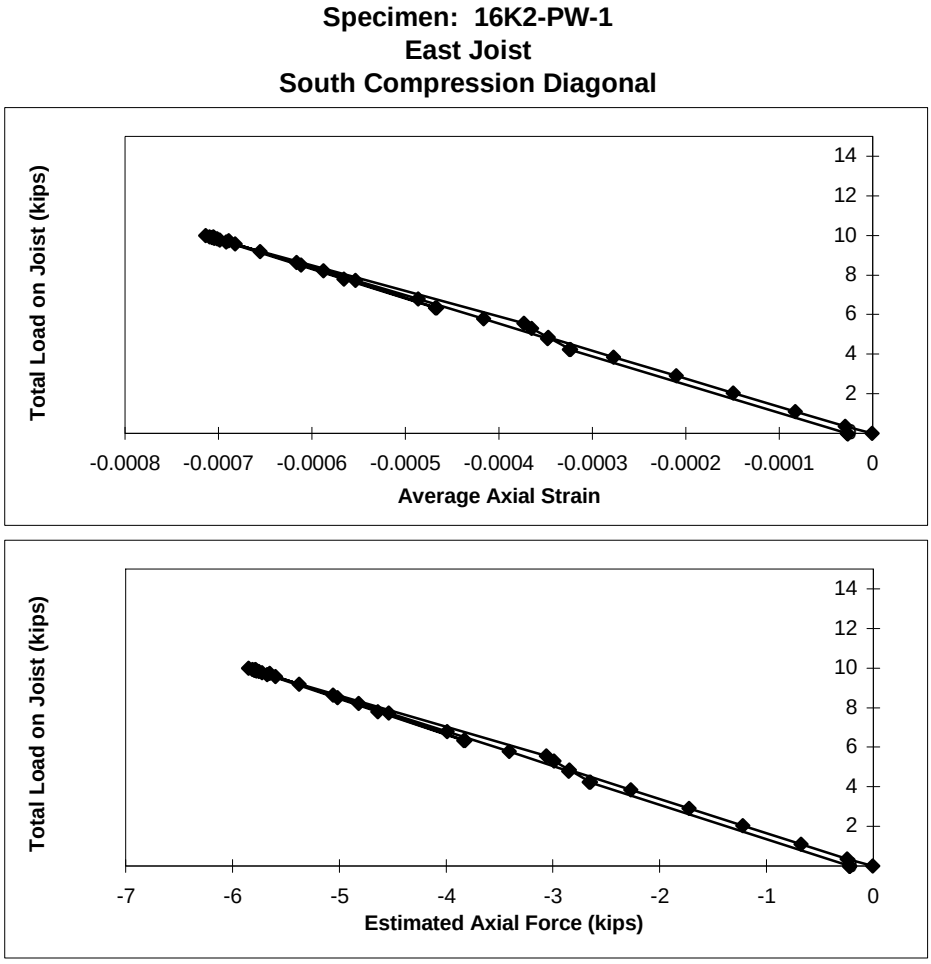

Figure C.2 16K2-PW-1 East Joist South Compression Diagonal

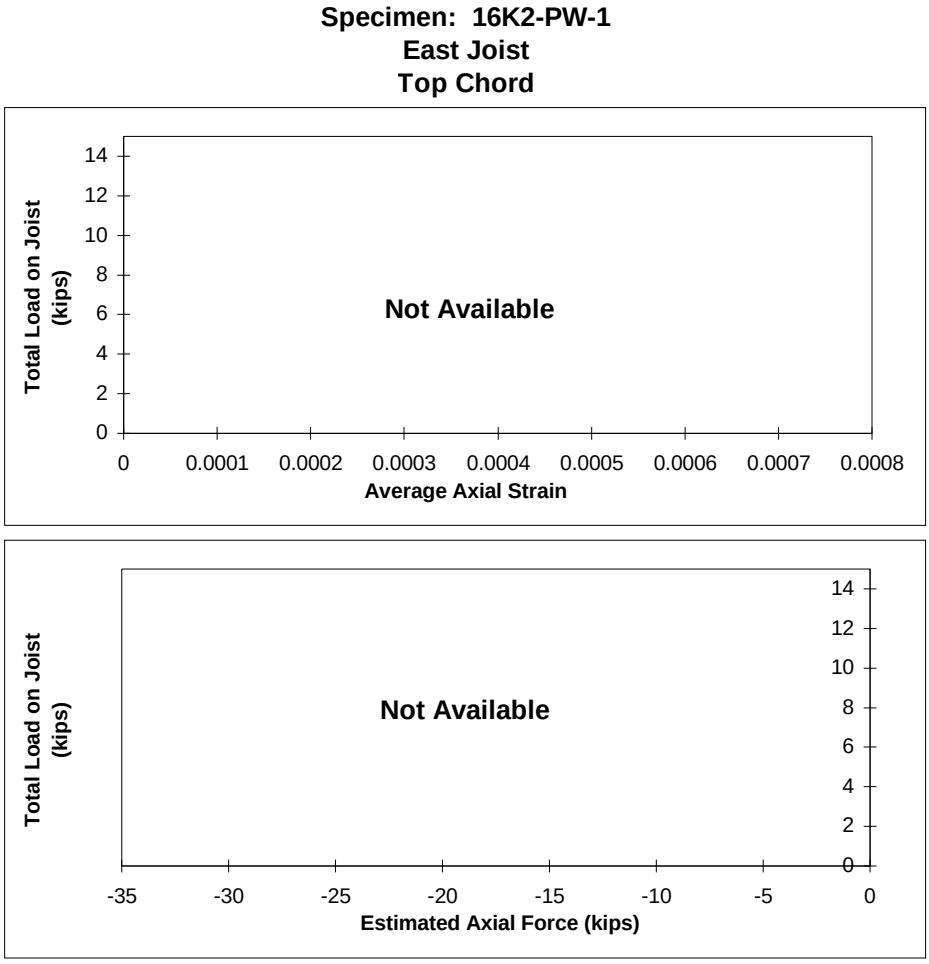

Figure C.3 16K2-PW-1 East Joist Top Chord

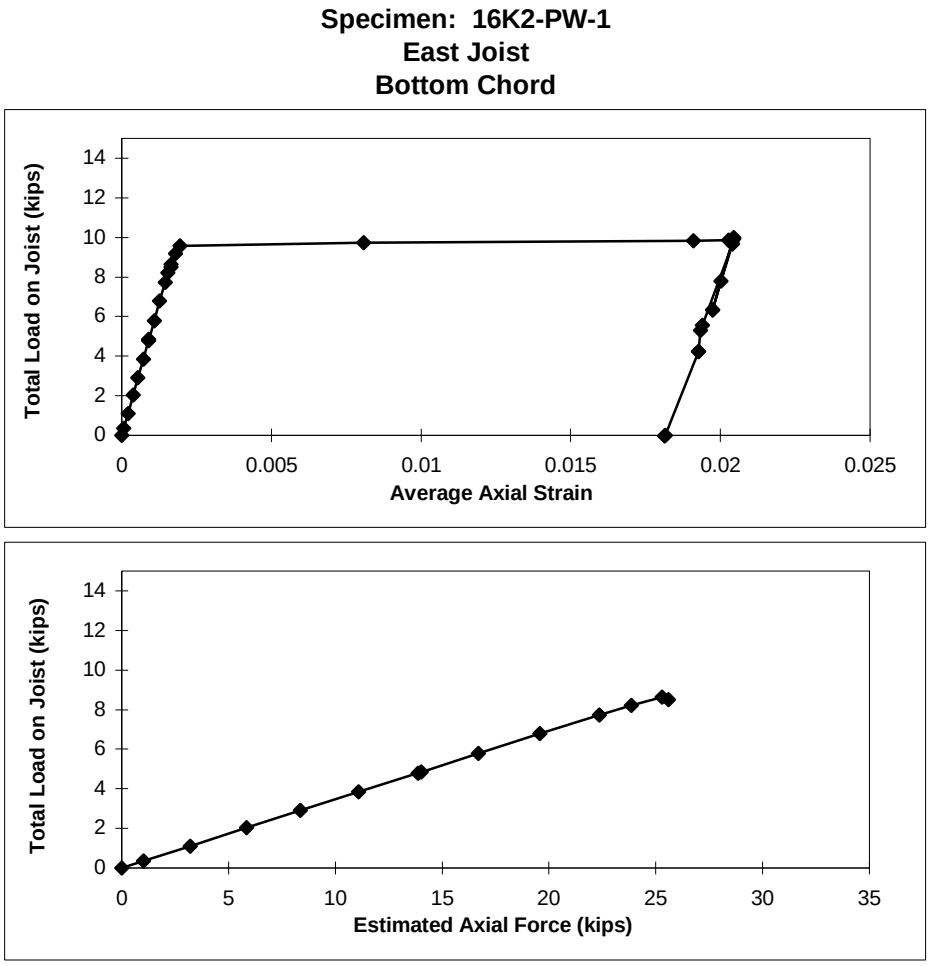

Figure C.4 16K2-PW-1 East Joist Bottom Chord

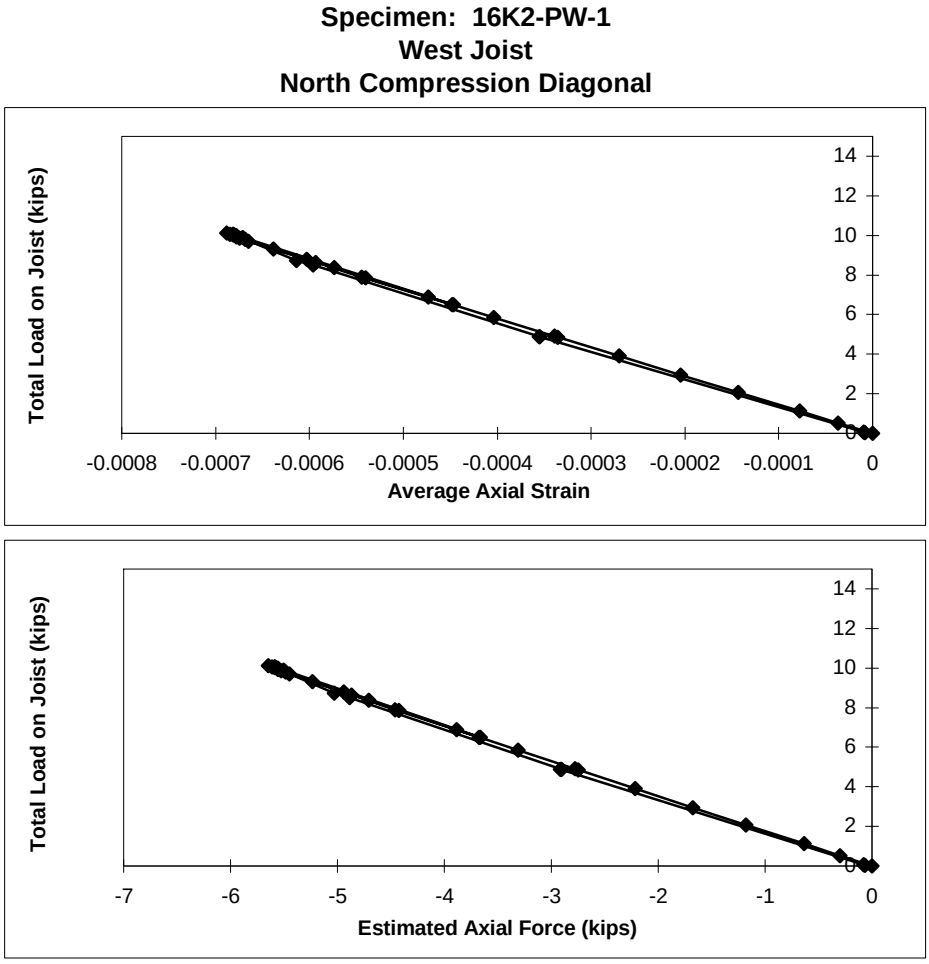

Figure C.5 16K2-PW-1 West Joist North Compression Diagonal

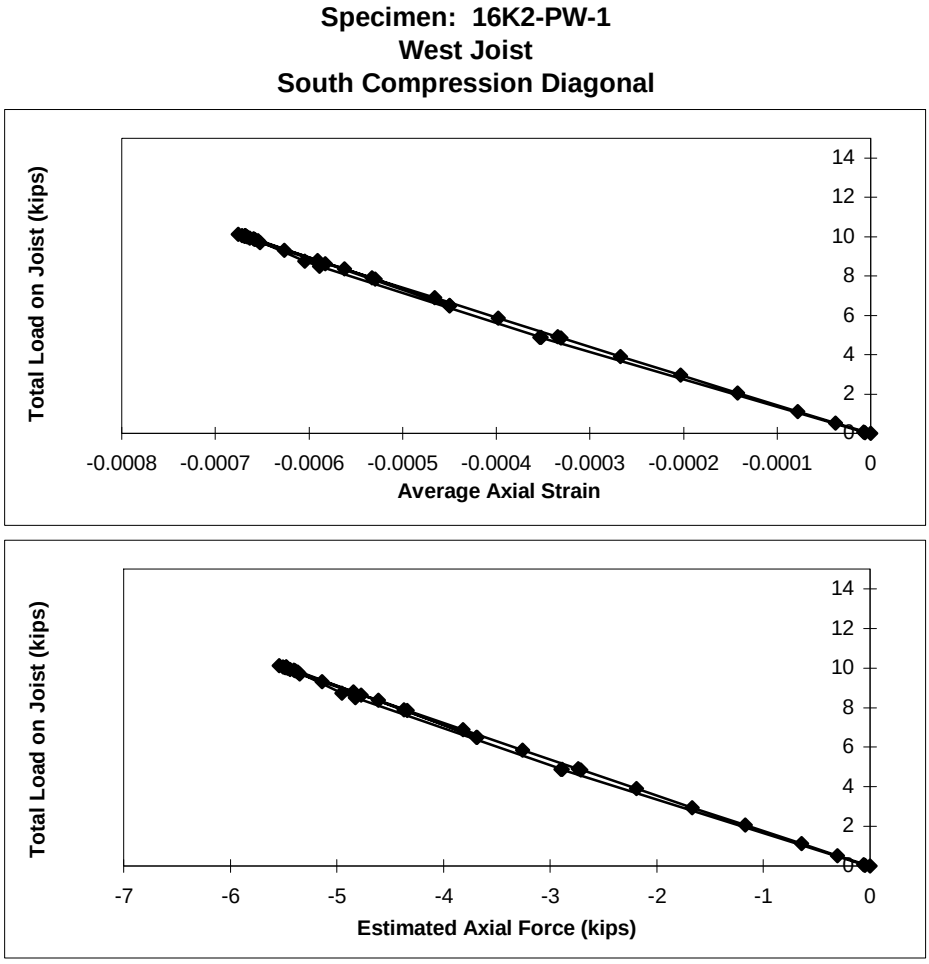

Figure C.6 16K2-PW-1 West Joist South Compression Diagonal

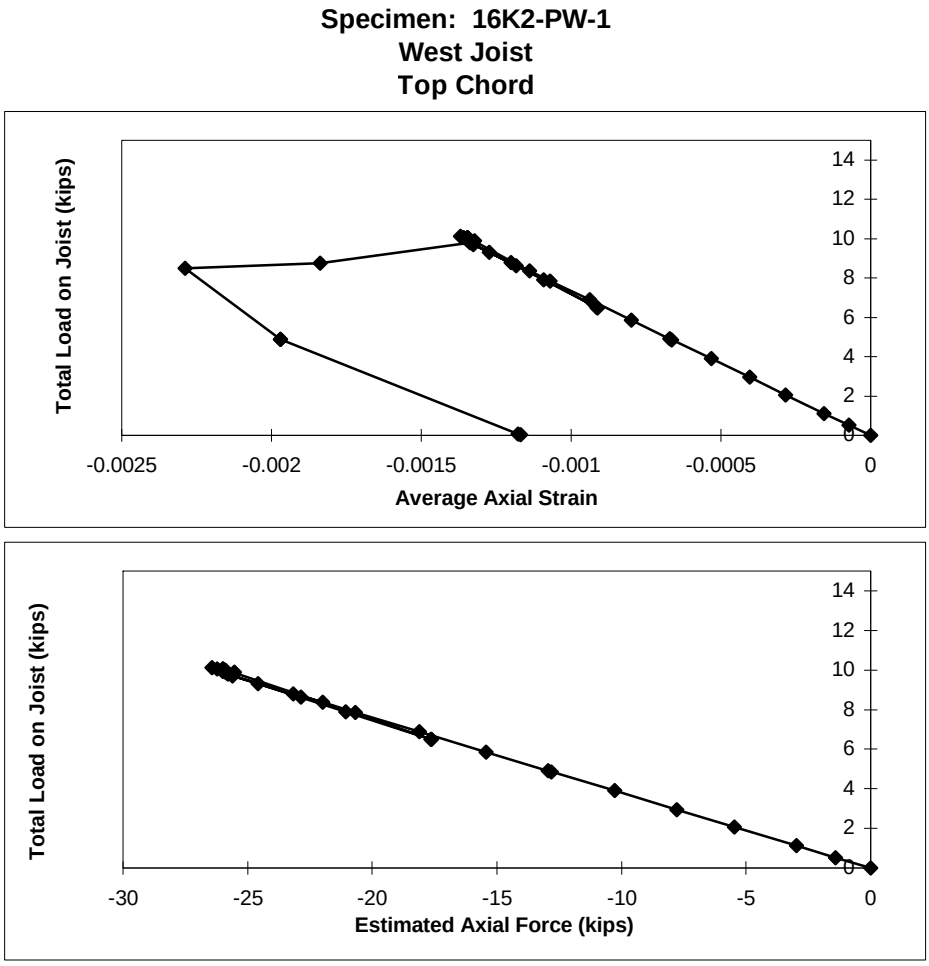

Figure C.7 16K2-PW-1 West Joist Top Chord

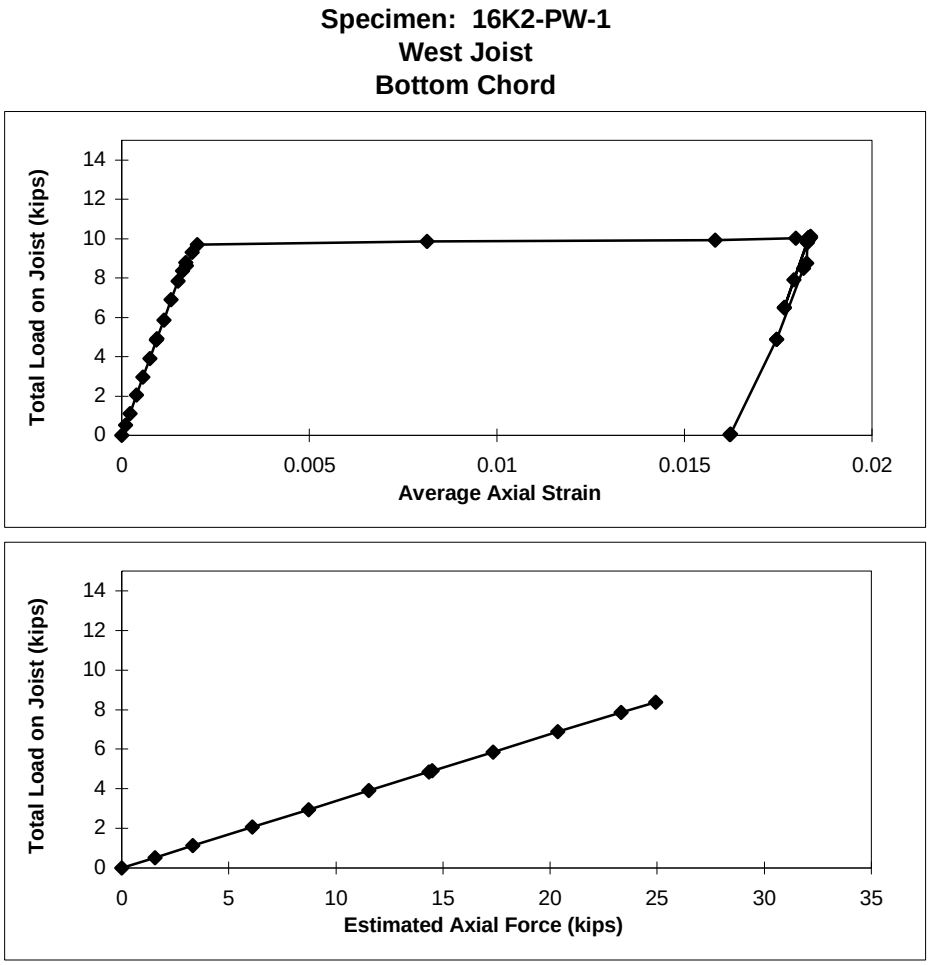

Figure C.8 16K2-PW-1 West Joist Bottom Chord

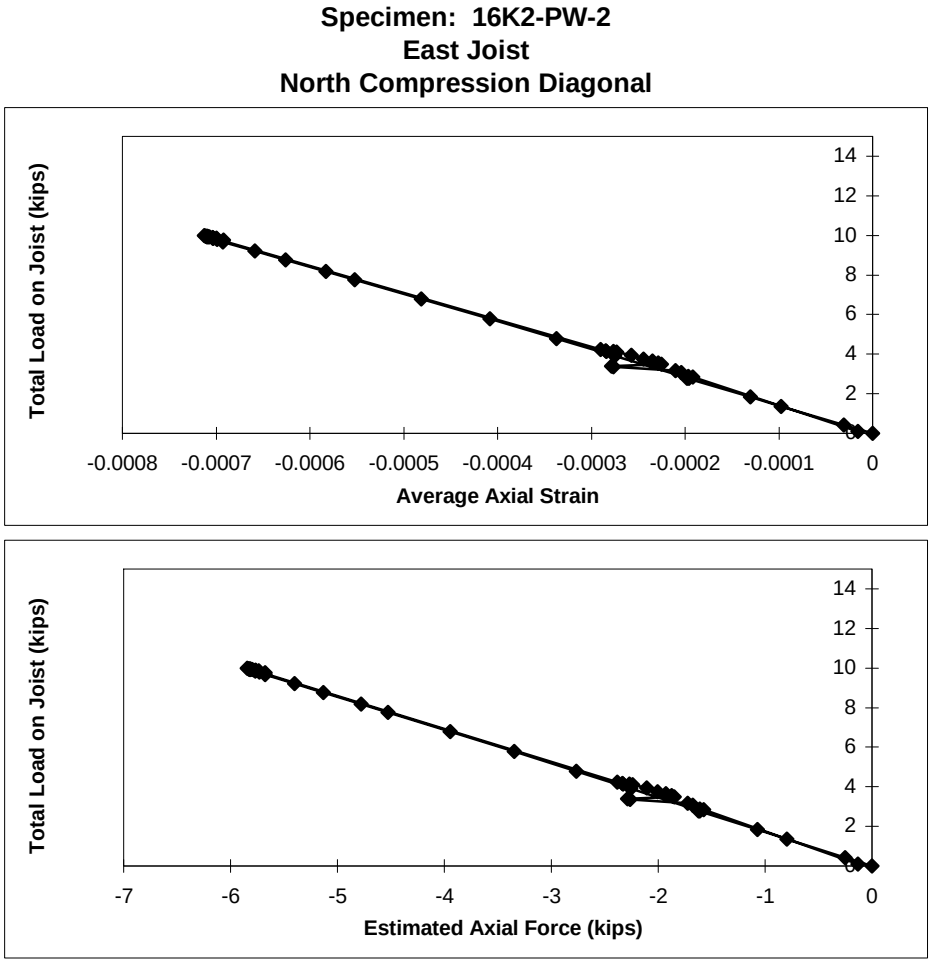

Figure C.9 16K2-PW-2 East Joist North Compression Diagonal

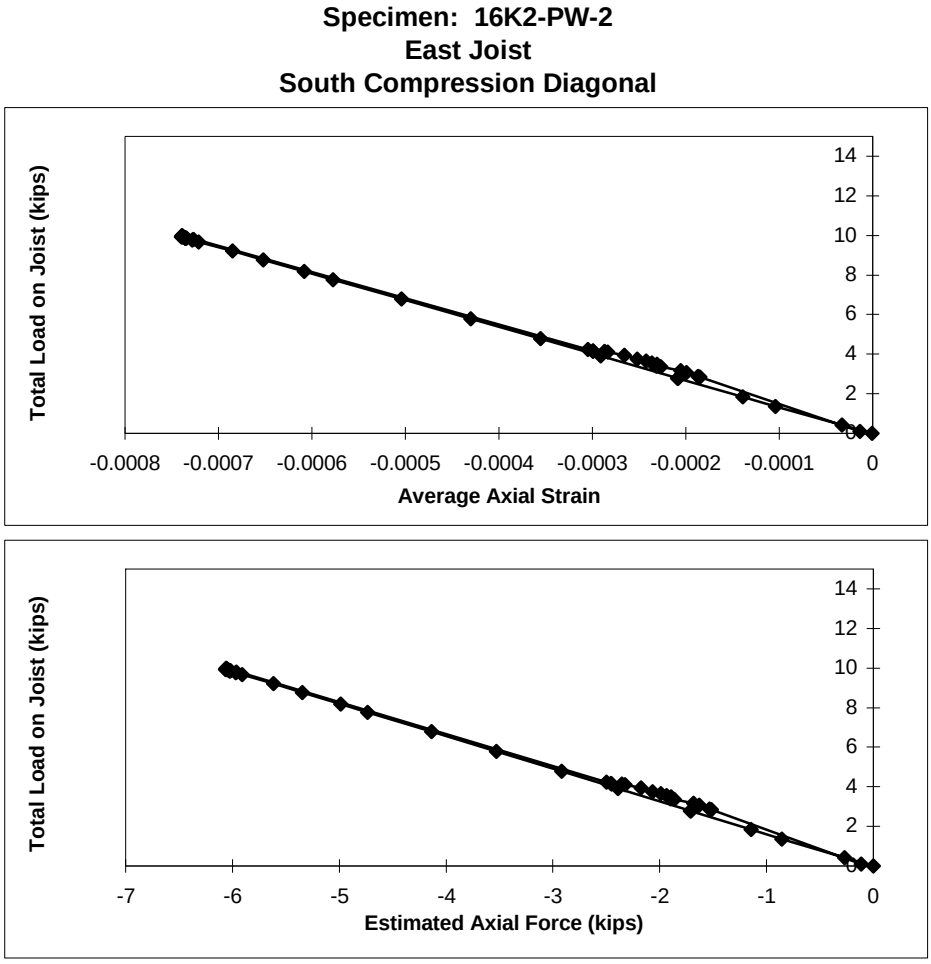

Figure C.10 16K2-PW-2 East Joist South Compression Diagonal

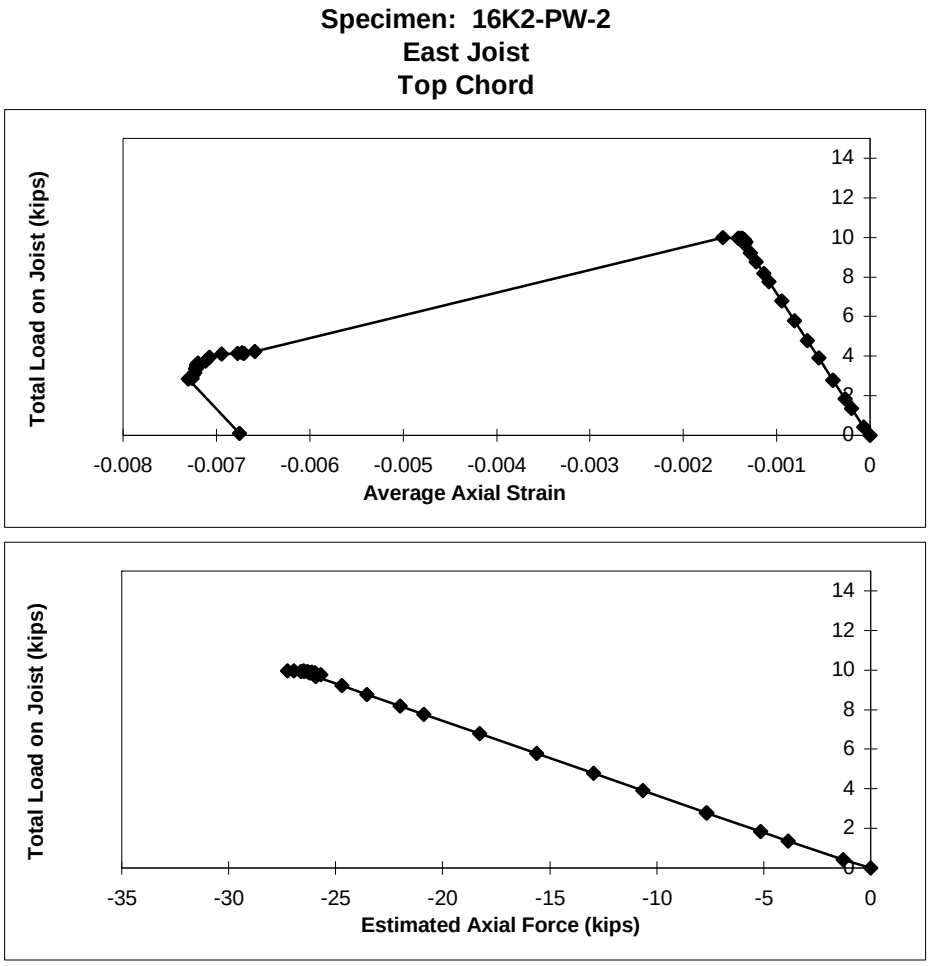

Figure C.11 16K2-PW-2 East Joist Top Chord

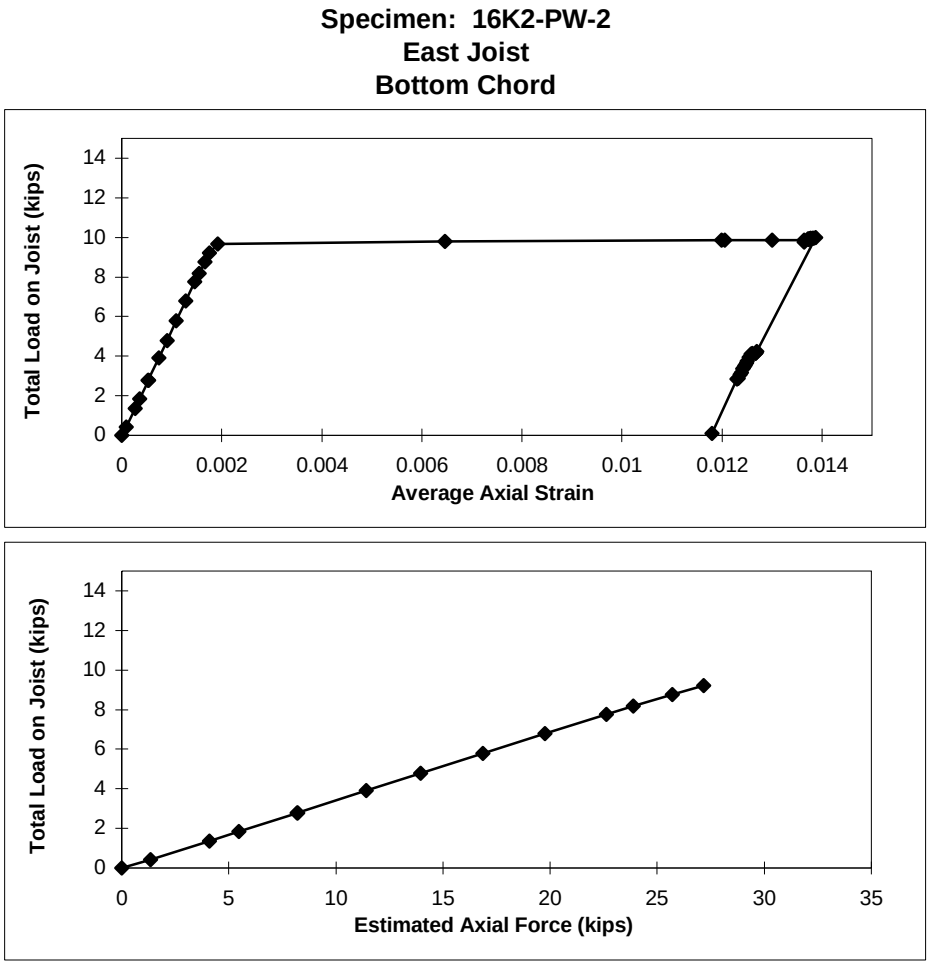

Figure C.12 16K2-PW-2 East Joist Bottom Chord

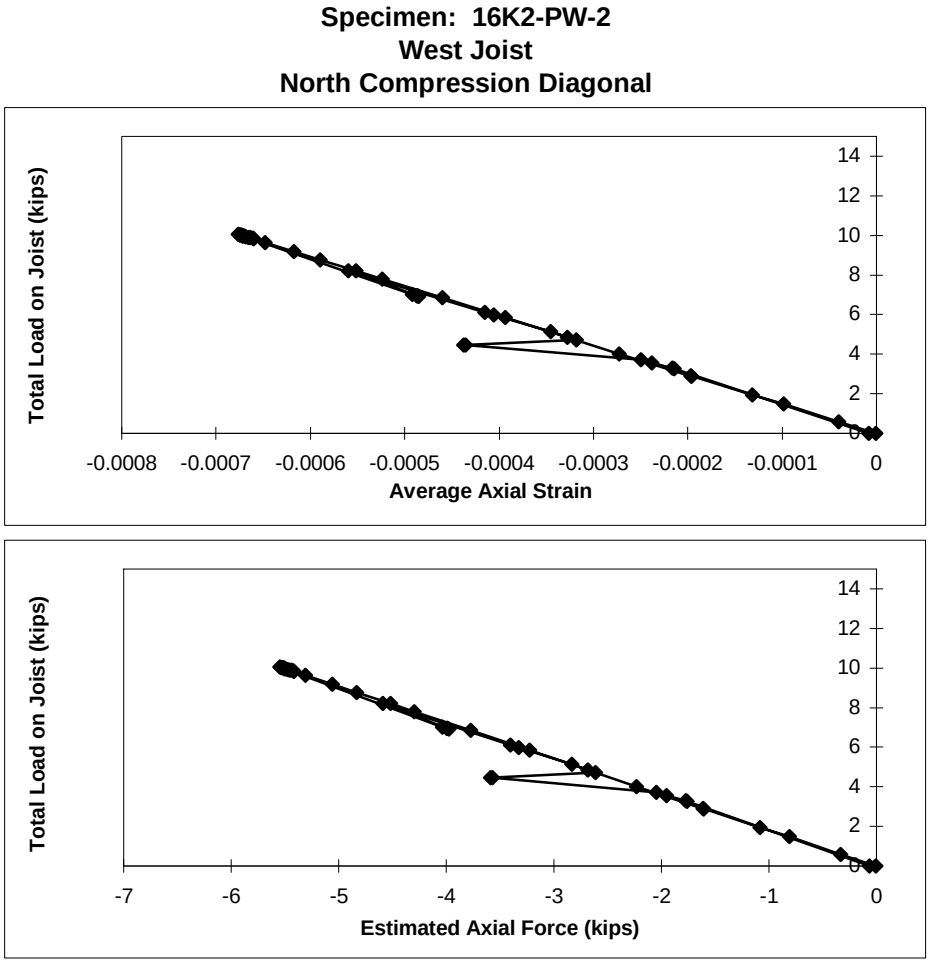

Figure C.13 16K2-PW-2 West Joist North Compression Diagonal

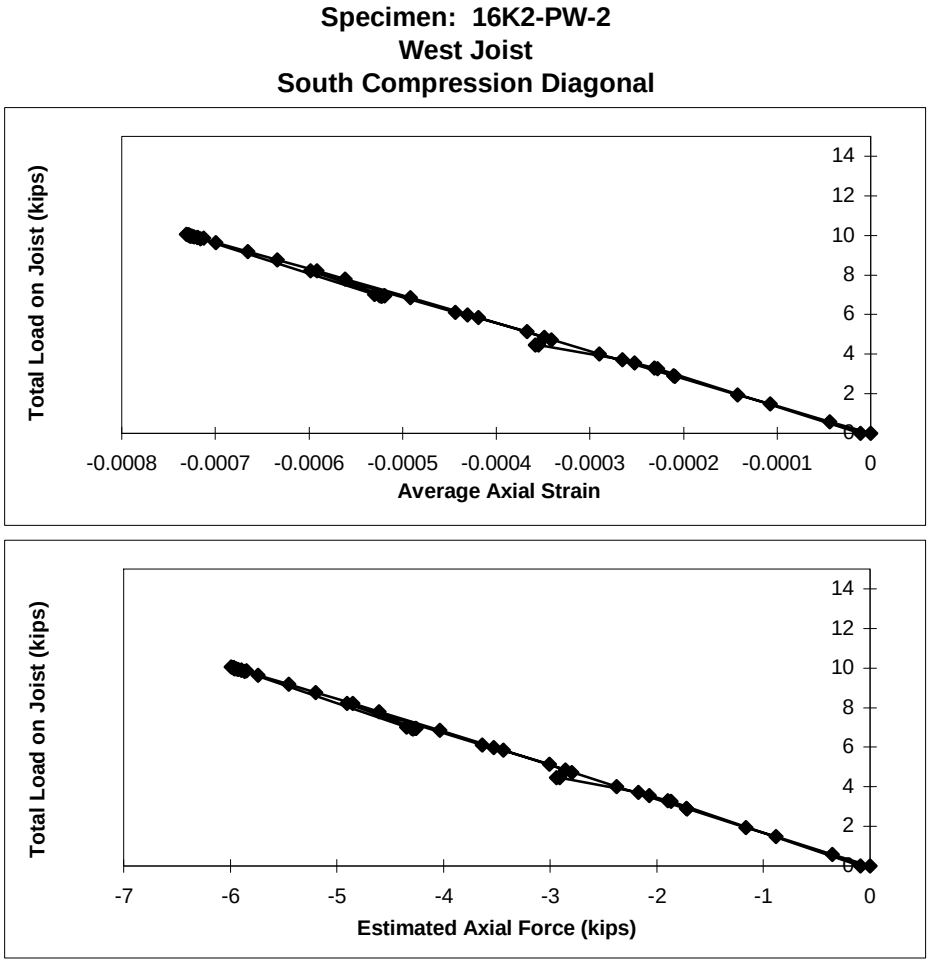

Figure C.14 16K2-PW-2 West Joist South Compression Diagonal

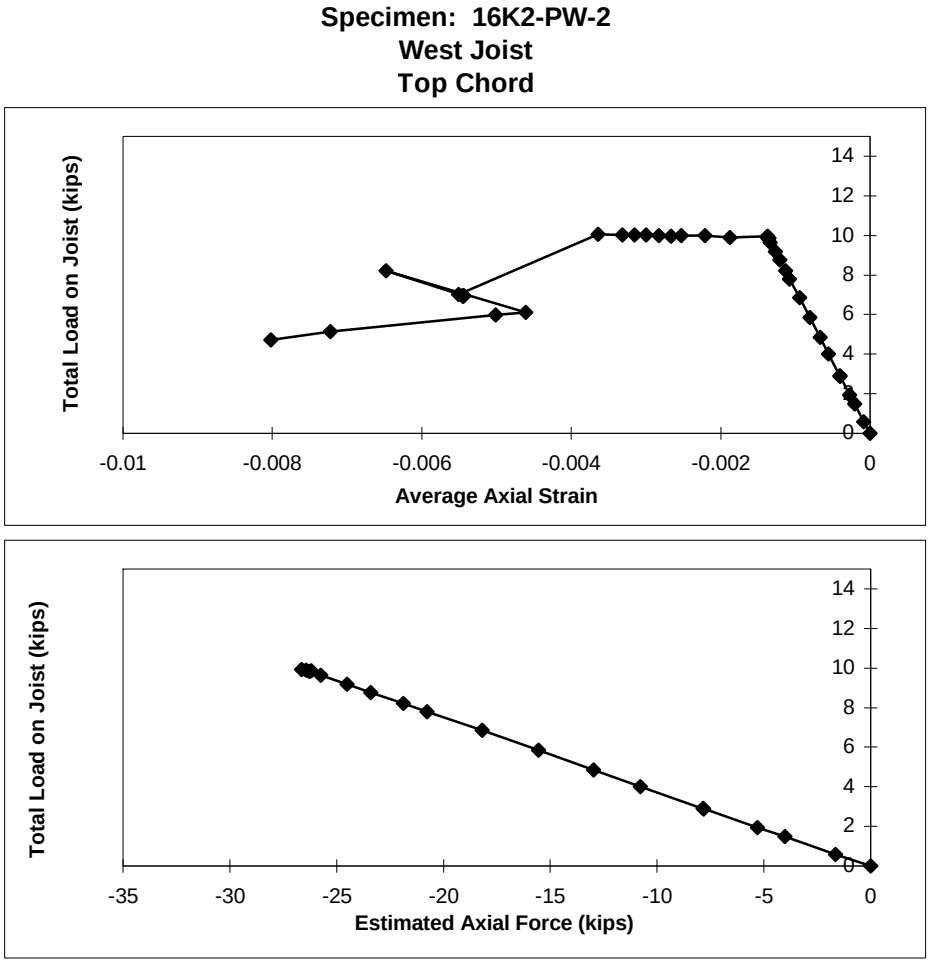

Figure C.15 16K2-PW-2 West Joist Top Chord

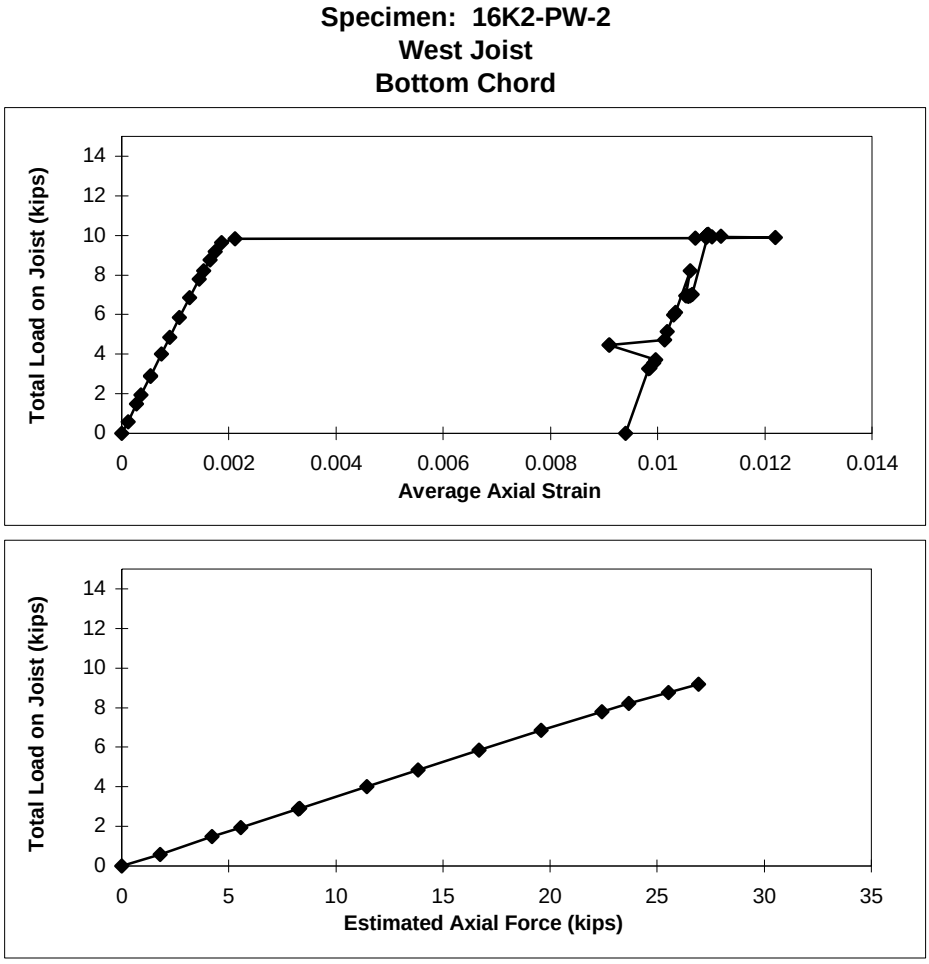

Figure C.16 16K2-PW-2 West Joist Bottom Chord

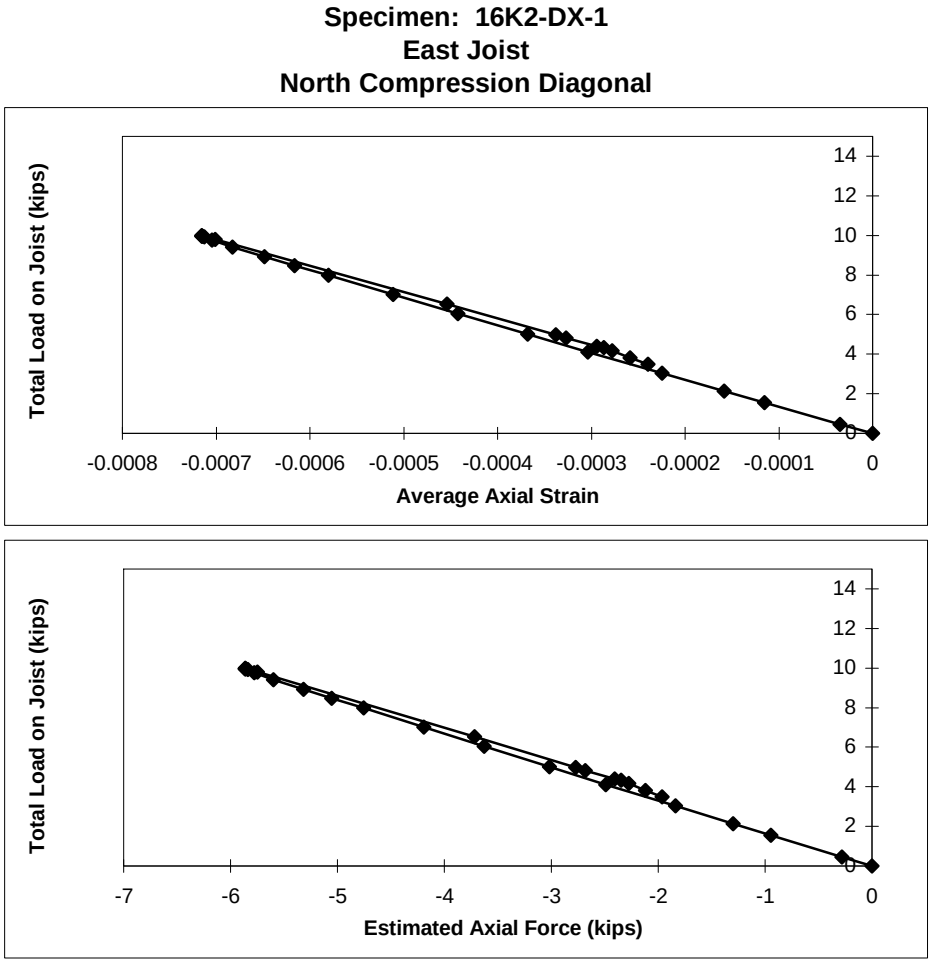

Figure C.17 16K2-DX-1 East Joist North Compression Diagonal

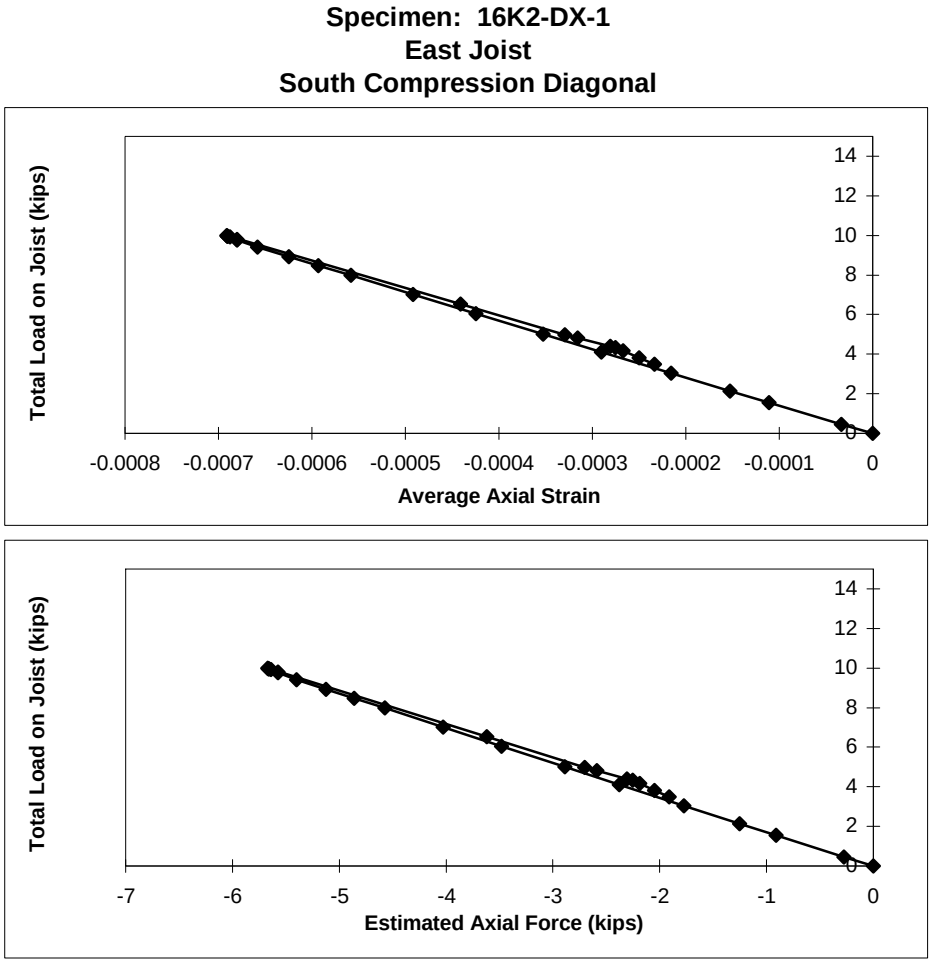

Figure C.18 16K2-DX-1 East Joist South Compression Diagonal

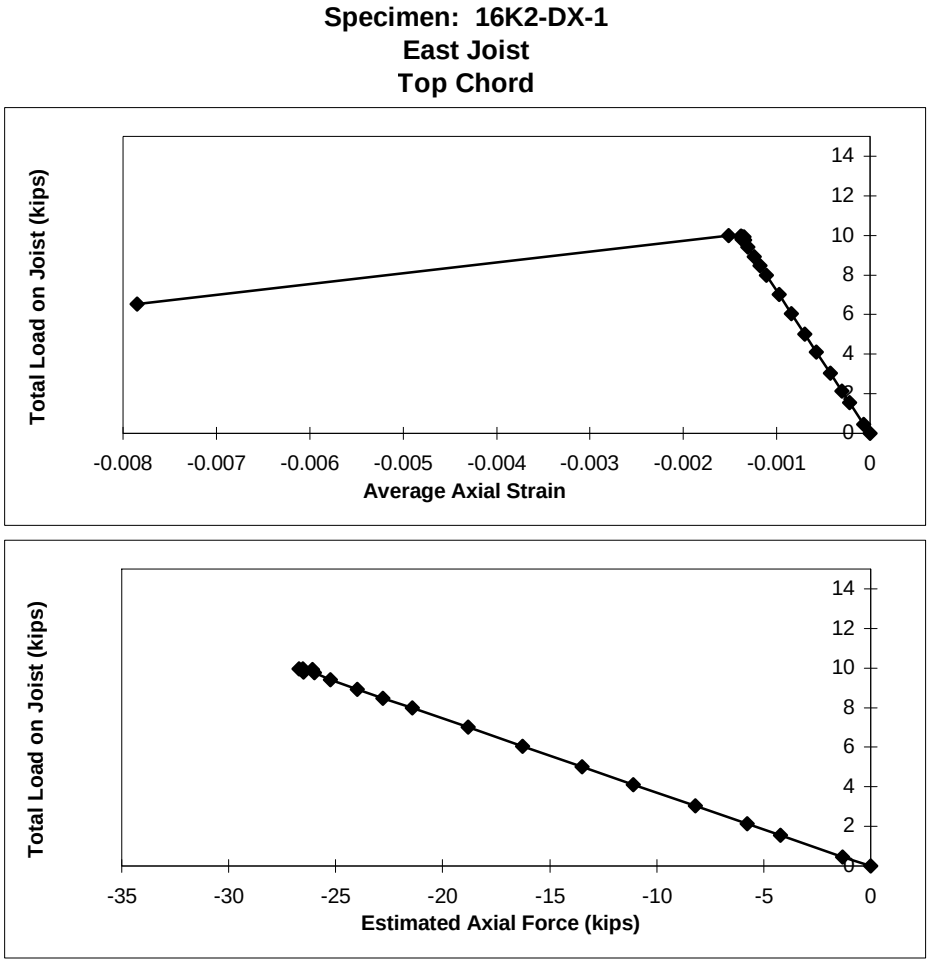

Figure C.19 16K2-DX-1 East Joist Top Chord

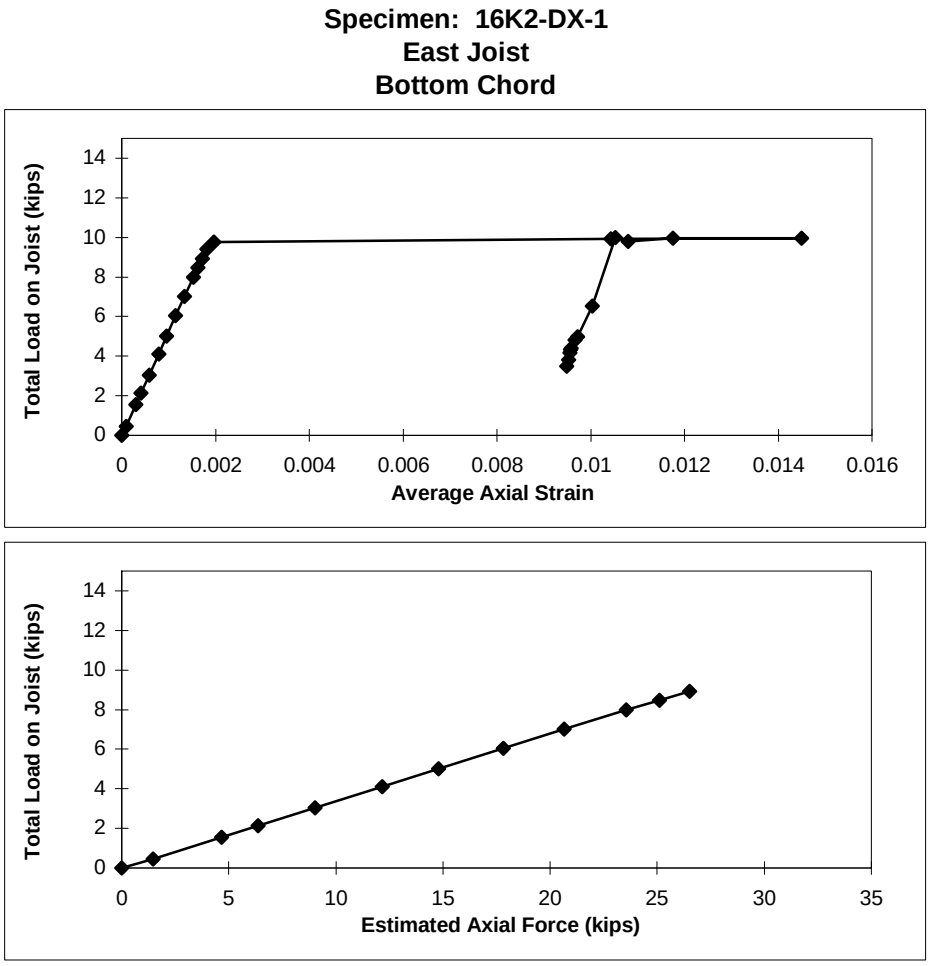

Figure C.20 16K2-DX-1 East Joist Bottom Chord

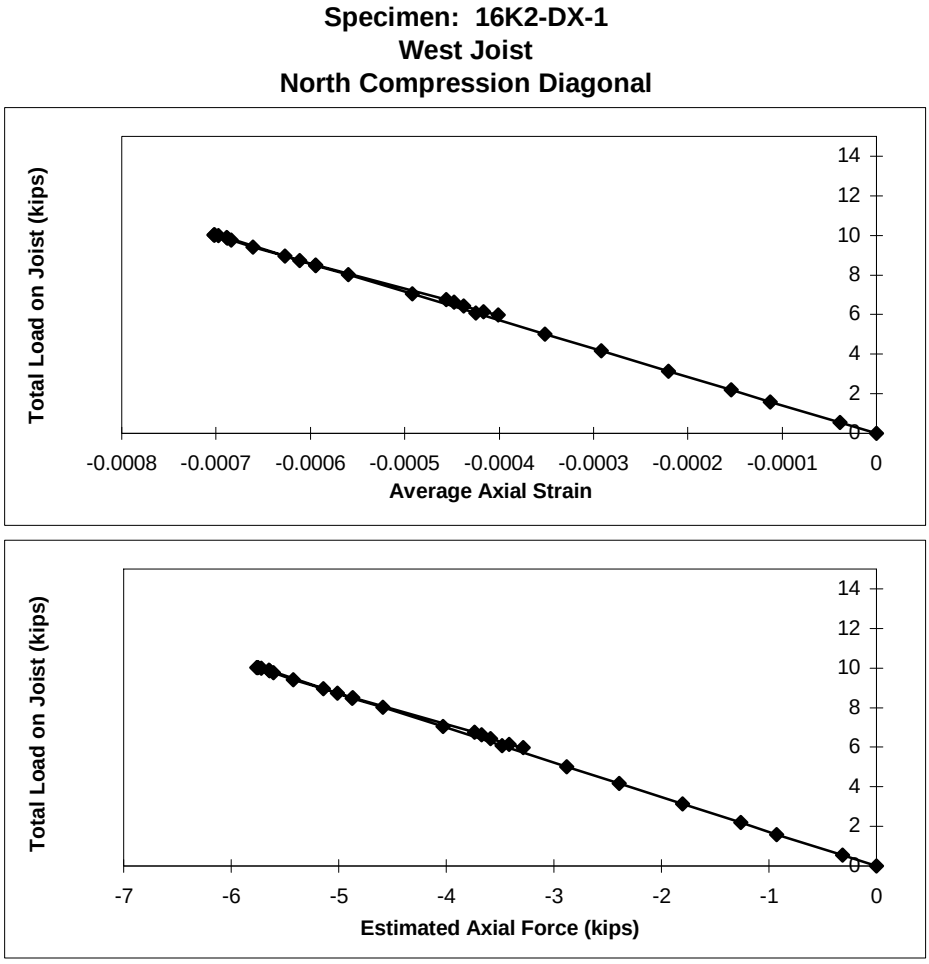

Figure C.21 16K2-DX-1 West Joist North Compression Diagonal

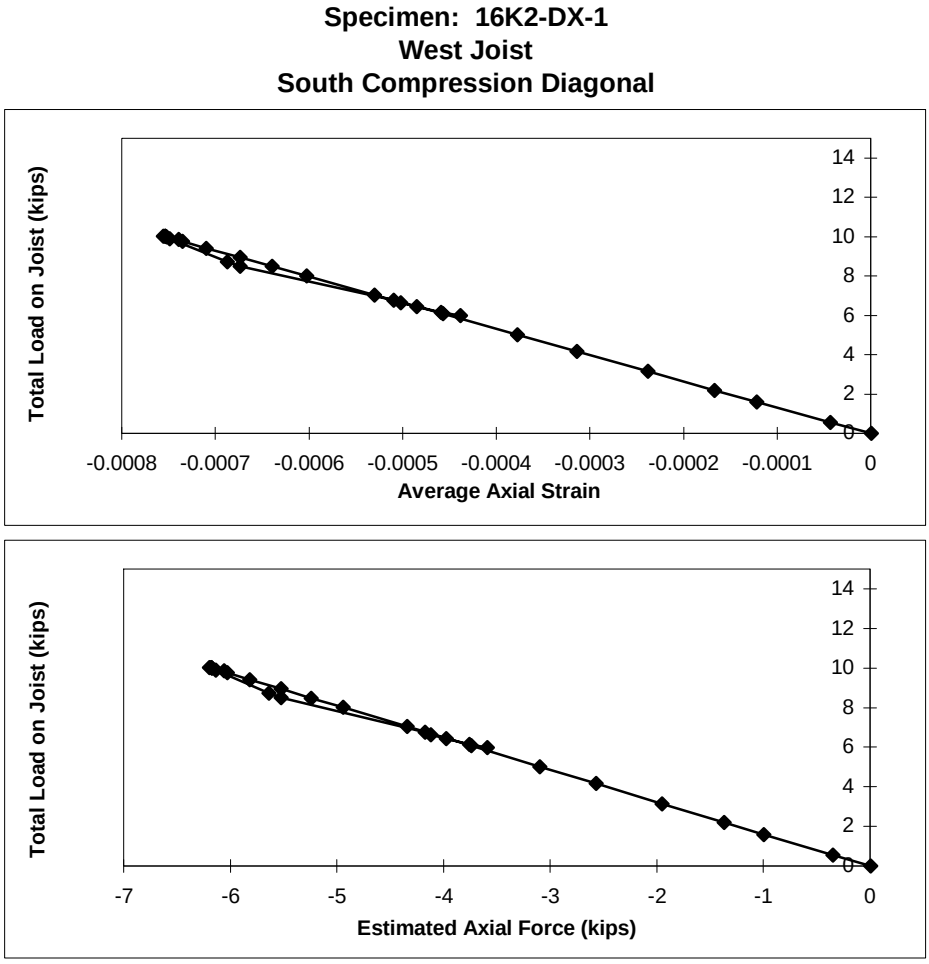

Figure C.22 16K2-DX-1 West Joist South Compression Diagonal

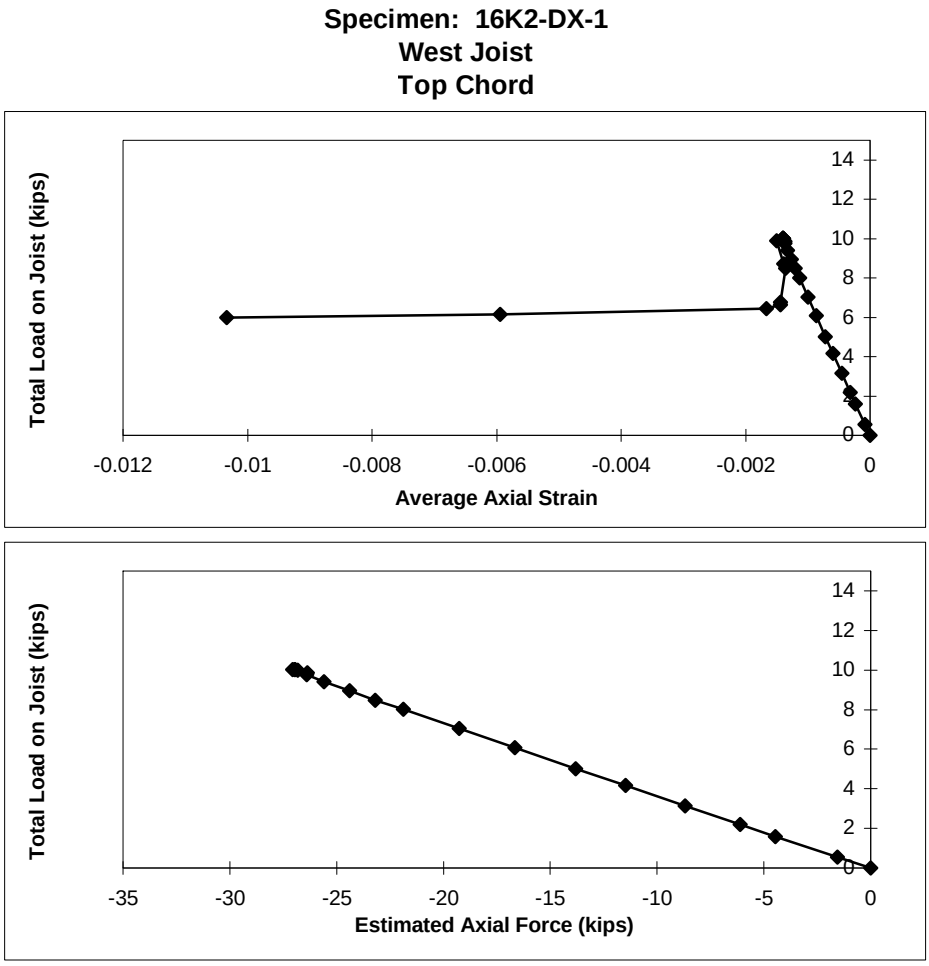

Figure C.23 16K2-DX-1 West Joist Top Chord

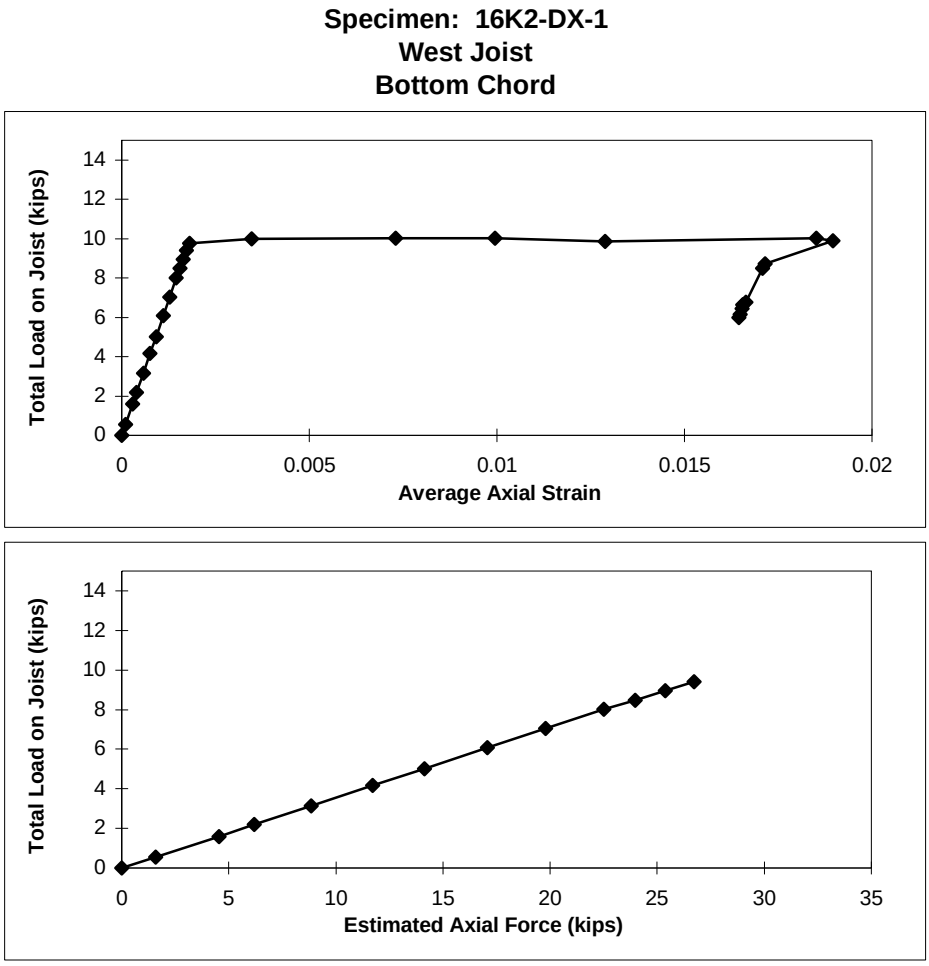

Figure C.24 16K2-DX-1 West Joist Bottom Chord

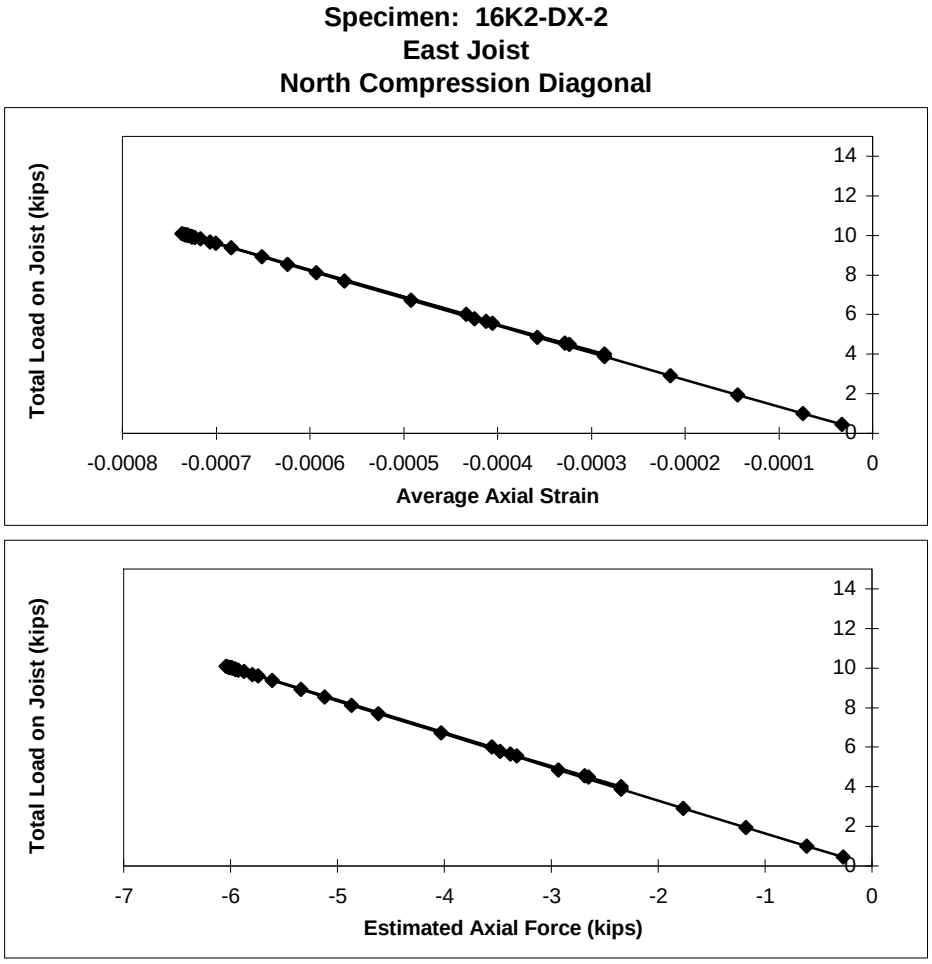

Figure C.25 16K2-DX-2 East Joist North Compression Diagonal

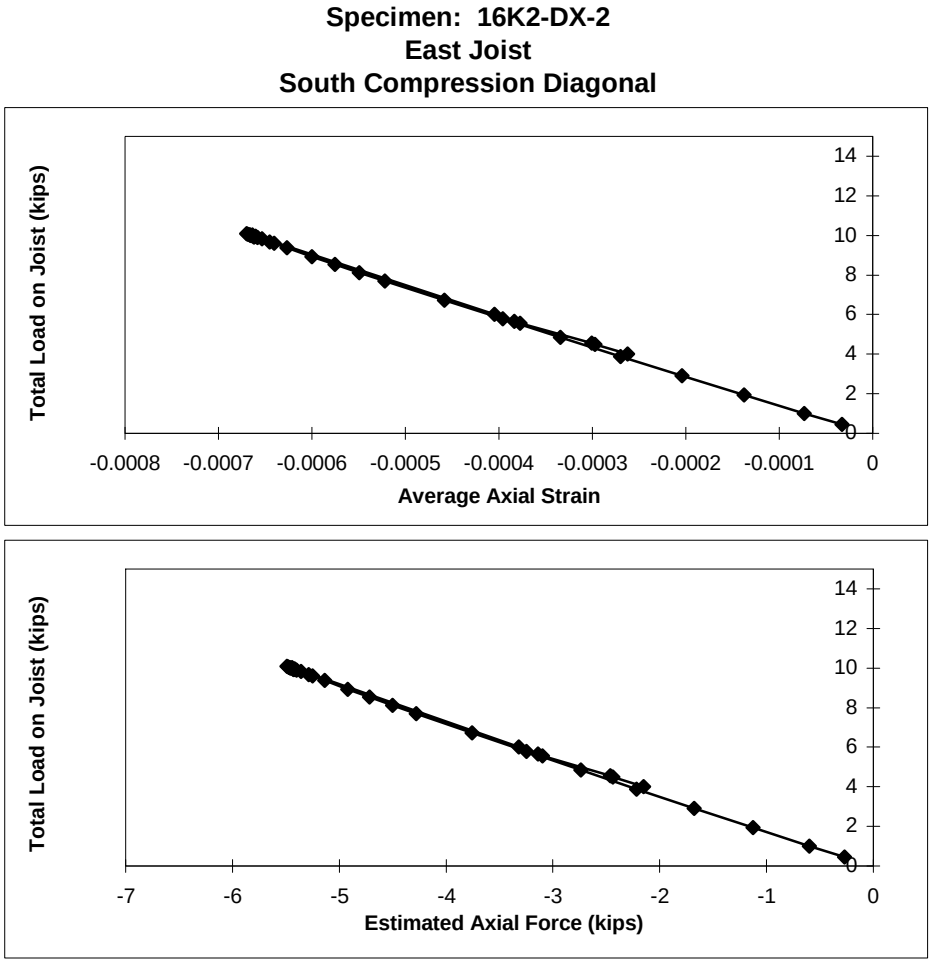

Figure C.26 16K2-DX-2 East Joist South Compression Diagonal

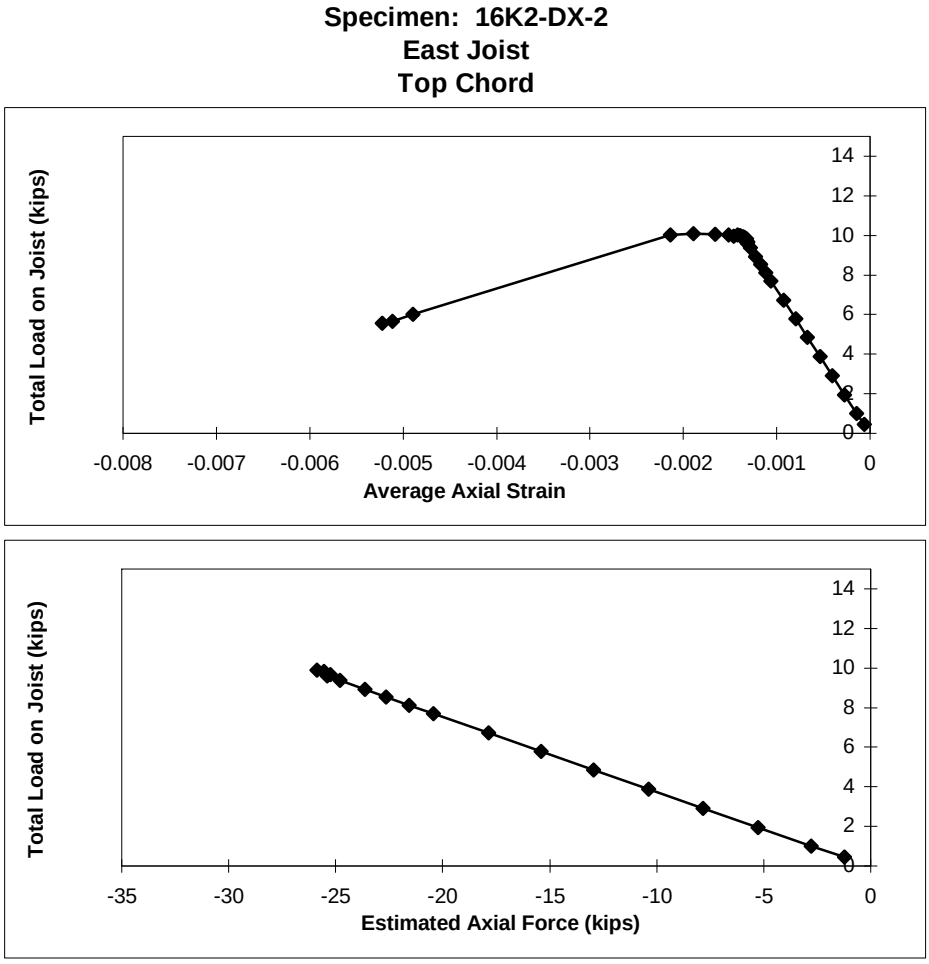

Figure C.27 16K2-DX-2 East Joist Top Chord

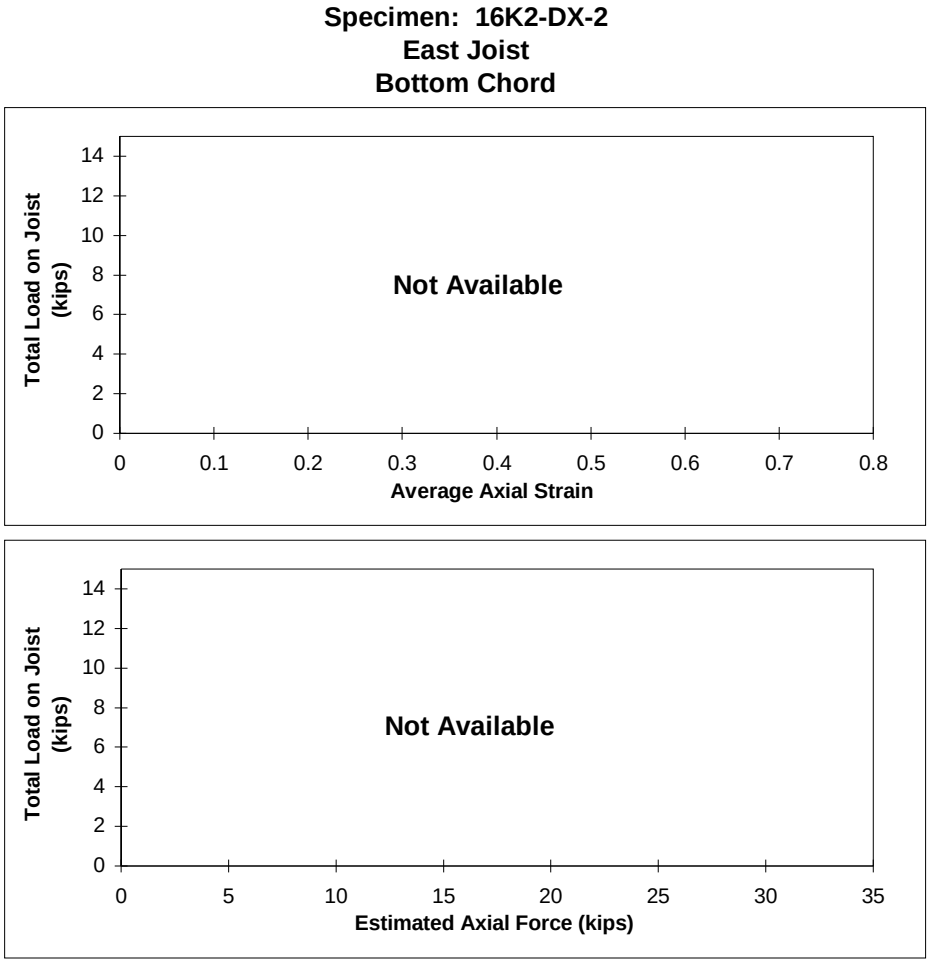

Figure C.28 16K2-DX-2 East Joist Bottom Chord

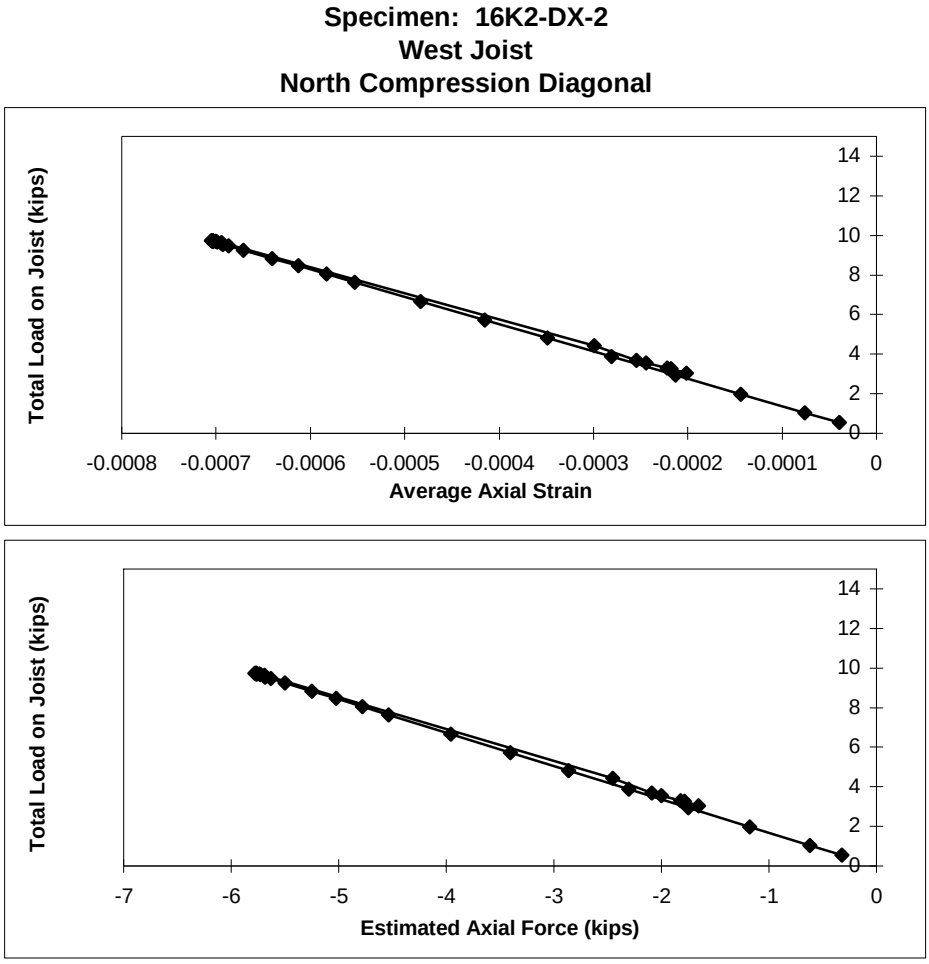

Figure C.29 16K2-DX-2 West Joist North Compression Diagonal

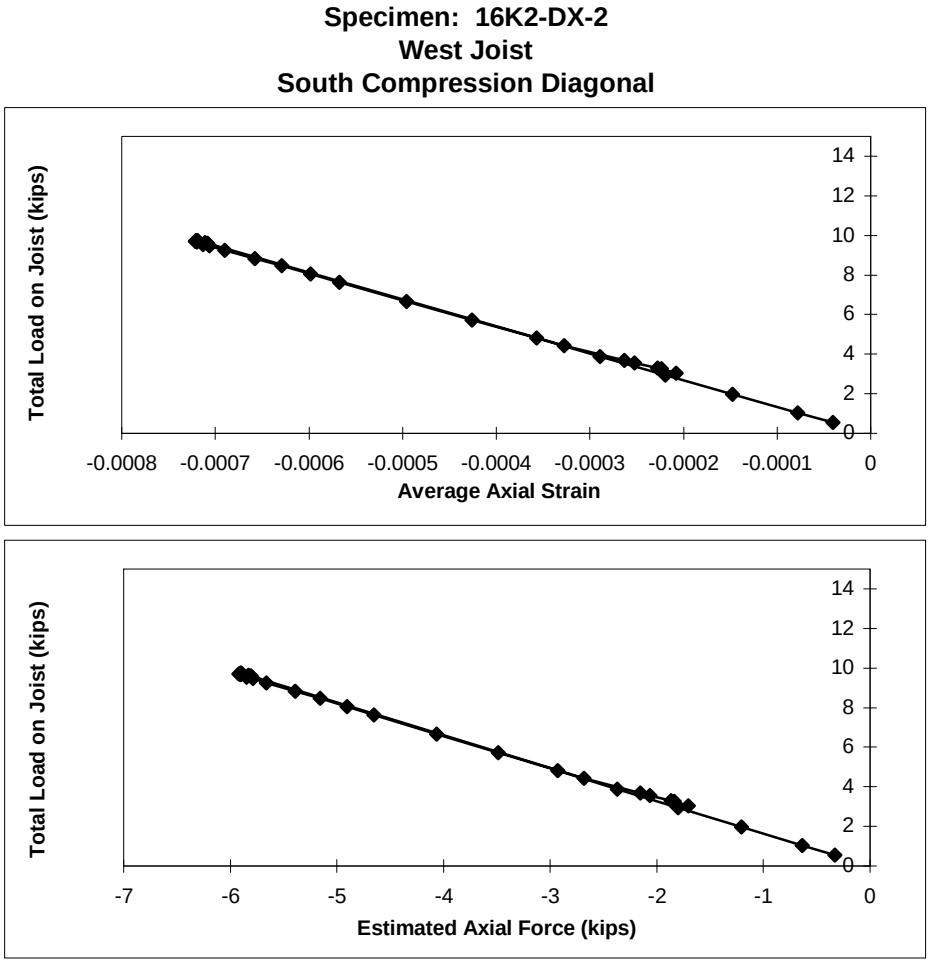

Figure C.30 16K2-DX-2 West Joist South Compression Diagonal

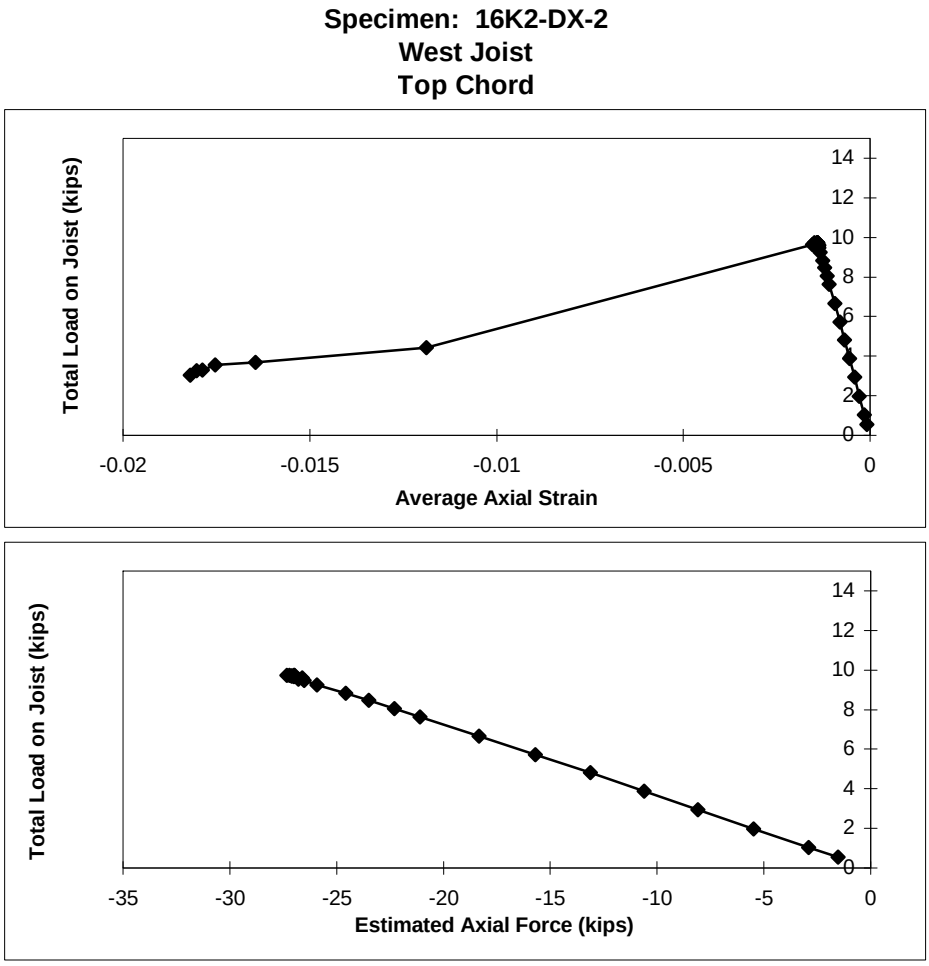

Figure C.31 16K2-DX-2 West Joist Top Chord

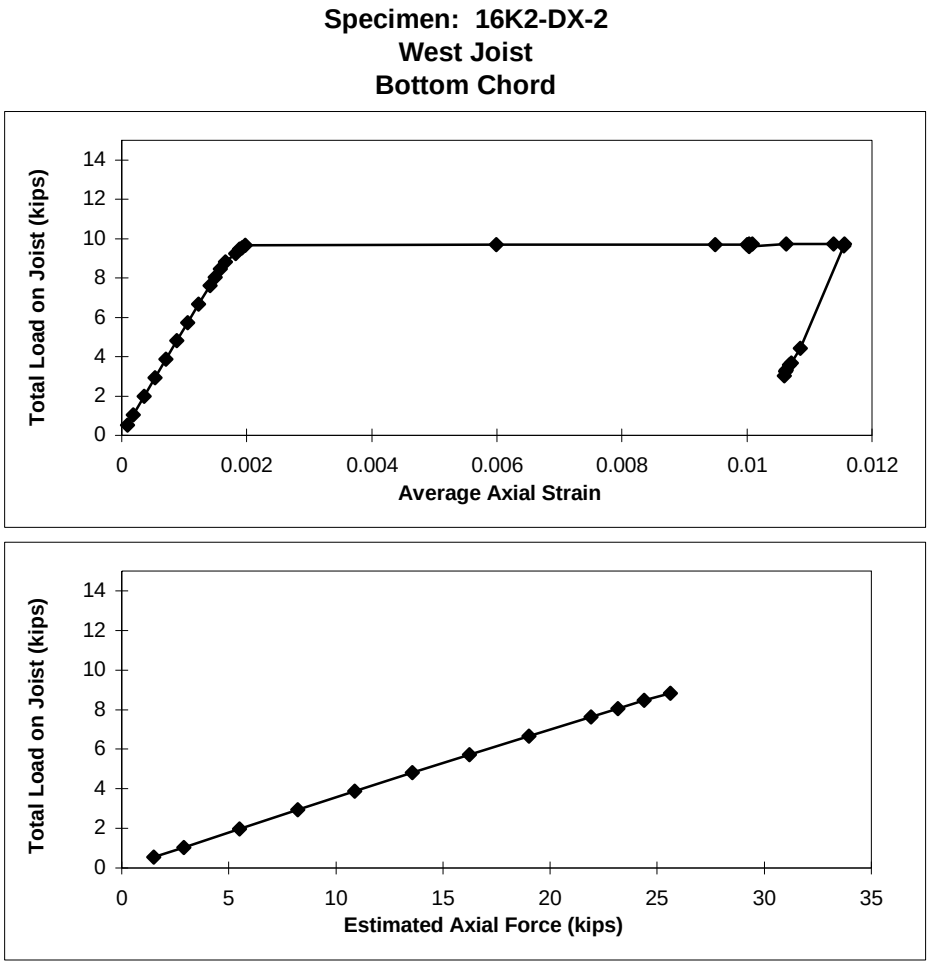

Figure C.32 16K2-DX-2 West Joist Bottom Chord

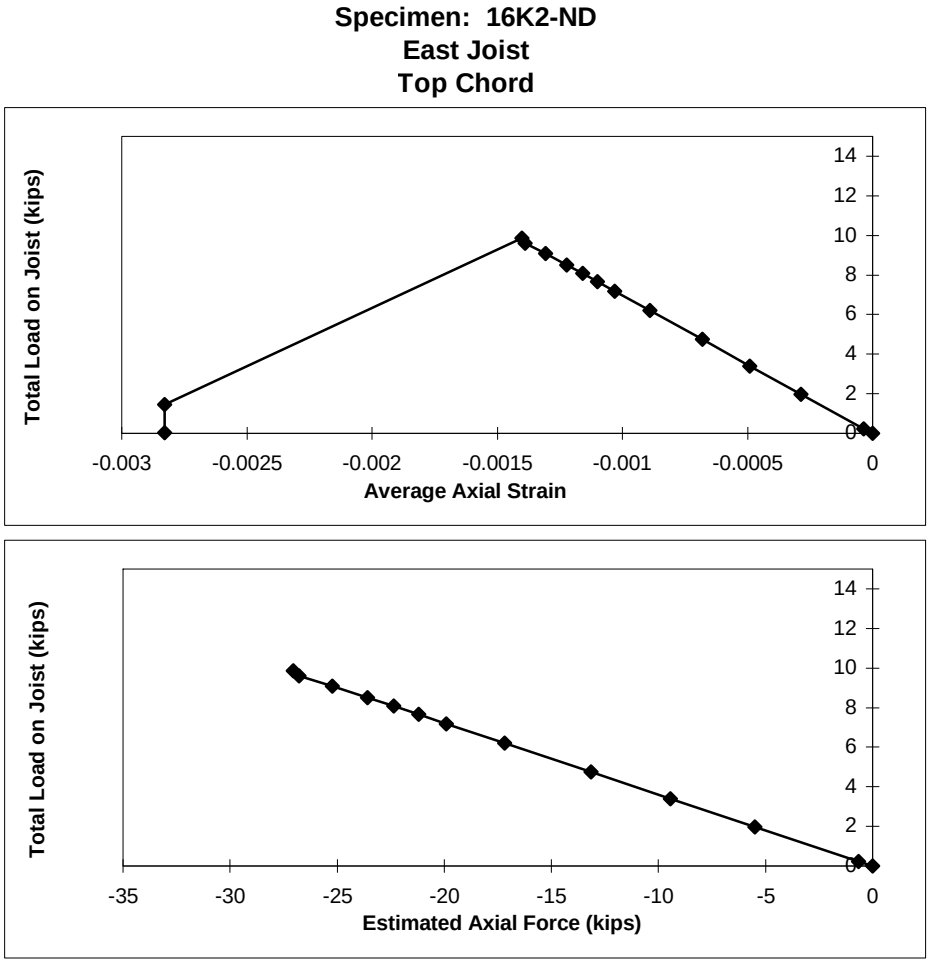

Figure C.33 16K2-ND East Joist Top Chord

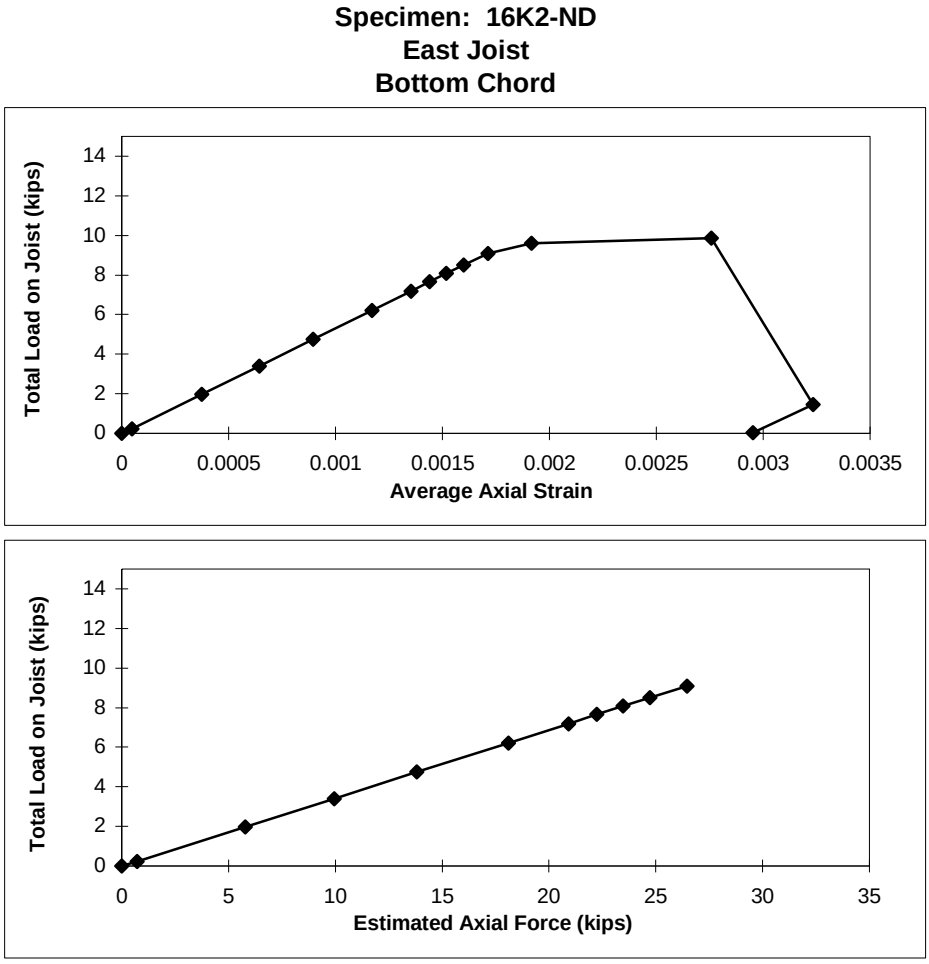

Figure C.34 16K2-ND East Joist Bottom Chord

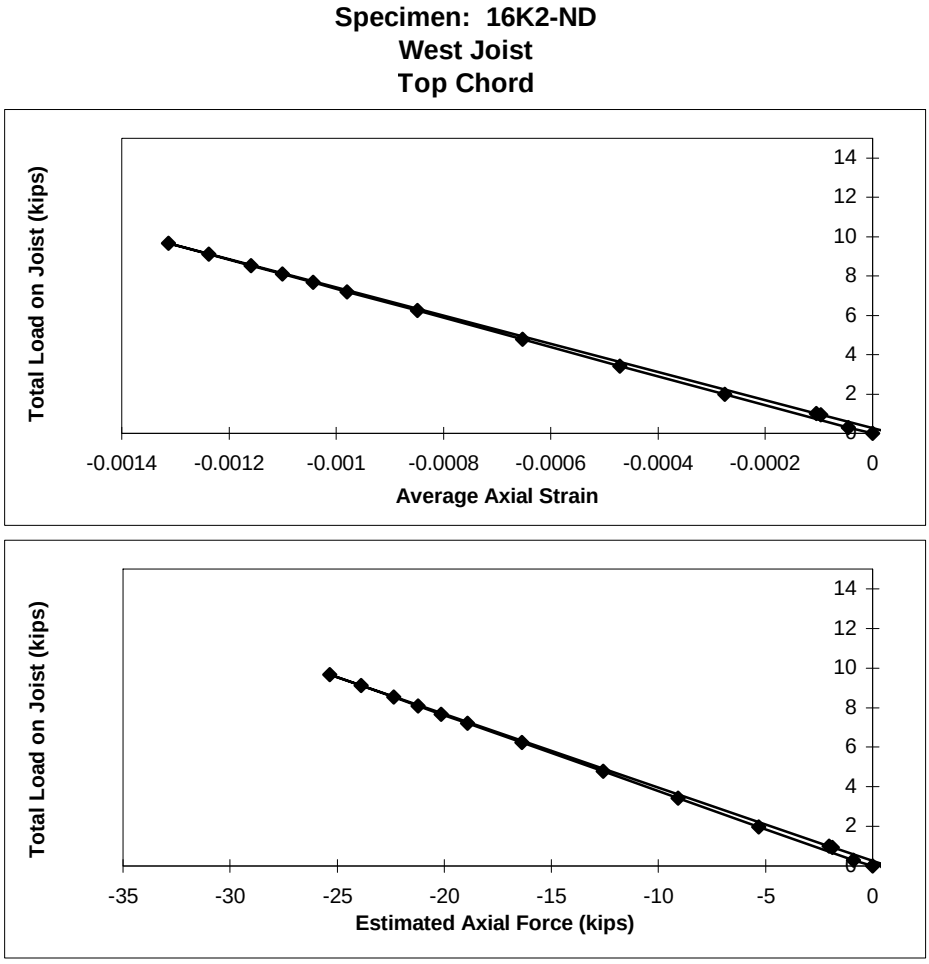

Figure C.35 16K2-ND West Joist Top Chord

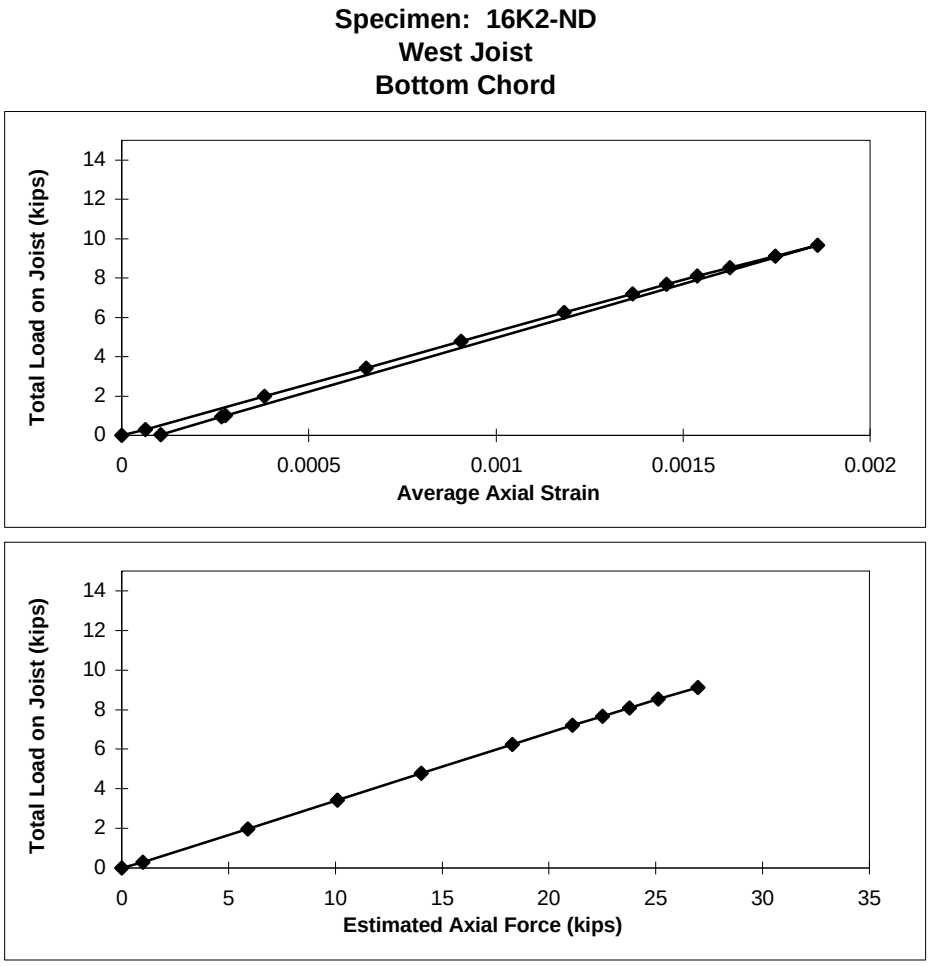

Figure C.36 16K2-ND West Joist Bottom Chord

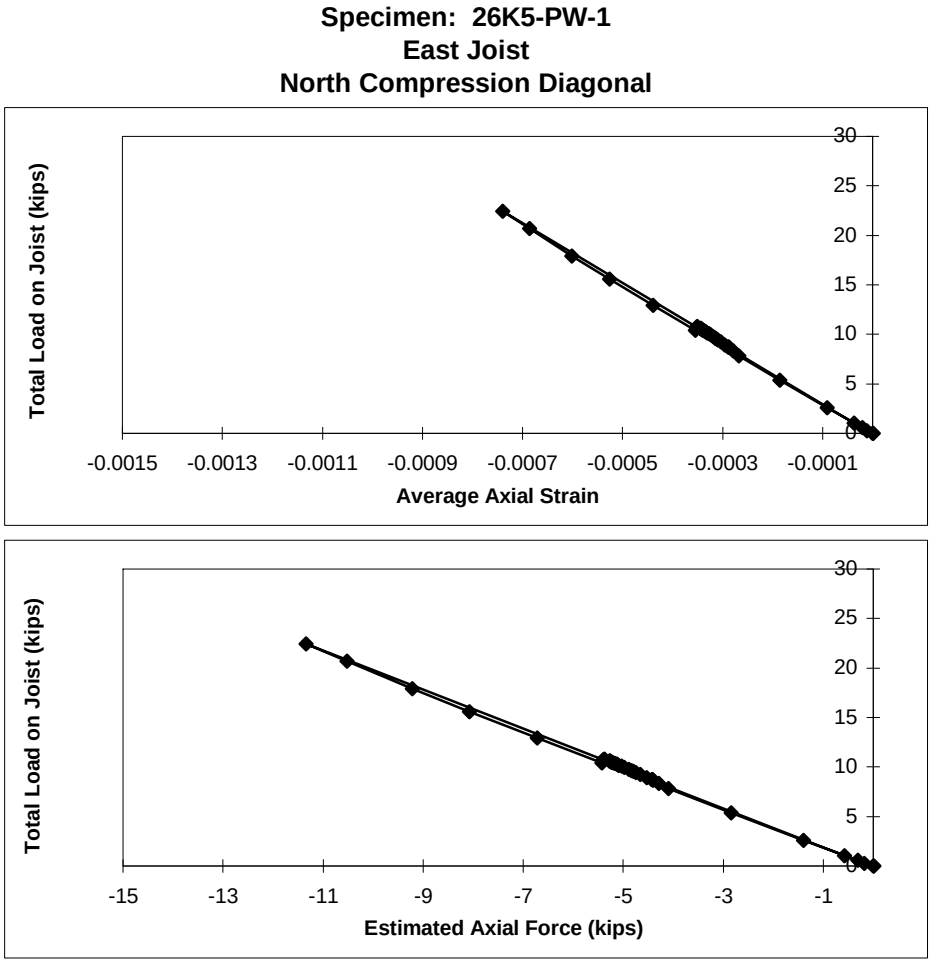

Figure C.37 26K5-PW-1 East Joist North Compression Diagonal

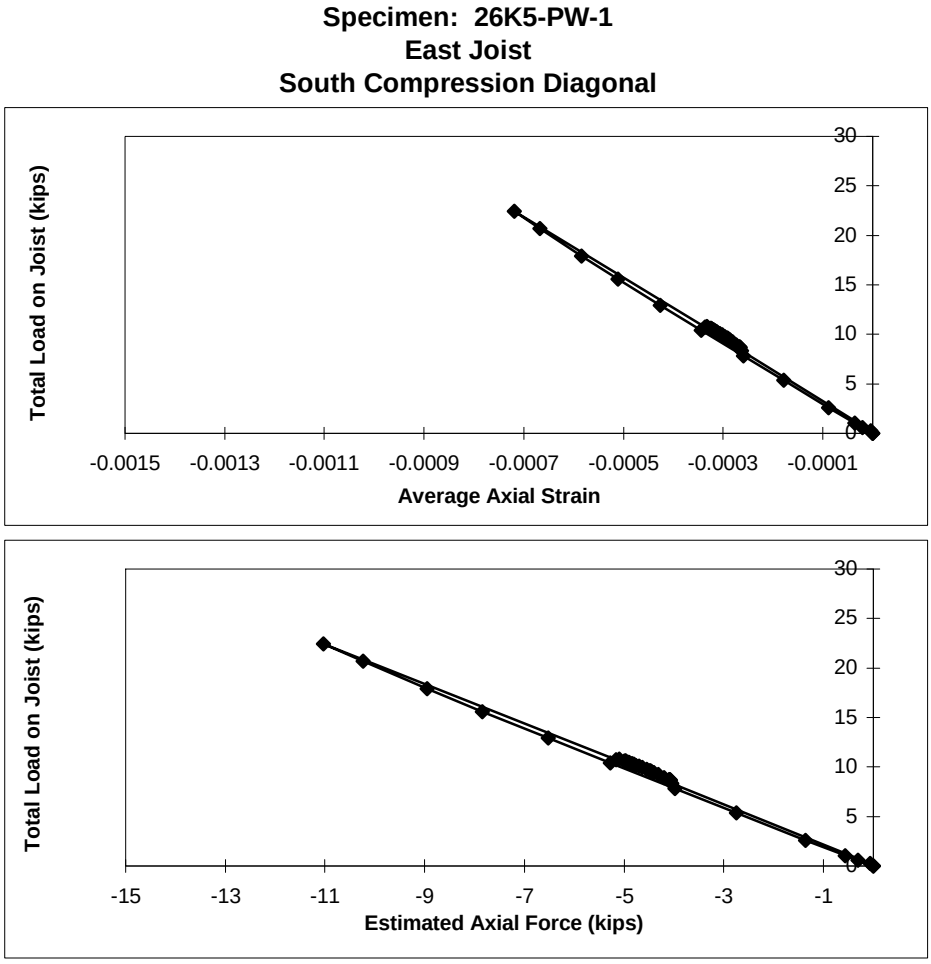

Figure C.38 26K5-PW-1 East Joist South Compression Diagonal

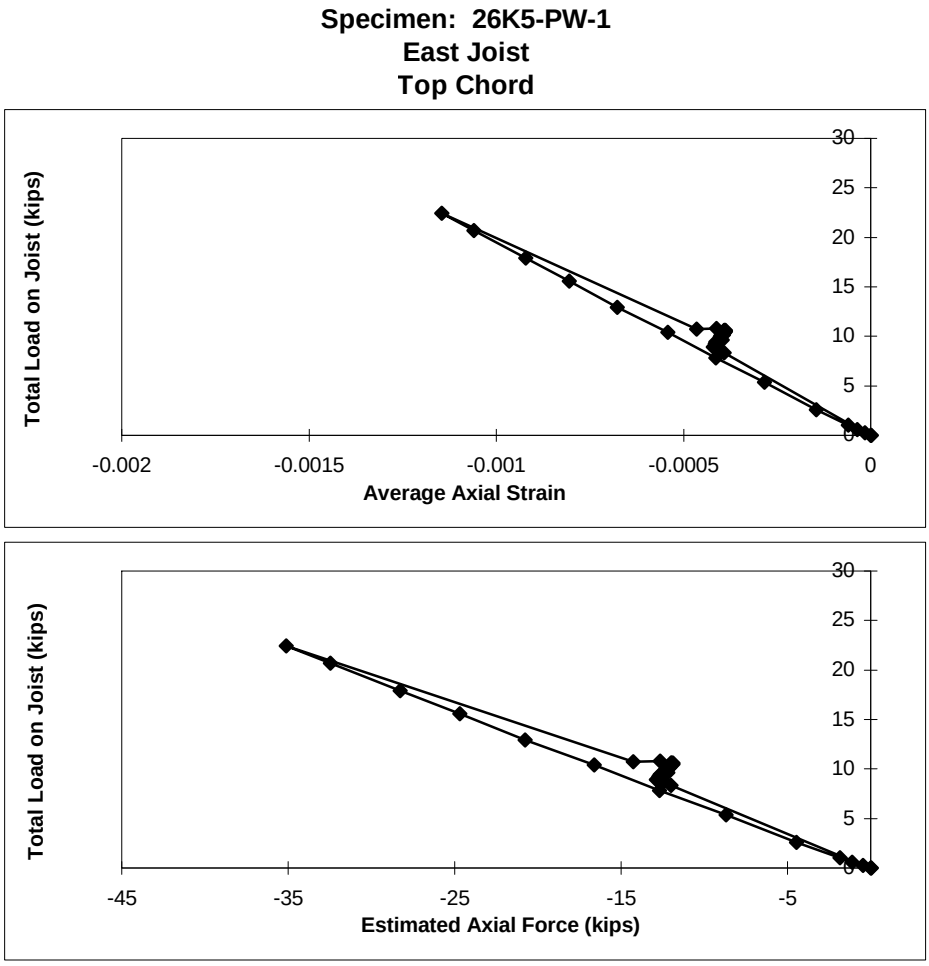

Figure C.39 26K5-PW-1 East Joist Top Chord

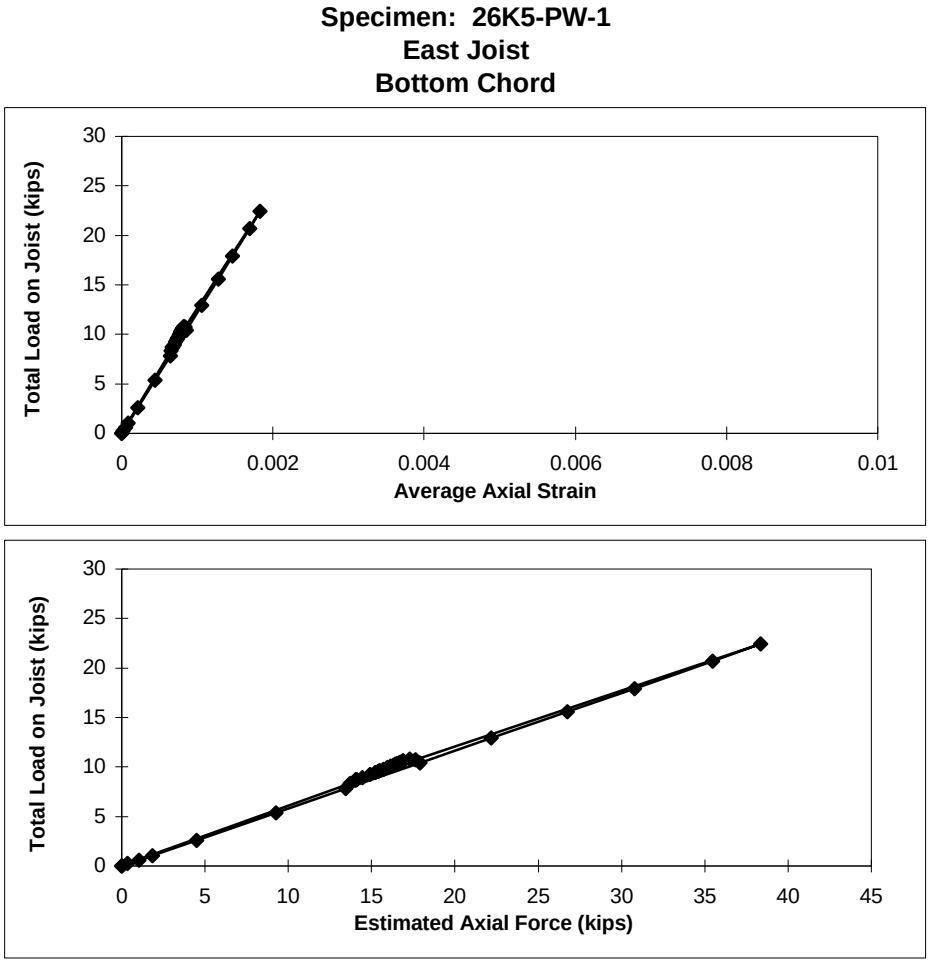

Figure C.40 26K5-PW-1 East Joist Bottom Chord

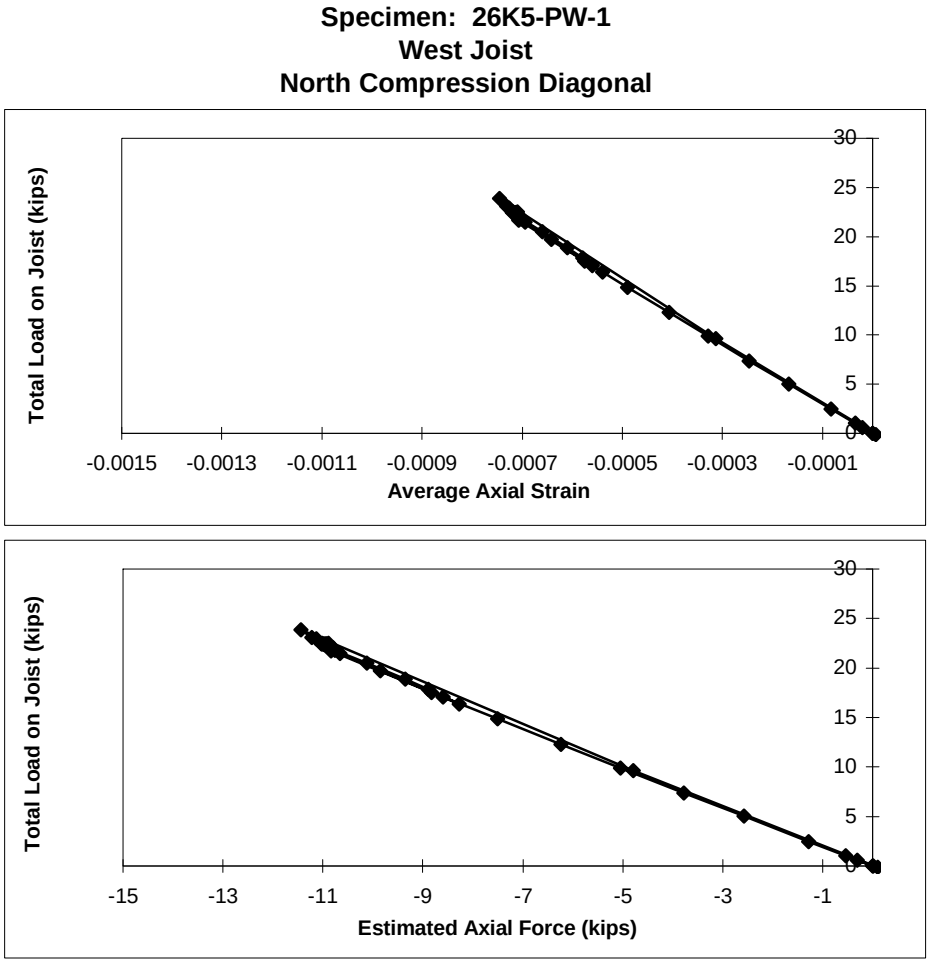

Figure C.41 26K5-PW-1 West Joist North Compression Diagonal

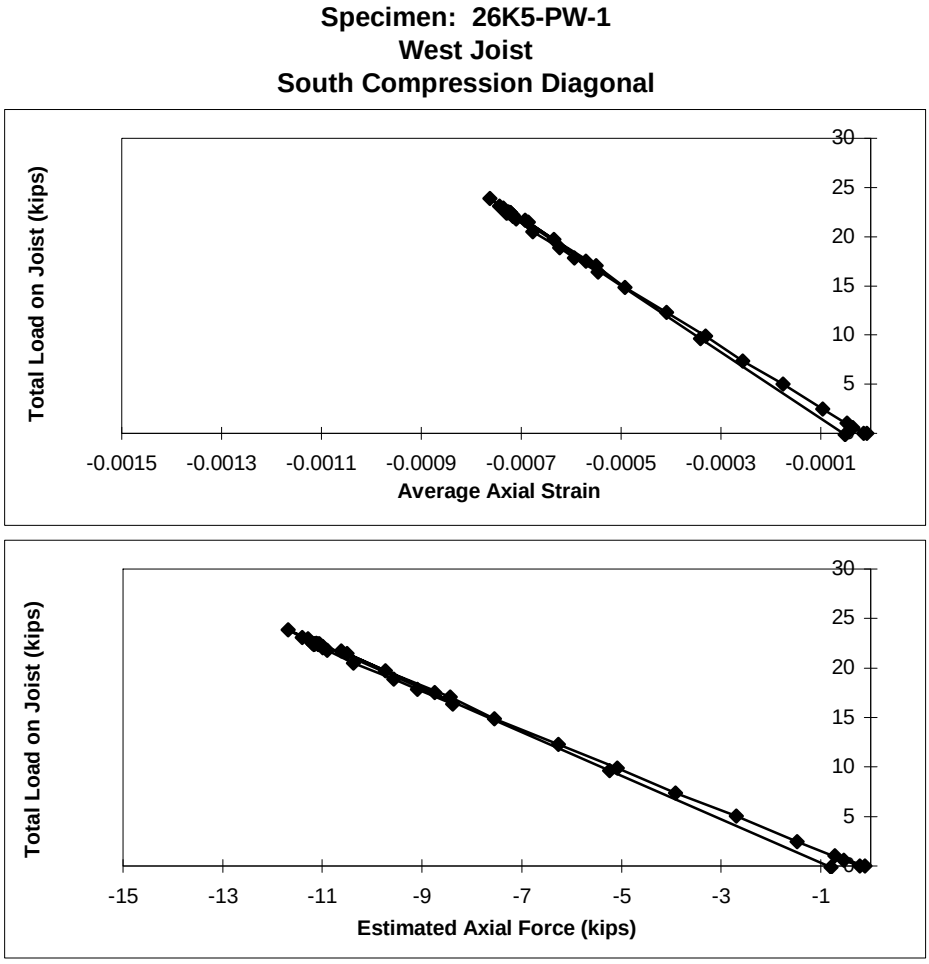

Figure C.42 26K5-PW-1 West Joist South Compression Diagonal

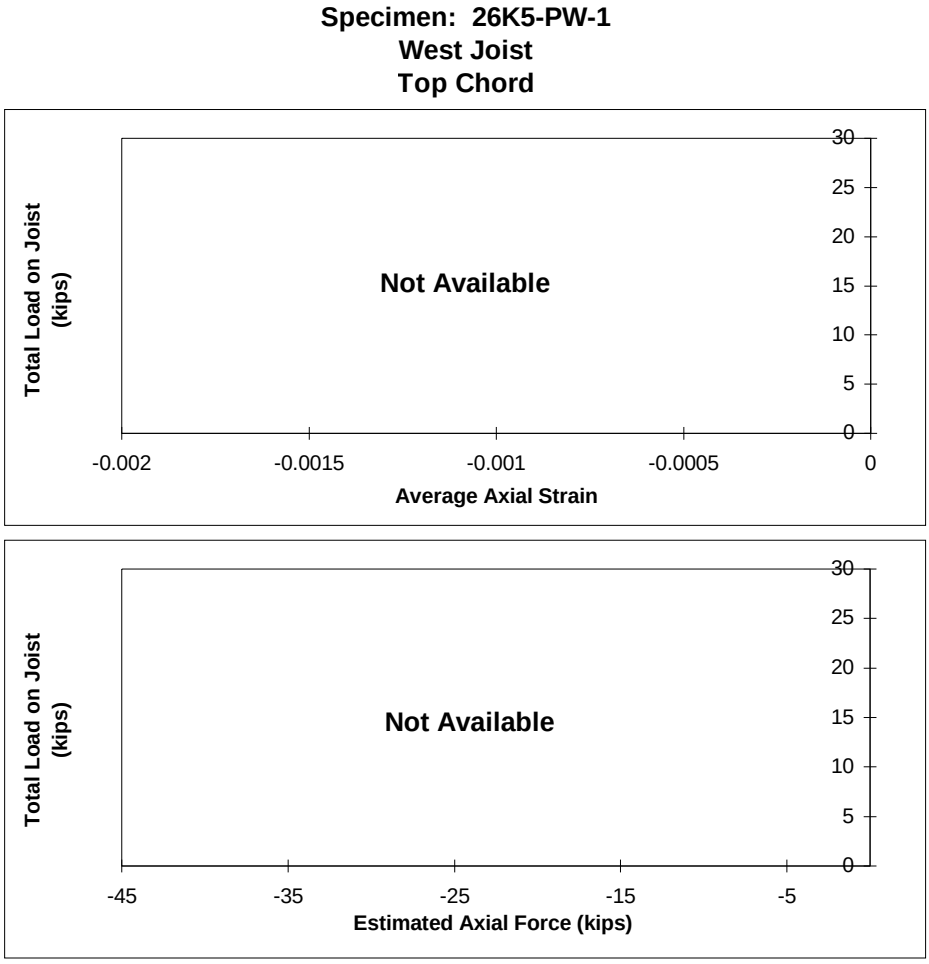

Figure C.43 26K5-PW-1 West Joist Top Chord

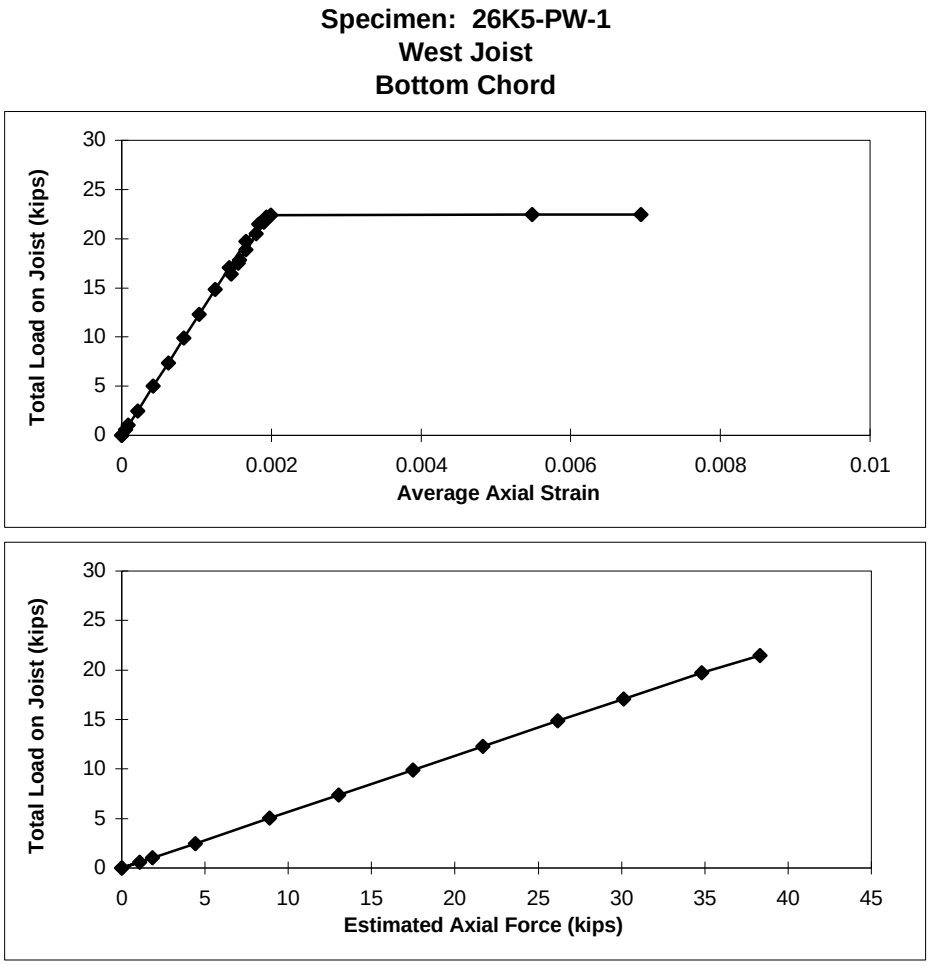

Figure C.44 26K5-PW-1 West Joist Bottom Chord

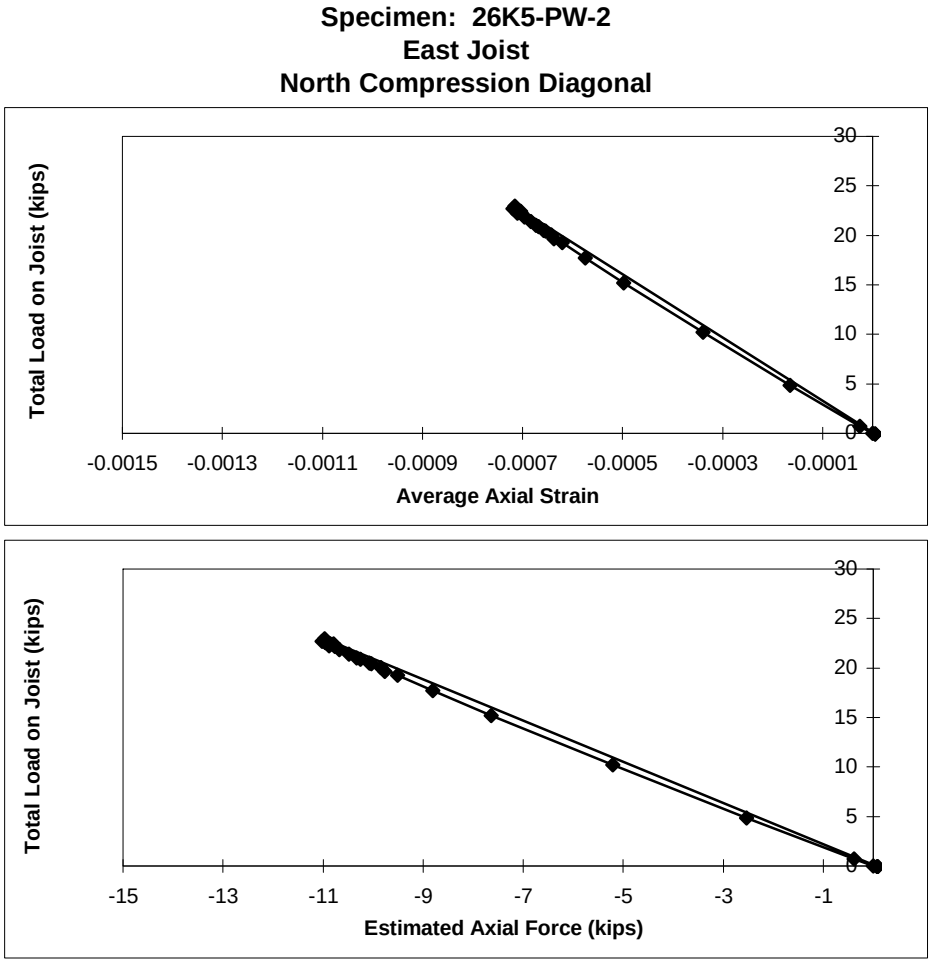

Figure C.45 26K5-PW-2 East Joist North Compression Diagonal

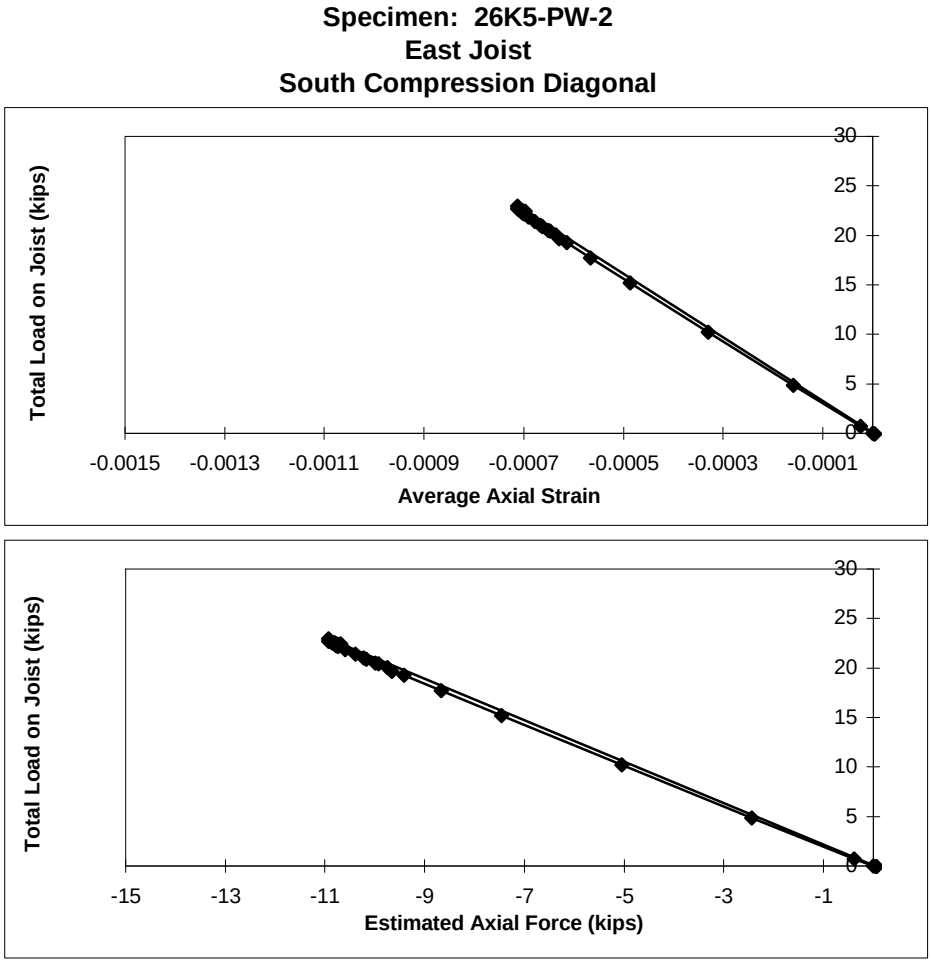

Figure C.46 26K5-PW-2 East Joist South Compression Diagonal

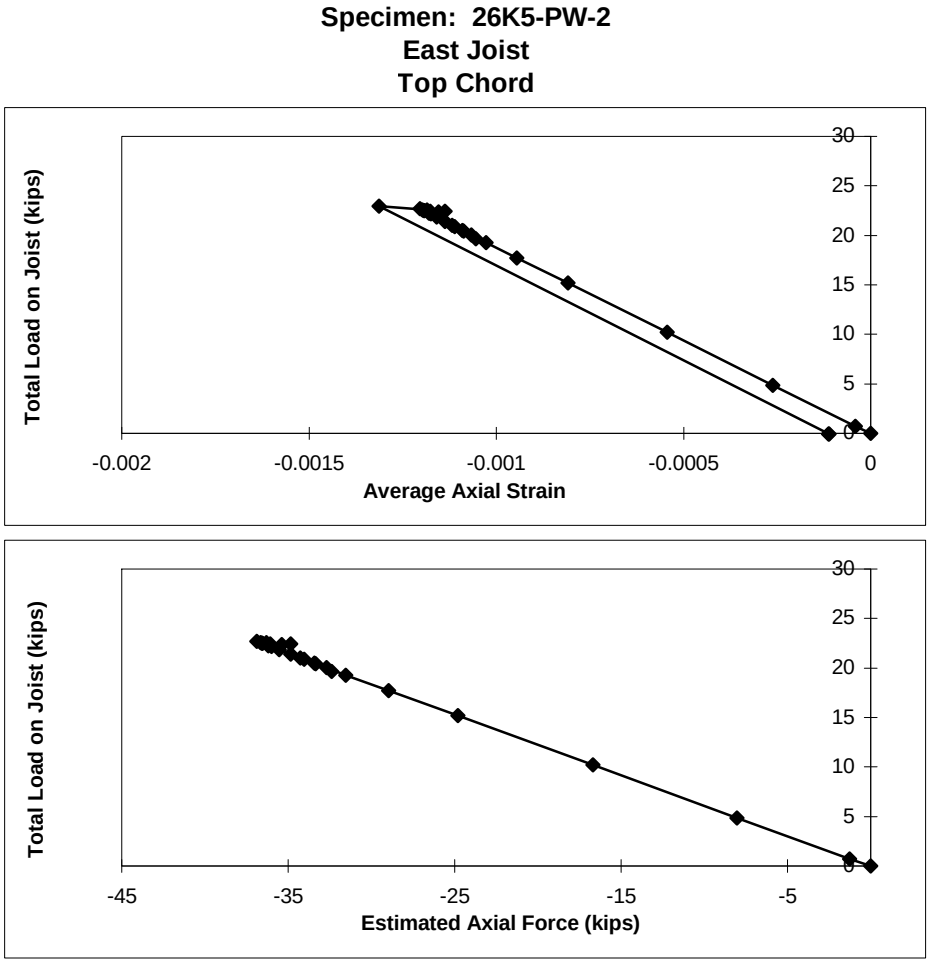

Figure C.47 26K5-PW-2 East Joist Top Chord

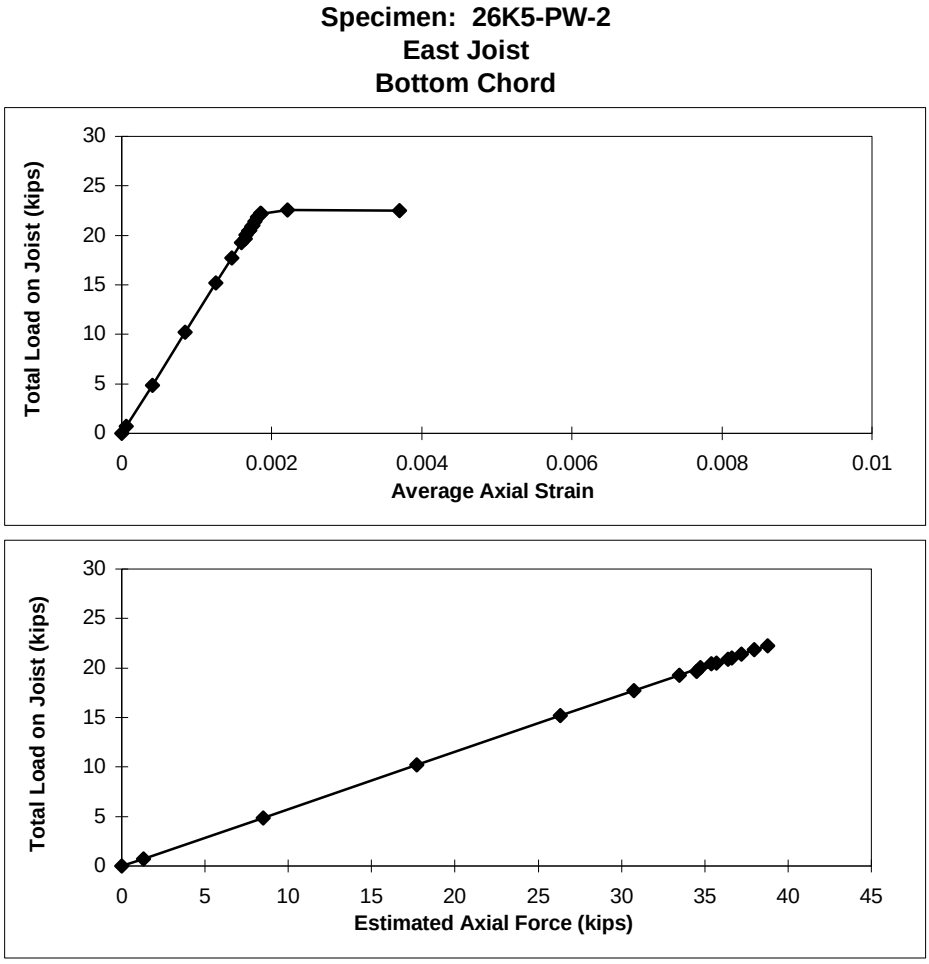

Figure C.48 26K5-PW-2 East Joist Bottom Chord

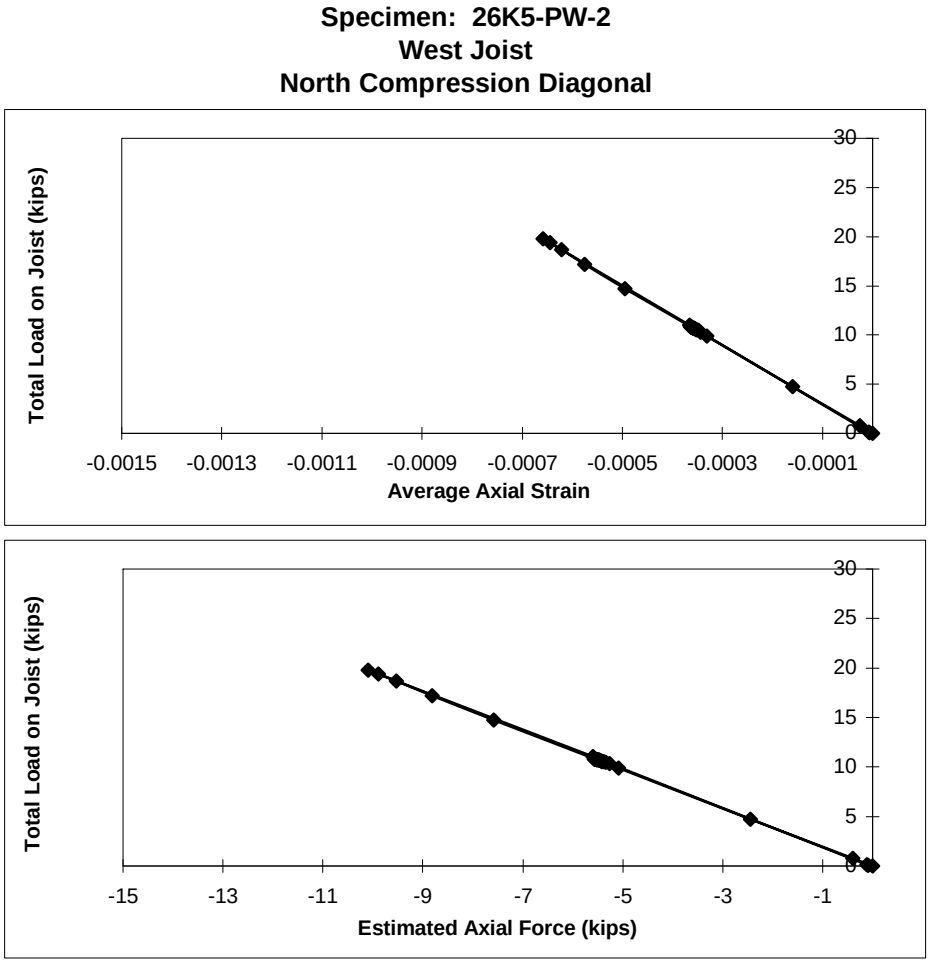

Figure C.49 26K5-PW-2 West Joist North Compression Diagonal

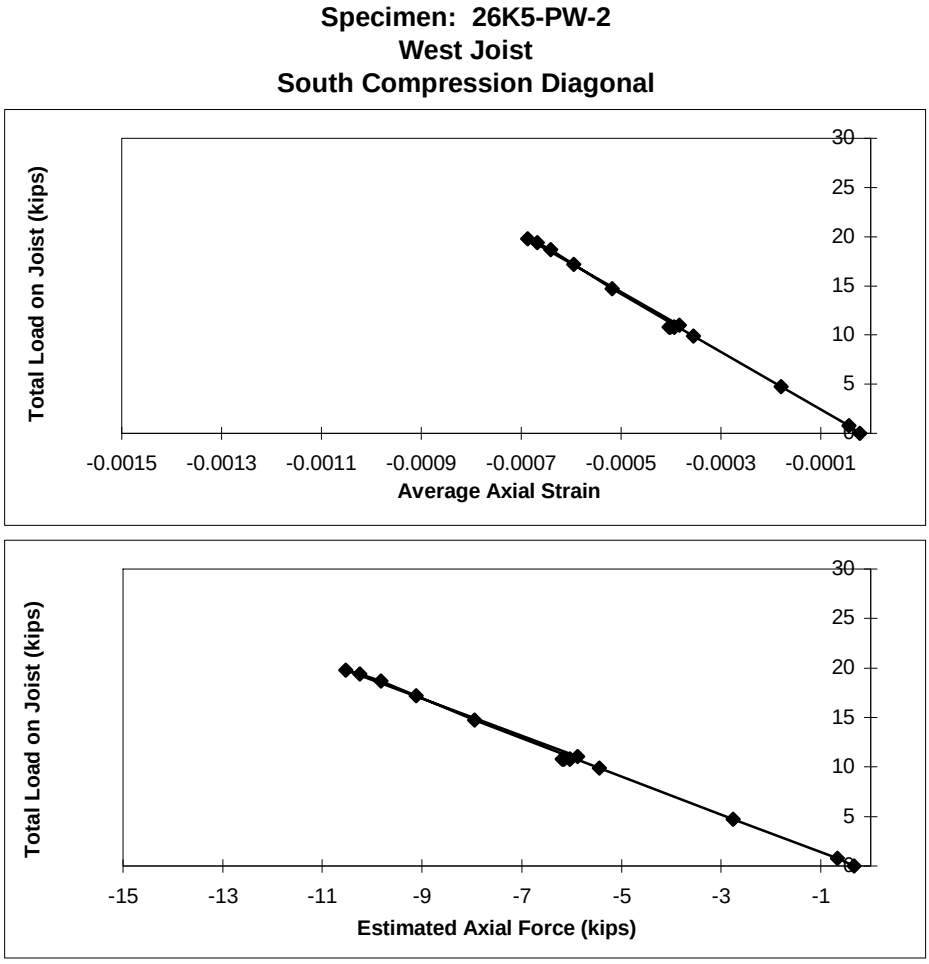

Figure C.50 26K5-PW-2 West Joist South Compression Diagonal

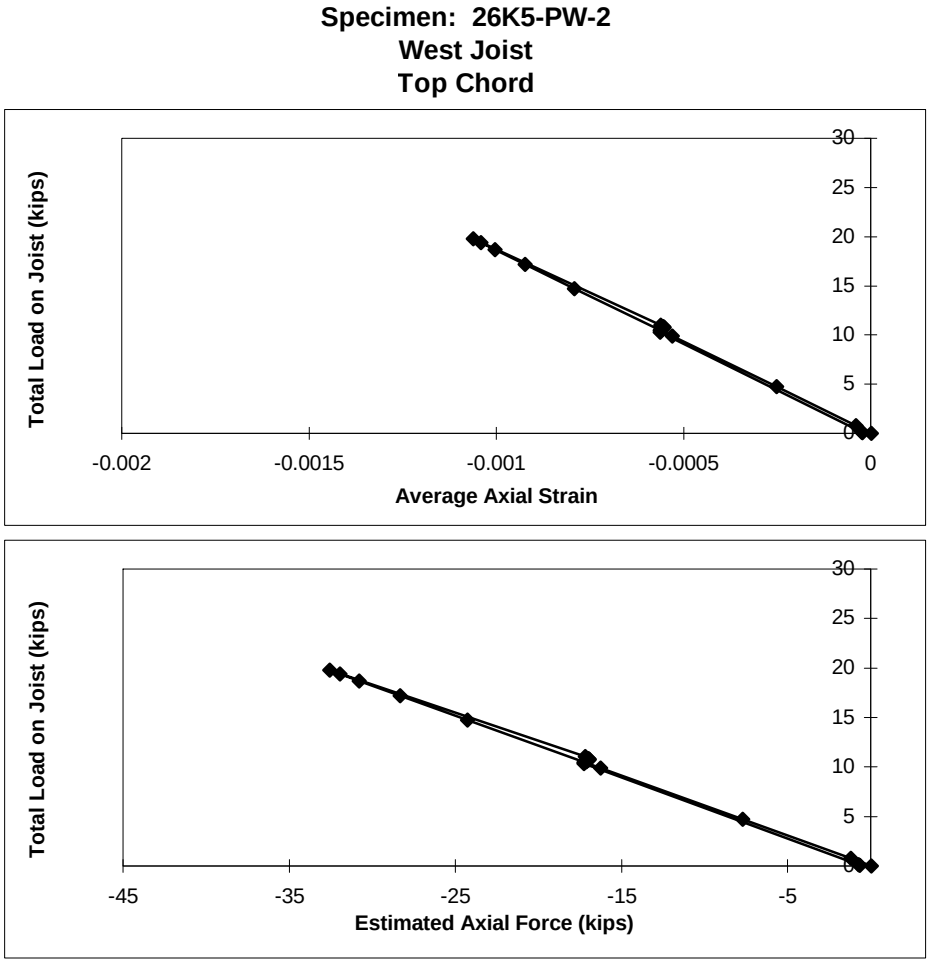

Figure C.51 26K5-PW-2 West Joist Top Chord

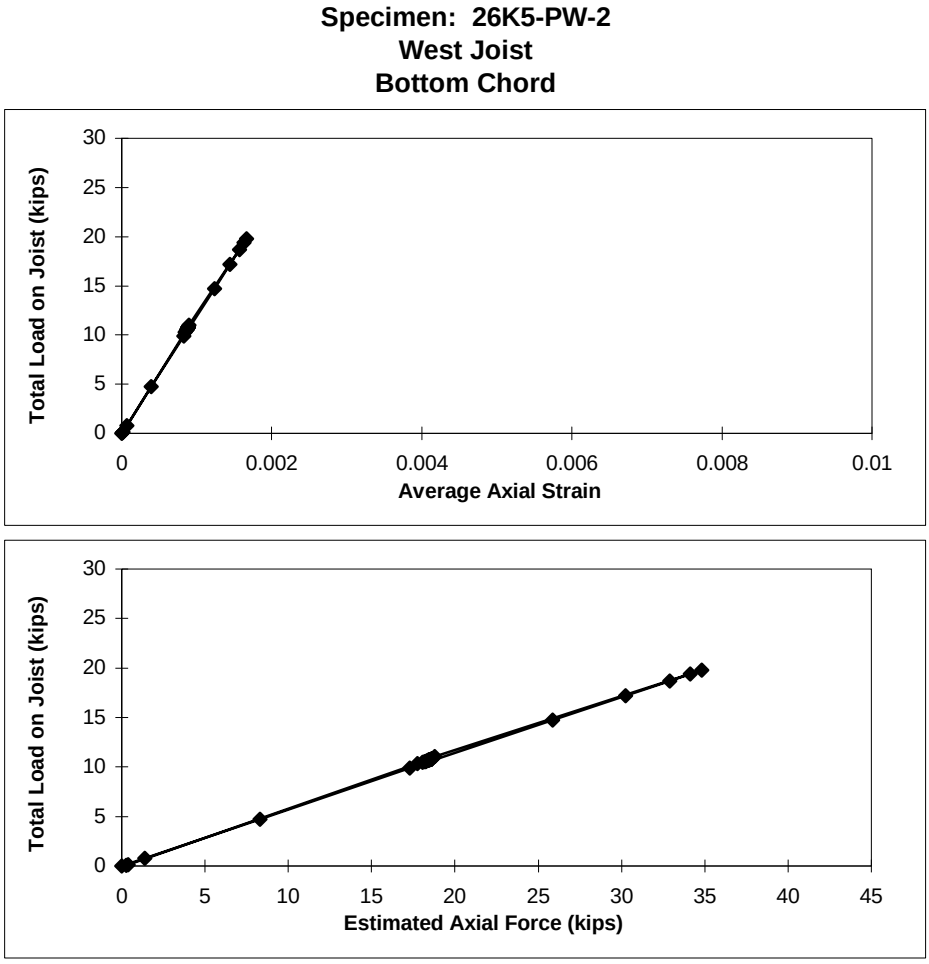

Figure C.52 26K5-PW-2 West Joist Bottom Chord

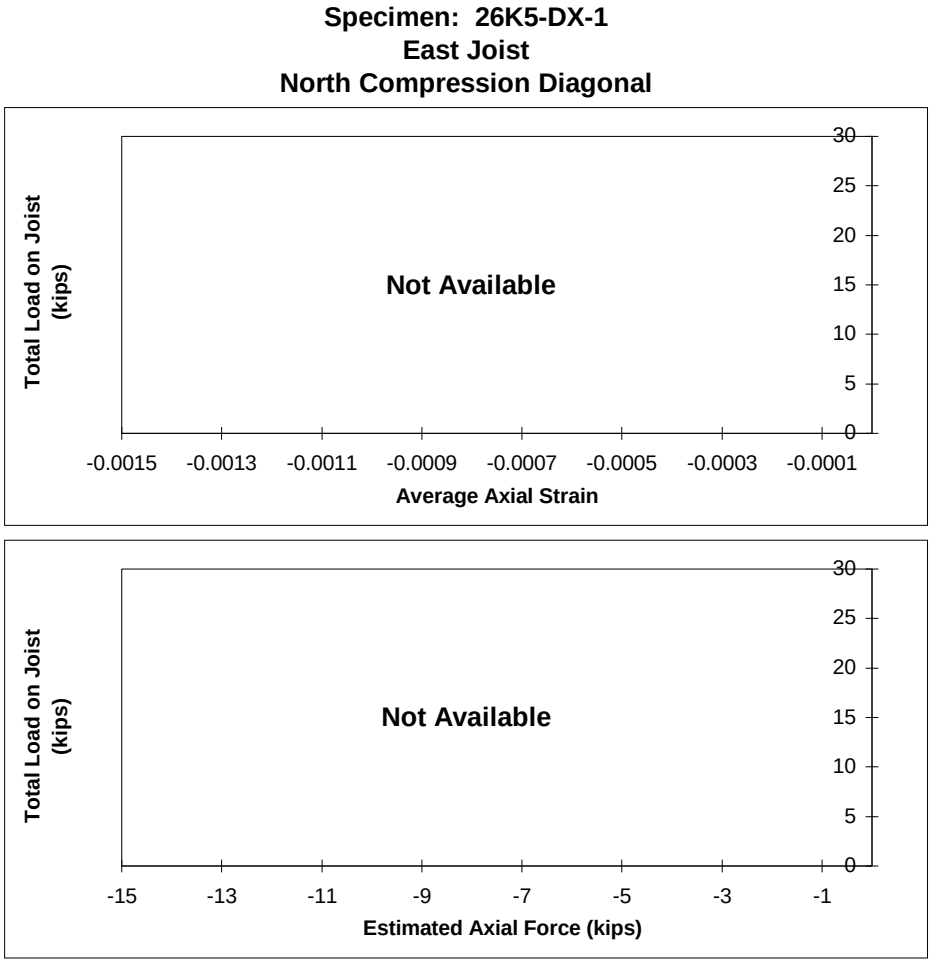

Figure C.53 26K5-DX-1 East Joist North Compression Diagonal

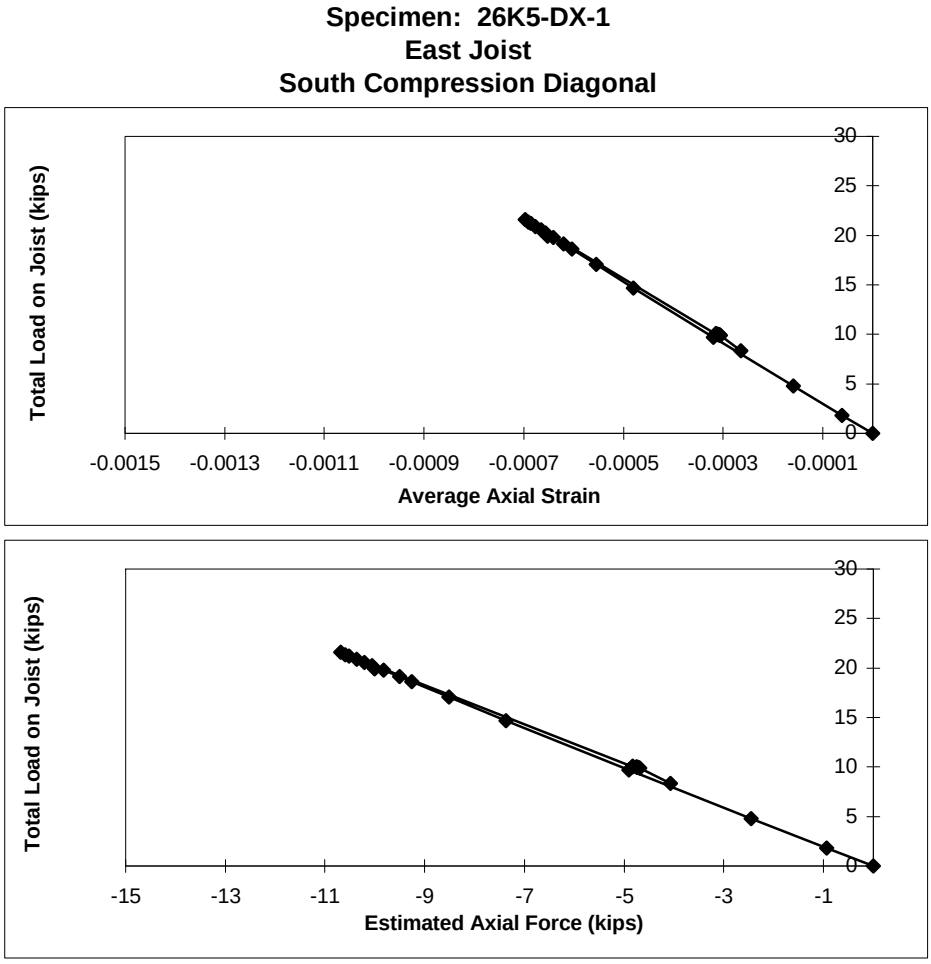

Figure C.54 26K5-DX-1 East Joist South Compression Diagonal

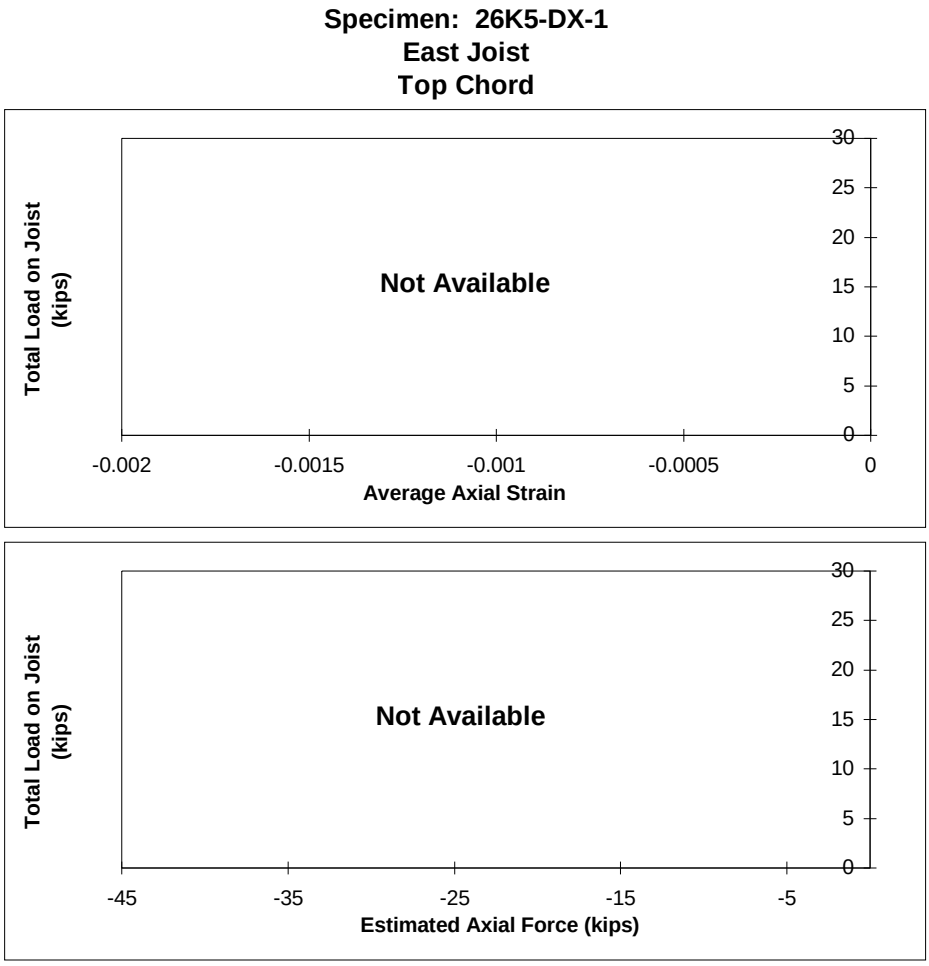

Figure C.55 26K5-DX-1 East Joist Top Chord

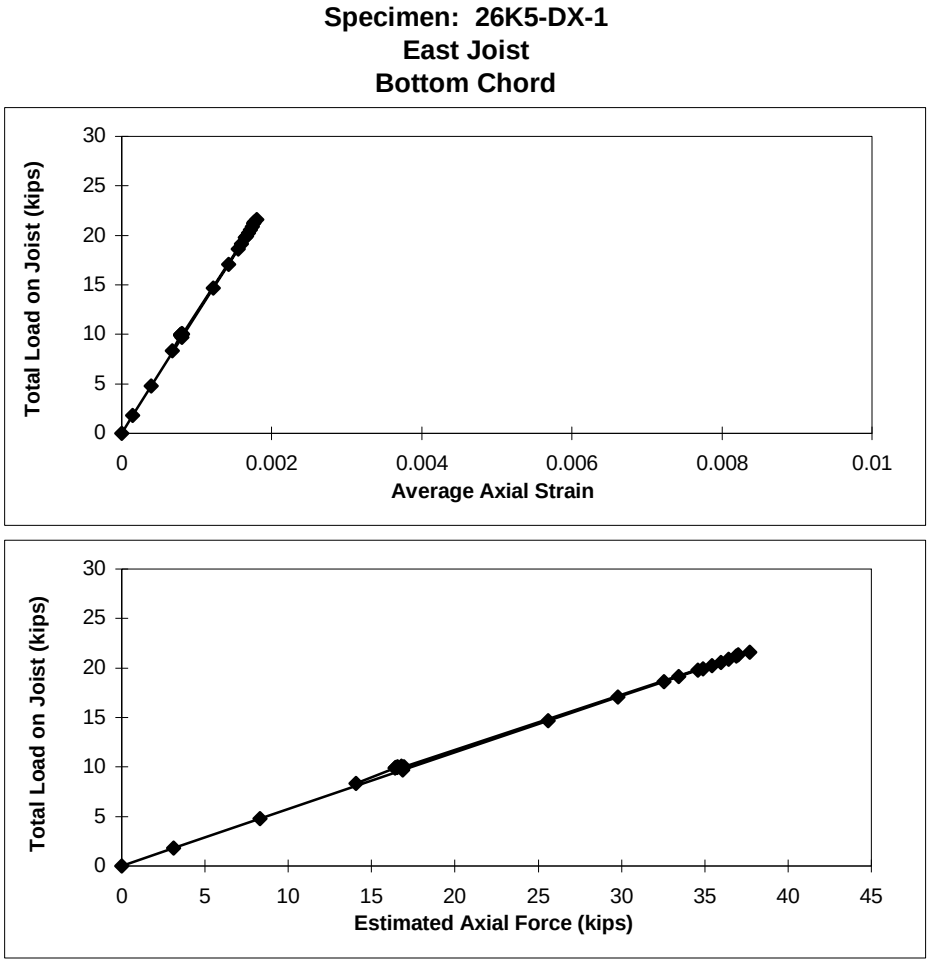

Figure C.56 26K5-DX-1 East Joist Bottom Chord

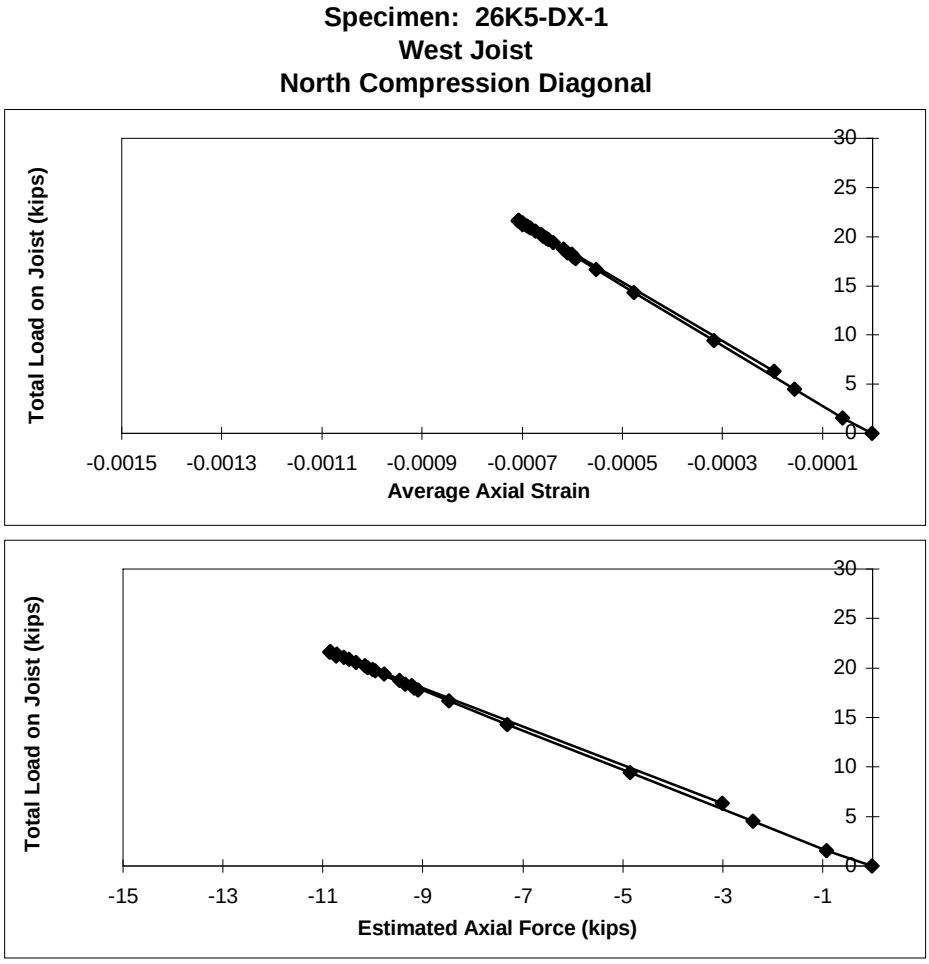

Figure C.57 26K5-DX-1 West Joist North Compression Diagonal

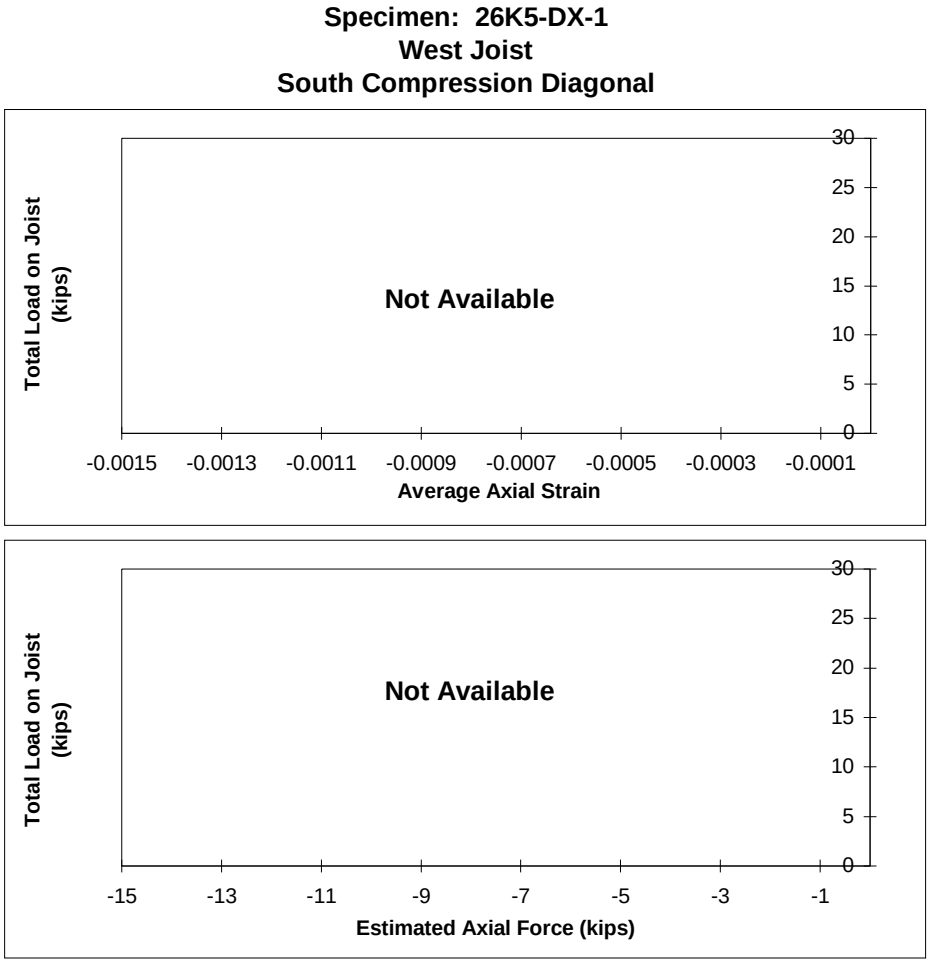

Figure C.58 26K5-DX-1 West Joist South Compression Diagonal

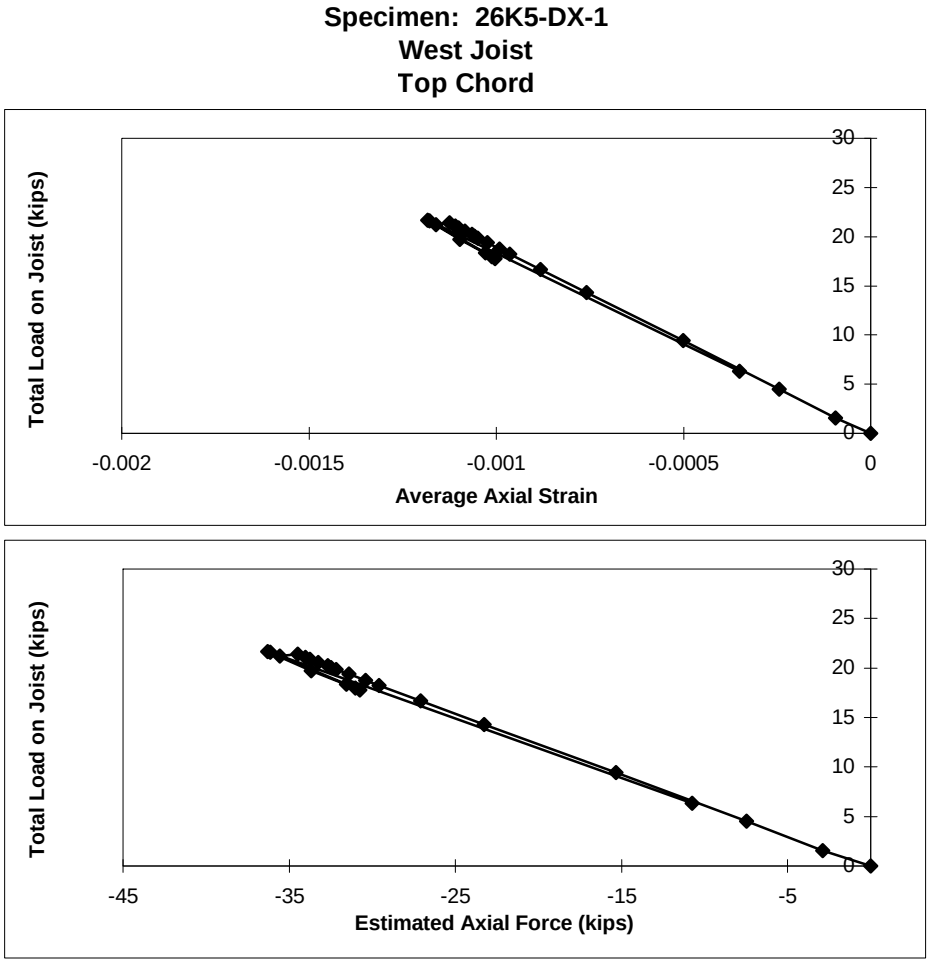

Figure C.59 26K5-DX-1 West Joist Top Chord

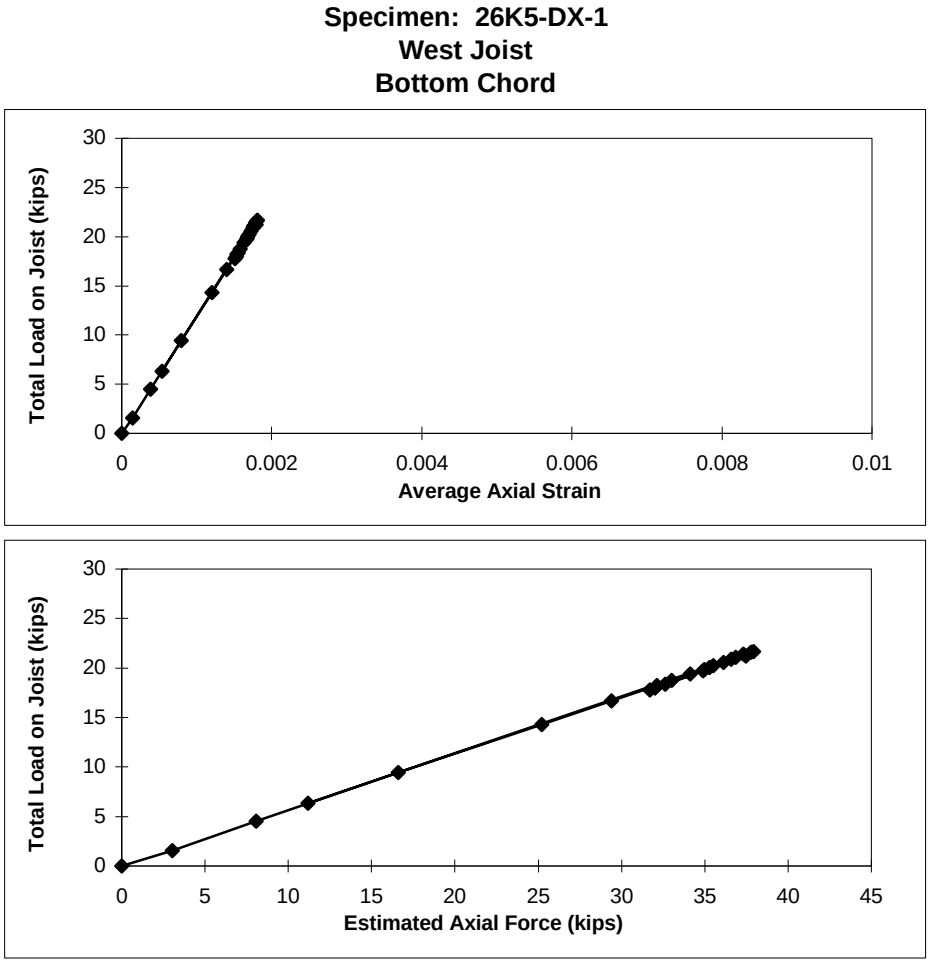

Figure C.60 26K5-DX-1 West Joist Bottom Chord

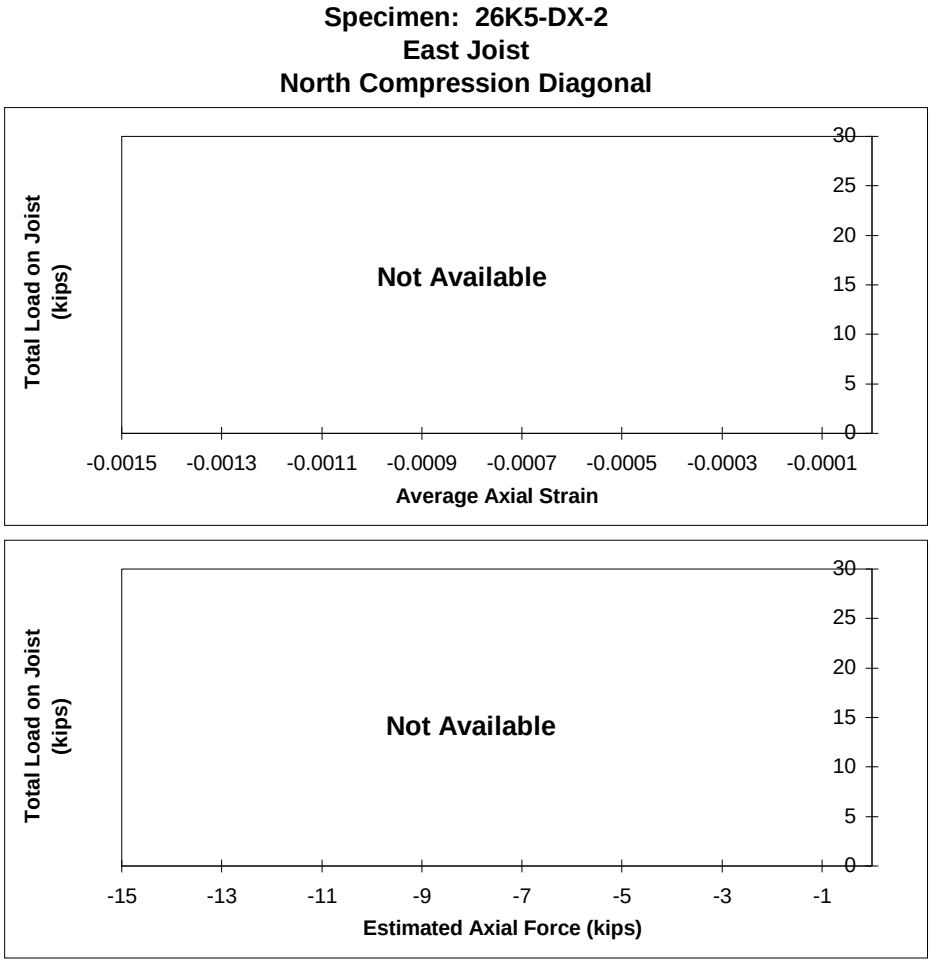

Figure C.61 26K5-DX-2 East Joist North Compression Diagonal

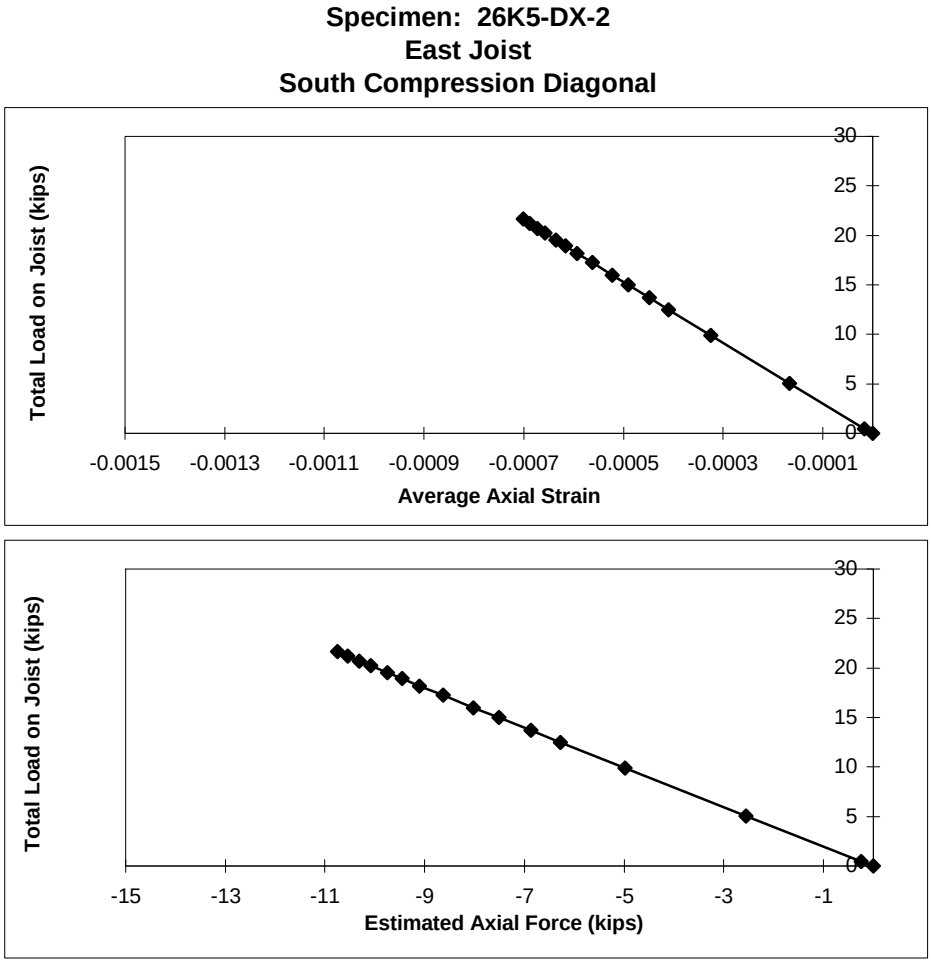

Figure C.62 26K5-DX-2 East Joist South Compression Diagonal

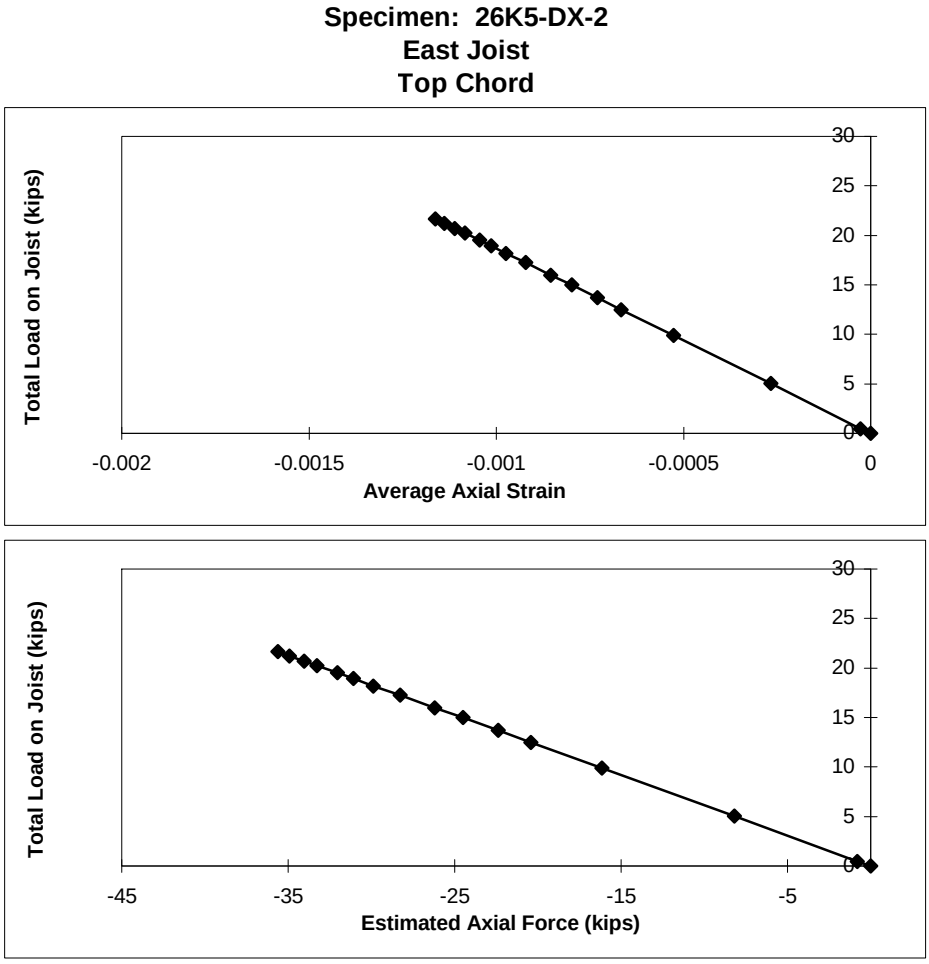

Figure C.63 26K5-DX-2 East Joist Top Chord

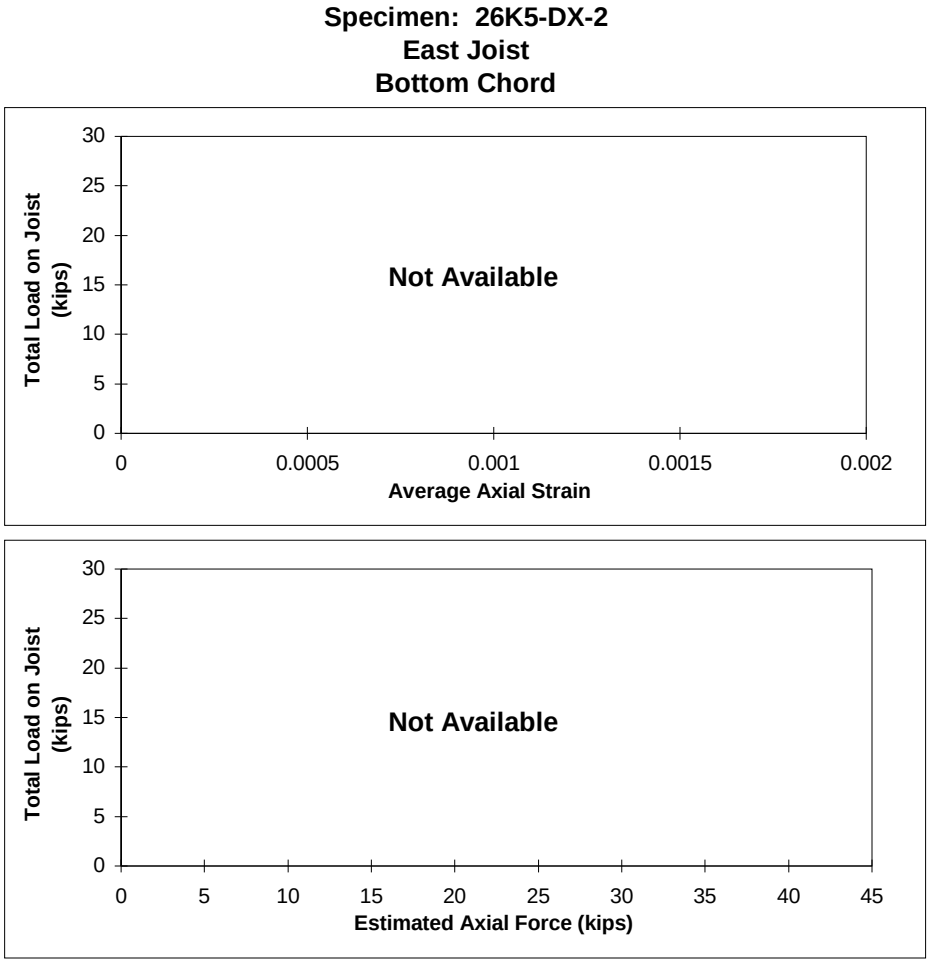

Figure C.64 26K5-DX-2 East Joist Bottom Chord

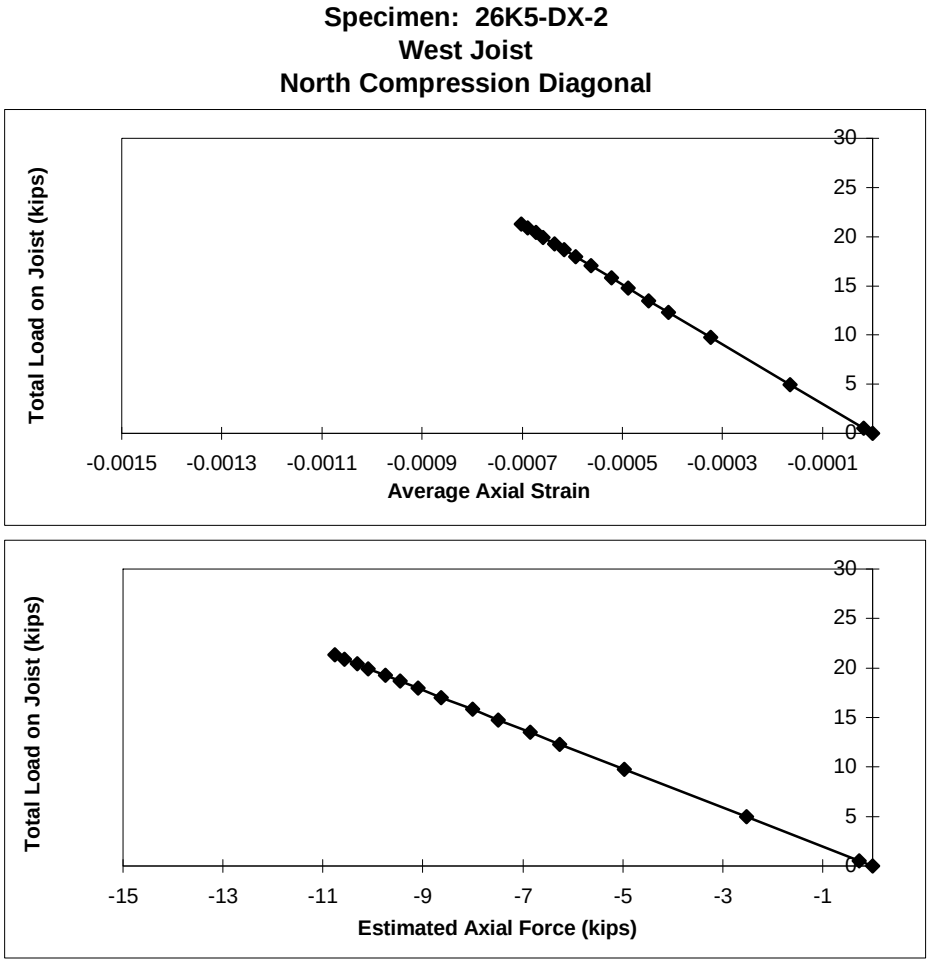

Figure C.65 26K5-DX-2 West Joist North Compression Diagonal

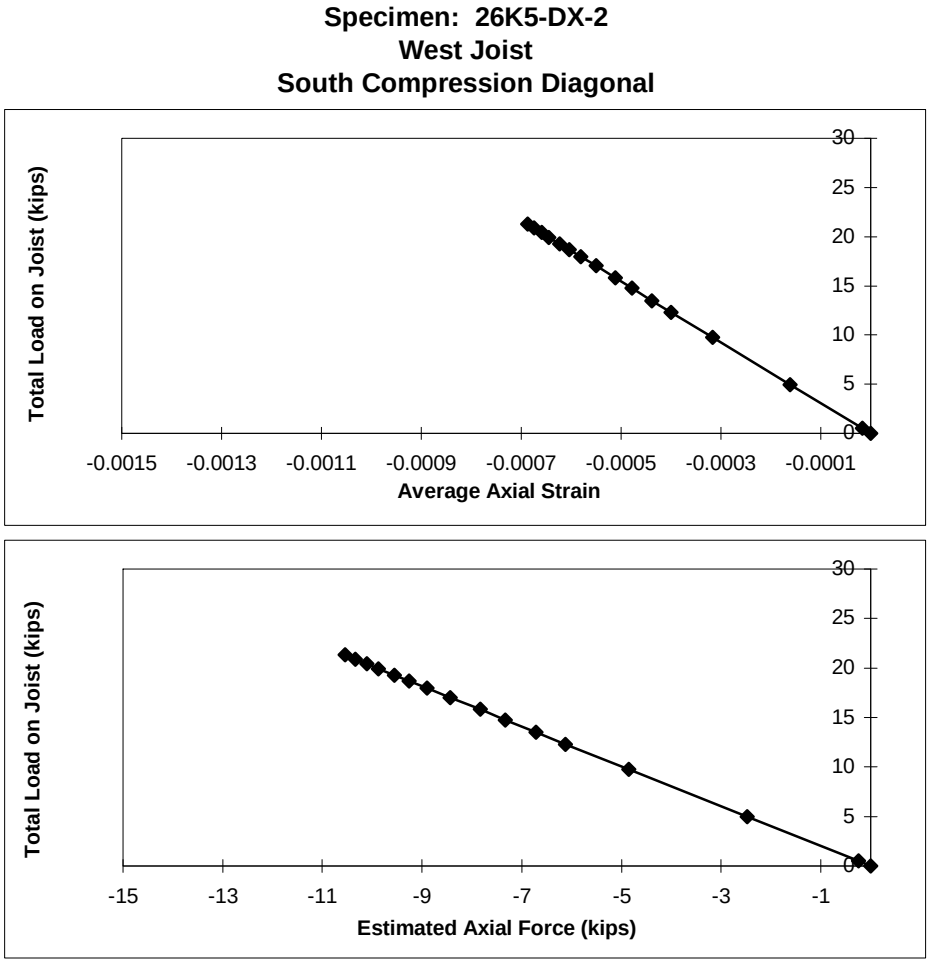

Figure C.66 26K5-DX-2 West Joist South Compression Diagonal

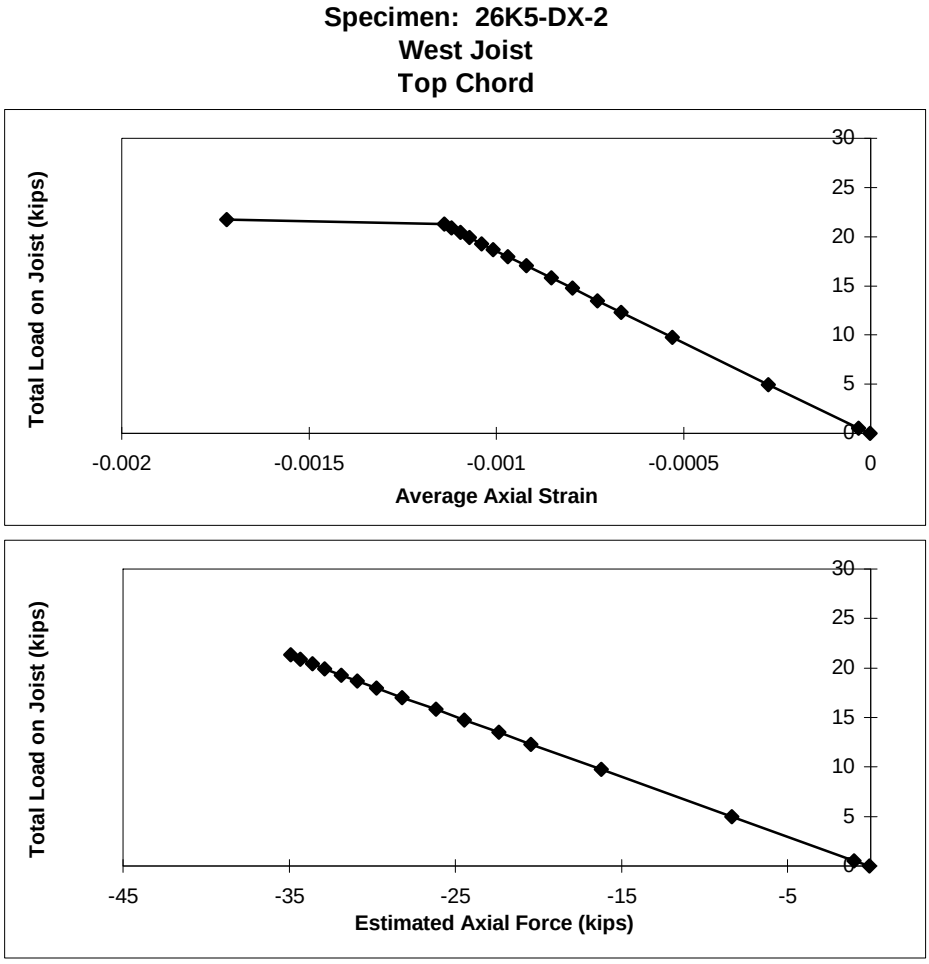

Figure C.67 26K5-DX-2 West Joist Top Chord

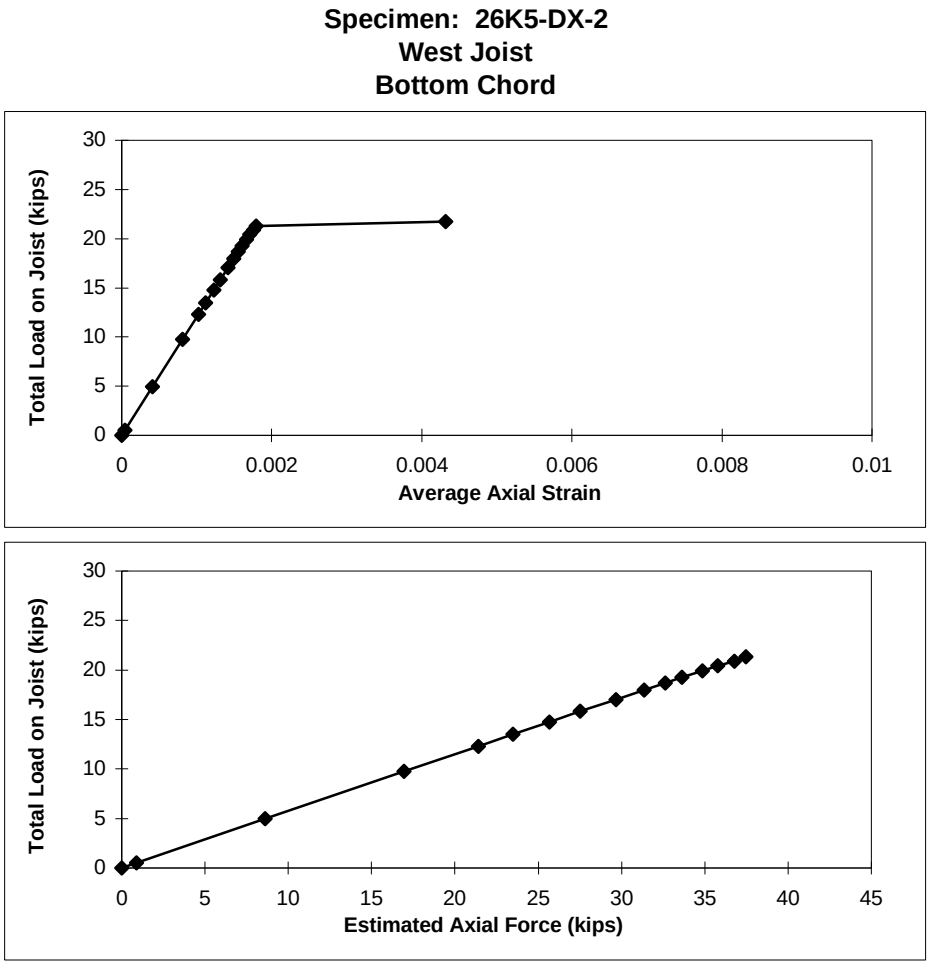

Figure C.68 26K5-DX-2 West Joist Bottom Chord

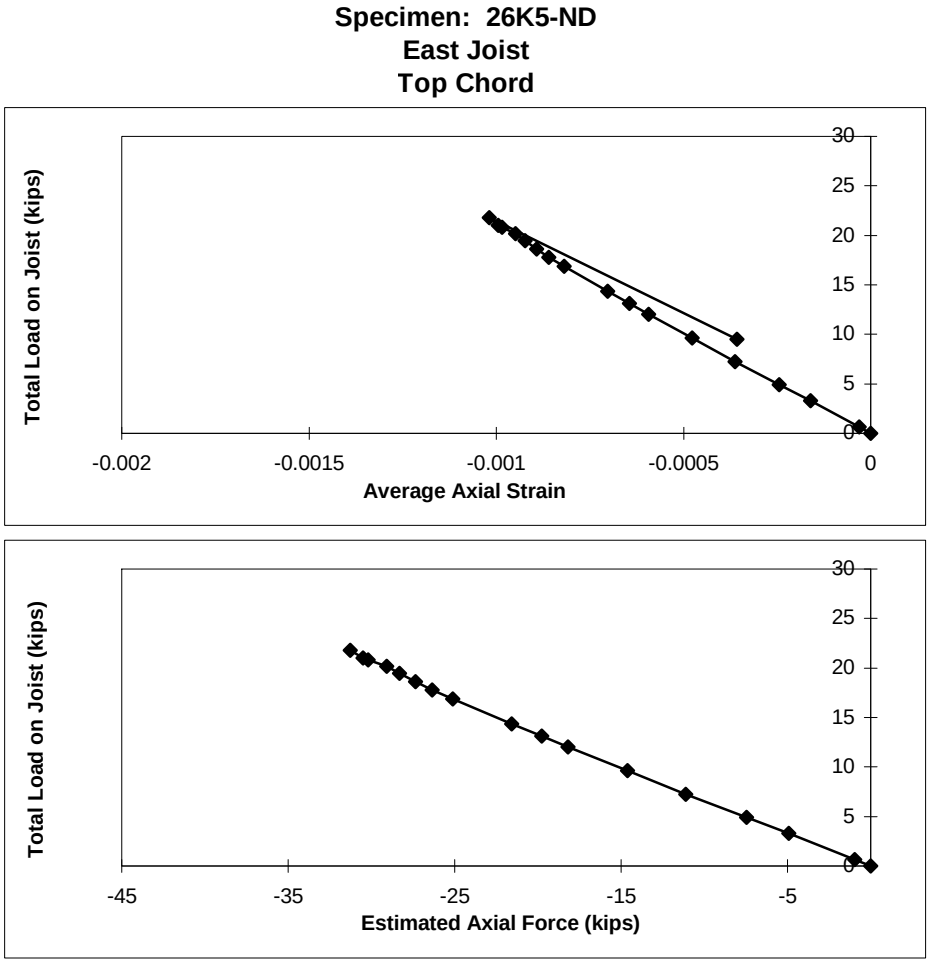

Figure C.69 26K5-ND East Joist Top Chord

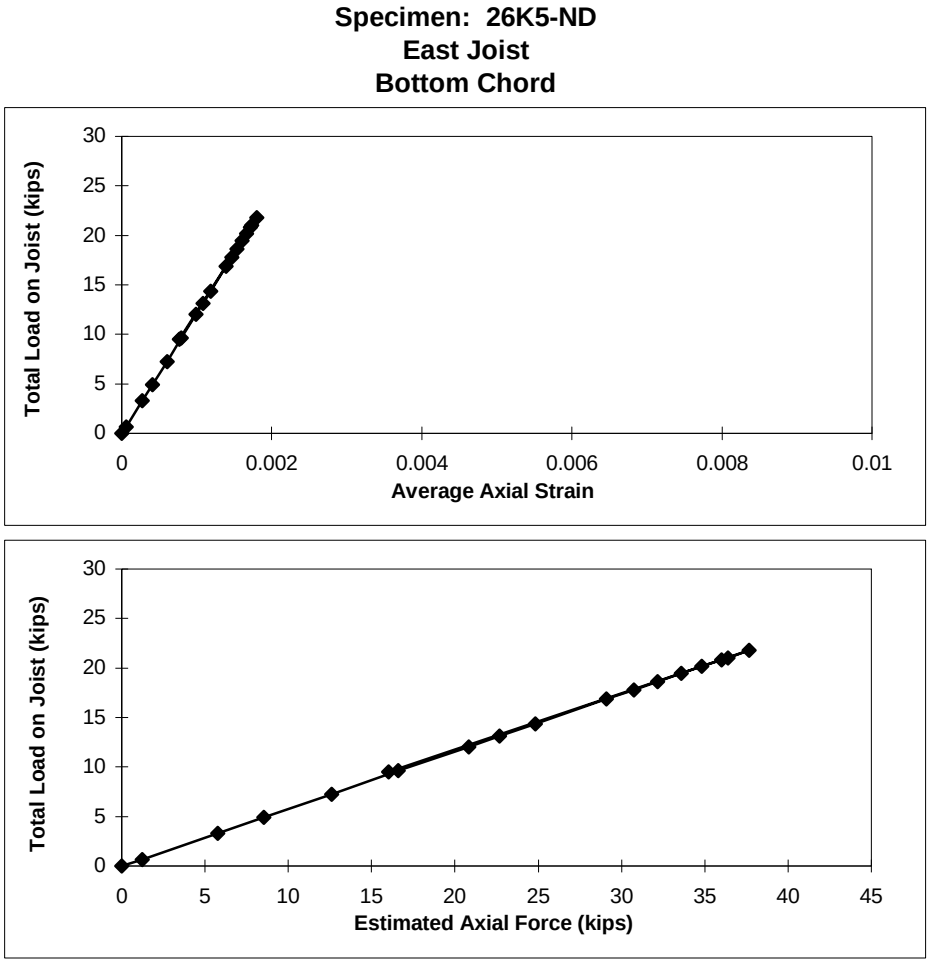

Figure C.70 26K5-ND East Joist Bottom Chord

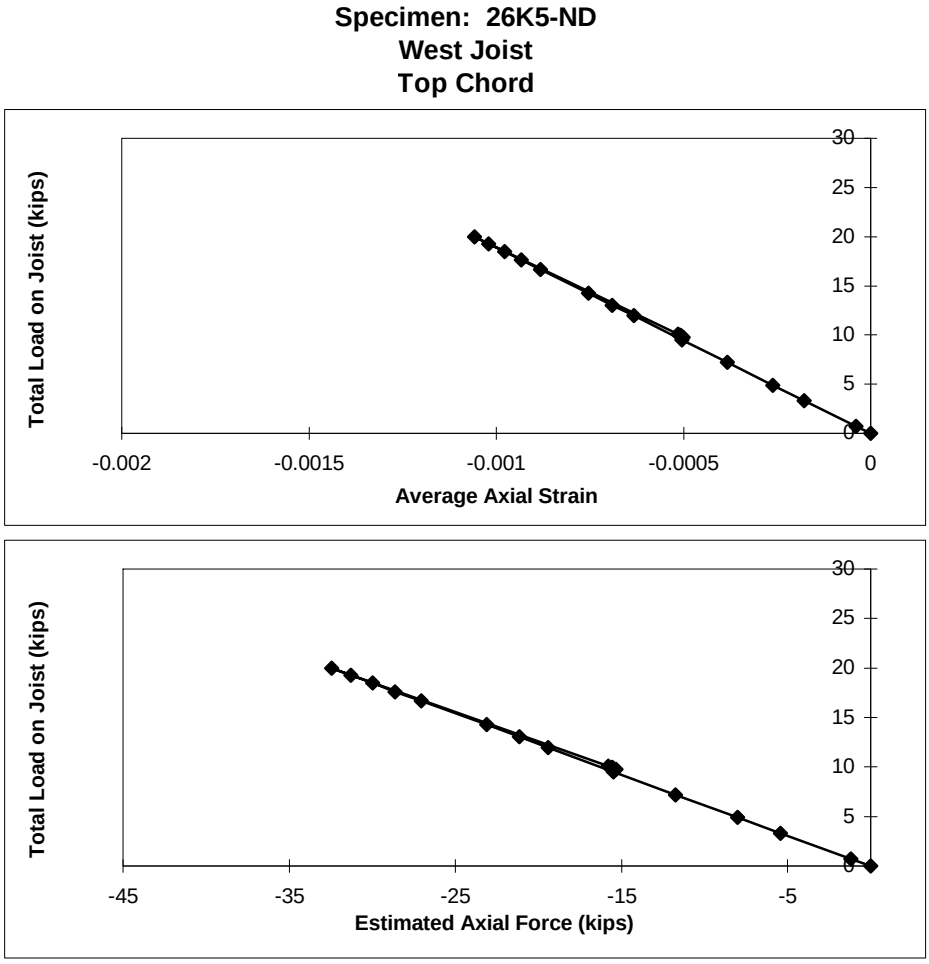

Figure C.71 26K5-ND West Joist Top Chord

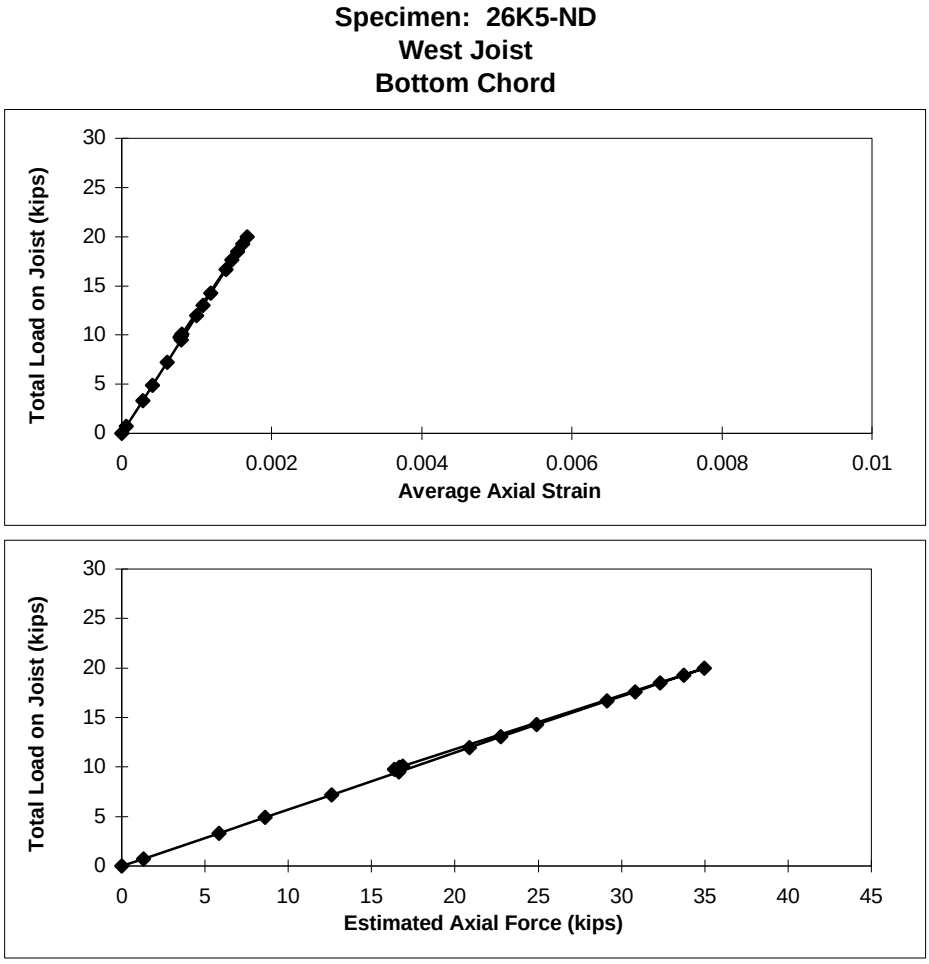

Figure C.72 26K5-ND West Joist Bottom Chord

Appendix D:

Force vs. Elongation Response for Double Angle Specimens

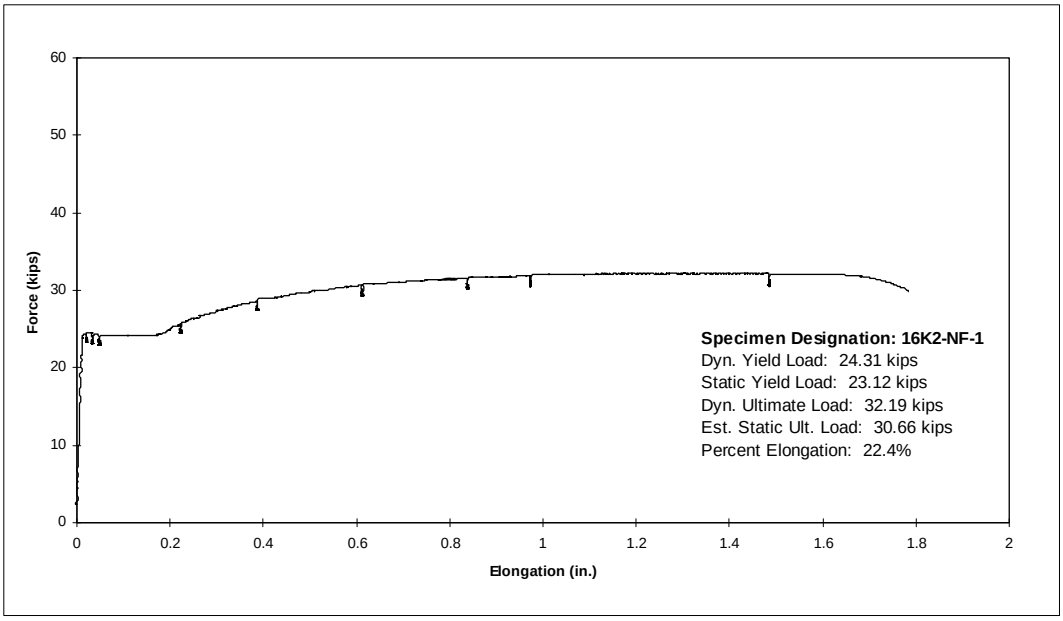

Figure D.1 Force vs. Elongation Response of Specimen 16K2-NF-1

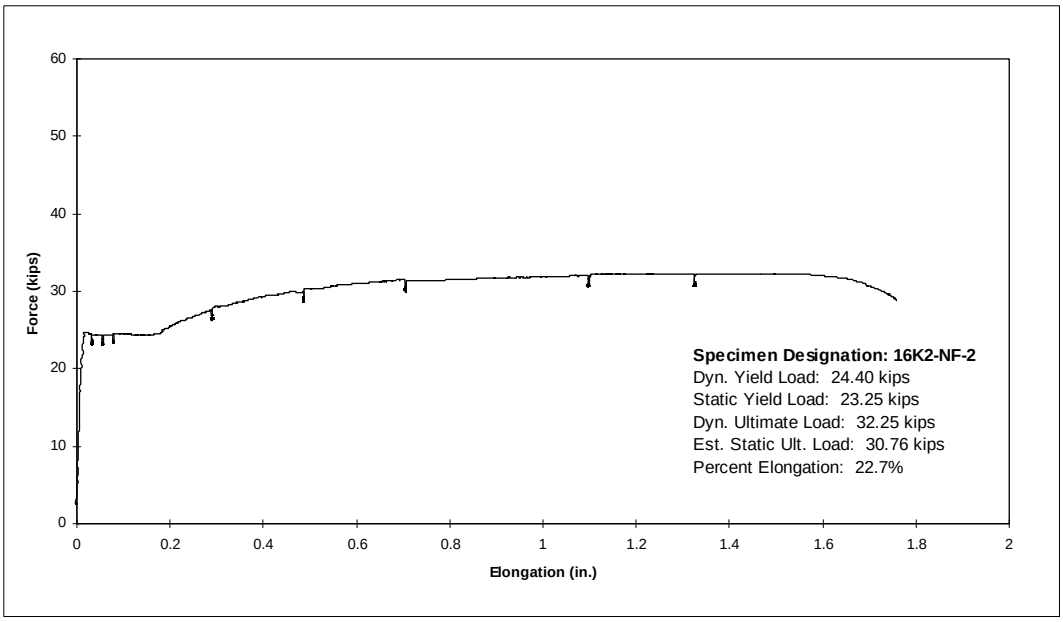

Figure D.2 Force vs. Elongation Response of Specimen 16K2-NF-2

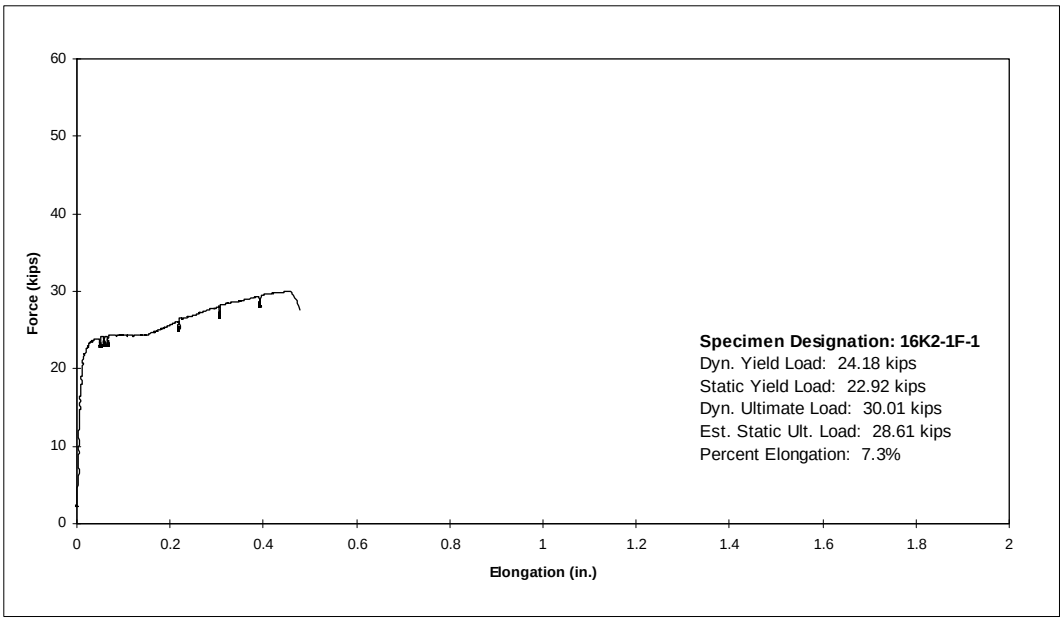

Figure D.3 Force vs. Elongation Response of Specimen 16K2-1F-1

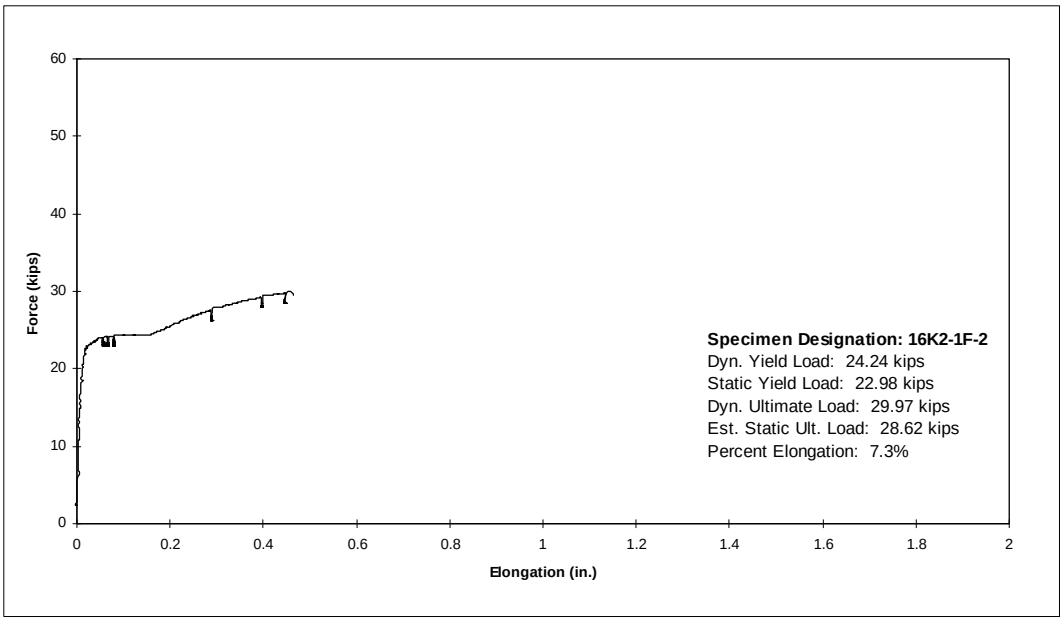

Figure D.4 Force vs. Elongation Response of Specimen 16K2-1F-2

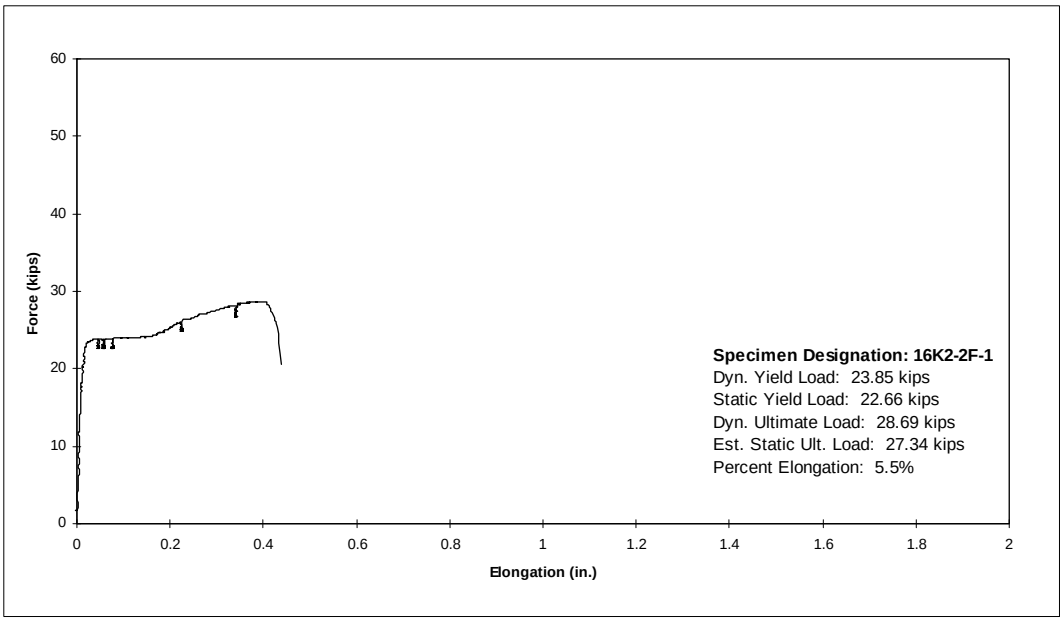

Figure D.5 Force vs. Elongation Response of Specimen 16K2-2F-1

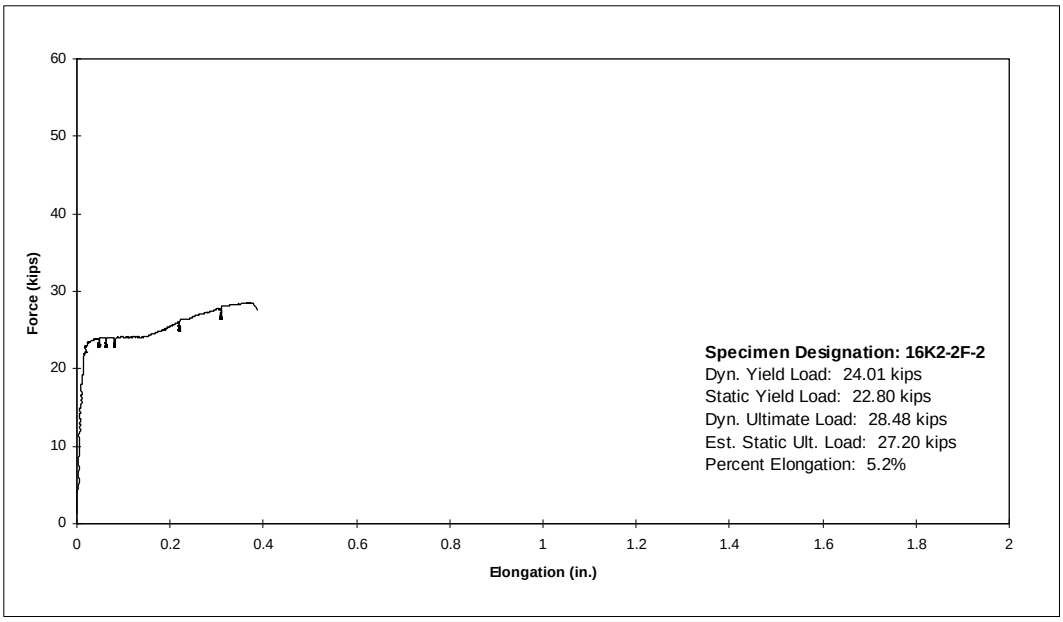

Figure D.6 Force vs. Elongation Response of Specimen 16K2-2F-2

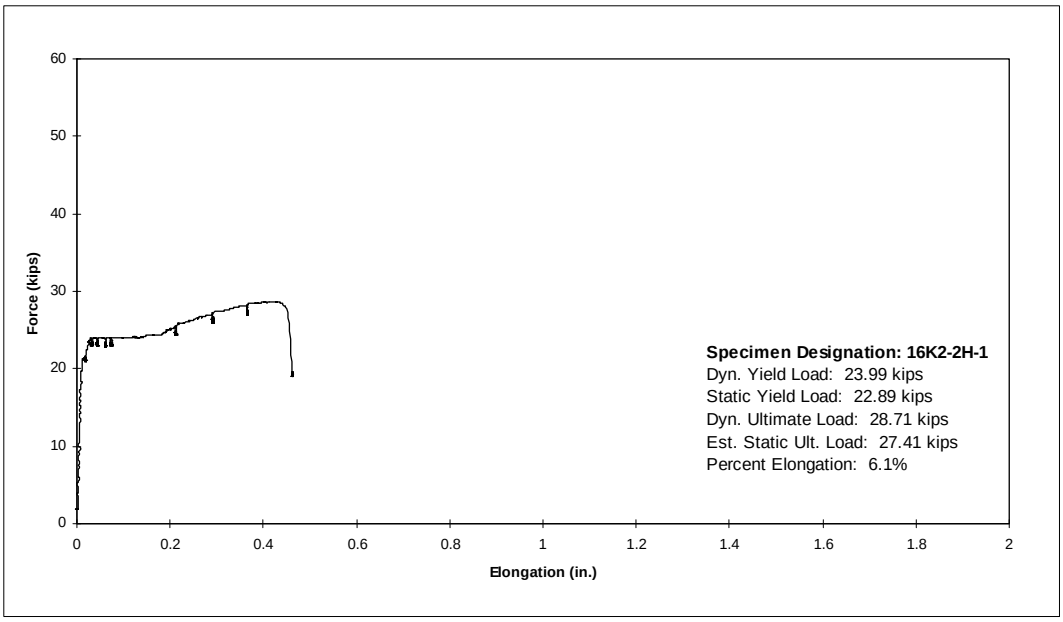

Figure D.7 Force vs. Elongation Response of Specimen 16K2-2H-1

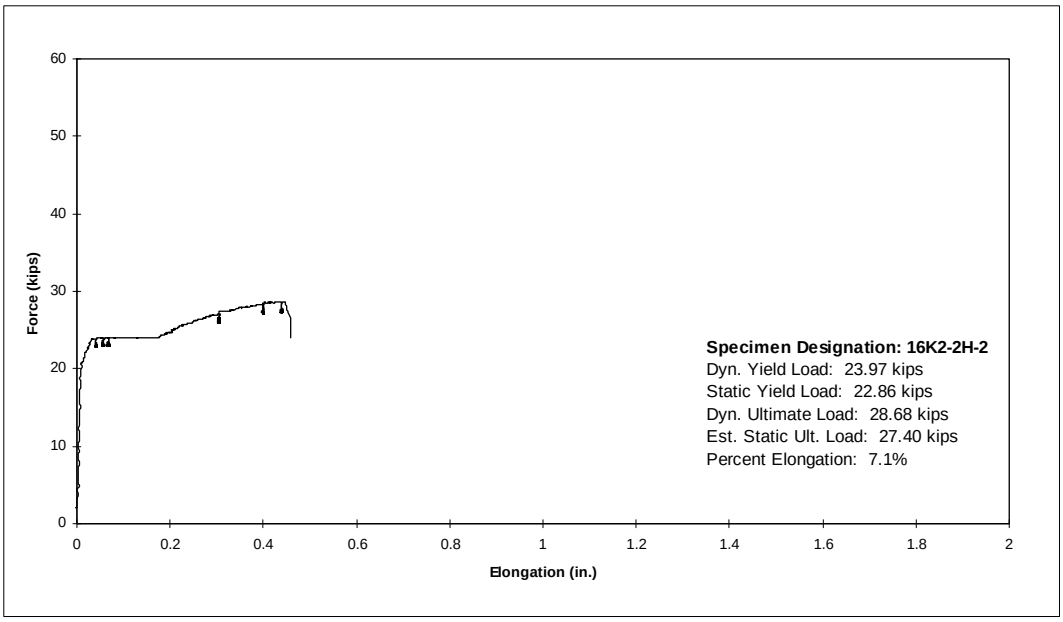

Figure D.8 Force vs. Elongation Response of Specimen 16K2-2H-2

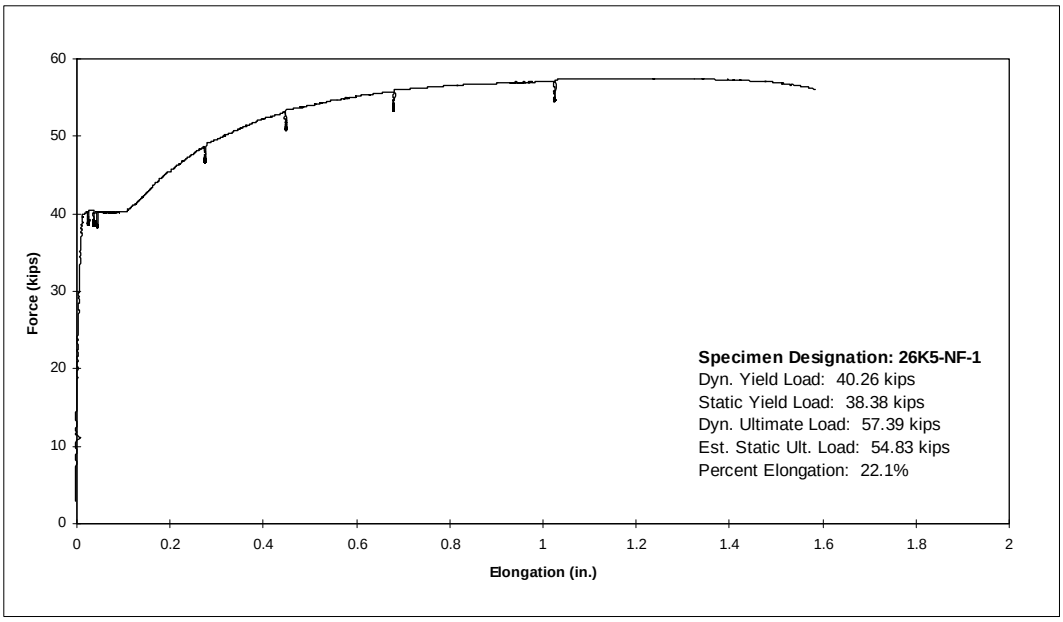

Figure D.9 Force vs. Elongation Response of Specimen 26K5-NF-1

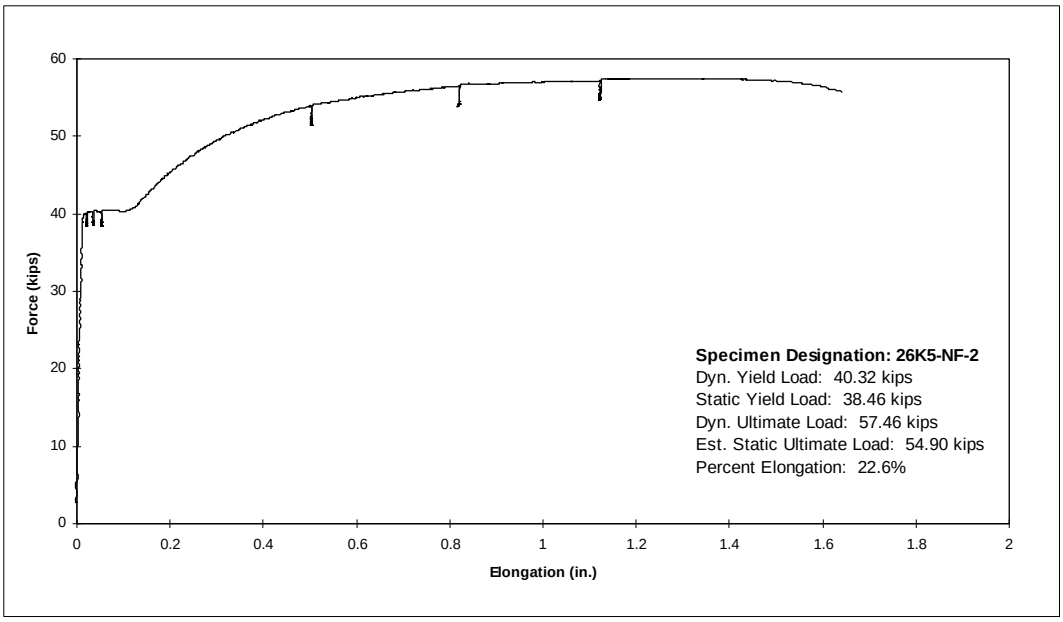

Figure D.10 Force vs. Elongation Response of Specimen 26K5-NF-2

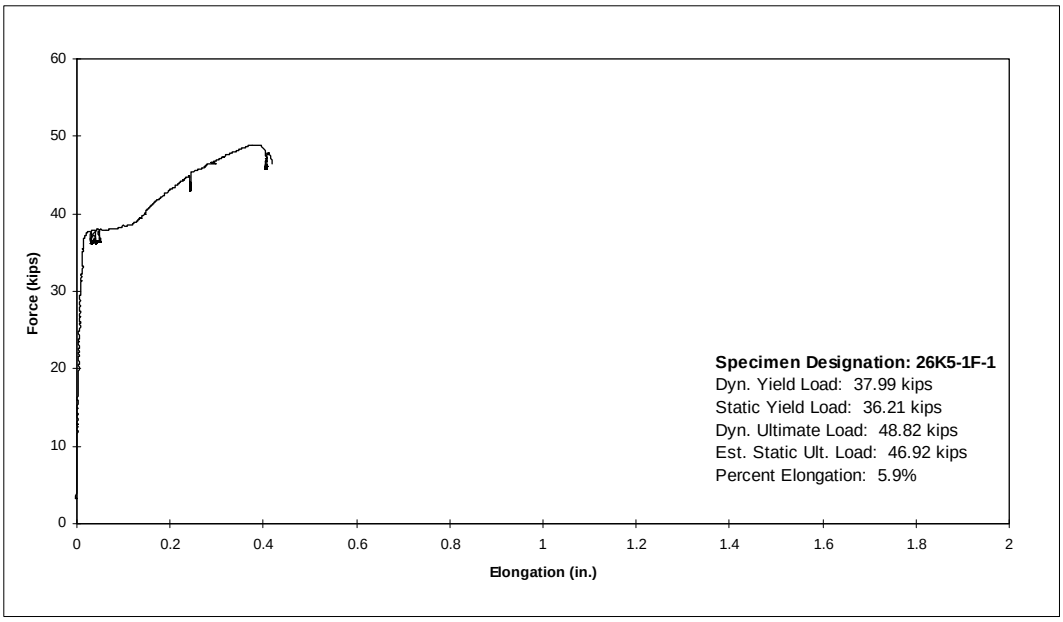

Figure D.11 Force vs. Elongation Response of Specimen 26K5-1F-1

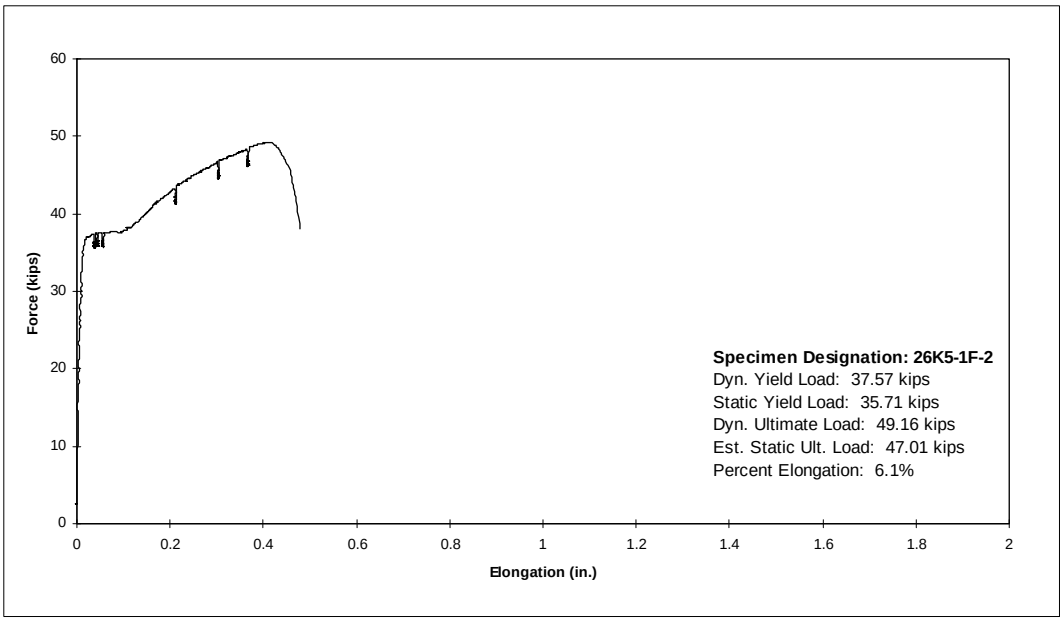

Figure D.12 Force vs. Elongation Response of Specimen 26K5-1F-2

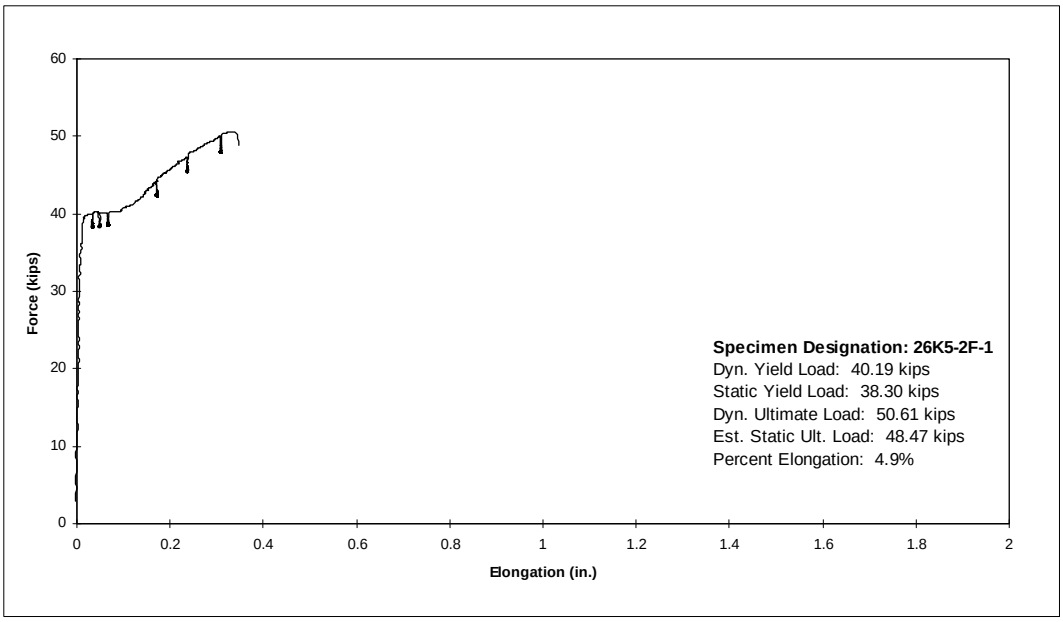

Figure D.13 Force vs. Elongation Response of Specimen 26K5-2F-1

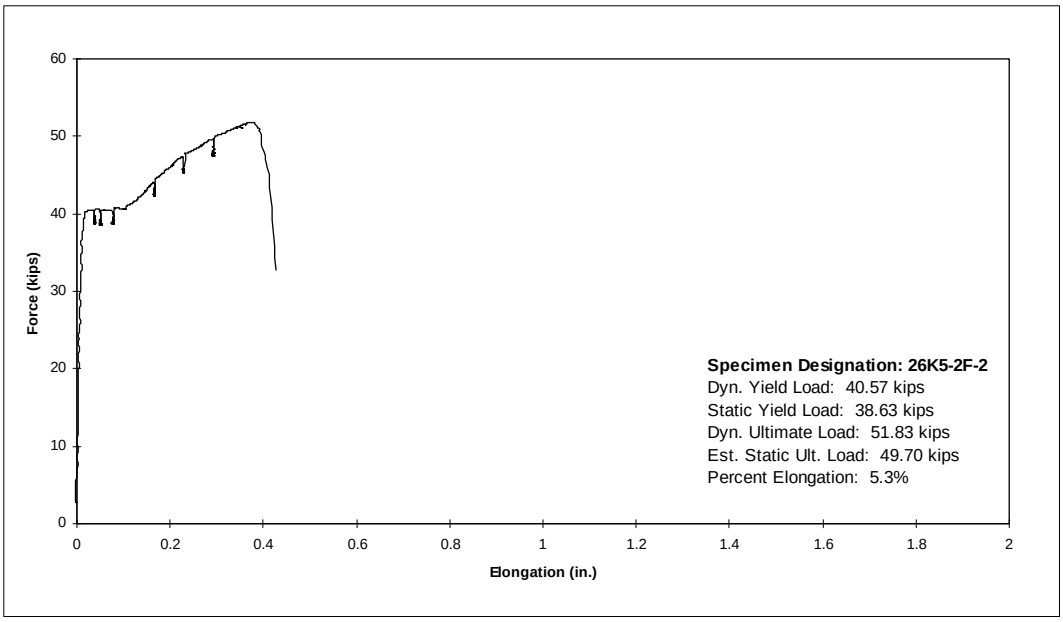

Figure D.14 Force vs. Elongation Response of Specimen 26K5-2F-2

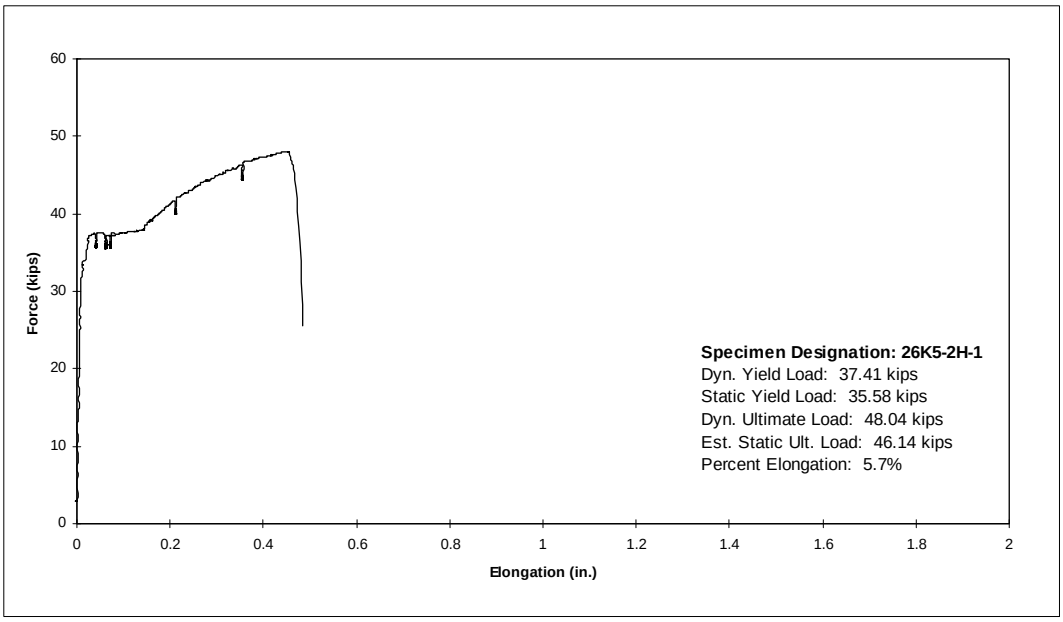

Figure D.15 Force vs. Elongation Response of Specimen 26K5-2H-1

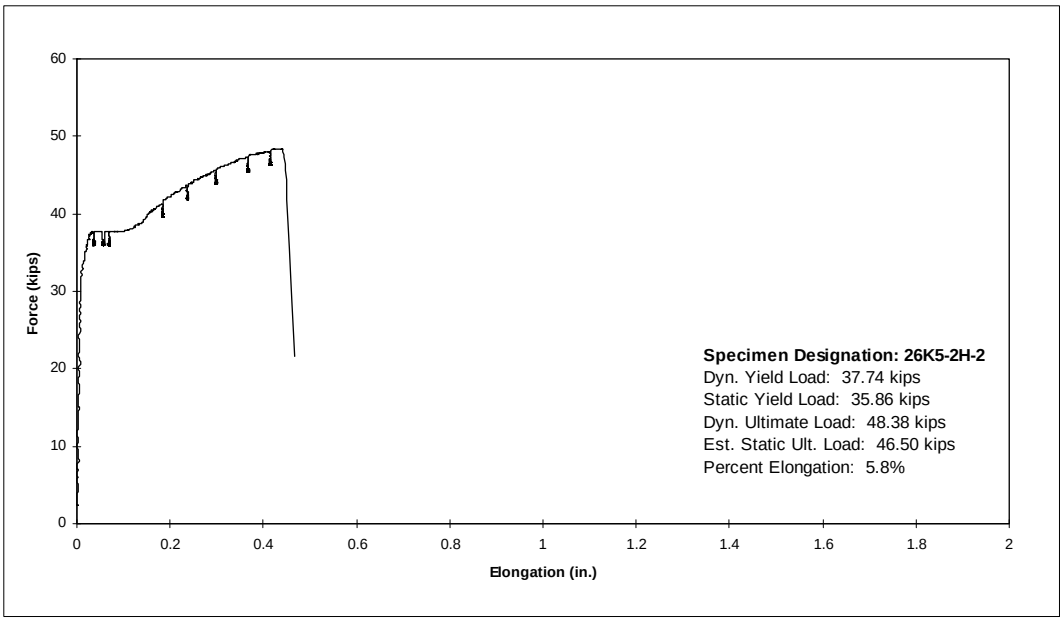

Figure D.16 Force vs. Elongation Response of Specimen 26K5-2H-2

References

American National Standards Institute, 1995. American National Standard for Construction and Demolition - Powder Actuated Fastening Systems - Safety Requirements, ANSI A10.3.

American Society for Testing and Materials, 1996. Annual Book of ASTM Standards: Iron and Steel Products, Volume 01.04, West Conshocken, PA.

American Society for Testing and Materials, 1987. Standard Test Methods for Strength of Powder Actuated Fasteners Installed in Structural Members, ASTM Designation E1190, Philadelphia, PA.

Glaser, N.J. and M.D. Engelhardt, 1994. An Overview of Power Driven Fastening for Steel Connections in the U.S. Construction Industry, *Report No. PMFSEL 94-1,* Phil M. Ferguson Structural Engineering Laboratory, The University of Texas at Austin, Austin, Texas.

Occupational Safety and Health Administration, 1981. Employment Safety and Health Guide: OSHA Standards for the Construction Industry, 29 CFR Part 1926, Commerce Clearing House, Inc.

Powder Actuated Tool Manufacturers' Institute, Inc., 1991. Powder Actuated Fastening Systems Basic Training Manual, PATMI Inc., St. Charles, MO.

Steel Joist Institute, 1994. Standard Specifications for Open Web Steel Joists - K Series, Steel Joist Institute.